University of Southampton

Novel DNA probes for sensitive DNA detection

James Alistair Richardson

A thesis submitted for the Degree of Doctor of Philosophy

Department of Chemistry

March 2010

Declaration

I hereby declare that this thesis is my own composition and that the work described is my own unless otherwise acknowledged. No part of this thesis has been submitted as part of any other previous application for a higher degree.

James. A. Richardson, March 2010

UNIVERSITY OF SOUTHAMPTON
FACULTY OF ENGINEERING, SCIENCE AND MATHEMATICS

SCHOOL OF CHEMISTRY

DOCTOR OF PHILOSOPHY

ABSTRACT

Novel DNA probes for sensitive DNA detection

James Alistair Richardson

The ability to detect and interrogate DNA sequences allows further understanding and diagnosis of genetic disease. The ability to perform such analysis of genetic material requires highly selective and reliable technologies. Furthermore techniques which can use simple and cheap equipment allow the use of such technologies for point of care analysis.

Described in this thesis are two novel DNA probe systems designed for mutation discrimination and sequence recognition of PCR products. A homogenous PCR system using HyBeacons® which utilise FRET to produce a three probe multiplex system and surface enhanced Raman detection method. Both of these systems allow multiplex detection of PCR products and mutation discrimination by melting temperature analysis. The research reported includes investigations into the effects of different modifications to improve the performance of HyBeacon® probes as well as the effect of different dyes in a FRET system, including unique changes in the optical properties of such dyes. Also a novel method of performing melting temperature analysis using an electrochemical potential is reported.

In addition to the detection methods described this thesis includes initial work into the stabilisation of quantum dot nanoparticles for their use in aqueous systems as a potential alternative to fluorescent organic molecules.

Contents

Abbreviations

A	Adenine
AFM	Atomic force microscopy
Ar	Aryl
BHQ	Black hole quencher
C	Cytosine
CCD	Charge-coupled devices
CFTR	Cystic fibrosis transmembrane conductance regulator
DABCYL	Dimethylaminophenylazobenzoic acid
DCM	Dichloromethane
DEPT	Distortionless enhancement by phase transfer
DHLA	Dihydrolipoic acid
DIPEA	N, N-diisopropylethylamine
DMAP	Dimethylaminopyridine
DMF	Dimethylformamide
DMSO	Dimethylsulphoxide
DMT	Dimethoxytrityl
DNA	Deoxyribosenucleic acid
DTT	Dithiothreitol
dT	Deoxythymine
dU	Deoxyuridine
EDC	1-ethyl-3-(3-dimethylaminopropyl) carbodiimide hydrochloride
ES	Electrospray
EtOAc	Ethyl acetate
FAM	Fluorescein
FESP	Force modulation etched Silicon probe
FISH	Fluorescence in situ hybridization
Fmoc	Fluorenylmethyloxycarbonyl
Fmoc -OSu	N-(9-Fluorenylmethoxycarbonyloxy) succinimide

FRET	Fluorescence resonance energy transfer
G	Guanine
HPLC	High performance liquid chromatography
HBTU	O-Benzotriazole-N,N,N’,N’-tetramethyl-uronium-hexafluoro-phosphate
HDA	Hexadecylamine
HPA	Hydroxypicolinic acid
HPLC	High performance liquid chromatography
IDU	5-iodo deoxyuridine
Kb	Kilobases
LED	Light emitting diode
HRMS	High resolution mass spectrometry
LRMS	Low resolution mass spectrometry
MAA	Mercaptoacetic acid
MALDI-TOF	Matrix assisted laser desorption ionisation time of flight
MeOH	Methanol
MPA	Mercaptopropionic acid
NMR	Nuclear magnetic resonance
PA	Picolinic acid
PCR	Polymerase chain reaction
PEG	Polyethylene glycol
PL	Photo luminescence
PLE	Photo luminescence excitation
ppm	Parts per million
RT-PCR	Real-time PCR
SAM	Self assembled monolayer
SBE	Single base extension
SERS	Surface enhance Raman spectroscopy
SNP	Single nucleotide polymorphism
T	Thymine
TAMRA	Tetramethyl-6-Carboxyrhodamine

TBE	Tris borate ethylenediaminetetraacetic acid
TEA	Triethylamine
THF	Tetrahydrofuran
TLC	Thin layer chromatography
TMSt	Trimethoxystilbene
TOPO	Trioctylphosphine oxide
U	Uridine
UV	Ultraviolet
QD	Quantum dot

Acknowledgements

I would like to thank my supervisor Prof. Tom Brown for allowing me this opportunity and for the support, ideas and inspiration which have made the research possible, and to the EPSRC for providing funding.

Secondly I would like to thank all the people I have had the pleasure of collaborating with during the course of the research and for allowing me to work in such a range of environments, particularly Dr Sumeet Mahajan and Mr Jan Junis Rinderman.

I would like to thank past and present members of the Brown group that have made the work group such a pleasurable experience, also for the ideas and input into my research and for helping proof reading this thesis.

Thanks to ADTBio for oligonucleotide synthesis and purification, Dr John Langley and Miss Julie Herniman for access to the mass spectrometry facilities and Dr Neil Wells and Mrs Joan Street for the use of the NMR systems.

Finally I would like to thank my family for their continued support and encouragement throughout my PhD.

Chapter 1

1.0 Introduction

1.1 Nucleic acid structure

1.1.1 Primary structure

Nucleic acids are biological polymers built up from monomers called nucleotides, which are condensed together to form phosphodiester linkages between the monomers. Nucleotides consist of three main components, a nitrogen-containing heterocyclic base, a pentose sugar and a phosphodiester; heterocyclic bases bound only to a pentose sugar are termed nucleosides. There are five different heterocyclic bases, two purines (adenine and guanine) and three pyrimidines (cytosine, thymine and uracil), with adenine, cytosine and guanine being common to both DNA and RNA, and thymine and uracil being specific to DNA and RNA respectively.

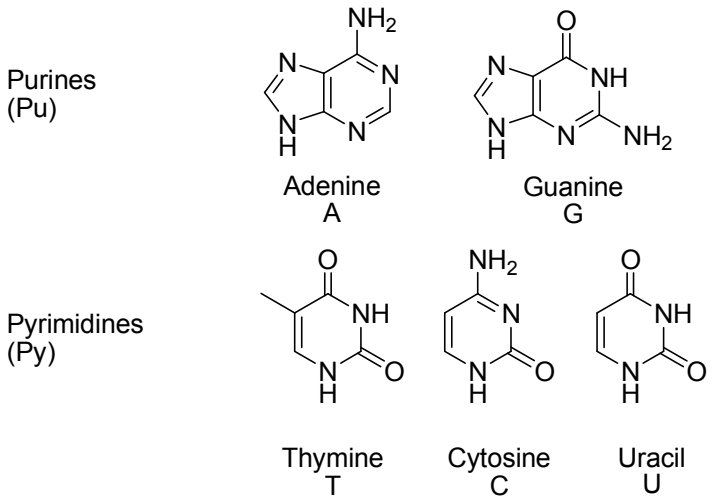

Figure 1.1 The five common heterocycles found in nucleic acids.

These heterocyclic bases are connected covalently by the *N* 9 of purines or the *N* 1 of pyrimidines to the C 1' position of the pentose sugar which is either a deoxyribose (in DNA) or a ribose (in RNA), fixing the sugar ring into a five-membered furanose configuration. This fixed configuration most commonly results in a β *N*-glycosylic bond[1], where the heterocyclic base adopts an orientation above the furanose ring, on the same side

as the base and the 5'-hydroxyl group of the sugar. Further possibilities exist by rotation around this glycosylic bond resulting in two possible extreme configurations, *syn* or *anti*.

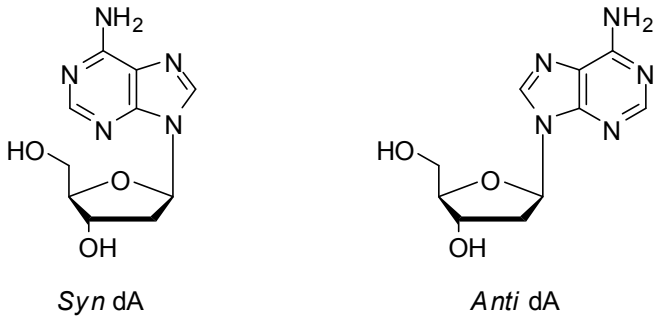

Figure 1.2 *syn* and *anti* configurations of dA nucleoside.

These monomeric nucleotides are condensed together in a chain-like fashion from the phosphodiesters between the 3' hydroxyl of one ribose and the 5' hydroxyl of another ribose. This linkage provides the DNA or RNA chain with a 5' to 3' directionality and at physiological pH a polyanionic phosphodiester backbone.

1.1.2 Secondary structure

The elucidation of the characteristic double helical secondary structure of DNA by James Watson and Francis Crick was published in 1953 in the journal Nature[2]. This discovery was dependent on work previously reported by Chargaff *et al* who formulated a rule stating that the ratio of purines to pyrimidines is always 1:1[3,4]. This ratio is invariable, regardless of the sequence of the nucleotides in the DNA strand. Moreover, the number of moles of adenine is equal to that of thymine and likewise for guanine and cytosine. This meant that the bases form purine-pyrimidine pairs and A only pairs with T, and G with C.

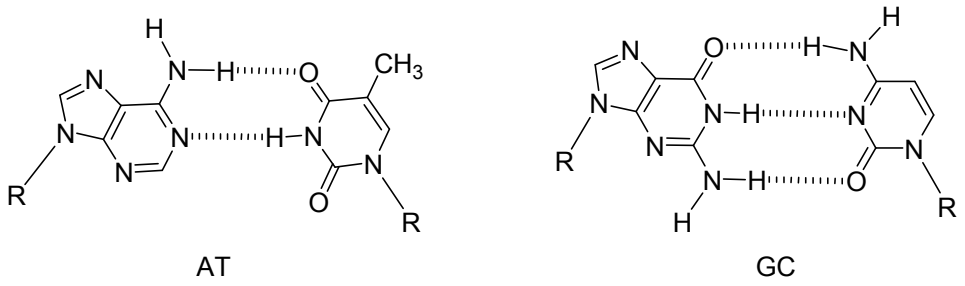

Figure 1.3 Watson-Crick base pairing in DNA.

This information provided evidence that the two strands of the double helix are complementary in sequence. Further information on the structure of DNA was provided by Maurice Wilkins and Rosalind Franklin who used X-ray crystallography to show that the secondary structure of DNA is highly crystalline and helical in structure. They proposed that the bases are within the core of the helix, exposing the negatively charged phosphodiester backbone. As well as providing information as to the helical structure of the DNA, Maurice Wilkins and Rosalind Franklin also discovered that this helical structure could be altered by varying the humidity. This allowed them to characterise both the 'A-form' of the helix in low humidity and the 'B-form' under high humidity.

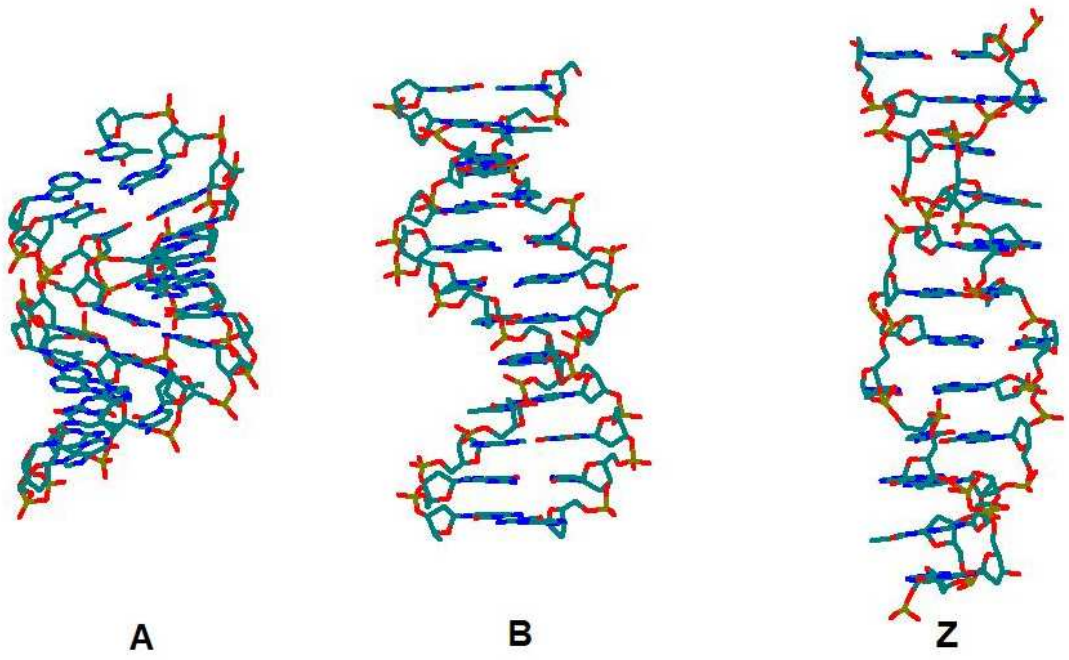

Figure 1.4 DNA duplexes of the A, B and Z forms.

From this James Watson and Francis Crick were able to deduce the structure of DNA in which two separate antiparallel strands wind in a helical fashion. At the centre of the helix structure lie the hydrophobic bases, which are planar and are stacked upon each other with the specific adenine-thymine and guanine-cytosine base-pairing. In this base-pairing, hydrogen bonds link the two strands of the helix together, imparting a right handed coil with around 10 base pairs making one complete turn of the helix in the most common B-form DNA. This helical structure gives rise to two grooves of unequal size, a minor groove and a major groove of 0.6 nm and 1.2 nm respectively. These grooves contain hydrogen bonding sites and can provide a source of interaction for both small molecules such as spermine and also large molecules such as proteins, or a third DNA strand.

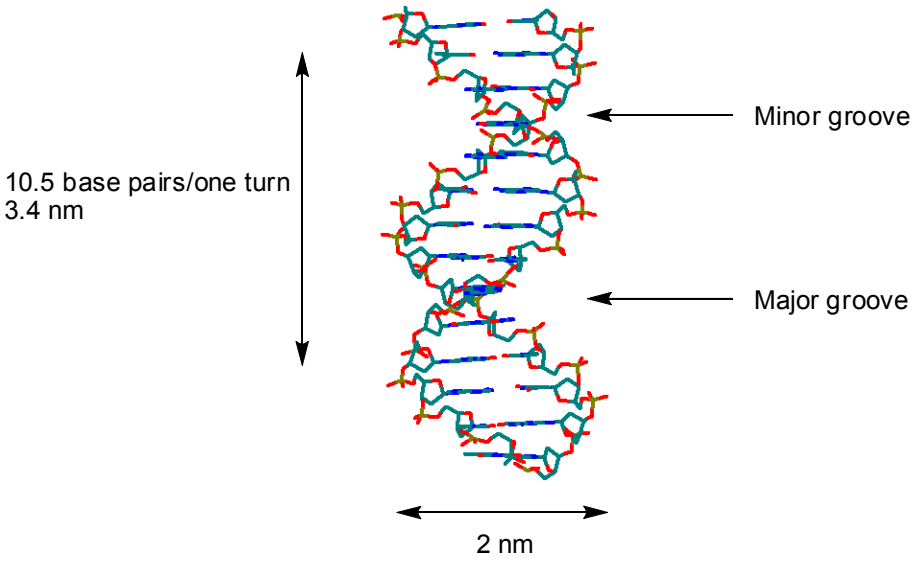

Figure 1.5 Structural dimensions of B-form DNA duplex.

1.13 PNA

Peptide nucleic acid or PNA is an artificial mimic of nucleic acids [5] and is made up of monomer subunits comprised of a heterocyclic base identical to that of DNA/RNA and a peptide-like backbone in place of the pentose sugar and phosphodiester. PNA molecules are constructed using the same C to N directionality with the C terminus being comparable to the 3' of normal DNA, and N terminus being comparable to the 5' position. By using a peptide backbone the PNA molecules carries no formal negative charge, unlike the polyanionic backbone of DNA/RNA molecules. This results in an increase in the thermodynamic stability of PNA/PNA and PNA/DNA duplexes when compared to standard DNA/DNA duplexes as there is no interstrand repulsion from the backbones. Furthermore, this synthetic backbone provides the PNA with increased *in vivo* stability as it is difficult for enzymes to recognise the PNA resulting in a resistance to enzymatic degradation. This increased stability both thermally and enzymatically makes PNA a

suitable mimic for DNA probes as shorter probes can be used *in vivo* with increased lifetimes than DNA probes.

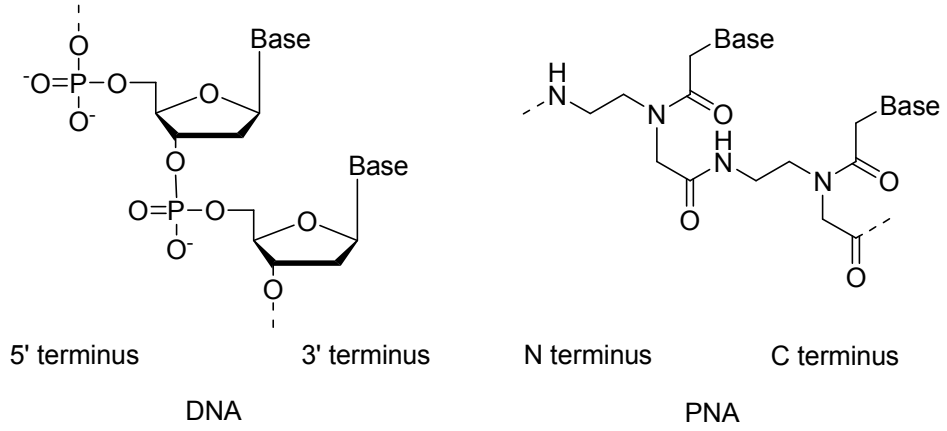

Figure 1.6 Comparison of DNA and PNA oligomers.

1.2 The Genetic code

The central dogma of biology is that DNA codes for RNA, which codes for proteins, and so the individual sequences of amino acids within proteins are initially coded for within the sequence of DNA nucleotides which makes up the genome. Genomic DNA is grouped into genes, and in eukaryotic cells this can further be divided into non-coding introns and coding exons which contain tri-nucleotide sequences called codons. Organisms can have as little as 500 or as many as 50,000 genes[6]; these genes are stored in one or more chromosomes within the organism. The human genome contains 3×10^9 base pairs, only 3-5% of these coding for the 3×10^5 genes contained within the 23 chromosomes[7].

The process of producing proteins starts with transcription, where the information coded within the DNA is transcribed into RNA by the enzymatic copying of the DNA with RNA polymerase producing a complementary mRNA strand. This mRNA strand is then decoded by the ribosomes which translate the codons into amino acids and so define the primary

structure of the peptides produced. There are a maximum of 64 possible codons, coding for 20 natural amino acids, this means that many of them code for the same amino acid (degeneracy). Some codons are used for start, stop and nonsense signals to differentiate between regions that code for separate proteins.

1.3 DNA labelling

1.3.1 Fluorescent labels

Fluorescent labelling of DNA is used throughout the life sciences and is hugely important in DNA diagnostics. It provides a simple and safe method for the detection and identification of labels and also allows further more detailed analysis due to the ability to manipulate the signal. This has led to fluorescent labels being a major contributing factor in the rapid development of DNA sequencing and genetic analysis, by allowing more advanced high-throughput techniques[8,9].

1.3.1.1 Organic fluorophores

There are vast numbers of fluorescent organic molecules which can be used for DNA labelling, many of which are modified to produce dyes of varying optical characteristics. These dyes tend to be planar aromatic molecules, the fluorescence properties of which are highly sensitive to chemical modifications.

Particularly popular classes of dyes are the fluorescein and rhodamine based dyes, which are based on modified carboxyfluorescein and rhodamine (Figure 1.7).

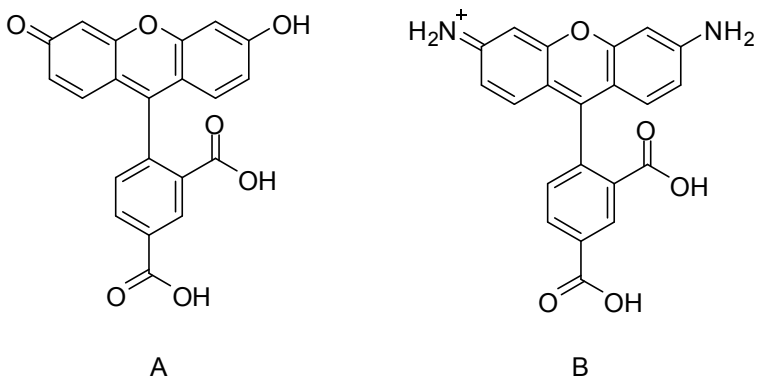

Figure 1.7 Structure of 5-carboxyfluorescein (A) and 5-carboxyrhodamine (B).

Carboxyfluorescein has excitation and emission wavelength maxima of 494 nm and 525 nm respectively. Chemical modification yields dyes such as hexachlorofluorescein and similarly rhodamine can be modified to produce dyes such as Texas red. These fluorescein and rhodamine analogues have different excitation and emission wavelengths to fluorescein and rhodamine.

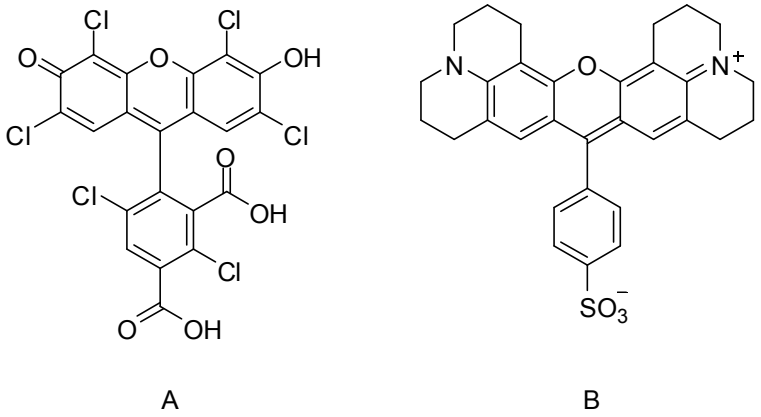

Figure 1.8 Structure of hexachlorofluorescein (A) and texas red (B).

This means that almost all wavelengths in the visible region can be covered, making the fluorescein dyes very useful. Carboxyfluorescein has become widely used as it has many desirable properties including a very high quantum yield (0.96 in 0.1 M NaOH)[10], good chemical stability and ease of use when labelling. It is available modified with a variety of

functional groups and can be conjugated to DNA bases for use in solid phase oligonucleotide synthesis. One of the most useful functionalised forms of this type of dye is the active ester, typically N-hydroxysuccinimide[11]. Active esters allow efficient coupling of the dye to primary amines which can easily be incorporated into oligonucleotides at either terminus and at internal positions, resulting in a chemically stable amide bond. This is a highly flexible method of labelling as it can be performed on the CPG oligonucleotide synthesis resin. This allows the oligonucleotide synthesis resin to be separated after oligonucleotide assembly and then labelled with different dyes reducing the need for multiple syntheses. However this technique can only be used to label an oligonucleotide with one type of dye in any given synthesis due the lack of selectivity when using multiple amines. Alternatively modified bases can be used which already contain a dye label. Thymidine modified at the 5 position with fluorescent dyes attached to an alkyl chain is used in the majority of cases as it is simple to synthesise, but adenine, cytosine and guanine can also be purchased modified with fluorescent dyes. These modified monomers utilise the standard protecting and activating groups for DNA synthesis, with a dimethoxytrityl group at the 5' and a phosphoramidite at the 3'.

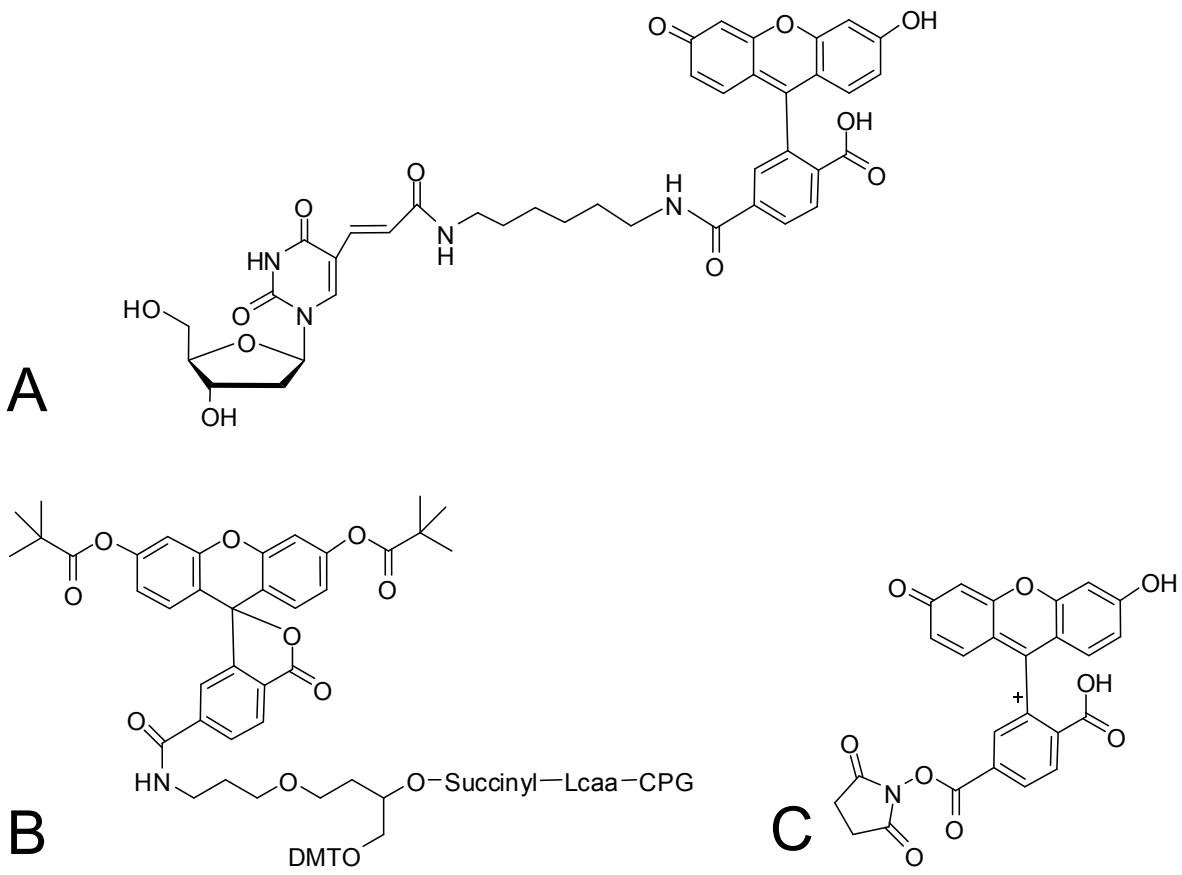

Figure 1.9 Addition of fluorescein into oligonucleotides; **A**, Commercially available FAM dT in its form in an oligonucleotide; **B**, Modified CPG resin for 3' labeling; **C**, FAM NHS ester for amino labelling.

These monomers can be used on DNA synthesisers alongside standard unmodified bases during oligonucleotide assembly. It also allows the oligonucleotide to be labelled with multiple dyes as the individual phosphoramidite monomers are incorporated stepwise into the oligonucleotide. This further increases the versatility of the labelled oligonucleotides, enabling them to be used in various applications.

Due to its relatively low cost and favourable fluorescent properties, fluorescein is widely used in biophysical techniques such as real-time PCR, and equipment is designed specifically for fluorescein (e.g. Roche LightCycler). This has meant that its use as a label

for DNA based analytical techniques has been thoroughly investigated and optimised. However it does have some limitations, including pH sensitivity[12], broad emission spectra and susceptibility to photobleaching[13]. The limitations of fluorescein-based dyes have led to the synthesis and use of other families of dyes including the cyanine dyes. Cyanine dyes have higher extinction coefficients than fluorescein, and their fluorescence is relatively pH insensitive, although their quantum yields are lower than fluorescein[14]. They too can be modified to cover a broad range of the visible and near-IR region of the electromagnetic spectrum by either varying the length of the polymethine chain or modifying the heterocyclic rings in the molecule[15-17]. The cyanine dyes are commercially available both as active esters and phosphoramidite monomers suitable for 5'-, 3'- or internal oligonucleotide labelling. This makes them versatile, just like the fluorescein dyes, and also useful for labelling during oligonucleotide synthesis.

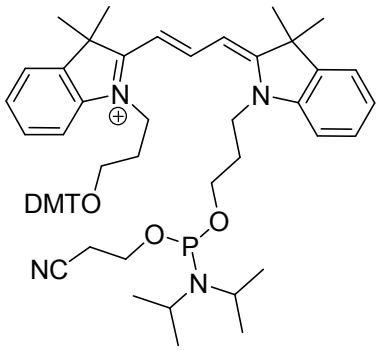

Figure 1.10 Cy3 phosphoramidite for incorporation into an oligonucleotide sequence.

Both of these families of dyes can be used to label DNA covalently (i.e. by chemical bond formation). However some dyes exist which can be used to label DNA without the formation of chemical bonds, but through electrostatic and hydrophobic interactions. These "DNA binding dyes" are useful in applications such as low-cost genetic analysis. Dyes such as ethidium bromide and Sybr green are planar polycyclic aromatic dyes which carry a formal positive charge. These dyes can bind in the minor groove or in the hydrophobic region between the base pairs forming π–π stacking similar to the base pairs themselves[1]. Also, as the dyes carry a positive charge, the polyanionic backbones of the DNA duplex

contribute to binding and increase the stability of the complex. Such dyes have enhanced fluorescence when bound to double stranded DNA (intercalating dyes and minor-groove binders can only bind to *double stranded* DNA). This makes them extremely useful for fluorescence melting and applications such as real-time PCR when, for cost-related reasons, modified primers, labelled dNTPs etc are not suitable.

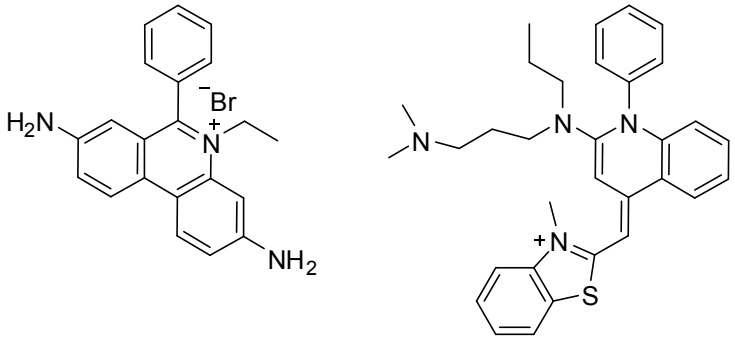

Figure 1.11 Two common DNA binding dyes, ethidium bromide (left) and SYBR green (right).

1.3.1.2 Quantum dots

Quantum dots are semi conductor nanocrystals with a diameter in the region of 3-8 nm depending on the semi conductor material. These nanocrystals exhibit fluorescence with a high quantum yield (0.50)[18], narrow emission spectra (FWHM ~30 nm) and broad excitation spectra. These optical characteristics occur due to an effect known as quantum confinement brought about by the nanoscale size of the quantum dots[19]. When a material is excited, it creates an electron hole pair known as an exciton, and the spacing between the electron and hole is known as the Bohr radius. When the material is of a similar size to the Bohr radius the electron wavefunction is bound by the confinement in size, resulting in well-defined discrete energy levels. This is similar to the defined number of mechanical wave patterns on a string, differentiating the nanocrystal from the bulk material. In quantum dots, the confinement is in 3 dimensions; confinement in either one or two dimensions gives quantum wells and quantum wires respectfully. Confinement in all 3

dimensions results in discrete energy levels predicted by the particle in a box theory. This size related quantum effect results in the tuneability of the optical properties of the quantum dot. By reducing the size of the nanocrystal the confinement is increased and so the energy gap between the energy levels increases resulting in a blue shift in emission. This size tuneability can also be explained by Heisenberg's uncertainty principle, as with greater localisation of the wavefunction there is an increased uncertainty in momentum which results in an increase in the energy gap between discrete energy levels.

Quantum dots are spherical with faceted surfaces due to the anisotropic growth of the crystal, usually CdSe in a wurtzite structure. Quantum dots with a diameter of 4.5 nm will contain somewhere in the region of 1800 atoms, which leaves a high fraction of atoms at the crystal surface. Many of these atoms have uncoordinated bonds which can react chemically and so they are coordinated with Lewis base organic surfactants such as long chain amines and tri-octylphosphine oxide (TOPO). CdSe nanocrystals are prone to photo-oxidation due to the interaction of the electron-hole pair at the surface with uncoordinated selenium atoms. This reduces the quantum yield of the quantum dot and so the CdSe core is often coated with a higher bandgap material, in many cases ZnS, increasing the quantum yield to 0.5-0.6. This higher bandgap material confines the holes to the core of the quantum dot due to the energy difference in the bandgaps, reducing the photo-oxidation. This interaction between the electron-hole pair and the surface also gives rise to other quenching mechanisms with molecules at the surface such as water or oxygen. This makes the quantum dots highly susceptible to quenching and as such the choice of coordinating ligand is important. By using Lewis base organic surfactants a hydrophobic shell is produced around the quantum dot, preventing contact with water molecules and providing solubility in organic solvents. For use in aqueous systems the surface of the quantum dot needs to be modified to allow aqueous solubility and/or protection from the aqueous environment. The most common method for such modification is the use of small, carboxylic acid functionalised molecules such as mercaptoacetic acid[20-22] or mercaptopropionic[23-25] acid, with MPA coated Quantum dots having greater stability[26]. By performing ligand exchange with the TOPO or hexadecylamine (HDA), a shell of zinc-sulphur bound molecules is created providing an exterior acid-functionalised surface.

Similarly dithiothreitol has also been shown to be a suitable small molecule for the coating of Quantum dots, providing aqueous solubility and stability[27]. These coatings have two advantages; they allow the solubilisation of Quantum dots in an aqueous environment whilst retaining fluorescence; and they also allow further modification of the quantum dots by providing many reactive sites on the exterior of the protective shell. These small molecule based systems have been shown to have limited lifetimes, with precipitation occurring in as little as one to two weeks[20,24], but have be implemented in systems such as molecular beacons, in conjunction with traditional organic dyes as fluorescence quenchers[22].

As an alternative to small molecule ligands, large linear polymers[28] or branched organic dendrons[29] containing hydrophobic inner regions and hydrophilic exteriors can be used to build up a hydrophobic shell around the quantum dot with a hydrophilic exterior. This has allowed quantum dots to be used to passively label tumour cells *in vivo* by taking advantage of the enhanced permeability and retention of tumour cells and the lack of lymphatic drainage in tumours.

Similarly quantum dots can be encapsulated within polymer microbeads[30] to provide fluorescent quantum dots which are totally shielded from their local environment. This can also increase the potential uses for the quantum dots by encapsulating multiple quantum dots within one microbead. By changing the colour/size and number of specific quantum dots within the microbead a barcode type system can be created. This can provide as many as 10,000-40,000 different codes from just 5-6 colours and 6 different intensities. However this type of protection does limit the use of the quantum dot, as it is isolated from the local environment.

1.3.1.3 Lanthanide labels

Lanthanide chelates can be used to label DNA giving long fluorescence lifetimes (up to 2 ms), narrow emission spectra and large Stokes shifts[31,32], with excitation wavelengths within the UV and emission in the visible spectrum. This makes them particularly useful for FRET and time-resolved experiments and has allowed them to be used for distance measurements within DNA duplexes using an organic dye acceptor molecule[31].

Similar to the organic molecule DNA binding dyes, intercalating fluorescent lanthanides can be used for DNA labelling. Lanthanide-based intercalators which bind specifically to double stranded DNA have been used to monitor the capturing of DNA by surface bound probe strands with quantitative results[33]. This allows both the detection of the target DNA as well as determination of the concentration.

1.3.2 Raman labels

Raman labels are molecules which can be used to provide a unique signature when analysed by Raman spectroscopy and can be specifically or non-specifically bound to a target. Raman labels have been used to label biological molecules since the early 1970's and have allowed Raman spectroscopy to be used as a tool for monitoring interactions such as protein-ligand interactions through the use of molecules such as methyl orange[34].

For a molecule to perform well as a Raman label it requires a highly polarisable extended π-electron chain[35]. This means that many commercially available labels designed for use in fluorescent assays such as fluorescent dyes and quenchers are highly suitable, as are simple molecules such as benzene. Furthermore due to the highly specific nature of Raman spectroscopy and its sensitivity to the π-electron system, small changes can result in observable changes in the Raman spectrum. Texas red is a commonly used fluorescent dye and is largely available for the labelling of biomolecules as a mixed isomer. The two

isomers (Figure 1.12) have very similar emission spectra and so for fluorescent applications there is no significant difference. However when analysed by Raman spectroscopy the two isomers appear different.

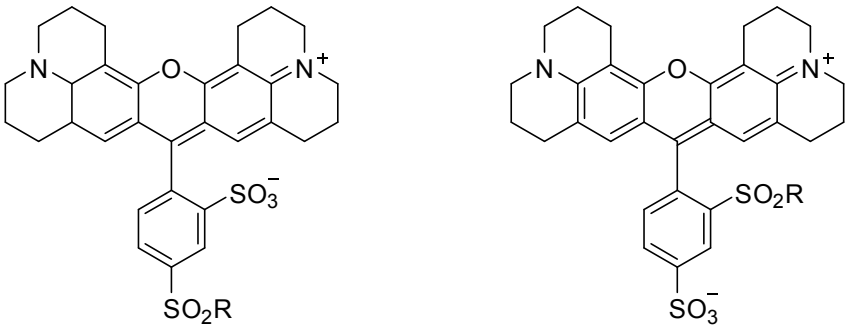

Figure 1.12 Two regioisomers of Texas Red.

This high selectivity and precision means that the Raman labels have a much higher potential in multiplexing[36,37] than their fluorescent counterparts.

1.3.3 Radioactive labels

Radioactive labels were the first labels used to create DNA probes and are still in use today for labelling of both DNA and other biomolecules. Radio-labelling of DNA can be performed at both the 3' and 5' ends of the DNA and utilises radioactive deoxyribonucleoside triphosphates which are enzymatically incorporated into the DNA by techniques such as PCR[38,39]. By labelling DNA with a radioactive marker Edwin Southern was able to demonstrate the use of a radio-labelled DNA probe through the development of Southern blotting[40]. This technique uses restriction enzymes to cut large nucleic acids into fragments which are then separated by gel electrophoresis and then fixed onto a membrane. The radio-labelled probe can then be introduced to the membrane and the radioactive signal can be observed to show the presence or lack of a specific DNA sequence.

Radiolabelling has a high level of sensitivity, with ^{125}I having a lower detection limit of around 10 amol. However there are numerous disadvantages of using radio labels. Due to the radioactive nature of the labels they are hazardous to work with, this also makes them more difficult to dispose of. This can be reduced by using labels with a shorter half-life such as ^{32}P which has a half-life of around 14 days, however this in itself produces its own problems. By having a short half-life the probes will not last long, as the signal rapidly reduces, also this makes the reagents expensive to buy and very limited in shelf life. This makes radio-labelled DNA probes not suited to commercial or high throughput analysis where reusability and reproducibility are important.

1.3.4 Mass tags

Molecular weight specific markers known as mass tags can be used to label DNA and allow detection of cleaved tags by mass spectrometry. This can be used to detect the presence of SNPs within a sequence of interest through using single base extension methods[41]. A primer labelled with a 5' photocleavable mass tag is used which locates next to the SNP location. A single base extension is then performed using a mixture of the four dideoxynucleotides, one of which has a biotin modification. This results in the SBE product containing a 3' biotin modification if the desired variant is present. This product can then be captured using streptavidin-coated beads and the mass tag is then cleaved allowing it to be detected by mass spectrometry. The presence of a positive signal in the mass spectra confirms the identity of the nucleotide at the SBE site as the biotinylated dideoxynucleotide, so confirming the presence or absence of a SNP at that site.

1.4 Principles of fluorescence

Fluorescence is the relaxation back to the ground state resulting in radiation of a photon of a lower energy after absorption of photons by a species resulting in an excited state. It differs from phosphorescence electronically by electron spin coupling and physically by fluorescence lifetimes. Naturally occurring fluorophores have been known since as early as 1845, when Sir John Frederick William Herschel observed the blue emission from the quinine found in tonic water. Since the early observations of fluorescence it became a phenomenon widely used as an analytical tool in the areas of biophysics and biochemistry. In the last 20 years this has progressed further and now its use is widespread throughout industry in applications such as medical diagnostics. Even to this date novel uses of fluorescence are being developed and techniques are being improved and modified.

1.4.1 Mechanism of fluorescence

When light of a particular wavelength is absorbed by a fluorophore it causes an electron to be promoted into a higher energy level, before undergoing non-radiative internal conversion followed by emission of a lower energy photon. This occurs through a series of well defined energy levels and can be depicted by a Jablonski diagram (figure 1.13)

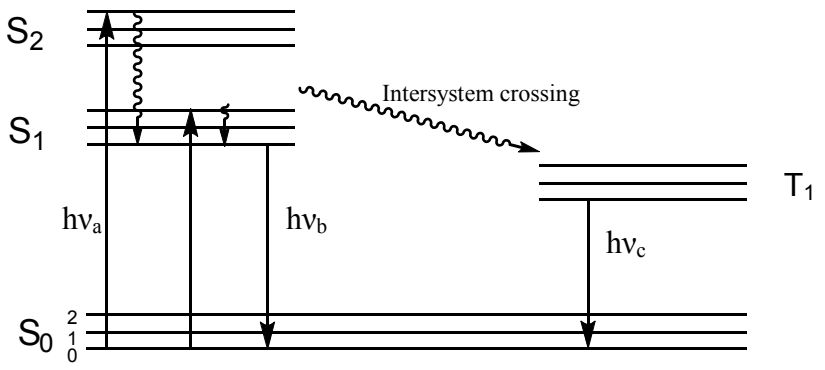

Figure 1.13 Jablonski diagram illustrating path of an excited electron resulting in either fluorescence or phosphorescence.

The energy gap between the S_0 (ground state) and S_1 (excited state) energy levels is sufficiently high that thermal energy is not enough to promote electrons into the S_1 energy level and so light is used. Upon absorption of light $h\nu_a$ the fluorophore is excited into a higher energy level of S_1 or S_2 and then undergoes non-radiative relaxation to the lowest S_1 vibrational energy level. This process is called internal conversion and occurs on a 10^{-12}s scale, so at a much faster rate than the fluorescence lifetime 10^{-8}s. The excited fluorophore can then return to the ground state S_0 emitting a photon $h\nu_b$, typically to a higher ground state such as $S_0$1 which then experiences further internal conversion to reach the lowest energy ground state. This process differs to phosphorescence, where an excited state species can undergo a process called intersystem crossing, by which a forbidden singlet S_1 to triplet T_1 spin conversion occurs before the emission of a photon $h\nu_c$. Due to the forbidden nature of this intersystem crossing the emission rate is several orders of magnitude slower resulting in long emission lifetimes. Due to the internal conversion process $h\nu_a$ is higher in energy than $h\nu_b$, the excitation wavelength is of higher frequency than the emission wavelength, and the resulting energy difference is lost as thermal energy. This process was initially observed in 1852 by Sir G. G. Stokes, and so carries the name Stokes shift. The Stokes shift for different fluorophores can be as little as 20 nm to as much as 200 nm and can be influenced by factors such as solvent, excited state reactions, formation of excimers and energy transfer. The efficiency of the process as a whole can be measured by the number of photons emitted relative to the number of fluorescence photons

absorbed, this is known as the fluorescence quantum yield. The quantum yield is essentially a balance between the rate of emission and the rate of non-radiative decay. The quantum yield of a fluorophore can be calculated by comparing it with a known standard (Table 1.1) and using the following formula.

$$Q = Q_R \frac{I}{I_R} \frac{OD_R}{OD} \frac{n^2}{n_R^2}$$

Figure 1.14. Formula for calculating quantum yields, Q = quantum yield, Q_R = quantum yield of reference, I = integrated intensity, I_R = integrated intensity of reference, OD = optical density of sample, OD_R = optical density of reference, n = refractive index of sample and n_R = refractive index of reference.

Fluorophores with a higher quantum yield can appear brighter, however it is not the only factor in determining the effectiveness of a fluorophore; the extinction coefficient is also very important. This is a measure of the amount of light that is absorbed by a species as a function of concentration. The ideal fluorophore would have a high quantum yield as well as a high extinction coefficient, if either of these factors are low then the brightness of a fluorophore will not be high.

Compound	Solvent	λ_{ex} (nm)	T (ºC)	Quantum yield
Quinine sulphate	0.1 M H_2SO_4	350	22	0.577
Fluorescein	0.1 M NaOH	496	22	0.95
Phenol	Water	275	23	0.14

Table 1.1. Examples of quantum yield standards and the relevant conditions[42].

1.4.2 Fluorescence quenching

Fluorescence quenching is a process which can reduce the emission intensity of a sample and can occur by different mechanisms, namely collisional, Förster/fluorescence resonance

energy transfer and static quenching. Collisional or Dexter quenching is when an excited state species comes into contact with a quencher resulting in the deactivation of the excited state species with no radiative decay. This process requires the two species to come into contact whilst the fluorophore is in the excited state and so the longer the fluorescence lifetime the more efficient this process. However despite the electronic interaction between the two species neither species is altered. FRET quenching occurs when energy is transferred from an excited fluorophore to an acceptor species which then loses the energy in a non radiative manner. The efficiency and mechanism of this process is discussed in part 1.4.3. Both collisional and FRET quenching are dynamic processes as they require the fluorophore to be in the excited state. The third mechanism of quenching, static quenching does not require the fluorophore to be in the excited state. In static quenching the fluorophore complexes with the quencher species whilst in the ground state, resulting in a complex with its own unique properties. Often this can be observed through a change in the absorption spectra from the individual fluorophore and quencher to the complex of the two. An example of a commonly used fluorophore is dabcyl (Figure 1.15), which is widely used in molecular biology particularly in a fluorophore-quencher pair with fluorescein.

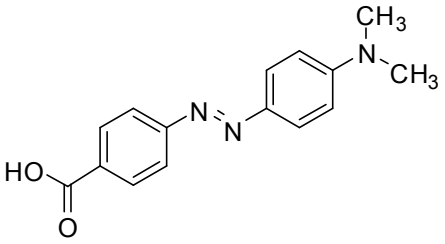

Figure 1.15. Structure of dabcyl, one of the most common quenchers in molecular biology.

1.4.3 FRET

As well as being a quenching mechanism as discussed in 1.4.2 FRET can be used as a method for modifying the observed fluorescence from a sample by shifting the emission

wavelength to one of a lower energy. This process involves the non-radiative transfer of energy from an excited state donor fluorophore to a ground state acceptor fluorophore *via* dipole-dipole coupling. This results in an excited acceptor fluorophore which then relaxes back to the ground state yielding emission at the wavelength corresponding to the acceptor fluorophore. The efficiency of this process depends on the spectral characteristics of both donor and acceptor as well as the distance between them and the relative orientation of the two dipoles. Typically FRET will occur over distances of around 0.5-10 nm[43] (known as Förster distances) making it an ideal technique for measuring distances and interactions between biomolecules[44]. The efficiency of FRET increases with the overlap of the wavelength of the donor emission and the acceptor absorption. A good example of an efficient FRET pair is fluorescein and JOE. Fluorescein has an emission wavelength of 525 nm and JOE has an absorption wavelength of 525 nm (Figure 1.16). This means if both the fluorescein and JOE are within ~6 nm of each other excitation of the fluorescein at 494 nm will result in emission from the JOE at 555 nm (Figure 1.16).

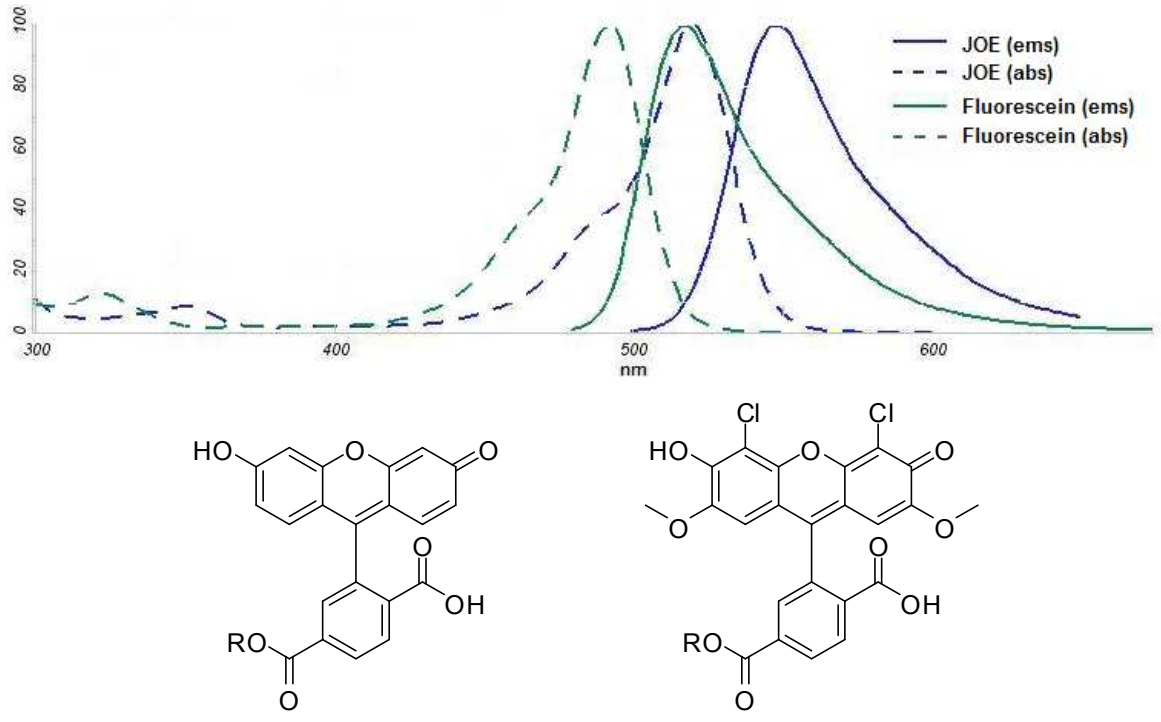

Figure 1.16. Spectral overlap and structures of fluorescein (left) and JOE (right).

1.4.4 Fluorescence detection

The equipment used for the detection of fluorescence can vary widely depending on use. Modern probing technologies are designed so that the simplest equipment possible can be used, however some experiments require much more complexity. Fluorescence at its simplest occurs when light of wavelength X is used to excite a sample, resulting in emission of light of wavelength >X. For many techniques this is all that is required to produce the desired results and so simple equipment can be used. For example in monitoring real-time PCR using a DNA binding dye such as SYBR green, a single fixed excitation wavelength is required. This means that low power, low cost and long lifetime light sources such as LEDs can be used. The emitted light passes through a longpass filter to remove any excitation light and then the emission is detected by a CCD detector giving a measure of fluorescence intensity. More advanced detection methods are found in machines such as the Roche LightCyclers, which utilise either a single or multiple fixed excitation sources, again LEDs, and multiple fixed wavelength emission channels, using dichroic mirrors and filters to separate the emission light into separate detectable wavelengths (Figure 1.17). These two types of machine use relatively simple and low cost components. Their major limitation is that the excitation and emission wavelengths are fixed, so the equipment cannot be tailored to suit specific dyes. In many commercial applications this is not a problem as there is a vast range of suitable commercially available dyes. Fluorimeters/spectrofluorimeters are more sophisticated and use a high intensity light source which passes through a monochromator, allowing the operator to choose the specific wavelength of excitation light to be used. The monochromatic light then passes through the sample causing excitation. The emitted light then passes through another monochromator (as well as a series of filters and variable slits) before being detected by a device such as a CCD detector or photomultiplier tube. This also allows the user defined emission wavelength to be detected, or even a scan to be performed over a range of emission wavelengths. This type of detection is avoided in many commercial applications due the increased complexity, size and cost of the equipment, but for some experimentals it is essential.

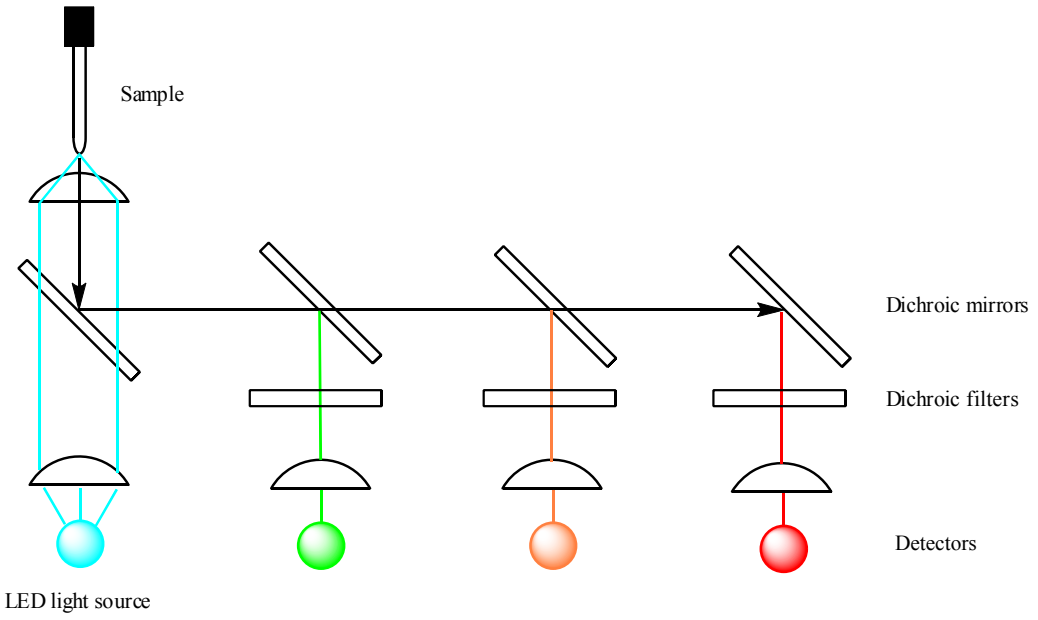

Figure 1.17. Schematic of the LightCycler optics.

As well as the equipment, the contents and orientation of the sample can have an effect on the quality of the fluorescence detection. In the case of many detection machines the emission light is collect at 90º to the excitation light for the simple reason that the excitation light will not then pass directly into the detection components. This can reduce the need for some filters and makes separating the emission from the excitation light much easier. The sample to be analysed must be have a concentration within a certain window, too low and the fluorescence may be below the detection limit of the machine and so no signal (or a noisy signal) will be observed, too high and the optical density could be high enough that not all of the excitation light passes through the sample resulting in lower readings than expected. This is called the inner filter effect and can be observed by seeing fluorescence from the surface of a sample but not throughout. It was first observed by George Gabriel Stokes in 1852.

1.4.5 Fluorescence polarisation

Polarised light can be used alongside fluorescence to provide information about the size, structure and binding of a species. Fluorophores will absorb light with a specific alignment and so by exciting a sample of fluorophores with polarised light only the fluorophores with this correct alignment will be excited. During the lifetime of the excited state the fluorophore can rotate before emission, resulting in the emission having a random alignment, known as fluorescence anisotropy. With fluorophores such as fluorescent proteins this can provide information about the size of the protein as larger proteins will rotate more slowly than smaller ones. Similar to this, the binding of a small fluorophore to a large species can be monitored, as before binding the fluorophore will be able to rotate freely, but when it is bound to the larger species the rotation will be slower. This has been used as a tool to monitor the interactions between DNA-binding proteins and DNA duplexes[45].

1.4.6 Time resolved fluorimetry

Time resolved fluorescence is the measure of emission intensity as a function of time and can be used to provide more detailed information about the fluorophore than the emission spectra alone. This has been particularly useful in biology. For example a protein containing two tryptophan residues will have identical emission spectra for the two residues. However if time resolved fluorimetry is used, the decay rates for the two residues can differ depending on the accessibility of non-radiative decay processes. This allows the two residues to be resolved, thereby providing more detailed information about the locations of the individual residues [10]. Time resolved measurements can also be used alongside FRET to study the binding of two different FRET-capable species, particularly in the area of protein-protein and protein-substrate interactions[46]. To measure time resolved fluorescence, very sensitive equipment is required, the excitation source (typically a laser) has to be capable of providing pulses of excitation light with a duration less than the

fluorescence lifetime of the sample. This also means that the detection equipment has to be equally sensitive and in some cases can even include single photon detectors. This then limits time resolved fluorimetry to specialised research laboratories and so it is not used in high-throughput analysis but more for the understanding of fundamental interactions.

1.5 Principles of Raman spectroscopy

Raman spectroscopy is the study of the inelastic scattering of light by a species and was first observed in 1928 by Sir Chandrasekhara Venkata Raman[47] and separately by Grigory Landsberg and Leonid Mandelstam[48], although it was theorised previously by Adolf Gustav Smekal in 1923. Similarly to fluorescence the inelastic scattering can be from electronic energy levels described by Raman as 'feeble fluorescence' but also from vibrational and rotational energy levels. The use of Raman spectroscopy has not been as widespread as fluorescence throughout bio-analytical research, however more advanced and sensitive forms of Raman spectroscopy such as surface enhanced Raman spectroscopy and the use of resonant Raman spectroscopy have led to the development of more bio-analytical based techniques.

1.5.1 Nature of Raman spectroscopy

In Raman spectroscopy the majority of the excitation light is scattered elastically, known as Rayleigh scattering. However a small portion of the excitation light can be scattered inelastically, giving radiation of a different wavelength to the excitation light, either Stokes or anti-Stokes. After excitation of the species if the relaxation occurs to a higher vibrational level in the ground state the photon emitted has a lower energy than the excitation light (Stokes). If the excitation occurs from a higher vibrational energy level in the ground state and relaxes to a lower vibrational energy level in the ground state it results

in a photon of higher energy than the excitation light (anti-Stokes). This process can be demonstrated using an energy level diagram (Figure 1.18).

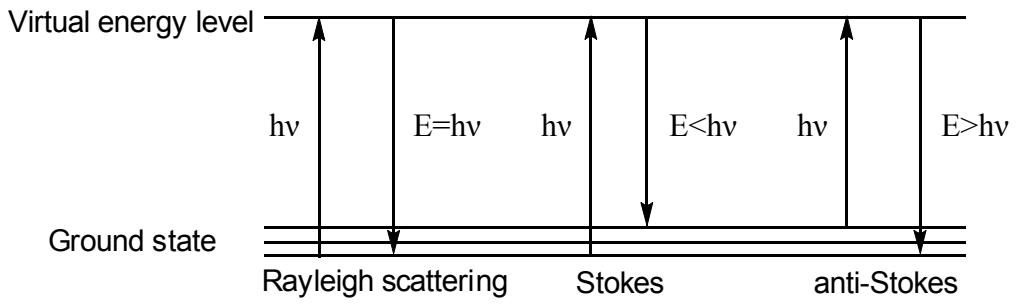

Figure 1.18. Energy level diagram of light scattering.

Due to the different vibrational energy levels of a molecule there can be multiple Stokes and anti-Stokes lines. This gives the molecule a unique fingerprint and is one of the main advantages of Raman spectroscopy. It allows the molecule to be identified amongst other signals as the resulting spectra are very specific, unlike fluorescence spectra which have much more limited information content. Furthermore Raman spectroscopy can take place using any excitation light unlike the specific excitation wavelength required for fluorescence. However due to the low proportion of inelastically scattered photons Raman is a weak technique and has a much lower sensitivity when compared to fluorescence.

1.5.2 Surface enhanced Raman spectroscopy

Surface enhanced Raman spectroscopy uses metallic surfaces to increase the observed Raman signal from a molecule and is a fairly recent technique being first observed in 1974 by Fleischman *et al* who observed an unusually large Raman signal for pyridine adsorbed onto a rough silver surface[49]. The enhanced signal can be as much as 10^{14}-10^{15} times stronger than the bulk signal giving SERS the sensitivity required for single molecule studies[50], although in the majority of SERS an enhancement of 10^{6} is observed. This huge

increase in sensitivity can be attributed to the excitation of surface plasmons[51]. The discovery of the predictable source of the Raman enhancement led to the development of SERS substrates which would produce this phenomenon, such as rough silver and alkali metals, gold and colloidal nanoparticles[52]. The limiting factor with the majority of these surfaces is the irreproducibility of the enhancement due to their rough nature. This means that the surfaces are not suited to commercial applications as some areas of the surface will have a greater enhancement than others. However due to the highly distance dependent nature of the enhancement, the signal from the bulk solution is negligible, making the technique useful in specialised applications.

1.5.3 Resonant Raman spectroscopy

Resonant Raman spectroscopy uses an excitation wavelength which is near to the absorption maximum of the molecule of interest. This means that instead of the molecule being excited to a virtual state as with normal Raman spectroscopy it is excited to a higher electronic state. The vibrational modes which are associated with that electronic transition then result in a much greater Raman scattering and so an increase in signal of more than four orders of magnitude[53]. This further enhancement combined with SERS increases the sensitivity of Raman based techniques. Sensitivity comparable to fluorescence can be achieved[54] and due to the molecule-specific nature of Raman spectra, labels with similar absorption maxima are likely to have unique spectra (unlike fluorescence).

1.6 Fluorescence applications in molecular biology

Fluorescence has been widely used as a tool in molecular biology, allowing the study of interactions between biomolecules as well as monitoring rates of reaction. Applications include the development of real-time PCR monitored by fluorescence[55], measuring interaction between proteins[44] and most recently the study of single molecules[56].

1.6.1 PCR

The polymerase chain reaction is a process which is used to exponentially amplify a target region of DNA, producing many millions of copies from as little as a few starting DNA molecules of lengths of up to 40 Kb[57]. PCR has now become commonplace in the analysis of genetic material for genetic diseases[58,59], genome sequencing[9] and forensic analysis[60]. PCR uses a DNA polymerase enzyme to build the copied strands from the template during a series of thermocycling stages. Specialised "hot-start" DNA polymerases can be used which require an initial step of heating which activates the inactive enzyme. This helps to alleviate some of the problems of PCR which arise from the formation of primer dimers and non-specific binding of the primers to other regions of the template. Such enzymes need to be thermally stable to withstand the repetitive cycling of high temperatures, an example of this is Taq-polymerase which was originally isolated from the bacterium thermos aquaticus[61]. The primer pairs used in PCR are short oligonucleotide sequences in the region of 17-30 bases with a similar G C content to ensure similar melting temperatures. The sequence of each primer is complementary to loci on either side of the region to be amplified. The design of these primers is important as they must have minimal secondary structure and not be capable of forming primer dimers or binding to other areas within the region of interest. As well as the primers and enzyme the reaction requires deoxyribonucleoside triphosphates which are the building blocks used by the enzyme to produce the copies of DNA. The reaction takes place using a buffer to control the pH and Mg^{2+} which is essential for the enzyme to work. The first step in the PCR reaction is

heating the sample to 95ºC to denature the template DNA and to activate the enzyme if required. This is then followed by cooling the reaction mixture to a predetermined annealing temperature which allows the primers to anneal to the template, this is in the region of 55 ºC. The mixture is then heated to 70 ºC which allows extension from the 3' end of the PCR primer resulting in synthesis of the product strand. The whole process can be repeated many times, cycling between the three temperatures resulting in an exponential growth of the product as the amplicons from one cycle act as templates for the next.

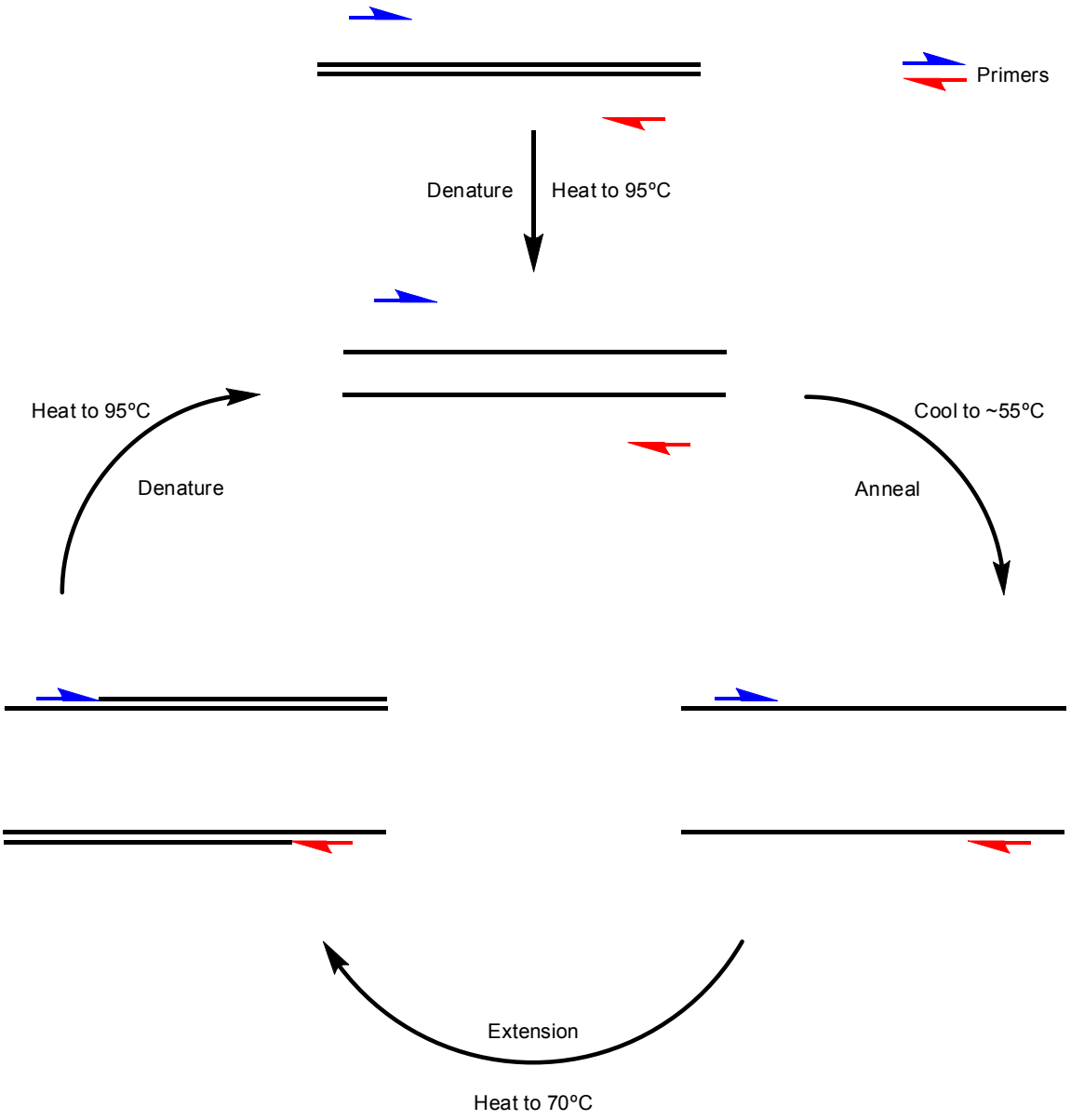

Figure 1.19. Thermal cycles used in PCR.

During the first few cycles the products are not entirely the same due to the action of the DNA polymerase which will keep extending the product until the end of the template or until the enzyme falls off the template, or until the next thermal cycle begins. This means that some of the initial PCR products have longer ends, however as the PCR reaction progresses PCR products are produced exponentially which terminate at the primer 5' ends (Figure 1.20).

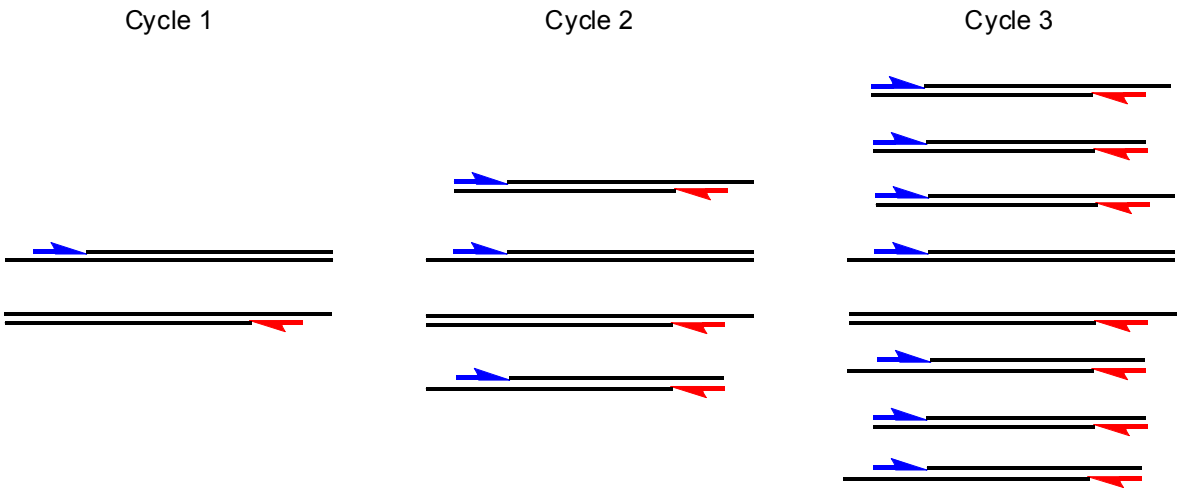

Figure 1.20. PCR products from the first few cycles.

To detect the presence of the PCR products traditionally a portion of the PCR mixture is analysed by agarose gel electrophoresis alongside a DNA stepladder usually containing multiple DNA sequences differing in length by 25 or 50 base pairs, thus allowing the length of the PCR product to be determined. A negative control which contains all the PCR reagents and DNA polymerase but no template must also be used to determine whether the PCR preparation was sterile and that the PCR products are not amplicons of a contaminant sequence. Alternatively the PCR reaction can be quantified in real-time as the reaction progresses (real-time PCR;RT-PCR) RT-PCR uses a fluorescent signal to provide information about the quantity of PCR product present. The simplest method of achieving this is by the addition of a DNA binding dye to the PCR reaction mixture which selectively binds to double stranded DNA resulting in an increase in fluorescence intensity. One

example of such a dye is SYBR green[62] which has similar optical properties to fluorescein. Other methods of introducing the fluorescent signal are the use of fluorescent probes which are discussed in section 1.7.

As well as the standard and RT-PCR methods described above, there are other PCR methodologies for different applications. One example of this is asymmetric PCR which produces much more of one amplicon strand than the other. This is achieved by having a large excess of one primer, this results in the limited primer being used up and subsequent cycles resulting in the production of one product strand. However this process loses the exponential nature of PCR. Once the lesser primer is used up further product is produced at a linear rate and so more cycles are required[63]. This technique is particularly useful when using DNA probes for the interrogation of the PCR product, because with standard symmetric PCR the double stranded products are very stable, making the annealing of a short DNA probe unfavourable. Consequently probe-target binding is a relatively rare event. By producing one strand in excess there is much less competition between the PCR products and the probe, resulting in more probe-target duplexes being formed and consequently more successful probing.

PCR can also be used for genotyping by the use of allele-specific or amplification refractory mutation system (ARMS) PCR. ARMS PCR uses primers which have a 3' end complementary to the mismatch (single point mutation or SNP) and so the PCR reaction is only successful if the mismatch is present[64-66]. This allows simple probe-free low cost analysis.

1.6.2 FISH

Fluorescence *in situ* hybridisation (FISH) involves the use of sequence-specific fluorescent probes tolabel regions of DNA to identify specific localised sequences within a chromosome[67]. This can be used in the detection of diseases such as Down syndrome, translocations responsible for cancer as well as the identification of pathogens. Multiple FISH probes can also be used in a multiplex analysis to provide more detailed information about a genome such as chromosome deletions[68]. The medical diagnostic capabilities of FISH have led to particular advances in high throughput analysis using modern micro fabrication techniques to produce lab on a chip analysis. These high throughput chips have reduced the cost of testing for disease by 10-fold in some cases [69]. Chip-based FISH provides a low cost and simple method of genetic analysis/detection. Furthermore by miniaturisation of FISH, point of care diagnosis becomes possible and therefore the speed of diagnosis is increased. The label used for FISH can either be a fluorescent organic molecule such as the common dyes mentioned in section *1.3.1.1* or quantum dots[30]. Both of these labelling methods result in highly fluorescent probes suitable for the high throughput systems.

1.7 DNA probing strategies

Probing strategies are important in DNA diagnostics as they provide a means of early detection of genetic diseases or pathogens. There are many different probe systems for DNA analysis even though DNA sequencing is considered to be the gold standard[70]. Despite recent advances in the cost and speed of genome sequencing[9], probing strategies are still cheaper and quicker for the detection of known genetic disease and pathogens. Due to the simplicity of many probing strategies, point of care analysis and detection of pathogens in the field is possible, whereas genome sequencing requires much more advanced equipment and so is purely a lab-based technique. Currently homogenous

methodologies which take place in a single tube/container are preferred due to their ease of use and high resistance against contamination.

1.7.1 HyBeacon probes

HyBeacon probes are fluorescently labelled single stranded oligonucleotide probes with no significant secondary structure which produce a signal change upon duplex melting (Figure 1.21).

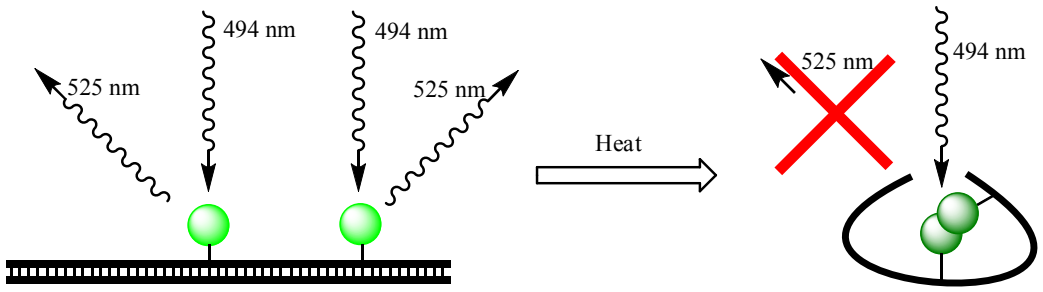

Figure 1.21. Mode of action of a HyBeacon probe displaying fluorescence in the rigid linear double stranded form and a quenched single stranded form.

Hybeacons are valuable tools in the detection of genetic variation, identification of genetic disease and response to medication[71]. Such probes are designed to provide melting temperature analysis for identifying specific mutations within the sequence of interest such as base substitutions, insertions or deletions. HyBeacons provide a simple, homogenous method of analysis which requires no post-amplification manipulation of sample material[72], reducing handling time and risk of contamination. When compared to other homogeneous techniques HyBeacons are much simpler due to the use of the DNA bases and fluorophore-fluorophore interactions to provide quenching, resulting in fewer design constraints and inexpensive oligonucleotide synthesis[71]. Traditionally HyBeacon probes have contained either a single dye addition[33, 34], two dye additions[73] or two dye additions with a 5' stabilising moiety[74] using the change in emission intensity between the linear double

stranded form and the compact single stranded form (due to hydrophobic interactions) to provide the melting temperature analysis. HyBeacons have been synthesised with 6-carboxyfluorescein (FAM), tetrachloro-6-carboxyfluorescein (TET) and hexachlorofluorescein (HEX) providing probes with emission wavelengths of 525 nm, 536 nm and 556 nm respectively[33]. However this is limiting in terms of multiplexing due to the spectral overlaps of the excitation and emission spectra of each of the dyes, as well as the individual excitation wavelengths required for each dye.

1.7.2 Molecular beacons

Molecular beacons are single stranded probes with a highly defined secondary structure for homogenous analysis of PCR products, particularly in RT-PCR[75]. They are designed using a stem and loop type structure which allows them to be fluorescent in the presence of a complementary target sequence but non-fluorescent when there is no target present, or the temperature is above the probe-target melting temperature. The loop region of the probe contains a sequence complementary to the sequence of interest in the target, this is typically 15-35 nucleotides long[76]. Either side of this are shorter 5-8 nucleotide complementary regions, which in the lack of a target sequence hybridise, forming the stem-loop conformation of the probe. Both ends of the probes are labelled, one with a fluorophore and one with a quencher. When in close proximity in the stem-loop configuration the fluorophore is quenched and there is little or no observable fluorescence. However when the probe is hybridised to a target sequence, the fluorophore and quencher are at their maximum possible distance apart resulting in a fluorescent signal (Figure 1.22).

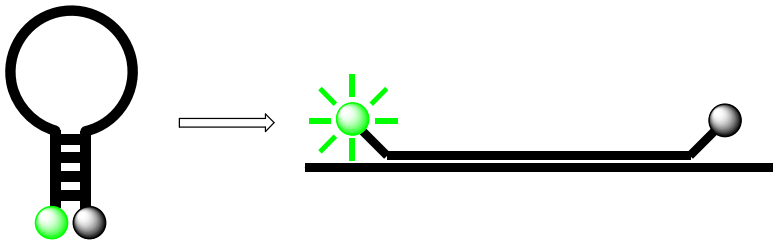

Figure 1.22. Mechanism of molecular beacon melting analysis.

As well as sequence recognition molecular beacons can be used for the detection of SNPs in both heterozygote and homozygote samples. By using molecular beacons with different fluorophores which have loop sequences complementary to either wild type or mutant samples, multiple SNPs can be detected[77]. Due to the instability of the probe-target duplex containing an SNP the relevant molecular beacon containing the complementary sequence to the SNP will bind preferentially. This means that by monitoring the different colours of the fluorescent signal and their relative intensities, allele discrimination can be performed[78,79]. These probes can be contained within a single PCR reaction tube, allowing direct homogenous analysis of PCR products[80]. Molecular beacons can utilise a variety of fluorophore-quencher combinations, including traditional organic fluorophores such as fluorescein, coumarin, Texas red[37, 38, 42], quantum dot fluorophores[81] and even gold nanoparticles as quenchers[82]. Molecular beacons have been modified further by the use of PNA based probes to produce highly stable shorter probes[83]. The PNA based molecular beacons exhibit very high selectivity for the complementary sequence and have a relatively low dependence on salt concentration.

1.7.3 Scorpion primers

Scorpion primers are self probing primers which have the ability to interrogate the PCR extension of itself (self-probing amplicons). The probing mechanism is similar to that of molecular beacons and uses a stem-loop system as described above, or a duplex probe

(Figure 1.23). In either case the probe is bound by one end to the 5' terminus of a PCR primer, and the probing region is complementary to the extension product of the primer in close proximity to the 3' terminus. Once the primer has been extended during PCR the probing region of the primer can then hybridise to this extension allowing sequence detection. With stem-loop scorpion primers, designing the stem region of the probe to be more stable than the extension product containing a mismatch it is possible to distinguish between different alleles[58]. In a homozygote wild type sample all of the PCR extension products result in a fluorescence probe and so a high level of fluorescence is observed. If a heterozygote sample containing a mutation is present only half the extended primers result in a fluorescent self probed product and so the total fluorescence is much lower. Similarly if the sample is a homozygote mutant then none of the PCR extension products are self probing and so there will be no observable fluorescence.

Duplex scorpion primers replace the stem-loop structure with a short duplex probe where the strand attached to the primer contains a fluorophore and the strand bound by Watson-Crick base pairing contains a quencher. Upon PCR extension the duplex region of the probe can be melted allowing the fluorophore labelled probe to bind to the extension product as with the stem-loop based scorpion probes allowing sequence detection and allele discrimination. The main advantage of duplex scorpion primers over stem-loop scorpion primers is that once the probing region is bound to the target the quencher is in solution and so distant from the fluorophore. This reduces the residual quenching present in both stem-loop scorpion primers and molecular beacons and so allows a higher fluorescent signal[84].

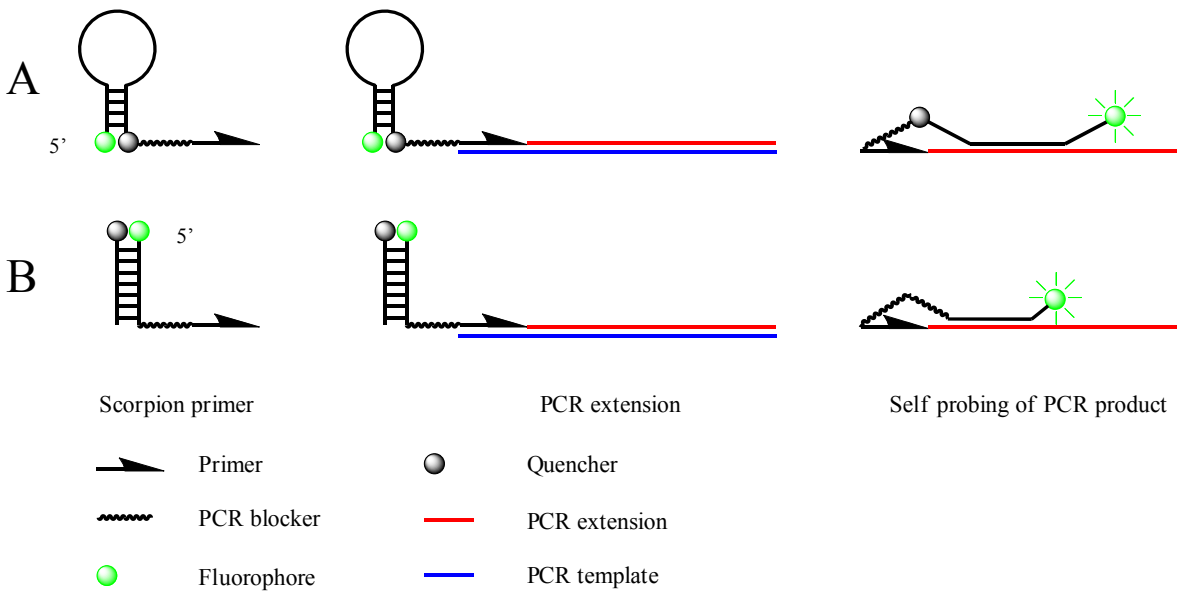

Figure 1.23. Mode of action of stem-loop (A) and duplex (B) scorpion primers.

The major advantage of self probing primers over a bimolecular approach is that it allows the probing to be intramolecular. Thus the probing is concentration-independent and therefore produces a more reliable and stable fluorescent signal and more accurate data than molecular beacons in RT-PCR[85].

1.7.4 Taqman probes

Taqman probes are single stranded probes which are used in quantitative RT-PCR. Like HyBeacons and scorpions they utilise DNA equence recognition and monitoring offluorescence intensity, but their mode of action is quite distinct. The Taqman probe consists of a single stranded oligonucleotide of around 20-30 bases in length containing a fluorophore and a quencher. In the single stranded form the probe is quenched due to the flexibility of the probe allowing the fluorophore and quencher to come into close contact during the fluorescence lifetime of the fluorophore[59]. During PCR the Taqman probe hybridises to the complementary region of the PCR product retaining a close proximity of

the fluorophore and quencher and so there is little observable fluorescence. During the extension step in the PCR reaction the Taq polymerase cleaves the probe due to its 5'-3' nucleolytic activity, producing mono and oligonucleotides[40], separating the fluorophore from the quencher and hence giving rise to an increase in the observed fluorescence. By monitoring the increase in the fluorescent signal the PCR reaction can be followed in real-time providing confirmation of sequence recognition/detection as well as quantification of the PCR product.

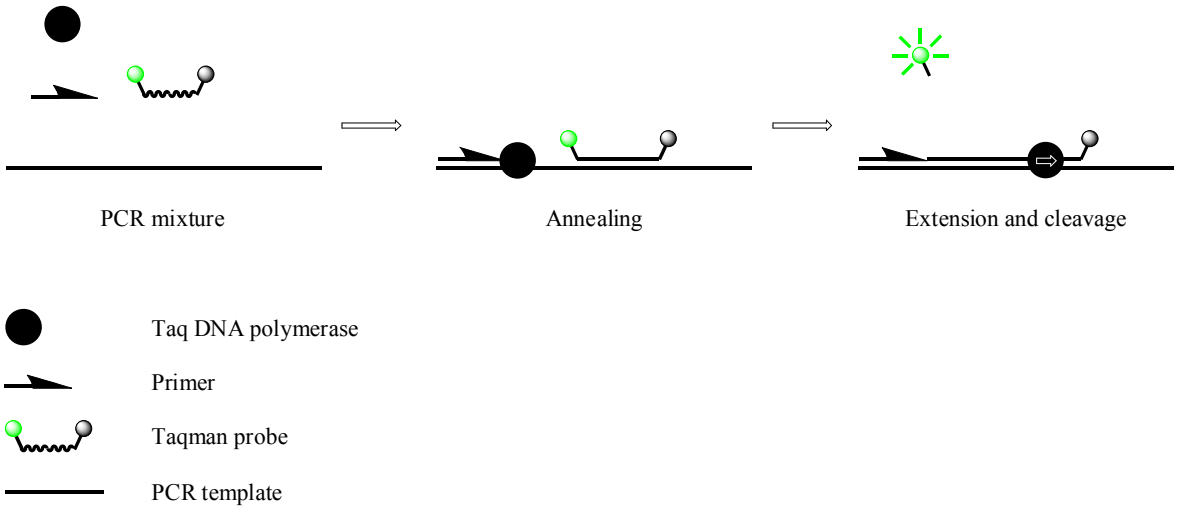

Figure 1.24. Mechanism of Taqman in quantitative RT-PCR.

The simplicity and homogenous nature of Taqman probes make them ideal for high throughput analysis. Miniaturised hand-held machines allow the use of Taqman probes for the detection of biological weapons in the field[86].

1.7.5 SERS

SERS has previously been demonstrated as a tool in DNA analysis using rough silver surfaces to detect target DNA sequences using a Raman labelled probe[87-89]. By immobilising DNA fragments to a SERS active substrate sequence-specific Raman labelled

probes can be washed over the sample DNA. If the sequence of interest is present, then the probe hybridises to the immobilised DNA bringing the Raman label into close proximity to with substrate giving a large Raman signal. This has been used to provide a simple sequence recognition method but provides no further information regarding SNPs. However SERS has been used in genotyping by using a combination of allele specific PCR and enhanced Raman by the aggregation of the silver nanoparticles[90]. This method does provide a more detailed analysis of sample DNA but the procedure requires significant post-amplification modification which requires increased handling time and risk of contamination. Further work includes the development of SERS beacons[91] which apply a mode of action similar to molecular beacons (Section 1.7.2).

However SERS does have significant advantages for DNA detection due to its ability to distinguish between multiple labelled oligonucleotides in a single sample[92]. Furthermore the high sensitivity and substrate distance dependence enable SERS to be potentially useful in the area of DNA detection and analysis.

1.7.6 Electrochemical melting

DNA is a highly negatively charged polymer and as such is susceptible to manipulation by the application of electrical potentials. The most common example of this is the use of gel electrophoresis where a potential is applied across a medium though which the DNA passes, causing a separation based upon the size of the DNA molecule as it is attracted towards the cathode. This principle combined with fluorescence detection was applied by Sosnowski *et al*[93] to accelerate DNA hybridisation across a gel permeation layer and to discriminate between SNPs by applying the potential, promoting denaturation and monitoring the change in fluorescent signal. A further example includes the use of a scanned potential to denature a duplex bound to a silicon surface[94]. This technique uses a surface-bound stem-loop structure similar to a molecular beacon with the DNA binding dye PicoGreen as the fluorescent reporter. This technique can be used to discriminate between

SNPs and is the first literature reference to a melting potential V_m, akin to the more common thermal melting temperature T_m. When the same approach was applied to linear oligonucleotides it was unable to generate significant differences between the SNPs. The precise mechanism of the electrochemical melting described is unknown, It is likely to be a combination of electrostatic repulsion, Joule heating and localised pH changes[93].

1.8 Aims and objectives

The aims of this PhD were to investigate methods of improving current fluorescence based methods for the detection and interrogation of DNA sequences. Furthermore the evaluation of quantum dots as a potential direct replacement of organic fluorophores for use in simple genetic analysis systems. A further objective of this PhD was to perform the initial experiments into a SERS-based detection method of PCR products for both sequence recognition and analysis.

All of these systems were being investigated with the aim of improving genetic analysis through reduced sample complexity, sample analysis time and increased multiplex detection.

Chapter 2

2.0 Quantum dot probes

2.1 Low Quantum yield Quantum dot probes

Stability studies and initial modification of quantum dots were performed using quantum dots (CdSe/ZnS core/shell) of various sizes from Nanoco (Manchester, UK). These quantum dots behaved normally and were fluorescent under qualitative UV illumination. However, when the fluorescence was determined quantitatively, their measured quantum yield was less than 0.01, opposed to the expected value of 0.3-0.5. This negated one of the key advantages of using quantum dots, which is the high quantum yield. The exact cause of the low quantum yield is unknown, although solvent interactions, absorption and emission spectra all remained as expected. The highly desirable optical properties of quantum dots make them ideal candidates for use in sensitive analytical systems, however, key physical and chemical properties need to be controlled. These include the chemical stability, solubility and modification of the quantum dots to allow use in traditional analytical methods. The following section describes the different approaches in controlling these unique properties of the quantum dots and their incorporation into DNA probes.

2.1.1 Aqueous stabilisation and stability

Quantum dots have a high quantum yield, narrow emission spectra and broad excitation spectra making them very good fluorophores. However, due to their size and interaction with their surroundings, their physical properties differ hugely from fluorescent molecules. The nanoparticle structure and high molecular weight give rise to high sensitivity to aggregation and manipulation by centrifugation. Furthermore, incomplete ligand coverage and "dangling bonds" can cause reduction in the luminescence of the quantum dots[95,96]. Quantum dot stability was measured using solutions of 532 nm quantum dots in toluene, to ascertain their optimum working conditions. Samples of CdSe/ZnS core shell quantum dots coated with HDA ligands in a solution of toluene, were excited at regular time intervals with a 329 nm light source and the emission intensity was recorded. A plot of emission intensity as a function of time shows a decay in the emission intensity, however,

the rate changes with time between illuminations. If the emission intensity is plotted as a function of scan number, the decay rates are similar for samples scanned at both 2 and 5 minute intervals (Figure 2.1).

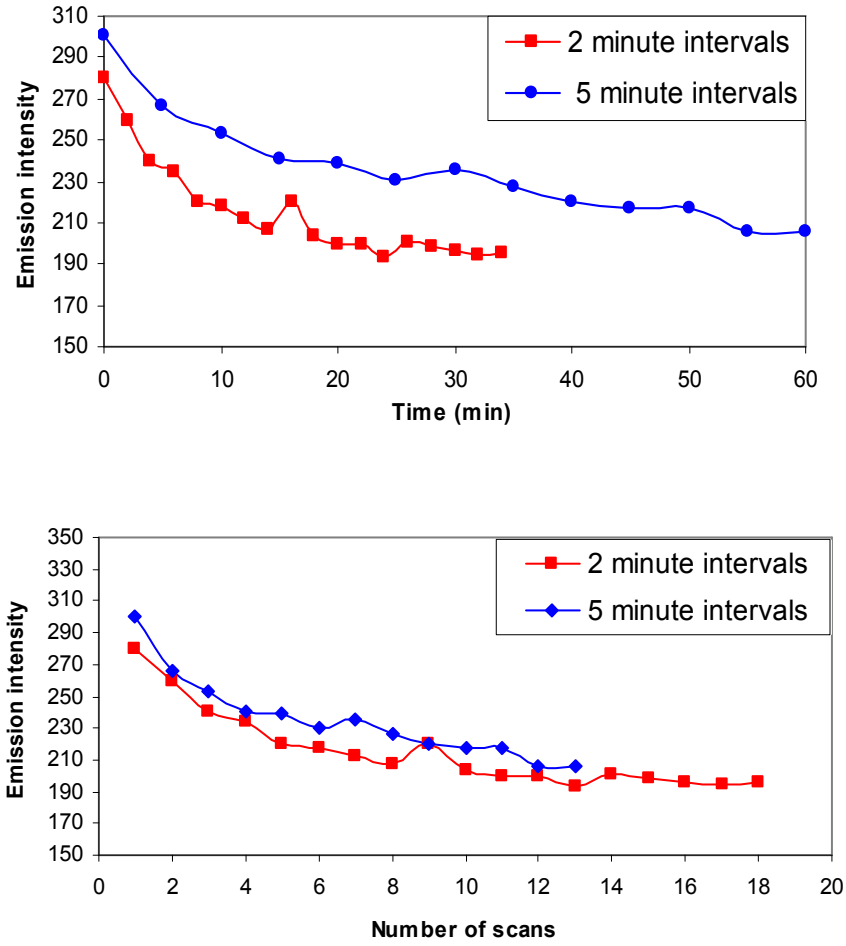

Figure 2.1. Emission intensities as a function of scans/time.

This scan-dependant decay indicates that the quantum dots are experiencing photobleaching, despite the reported resistance to phenomenon[97]. However, if the sample is allowed sufficient time, the emission intensity is recovered and the decay is not irreversible. Further samples were scanned three times in succession, displaying decay as expected and showing complete recovery when stored in the fridge overnight. The process

was reproducible and in some cases an increase in emission intensity was observed. This effect was prominent with samples prepared using toluene, however samples prepared using THF showed no recovery of emission even when left overnight (Figure 2.2). All samples were prepared using degassed solvents, under an inert atmosphere, to minimise dissolved molecular oxygen, which is a known quencher of quantum dots[98,99]. These emission intensity observations are highly representative of the sensitivity of quantum dots to their external environment and the solvent conditions.

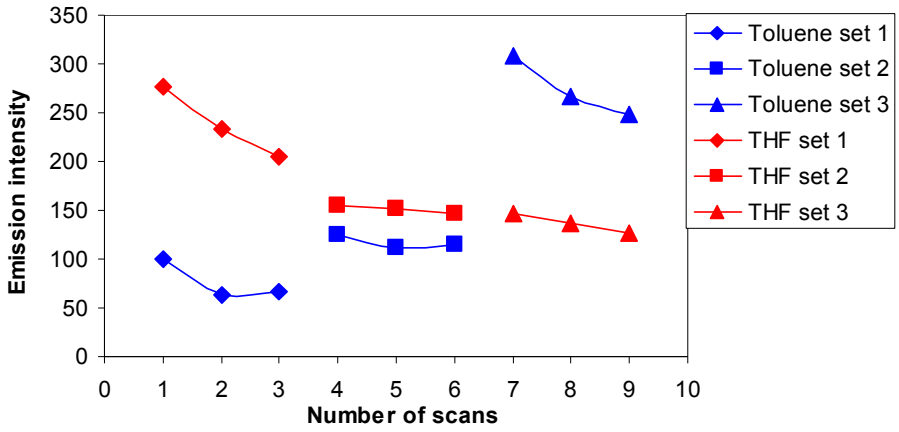

Figure 2.2. Emission intensity of quantum dot suspensions in toluene and THF with overnight storage between data sets.

One major disadvantage of materials in the nanometre scale is the tendency for the material to aggregate, in most cases causing precipitation. With many nanomaterials, aggregation has an effect solely on the physical properties of the material, which then behaves as bulk material. However, due to the quantum confinement in quantum dots, aggregation, which leads to the nanoparticles behaving as bulk material, results in a loss of the unique optical properties of the quantum dots, namely photoluminescence. Many quantum dot samples (>10) prepared in toluene appeared to experience precipitation when stored over a period of days. This precipitate appeared to retain the photoluminescence of the quantum dots indicating there was no degradation occurring. To increase this effect further, samples of quantum dots were evaporated to dryness resulting in large aggregations, which when

viewed under an optical microscope appeared to be disordered and were of uneven size. Due to the retained photoluminescence of the quantum dot aggregates, it can be assumed that the aggregation is not affecting the nanoparticles at a crystalline level and so the quantum confinement is not altered. However if HDA-coated quantum dots were suspended in water, then the suspension was no longer fluorescent and the precipitate did not display any of the properties observed with that prepared from toluene. Furthermore, when viewed under an optical microscope, there were no large aggregations visible, in contrast to the toluene samples. Either aggregation has a direct effect on the CdSe core, resulting in bulk behaviour, or more likely, quenching of the quantum dots occurs by trapping of excitons on the surface of the nanocrystal.

This poor solubility and high sensitivity to aqueous environments highlights the importance of creating a ligand system, which enables the quantum dots to retain their unique and desirable optical properties and still allow incorporation into oligonucleotide-based probes. To determine whether the effect of the aqueous environment was reversible, a series of extractions were performed using quantum dots suspended in water and one of DCM, THF, toluene or hexane as the organic phase. None of these extractions yielded fluorescent organic phases indicating that the quantum dots are permanently altered by the aqueous environment. To confirm this, quantum dots were suspended in mixtures of water and THF, which gave an instantaneous reduction in the observable fluorescence with no observable precipitation over a period of 3-5 minutes. This suggests that the quantum dots are not experiencing a rapid aggregation but quenching from the aqueous environment.

Currently, ligand exchange has proven to be the most common method of providing aqueous soluble quantum dots, with the ability to be used in DNA-based probes with small molecules such as mercaptoacetic acid and mercaptopropionic acid (as discussed in Section *1.3.1.2*). These ligand exchanges are quick and often require no chromatographic purification. Frequently the use of precipitation and centrifugation is sufficient to yield the aqueous soluble quantum dots. In addition, the use of acid groups to increase aqueous solubility also provides a source of functionalisation of the quantum dot surface. This approach has allowed quantum dots to be used in analytical systems intended for organic

fluorophores such as molecular beacons[22], despite the limited lifetime of these conjugates. To improve the stability of aqueous quantum dots, a series of peptides were used in ligand-exchange reactions with HDA-coated quantum dots. These peptides contained a thiol as the means for attachment, similar to the previously described small molecules and peptides[100-102], resulting in a stable bond between the sulphur and zinc in the ZnS-coated quantum dots. The thiol was introduced to the peptide at the N-terminus by using a terminal cysteine. This was followed by a series of hydrophobic amino acids then a series of hydrophilic amino acids, to produce a peptide containing a binding moiety and hydrophobic/hydrophilic regions (Figure 2.3).

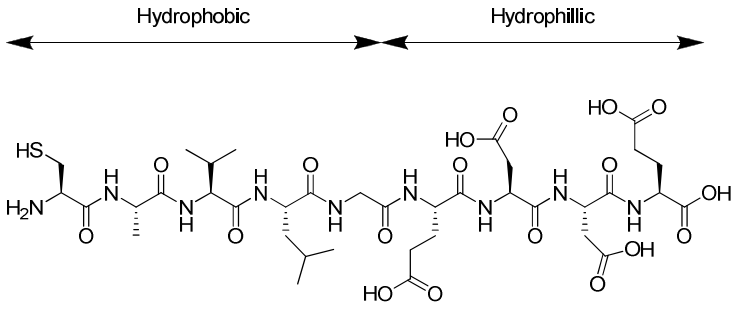

Figure 2.3. An example of the peptides used in quantum dot modification (peptide 3, peptides 1, 2, 4, 5 and 6; see Appendix Figure 9.1).

After ligand exchange of the HDA coating, a new functionalised quantum dot is produced with a two layer shell, a hydrophobic inner layer and a hydrophilic outer layer (Figure 2.4). By using a similar approach to the small molecule ligand exchange methods, organic soluble quantum dots precipitate once ligand exchange is complete, and the resulting precipitate can be centrifuged and washed to yield the product, removing any unmodified quantum dots and peptide. This technique is desirable due the ease and speed of the ligand exchange resulting in aqueous-soluble quantum dots in less than one hour. The resulting quantum dots can be re-suspended in aqueous solutions retaining their optical properties except for a 20 nm red-shift in the emission spectrum.

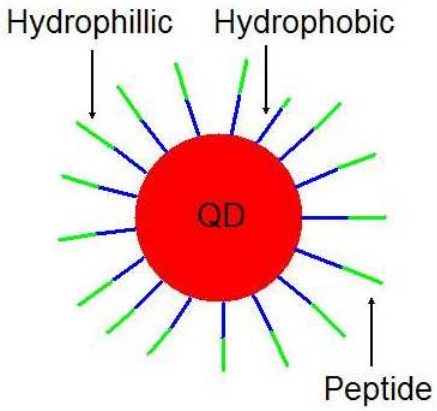

Figure 2.4. Schematic displaying hydrophobic/hydrophilic core/shell quantum dot peptide conjugate.

2.1.2 Oligonucleotide conjugation

Acid-functionalised quantum dots, produced by peptide ligand exchange, were used in oligonucleotide-labelling experiments to produce quantum dot-oligonucleotide conjugates for use in DNA probing systems. This was performed using labelling techniques, which are commonly used for the labelling of oligonucleotides with small organic molecules such as dyes and quenchers. Solid phase and solution-based techniques were applied, both of which used activated esters of the acid-functionalised quantum dots and amine-modified oligonucleotides.

2.1.2.1 Solution phase coupling

After ligand-exchange, the *N*-hydroxysuccinimide (NHS) or pentafluorophenol (PFP) active esters of the peptide-coated quantum dots were formed using standard conditions

(see experimental), which afforded quick reaction times, only requiring purification by small-scale gel filtration (Figure 2.5).

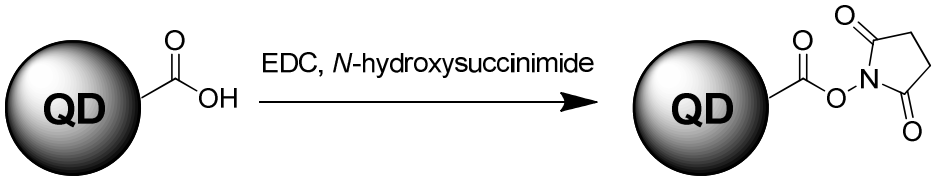

Figure 2.5. Reaction scheme for formation of active-ester quantum dots.

These reactive species could then be coupled using a suitable coupling agent such as 1-ethyl-3-(3-dimethylaminopropyl) (EDC) to the amine-modified oligonucleotide (Figure 2.6).

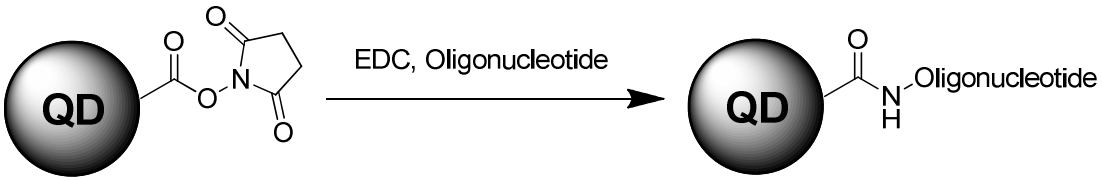

Figure 2.6. Reaction scheme for formation of quantum dot oligonucleotide conjugates.

To introduce the amine functionality into the oligonucleotide, one of three different modifications can be used, depending on the desired location of the amine. For 3'-modification, an amino C6-modifed CPG resin can be used, internal modifications can be incorporated anywhere within the sequence using an amino C6-dT monomer and 5'-modification can be achieved using an amino C6 phosphoramidite, all of which are commercially available monomers (Figure 2.7). Addition of these quantum dot active esters to the amine-modified oligonucleotide in buffer (pH 7-8) in a small volume (<500 μL) produced the quantum dot oligonucleotide conjugate with reaction times of less than 24 hours.

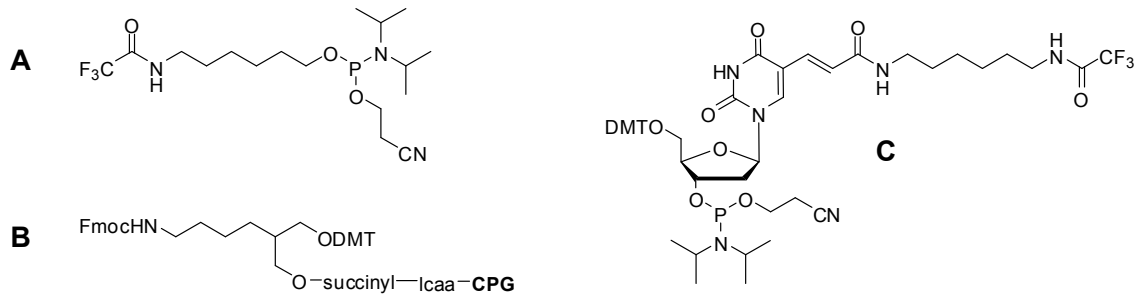

Figure 2.7. Monomers for amino modification of oligonucleotides; **A**, 5'-modification; **B**, 3'-modification; **C**, internal modification.

Initially, reverse-phase HPLC was used in an attempt to monitor and purify the reaction. However, little information could be obtained from the resulting traces which showed only a single, extremely noisy peak. The reaction mixtures were then analysed by large-scale gel filtration using the HPLC pumps and detector. At first, water was used as an eluent in order to reduce the exposure of the quantum dots to salt concentrations above 1 mM, however, no sign of separation was observed using either Superdex 75 or Superdex 200 purification resins. When phosphate buffer (pH 7.2) was used, separation was achieved only when using Superdex 75 resin, not Superdex 200 resin. The reaction mixture traces showed three peaks, which according to the retention times, were deduced to be the quantum dots, oligonucleotide and a potential conjugate of the two. However, when isolated, the quantum dot-conjugate did not display the characteristic quantum dot fluorescence properties, and it is also possible that either the increased salt concentration of the eluent or the metallic components of the HPLC pumps had an adverse effect on their optical properties.

Reaction mixtures were also loaded onto both agarose and polyacrylamide gels and analysed by gel electrophoresis, however, this did not yield any clear separation. After migration through the gel medium the gel was imaged using a 254 nm light source, which was unable to confirm the presence of any quantum dots by their fluorescence.

2.1.2.2 Solid phase coupling

After experiencing difficulties in purification of the peptide-modified quantum dots from the quantum dot-oligonucleotide conjugates, coupling was conducted on solid-support, in order to reduce the amount of purification required. Coupling the quantum dots to the oligonucleotide whilst the latter is attached to CPG resin, allows any unreacted quantum dots to be washed away leaving only the quantum dot-oligonucleotide conjugates and any unlabelled oligonucleotides. As previously mentioned, standard procedures used for small organic molecules were used; formation of a quantum dot active ester was followed by coupling to the oligonucleotide using a coupling reagent (EDC or HBTU). Once quantum dots were coupled to the resin-bound oligonucleotides, the resin displayed the optical characteristics of the quantum dots and their orange colour could clearly be seen (Figure 2.8).

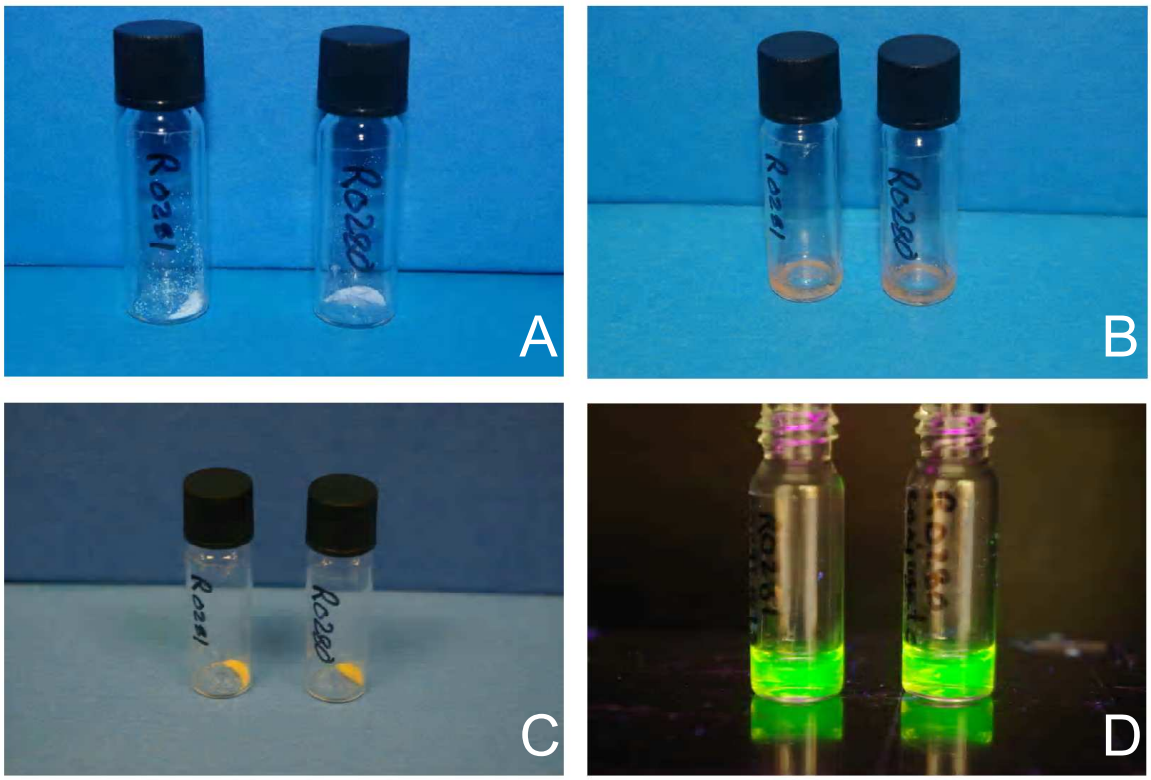

Figure 2.8. **A**, Amino-modified oligonucleotide bound to CPG resin (after standard automated DNA synthesis); **B**, CPG resin plus peptide activated ester modified-quantum dot solution.; **C**, Oligonucleotide- quantum dot conjugate bound to resin; **D**, Oligonucleotide-quantum dot conjugate cleaved from resin and illuminated at 365 nm.

The oligonucleotide could then be cleaved from the resin using a variety of standard oligonucleotide deprotection conditions resulting in a fluorescent solution. Initial experiments used a T_{12} oligonucleotide due to the milder deprotection conditions needed for a poly(dT) sequence but mixed sequence 25mer oligonucleotides were also used (for sequences see appendix Table 8.1). The quantum dot labelled CPG resin was divided into four different batches, and four deprotection conditions were used; *N*-methyl morpholine (NMM, 10 wt% in water), piperidine (20 wt% in DMF), DIPEA (5 wt% in acetonitrile) and methylamine (40 wt% in water). All produced fluorescent quantum dot oligonucleotide conjugates in solution, although aqueous methylamine was chosen for the remaining experiments, as the milder reagent and due to ease of removal by evaporation. These

labelled oligonucleotides exhibited the optical properties of the quantum dots, with addition of extra peaks in the photoluminescence excitation spectra below 260 nm. This is far below the normal spectra for 530 nm quantum dots, which have a lower cut off of approximately 280 nm (Figure 2.9). This extra excitation band was only present with quantum dot-oligonucleotide conjugates, and was not present with addition of unmodified oligonucleotides to peptide coated quantum dots.

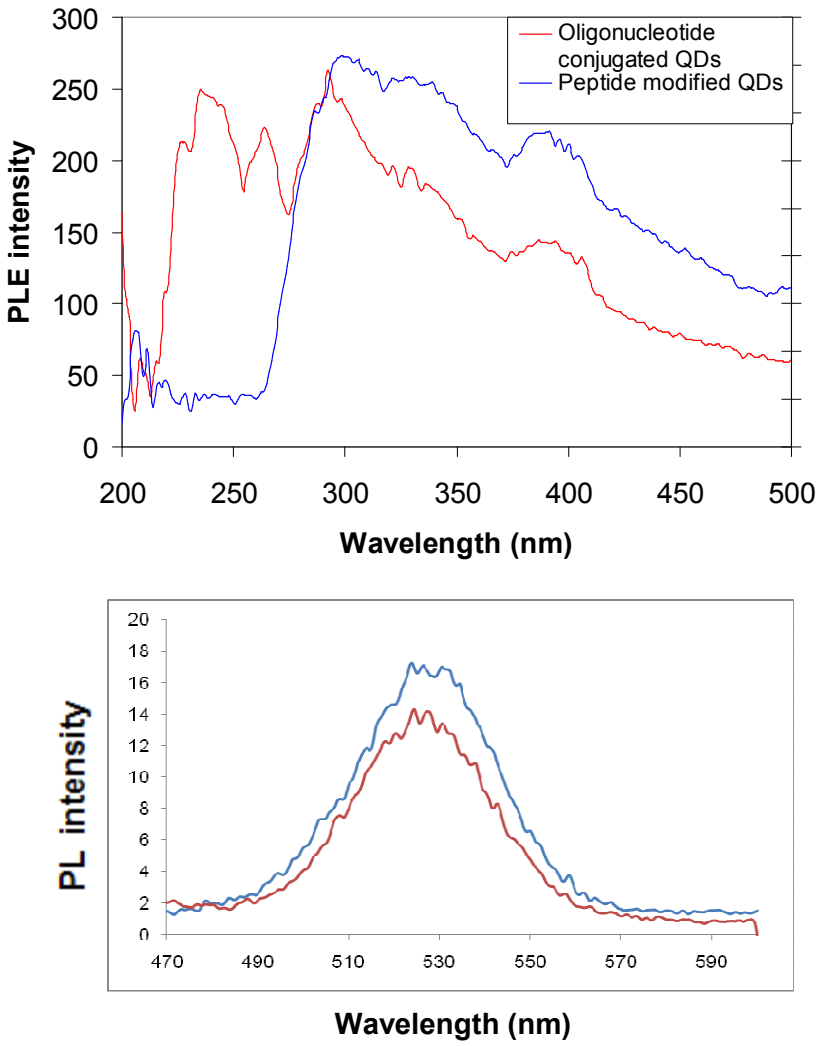

Figure 2.9. PLE (above) and PL (below) spectra of both peptide-coated quantum dots (red) and peptide-coated quantum dots conjugated to oligonucleotides.

Due to the normal absorption and emission spectra of the quantum dot remaining unchanged, the presence of the oligonucleotide is most likely not directly affecting the quantum dot's structure. This suggests energy transfer or the introduction of multiple negative charges from the phosphate backbone to the surface of the quantum dot are possible causes. It is known that quantum dots are highly sensitive to their external environment and surface trapping of excitons has an effect on their quantum yield. By introducing negative charges to the surface of the quantum dot it is possible that specific energetic pathways, within the quantum dot, could be affected.

To investigate the hybridisation properties of the quantum dot-oligonucleotide conjugates, two complementary oligonucleotides (25-mers) were synthesised, one with a 5'-amino modification and the other with 3'-DABCYL (for sequences see appendix Table 8.2). The 5'-amino modified oligonucleotide was conjugated to quantum dots with an emission wavelength of 532 nm. These two oligonucleotides were then hybridised and analysed by fluorescence melting using a Roche LightCycler®. This duplex should be quenched whilst hybridised, and upon melting an increase in the fluorescence should be observed as the DABCYL moiety and quantum dot become distant. However, this did not afford the expected results but instead showed a steady decrease in emission intensity as a function of temperature. This was most likely caused by inefficient hybridisation by the quantum dot oligonucleotides (due to oligonucleotide-QD interactions), so another oligonucleotide was synthesised with a 5'-amino modification complementary to the first amino-modified oligonucleotide. This strand was also conjugated to a sample of quantum dots before the two oligonucleotides were hybridised together. This would create a dumbbell-type structure with two quantum dots separated by a known, fixed distance, which could then be characterised by microscopy. These samples were imaged using atomic force microscopy (AFM) both dried or in an aqueous environment.

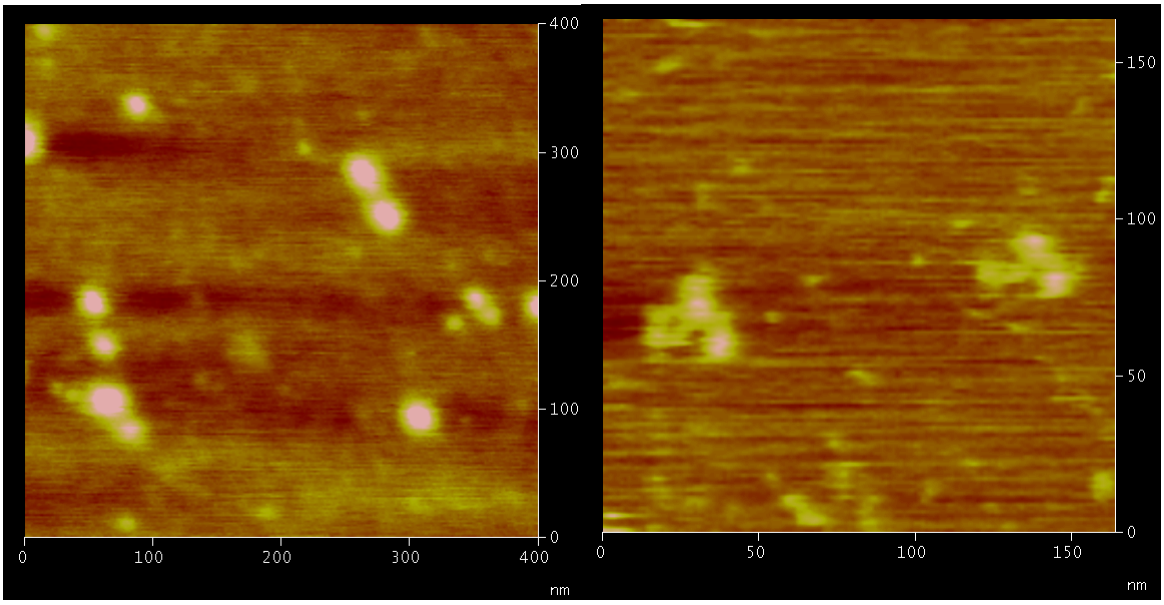

Figure 2.10. AFM images of oligonucleotide quantum dot dumbbell structures, dried (left) and in aqueous environment (right).

The dried samples displayed some features possessing the correct shape, however, when measured their sizes were too large, at more than double the size of the expected structures. The samples imaged in an aqueous environment had a repeating structure in all samples, which appeared to look like either two or three quantum dots bound together. The dimensions of these structures did match those of the intended structures and it is possible for more than one oligonucleotide to be bound to each quantum dot. However, these images were not clear enough to provide a definitive answer and with smaller structures AFM images can be interpreted incorrectly if the structure is not present in high frequency (Figure 2.10).

2.1.3 Unmodified oligonucleotide-quantum dot conjugates

Whilst the addition of unmodified oligonucleotides did not cause the increase in the PLE spectra below 260 nm, another effect was observed at lower energy wavelengths (<500

nm). The addition of free oligonucleotides into the peptide-coated quantum dot samples gave an extra emission peak at 460 nm and another excitation band at 490 nm. The intensity of the additional two peaks exhibits a concentration dependence with no saturation of the effect at up to a 40 times excess, and the 530 nm peak remains unaffected (Figure 2.11).

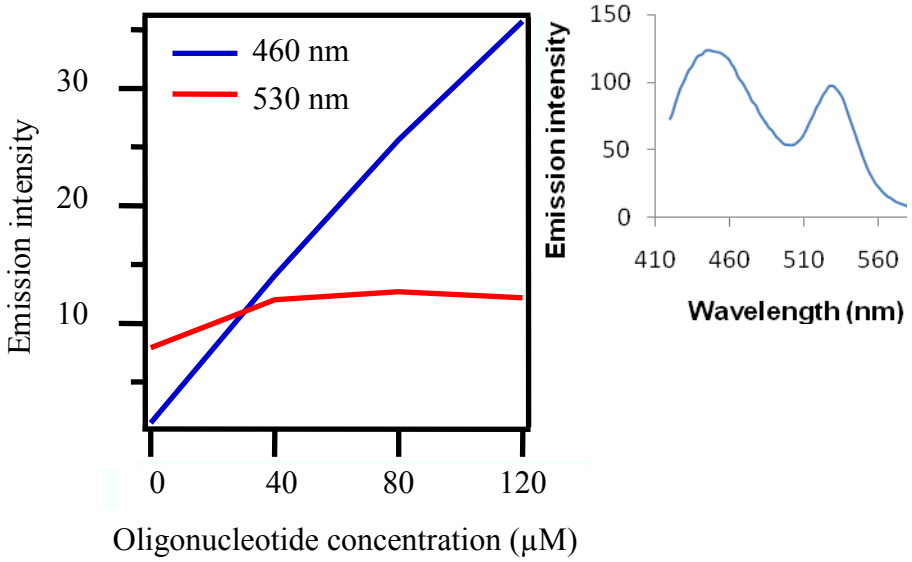

Figure 2.11. PL intensities as a function of oligonucleotide concentration and PL spectra (right).

Initial experiments used a mixed-sequence oligonucleotide, as used in previous conjugation experiments, which strongly displayed the new PL/PLE peaks. Changing the composition of the oligonucleotide led to differing intensities of the additional peaks. To determine whether there was a base dependency, a series of 23-mer oligonucleotides were synthesised, poly-dA, poly-dT, poly-dC and poly-d(GT). These were added together with dAMP, to peptide-coated quantum dots in a similar manner, and their PL and PLE spectra were recorded using excitation and emission wavelengths of 350 nm and 530 nm respectively. A clear dependence was shown on the presence of purine bases for the extra PLE peak, and poly-dA for the extra PL peak at 450 nm. No influence was exerted by dAMP on either the PL or PLE spectra suggesting that the effect is caused by oligonucleotides only and therefore potentially an effect of binding. Similar samples were

prepared using a mixed-sequence oligonucleotide at different concentrations. PL spectra were recorded at both 25 ºC and 65 ºC to determine whether there was a weak binding between the quantum dot and the oligonucleotide, however, no significant change was observed (Figure 2.12).

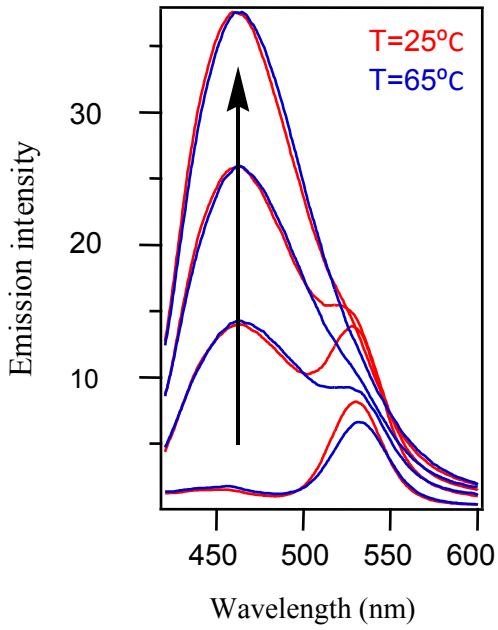

Figure 2.12. PL spectra of peptide-coated quantum dots with increasing oligonucleotide concentration (0, 40, 80 120 µM, indicated by arrow).

The precise mechanism for the production of these peaks is unknown. However, one system which could produce such peaks is ground state interactions such as an exciplex. Typical characteristics of an exciplex include additional absorption and emission peaks, although there are no previous examples of quantum dot-oligonucleotide exciplex systems. Alternatively, the additional emission peak at 450 nm may originate from alteration of the higher bandgap quantum dot surface material (ZnS). This could be rationalised as either an exciton or hole from the core material tunnelling into the surface material, or a separate exciton-hole pair from within the surface material. Further studies into these effects were halted, as the quantum yield of the quantum dots in use was significantly less than normal and therefore uncertainties arose about their precise structure.

2.2 High quantum yield quantum dot probes

Previous supplies of quantum dots displayed very low quantum yields, hence a different supplier was used and the quantum yield of the new quantum dots was measured as 0.45. Previously, all purchased quantum dots were supplied as a dry powder, which was subsequently re-suspended in a suitable organic solvent. New sources of quantum dots were supplied already suspended in toluene, and no suppliers were found who supplied quantum dots in their dry form.

2.2.1 Aqueous stabilisation and stability

The procedure for peptide coating, to provide aqueous stable/soluble quantum dots had to be modified as quantum dots were now supplied as a suspension in toluene. Due to the lack of companies supplying quantum dots as powders, a procedure was used which avoided evaporating the suspension to dryness. Instead, a co-evaporation was used; pyridine was added to the suspension in a 1:1 ratio, and the solvent volume was reduced by half. This process was repeated a number of times to produce a quantum dot suspension in a predominantly pyridine environment. These quantum dots could then be functionalised with the peptide coating using the same method as used previously (Section 2.1.1) to yield aqueous-soluble quantum dots. The quantum yield was then measured of these quantum dots, the pyridine-based suspension, the toluene suspension, and also a sample of quantum dots, which had been evaporated to dryness and re-suspended in pyridine. A significant reduction in quantum yield (50-70% reduction, Figure 2.13) was observed on removal/replacement of toluene.

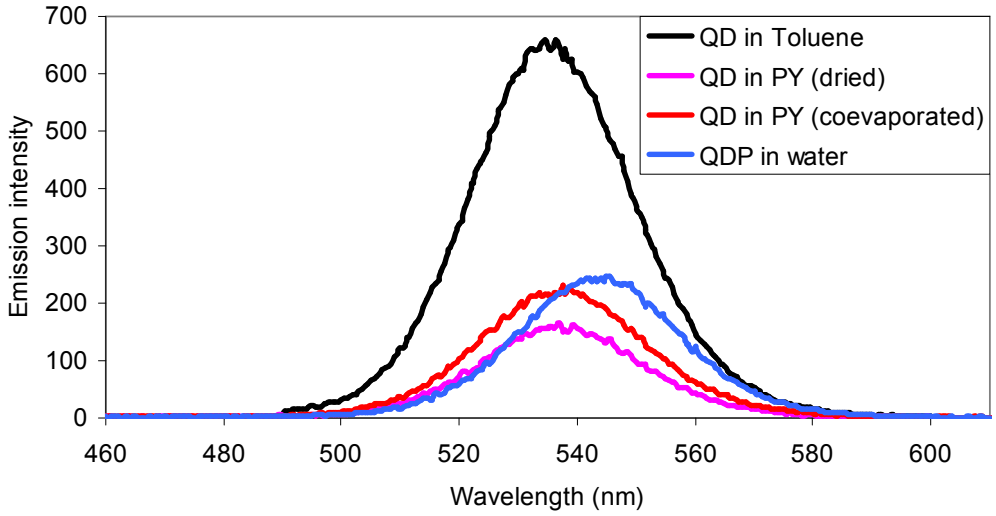

Figure 2.13. Emission spectra of quantum dot suspensions.

Drying the quantum dots before re-suspension gave quantum dots with a quantum yield 30% less than their co-evaporated equivalents. Interestingly, once the quantum dots had been modified with the peptide coating, the quantum yield was 30% higher than when suspended in pyridine. These changes in the quantum yield are further evidence to the sensitivity of quantum dots to their exterior environment, further highlighting that modification procedures must avoid drying of the quantum dots. Alternative peptide-modification techniques using a toluene-based precipitation were attempted in order to avoid the use of pyridine, and thus retain the higher quantum yield found with quantum dot-toluene suspensions. A similar method for addition of a peptide to the toluene suspension of quantum dots was used, however no precipitation occurred and the quantum dots remained in the toluene suspension.

Peptide-coated quantum dots, synthesised using a co-evaporated pyridine/toluene mix, were further analysed for their stability under typical conditions used in genetic analysis techniques. Thermal cycling of peptide-coated quantum dots in aqueous buffer displayed a temperature-dependant emission with an intensity difference of 40% between 28 ºC and 85 ºC. Quantum dots suspended in toluene were also analysed in a similar manner yielding the same outcome. This temperature dependence was reversible over the five cycles tested,

therefore further samples were incubated at 65 ºC for 2 hours using all six peptide quantum dot conjugates. This gave reductions in the quantum yield from 10% to 90%, depending on the peptide used (Table 2.1 for structures see appendix Fig 8.1).

	QY before incubation	QY after 65 degree incubation
QDP-1	0.10	0.09
QDP-2	0.22	0.11
QDP-3	0.09	0.01
QDP-4	0.18	0.07
QDP-5	0.18	0.04
QDP-6	0.14	0.09

Table 2.1. Quantum yield measurement of quantum dot-peptide conjugates, before and after incubation at 65 ºC in aqueous buffer for two hours.

This demonstrates that the peptide coating is insufficient protection for aqueous stable quantum dots in applications which require heating.

2.3 Conclusions

This thermal instability and temperature-dependant emission limits the possible uses of quantum dot-peptide conjugates in genetic analysis as almost all techniques require the use of heat for DNA amplification or interrogation. Furthermore, the high sensitivity to external environments leads to changes in the quantum yield and so quantitative measurement becomes difficult. These factors present a problem, particularly for their use as a replacement to organic fluorophores, in systems which require minimal modification.

Chapter 3

3.0 HyBeacon™ probes

3.0 HyBeacon™ probes

This chapter describes the modification of HyBeacon probes, investigating design changes and further development to improve multiplex capabilities. It also includes the analysis of Cyanine dyes and their effects/use within nucleic acid based detection systems.

3.1 Introduction

Previous HyBeacon probes have been proven in their use for homogenous PCR analysis using one or two additions of a single dye[71,73,103]. This approach has allowed mutation discrimination by melting temperature analysis within a PCR reaction. We have developed this system further through the use of FRET, to improve the multiplex capabilities of HyBeacon probes. This system is based around a single excitation wavelength for three probes, each probe possessing a different distinguishable emission wavelength.

During this development, the effectiveness of different dyes was analysed and their optical properties when incorporated into oligonucleotides investigated. This work includes a more detailed analysis of cyanine dyes and their temperature dependent emission.

We have also carried out a study on the FRET efficiency as a function of distance with a DNA scaffold using commercially available monomers, and have compared this with a suitable model, designed to include the variation in dye orientation due to the linker. This work has been completed with the help of Professor Pavlos Lagoudakis and Junis Rindermann of the hybrid optoelectronics group within the Department of Physics, University of Southampton, Southampton, UK.

3.2 Single dye HyBeacons

HyBeacons containing two additions of a single fluorescein have been established as homogenous PCR probes, proving mutation discrimination by melting temperature analysis. These probes have used commercially available monomers, such as the FAM-dT **1**, available from Glen Research (Figure 3.1).

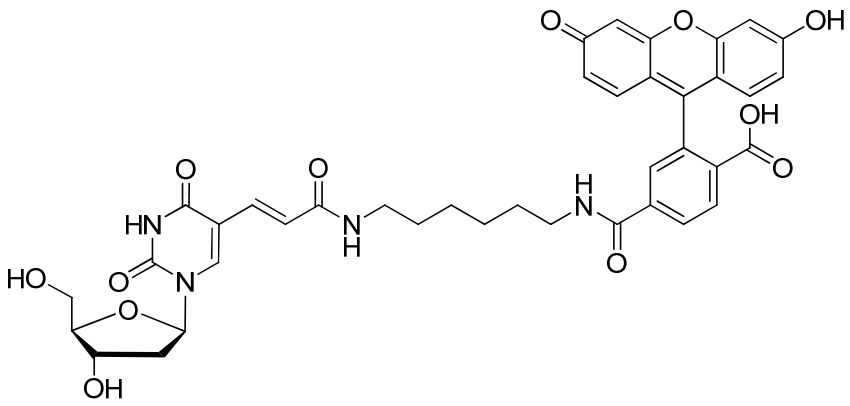

Figure 3.1. Structure of commercially available FAM-dT **1**.

A modified nucleoside analogue was synthesised, which had previously demonstrated potential antiviral properties,[104] and which incorporated a primary alcohol into the 5-position of the uracil base, with a three carbon chain (Figure 3.2) **2**.

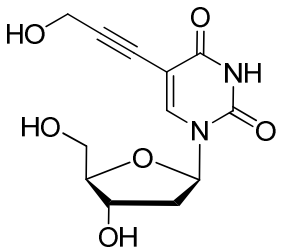

Figure 3.2. Structure of modified propargyl 2'-deoxyuridine containing a primary alcohol **2**.

This monomer was incorporated twice into a HyBeacon probe, which also contained a 5'-trimethoxystilbene (TMSt) group to improve probe stability[74,105,106] (Table 3.1, for target sequences see appendix Table 8.3).

Modification	Sequence
TMSt (**2**) Propargyl dU (**X**) Phosphate (**3**)	**2**CTTTCC**X**CCAC**X**GTTGC**3**

Table 3.1. W1282X probe sequence.

This sequence was designed to probe a region of the CFTR gene containing the W1282X mutation. This single base G to A mutation, in exon 20 results in a Trp residue becoming a STOP at position 1282. To protect the primary alcohol during oligonucleotide synthesis, a levulinyl protecting group was employed. This protecting group could be cleaved whilst the oligonucleotide was bound to the CPG resin and the resulting alcohol labeled using a fluorescein phosphoramidite. A labelled 2'-deoxyuridine with a phosphodiester linkage between the dye and the uracil base was produced (Figure 3.3) **3**.

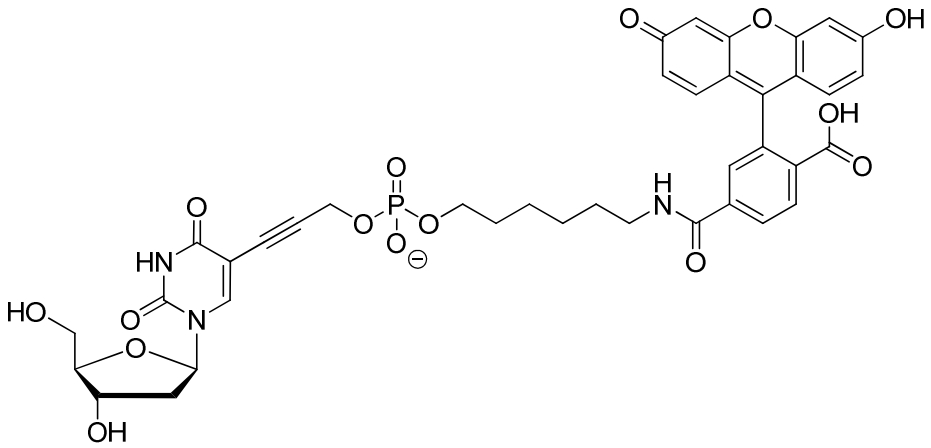

Figure 3.3. Structure of labelled propargyl-dU **3**.

Another HyBeacon was synthesised with the same sequence using the commercially available FAM-dT as a direct comparision. These probes were then analysed by fluorescence melting using a Roche LightCycler® with both the wild type and mutant sequences. The resulting melting curves showed a much smaller change in emission for the propargyl-dU HyBeacon and a smaller change in T_m between wild type and mutant type (Figure 3.4).

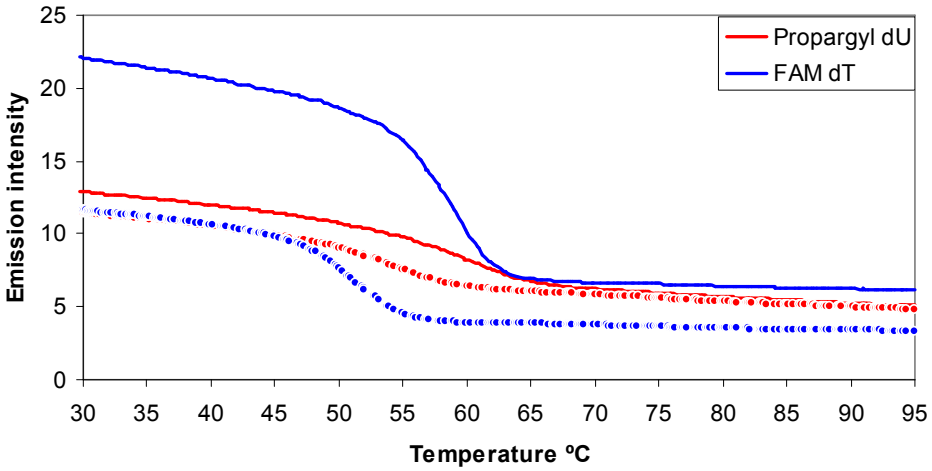

Figure 3.4. Melting curves of HyBeacons containing two fluorescein additions and a 5'-TMS, using either propargyl-dU **3** (red) or FAM-dT **1** (blue) modifications, with wild type (solid) and mutant (dashed) targets.

The low change in emission for the propargyl-dU **3** modified HyBeacon, is most likely due to the phosphodiester linkage introducing a negative charge between the dye and the nucleobase. This negative charge would create a repulsive force between the two dyes and between the dyes and the oligonucleotide, preventing them from coming into close proximity in the single strand state. This results in reduced quenching from the DNA bases as well as a reduction in potential fluorophore-fluorophore quenching (Figure 3.5).

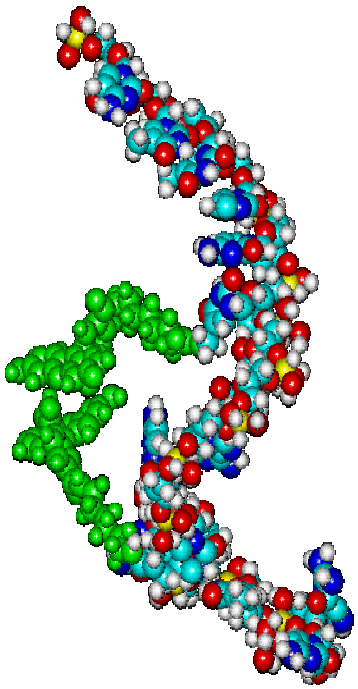

Figure 3.5. HyperChem 7.0 scale image of a HyBeacon probe, labelled with two FAM-dT **1** monomers (green) with no target, showing the length of the FAM-dT linker which allows the two fluoresceins to come into contact.

To overcome the dye-dye repulsion a new monomer synthesised by Dr. Qiang Xiao, which contained a primary amine incorporated at the 5-position of the uracil base using a 5-carbon linker (Figure 3.6).

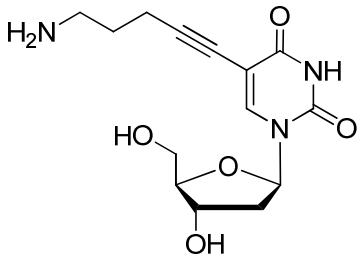

Figure 3.6. Structure of amino pentynyl dU monomer **4**.

This monomer was subsequently protected using an Fmoc protecting group for the primary amine, and the standard 4,4'-dimethoxytrityl and phosphoramidyl groups for the 5'- and 3'-

OH groups respectively. A new HyBeacon probe was then synthesised using this monomer in place of propargyl-dU **2** and was post-synthetically labelled with fluorescein NHS ester and analysed by fluorescence melting. Improvements were demonstrated over the propargyl-dU **3** HyBeacon, but this was not as successful as the FAM-dT HyBeacon. One major difficulty of post-synthetically labelling probes with two fluorophores, is that the efficiency of labelling decreases compared to labelling once only. This limits the use of such labelling techniques to single-dye HyBeacons, as low labelling efficiency results in increased cost and reduced effectiveness of the probes.

As well as variation of chosen dye, HyBeacon probes can be modified using end-capping moieties, to provide improved probe stability and single stranded quenching. All HyBeacon probes contain a 3'-modification, usually a 3'-phosphate or 3'-propanol, to prevent the HyBeacon acting as a PCR primer, which would result in extension of the probe and incorrect PCR products. Additionally, 5'-modification of HyBeacons using a TMSt functionality has been shown to improve both the stability and single-strand quenching of the probe.[74,105,106] Four different 3'-end capping moieties were synthesised by Dr. Nouha Ben-Gaied, using modified CPG resins, two anthraquinone and two pyrene (Figure 3.7), in order to improve mutation discrimination in HyBeacons.

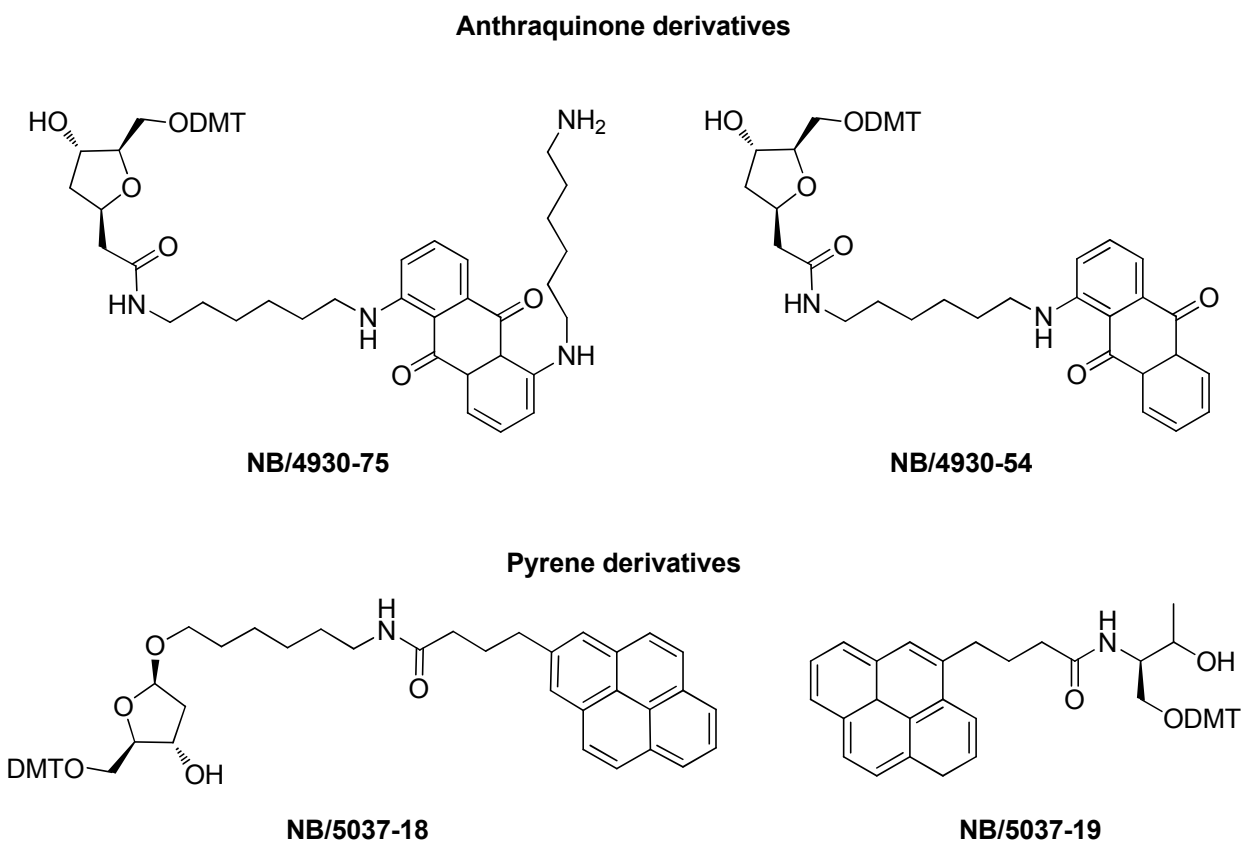

Figure 3.7. Structures of synthesised end-cap monomers for 3'-addition to HyBeacon probes.

A series of HyBeacons probes were synthesised using these end-caps, both with and without the commercially available 5'-trimethoxystilbene modification (Table 3.2). These probes were synthesised with two additions of fluorescein using FAM-dT **1** as the reporter dye, which allowed them to be compared to a previously synthesised HyBeacon containing only the two additions of fluorescein and a 3'-propanol terminus (for sequences see appendix Table 8.4).

HyBeacon	3' Modification	5' Modification
res0072	Anthraquinone	N/A
res0073	Anthraquinone-NH_2	N/A
res0074	Amido-Pyrene	N/A
res0075	Threoninyl-Pyrene	N/A
res0109	Anthraquinone	TMSt
res0110	Anthraquinone-NH_2	TMSt
res0111	Amido-Pyrene	TMSt
res0112	Threoninyl-Pyrene	TMSt
A0677	N/A	N/A

Table 3.2. HyBeacon probes synthesised containing combinations of different 3'- and 5'-end cap monomers.

These probes were analysed by fluorescence melting using a Roche LightCycler® 1.5 with both the wild type and the CYP2C9*2 (C to T) mutation from the cytochrome P450 gene, in 10 mM phosphate buffer containing 500 mM NaCl. Melting curve analysis allowed for accurate measurement of the melting temperature, and the effect of different end cap combinations could be assessed by both the wild type T_m and the ΔT_m between wild type and mutant (Table 3.3).

	Wild Type T_m (°C)	Mutant Type T_m (°C)	ΔT_m (°C)
res0072	68.9	60.3	8.6
res0073	68.7	58.0	10.7
res0074	68.9	60.2	8.7
res0075	68.9	62.2	6.7
res0109	71.0	60.6	10.4
res0110	68.5	60.2	8.3
res0111	70.8	61.5	9.3
res0112	71.0	62.9	8.1
A0677	69.0	61.7	7.3

Table 3.3. Melting temperatures of HyBeacon probes with different end cap combinations, comparing wild type and mutant templates.

The anthraquinone-capped HyBeacons had the largest ΔT_m, but the pyrene-modified HyBeacons have a slightly higher overall T_m. Largely, the melting temperatures were not hugely altered from the HyBeacon with no end-capping monomers (A0677), however, with the exception of res0075, the ΔT_m values were larger. The melting temperature analysis alone only shows small improvements, however, the shape of the melting curves is also important for fluorescent probes. Probes giving sharper melting transitions, with larger changes in emission, are easier to analyse and more suitable for multiplex detection. To quantify the change in emission, the quantum yields of the HyBeacons were measured in the single-stranded form and also double-stranded form, hybridised with the wild type target. These were compared to the HyBeacon with no end-cap (A0677) and a previously synthesised HyBeacon with only a TMSt cap (R0106). The emission spectra for each sample were recorded and compared to a known sample of fluorescein in 0.1 M aq. NaOH, using low optical densities (<0.01) to eliminate any inner filtering of the excitation beam. This allowed the quantum yield for each sample to be calculated, providing quantitative analysis of the change in emission between single- and double-stranded states (Figure 3.8).

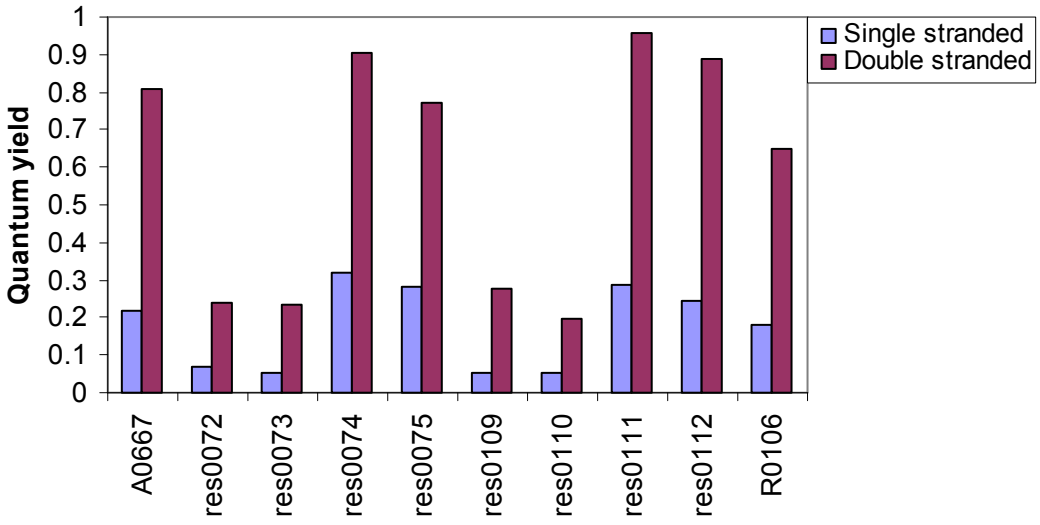

Figure 3.8. Quantum yield measurements of HyBeacons with different combinations of end cap monomers, in single- and double-stranded samples. Controls: A0667 and R0106.

The measured quantum yields demonstrate that the anthraquinone-modified probes (res0072, res0073, res0109, res0110) display significantly reduced quantum yields in both the single- and double-stranded samples. In contrast, the pyrene-modified HyBeacons (res 0074, res0075, res0111, res0112) retained the high quantum yield of the fluorescein in the double-stranded samples, but also had large reductions in the quantum yield in single stranded samples. There also appeared to be minimal difference between samples which contained both a 3'-modification and both 3'- and 5'-modifications. This means that the 3'-pyrene modification was the best in terms of emission intensity change, with minimal modification. However, as well as the melting temperature analysis and quantum yield analysis, the shape of the melting curve is also important, as a sharp melting curve produces a sharper peak from the calculated derivative curve (Figure 3.9). This allows for more accurate T_m calculations and therefore improved mutation discrimination and multiplex potential.

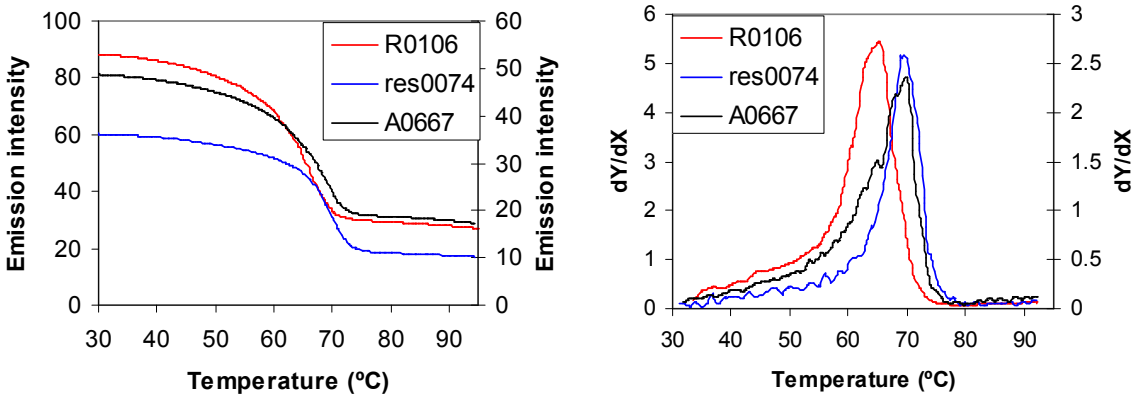

Figure 3.9. Melting curves (left) and subsequent derivatives (right) of HyBeacons labelled with two additions of fluorescein and a 3' pyrene (blue), 5'-TMS (red) and no end capping monomers (black).

Analysis of the melting curves showed that the HyBeacon without any end-capping monomers (A0667) has the broadest melting curve and the HyBeacon with the 3'-pyrene monomer has the sharpest. These results demonstrate that a HyBeacon containing a single 3'-pyrene has the advantages previously achieved using a 5'-TMS group, but with improved changes in emission intensity upon melting, slightly sharper melting curves, and the 3'-modification eliminates the need for further 3'-PCR blockers.

3.3 FRET-based HyBeacons

To improve the multiplex capabilities of HyBeacons, a new generation of HyBeacon probes was developed with three key properties; single excitation wavelength, multiple emission wavelengths and simple design. To achieve this, a FRET-based system was used, designed for use with simple detection equipment aimed at high throughput analysis. Due to the high performance and documented use of fluorescein as a HyBeacon, it was chosen as a suitable starting point for the FRET system. Also, due to the high popularity of fluorescein, many existing technologies are optimised for its use, such as the Roche LightCycler®.

These have an excitation wavelength ideal for fluorescein and multiple emission channels, therefore fluorescein was used as the FRET donor.

A short (Table 3.4, for target sequences see Appendix Table 8.3) oligonucleotide was synthesised using a sequence from the cystic fibrosis transconductance regulatory (CFTR) gene, which contains the W1282X SNP.

Modification	**Sequence**
Aminopentynyl dU (**X**) FAM dT (**F**) Phosphate (**3**)	CTTTCC**F**CCAC**X**GTTGC**3**

Table 3.4. W1282X FRET probe sequence

This oligonucleotide contained one addition of fluorescein using the commercially available FAM-dT **1**, one addition of aminopentynyl-dU **4** and a 3'-phosphate for blocking of PCR. After synthesis, the CPG resin was divided into two, and the aminopentynyl-dU moiety was labelled using standard solid-phase active ester coupling. One half was labelled with Texas Red and the other half labelled with JOE (Figure 3.10), to act as FRET acceptors, and the oligonucleotides were deprotected/cleaved from solid-support and purified by HPLC.

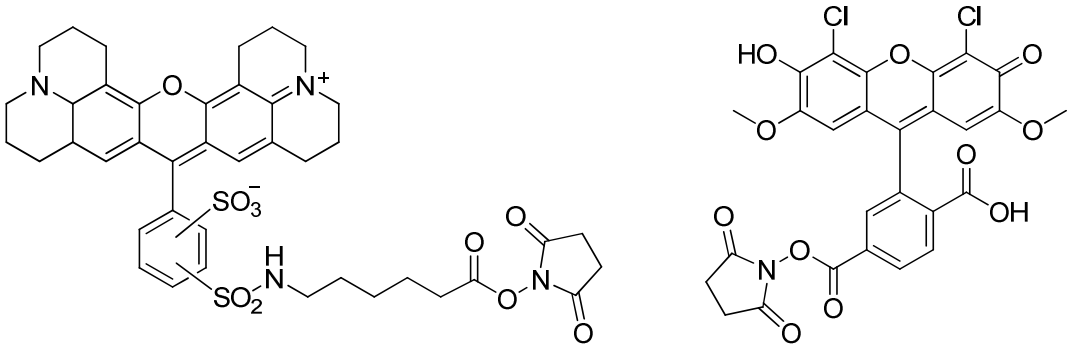

Figure 3.10. Structures of Texas Red (left) and JOE (right) NHS esters.

Both of these oligonucleotides were analysed by fluorescence melting using a Roche LightCycler® and standard PCR conditions. JOE has an absorption maximum at 525 nm and an emission maximum of 555 nm and so is an ideal FRET acceptor for use with fluorescein as a FRET donor. Texas Red has an absorption maximum of 589 nm and so has less spectral overlap with the emission of fluorescein, however, it has an emission maximum of 615 nm and is therefore distinguishable from the JOE emission and suitable for the second LightCycler® channel. Using channel 1 (530 nm) for the JOE acceptor HyBeacon, and channel 2 (645 nm) for the Texas Red acceptor HyBeacon, the fluorescence melting curves gave clear melting transitions (Figure 3.11), which could be used to derive the T_m. The Texas Red acceptor HyBeacon had residual emission in channel 1, as due to the lower FRET efficiency between the fluorescein and Texas Red.

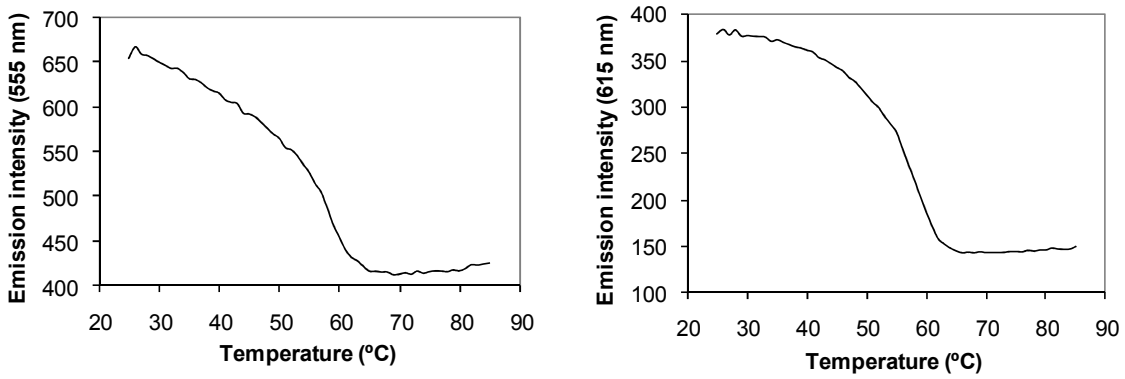

Figure 3.11. Melting curves of FRET HyBeacons with a FAM donor and either JOE acceptor (left) or Texas Red acceptor (right).

The single acceptor system did show reasonable emission changes upon melting, however, in order to improve quenching in the single-stranded form, a further two oligonucleotides were synthesised. These used the same W1282X probe sequence (appendix Table 8.5) containing a single addition of fluorescein, with two additions of the acceptor dye (JOE/Texas Red). These were then analysed in an identical manner to the previous single

acceptor HyBeacons, and demonstrated improved quenching in the single-stranded form Figure 3.12).

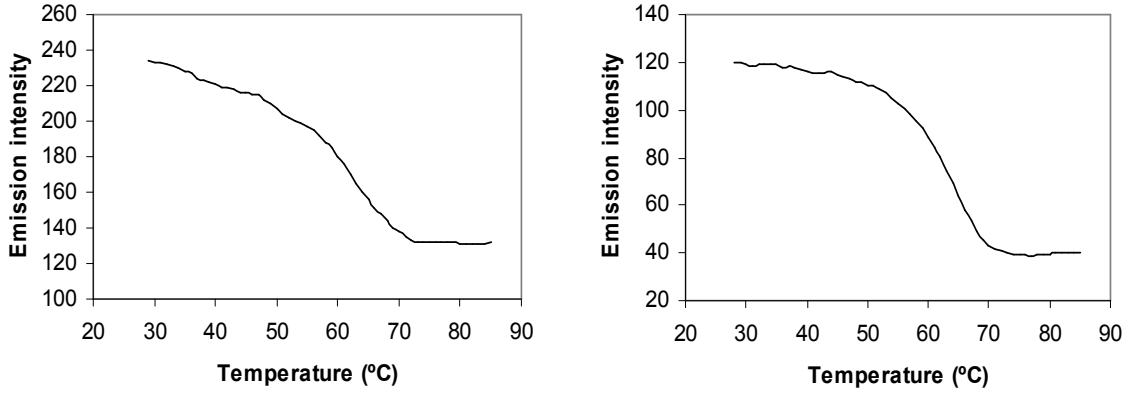

Figure 3.12. Melting curves of one-donor two-acceptor HyBeacons using the W1282X probe sequence.

This system worked effectively, however, a two probe system can be implemented without the use of FRET, to provide melting temperature analysis, with results not that dissimilar to the FRET system. The same one-donor two-acceptor approach was then applied to a three probe system, which used three different acceptor dyes, JOE, Texas Red and Cy5.5. Cy5.5 has an emission maximum of 707 nm providing little spectral overlap with JOE or Texas Red giving a distinguishable emission signal. However, due to the absorption maximum of 646 nm the FRET efficiency using FAM as a donor is low, although this is compensated for by incorporating two additions of Cy5.5, thus increasing the signal. Three HyBeacon probes were synthesised, each designed to target one of three different mutations within the CFTR gene, the ΔF508 (triple T deletion), R516G (A to G SNP) and C524X (C to A SNP). These mutations were chosen because the ΔF508 mutation accounts for 70% and 90% of the cystic fibrosis cases in the U.K. and U.S. respectively, and the R516G/C524X mutations having close proximity to the ΔF508 allowing a single template strand to be synthesised (appendix Table 8.6). These sequences provide a good test for mutation discrimination, as they cover unstable mutations such as the triple deletion as well as relatively stable G:T and G:A mismatches.

These HyBeacon probes were analysed individually using a Roche LightCycler® and standard PCR conditions. The melting curves were not as clearly resolved as previous FRET HyBeacons and the T_m values appeared to be much lower than expected (Figure 3.13), perhaps due to increase in un-natural lipophilic modification, in adding three dyes.

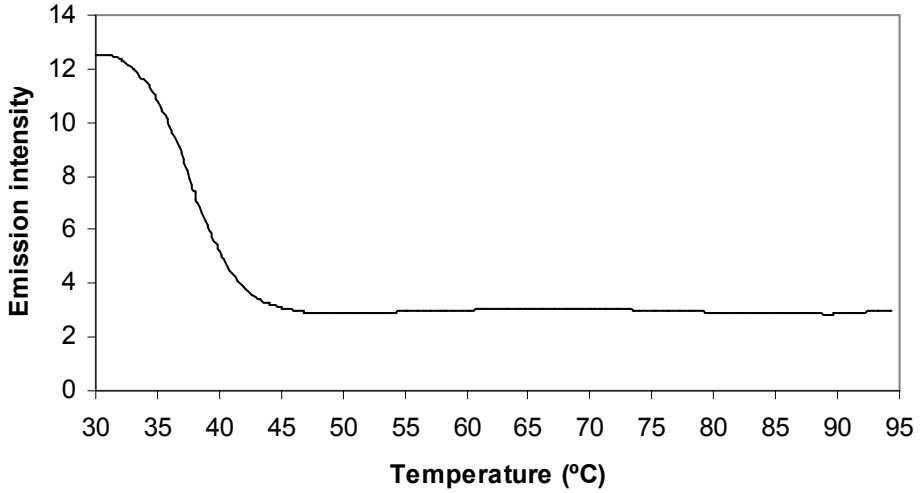

Figure 3.13. Melting curve of R516G probe labelled with a FAM donor and two Texas Red acceptor dyes with a T_m of 38 ºC.

These probes were re-synthesised using the same FAM-dT monomer **1** and aminopentynyl-dU **4** but were not labelled post-synthetically with the two additions of acceptor dye. The probes were then analysed individually in the same manner (using a LightCycler®) and conditions, and the melting temperatures were all above 56 ºC for the wild type samples. This confirms that the decrease in stabilisation is due to either the addition of the two acceptor dyes, the labelling process, or an inherent instability due to the probe sequence.

	Without acceptor dyes		With acceptor dyes	
	WT	**MT**	**WT**	**MT**
F508 probe	61.5	49.6	48.2	32.8
R516G probe	56.0	50.7	38.4	33.0
C524X probe	66.9	62.0	53.3	47.1

Table 3.2. Melting temperatures (ºC) of HyBeacon probes before and after post synthetic labelling with acceptor dye. WT = Wild Type, MT = Mutant Type.

One other possibility for the lower than expected HyBeacon stability is 5-endo-dig cyclisation of the aminopentynyl-dU monomer to form the furano-pyrimidine derivative (Figure 3.14). This monomer could not form a Watson-Crick base pair with A, and would therefore have a destabilising effect, which would be more prominent for double addition. This cyclisation was first observed by Cruickshank *et al.* and has been demonstrated by refluxing the alkynyl-dU nucleoside in methanol and triethylamine with a CuI catalyst, to provide the furano-pyrimidine[107-109]. However, there is a negligible chance of this cyclisation occurring under PCR conditions due to the lack of copper catalyst and there are currently no reported examples of this.

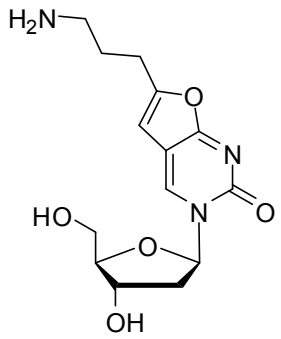

Figure 3.14. (2,3*H*)-Furano[2,3-*d*]pyrimidin-2(7*H*)-one product of aminopentynyl-dT monomer cyclisation.

There were two options for increasing probe stability, increase the length of the probe, or add stabilising monomers. Increasing the length would increase the melting temperature,

however, shorter probes are desired and the increased length would only mask the stabilisation problems occurred through modification. In order to overcome the instability problem, the probe length was increased by just two bases, and a commercially available trimethoxystilbene (TMSt figure 3.15) stabilising moiety was added to the 5'-end of the probe (for sequence see appendix Table 8.7). This has previously been demonstrated to increase stability and improve quenching in HyBeacon probes[74,105]. This endcap modification should overcome the destabilising effects of dye modification as well as aid in the single-stranded quenching, giving improved quenching over the previous single-acceptor dye HyBeacons. Furthermore, to eliminate any possibility of post-synthesis cyclisation of the aminopentynyl-dT monomer, a commercially available amino-C6-dT monomer **5** was used for the acceptor dye labelling.

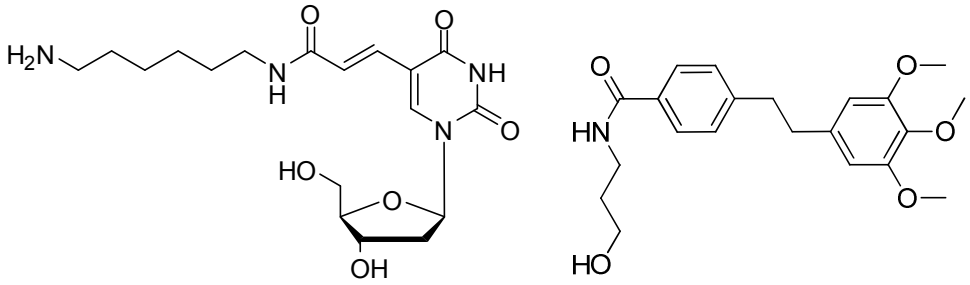

Figure 3.15. Structure of commercially-available amino-C6-dT monomer **5** (left) and TMSt (right).

These changes were applied to the R516G probe using Texas Red as the acceptor dye with only one addition, relying on the endcap modification providing extra quenching instead of the extra acceptor dye addition. This reduction in the acceptor dyes aids application, by retaining probe simplicity (increased difficulty and efficiency of oligonucleotide synthesis results from multiple labels, multiple active ester labelling has lower efficiency) as well as reducing overall cost of the probe. This monomer led to an increased T_m (14 ºC increase over two acceptor probe), whilst retaining a very good change in emission intensity upon melting (Figure 3.16).

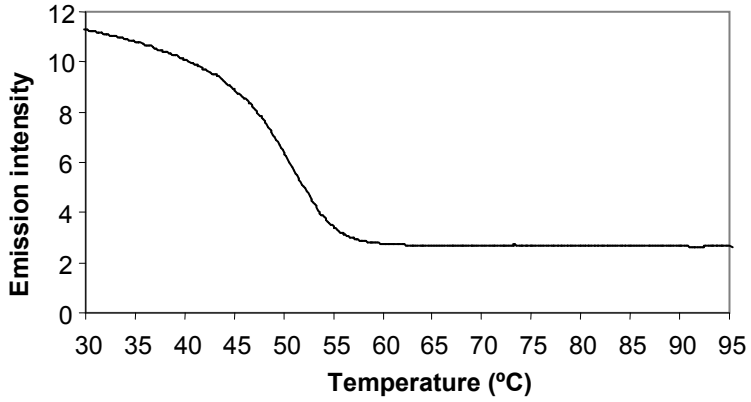

Figure 3.16. Melting curve of one-donor one-acceptor (Texas red) FRET HyBeacon with a 5'-TMS end cap.

This demonstrates the ability of end-capping monomers to improve the emission change in FRET HyBeacons similar to that of the traditional single-dye HyBeacons. To expand this further to the three probe system, three more HyBeacon probes were synthesised using the same three CFTR mutations and JOE, Texas Red and Cy5 as acceptor dyes (for sequence see appendix Table 8.7). Cy5 was used as the third acceptor dye instead of Cy5.5 (for structures see Appendix figure 8.2), in order to increase FRET efficiency to allow for the single addition. In an effort to reduce the number of modifications of the HyBeacon, a 3'-end capping monomer was used, as 3'-modifications are also essential for prevention of probe extension during PCR, thereby serving two purposes. This reduces the number of modifications required from four to three, increasing simplicity and potentially reducing costs. The 3'-end cap monomer chosen was a pyrene (NB/5037-19, using a CPG resin synthesised by Dr. Nouha Ben-Gaied) as this has shown large stabilisation and quenching effects in single-dye HyBeacons whilst retaining a good ΔT_m between wild type and mutant sequences. These probes were analysed individually by fluorescence melting using standard PCR conditions and both a LightCycler® and fluorimeter. When using the LightCycler®, clear melting curves with large changes in emission upon melting were obtained from the probes using JOE (channel 1) and Texas Red (channel 2) as acceptor

dyes. However, the probe which used Cy5 (channel 3) did not give a clear melting curve (Figure 3.17).

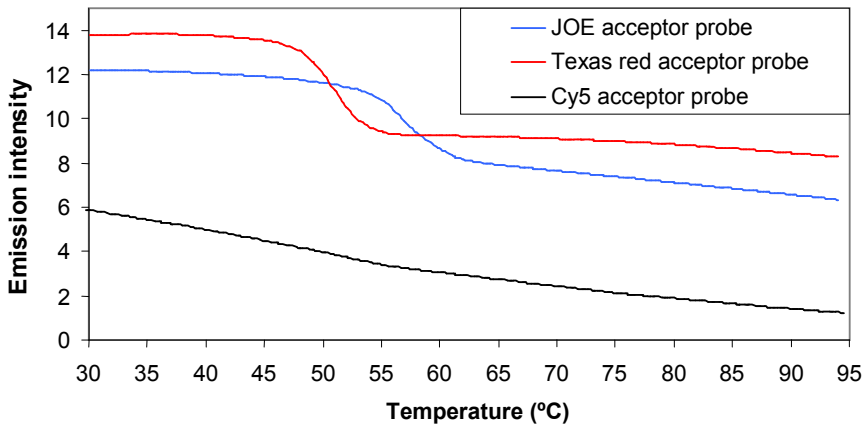

Figure 3.17. Individual melting curves of the three CFTR probes recorded using a LightCycler®.

The Cy5 probe displayed the characteristic steady decrease in emission previously observed with single-dye cyanine HyBeacons, which display no significant change in emission but temperature dependant emission. The probe was then re-synthesised and labelled with Alexa Fluor 647, which has similar optical properties to Cy5, is a modified cyanine dye and was analysed in the same way (Figure 3.18).

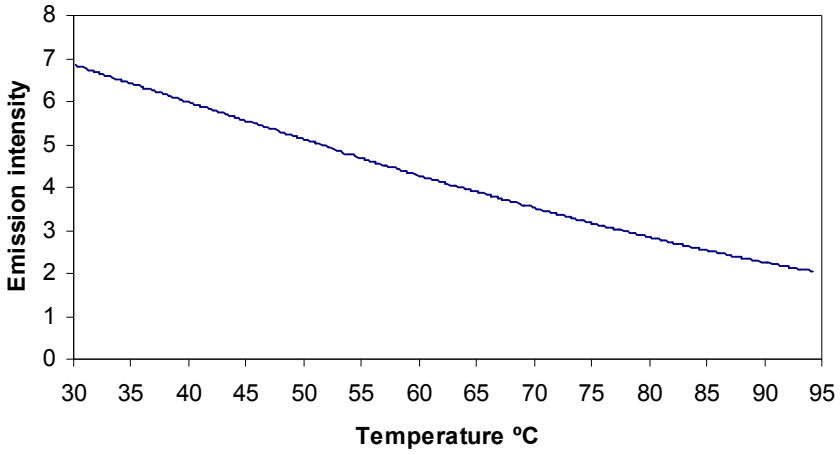

Figure 3.18. Melting curve of FRET HyBeacon using an Alexa Fluor 647 acceptor dye.

This gave the same temperature-dependant emission, demonstrating that this same effect is observed with another cyanine single-dye HyBeacons and not only Cy5. This limits the choice of dye available for the higher wavelength probe as the majority of dyes which emit in this region are cyanine-based so an alternative approach was needed. Femtosecond fluorescence measurements have shown that the quantum yield of the asymmetric cyanine dye thiazole orange is reduced from 0.4 to 0.1 by twisting of the molecule around the methine bridge[110] and so controlling the twisting could result in improve quantum yields.

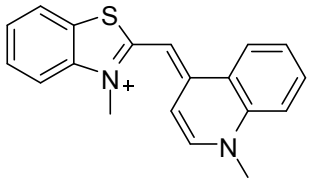

Figure 3.19. Structure of thiazole orange.

Furthermore the binding of cyanine dyes to DNA duplexes has been studied in detail with two models, which depend on the dye, half intercalation[111,112] and minor groove binding[113-115]. In many cases, the binding of the DNA facilitates an increase in the fluorescence of the

dye. Two new probes were synthesised to take advantage of the minor groove binding properties of the cyanine dyes, in order to facilitate binding of the dye and therefore increasing its emission intensity. The new probes were synthesised using the same sequence as the previous Cy5 HyBeacon, with and without the 3'-pyrene modification, except that amino-C6-dT was replaced with 2'-aminoethoxy-T, which places the label in the minor groove on a relatively short linker (for sequences see appendix Table 8.8). The new probes were then labelled with Cy5 and analysed by fluorescence melting using the LightCycler®. This gave clear melting curves for both probes, however, the probe without 3'-pyrene end-cap gave the best-shaped curve, as the pyrene moiety provides quenching in the double stranded form (Figure 3.20).

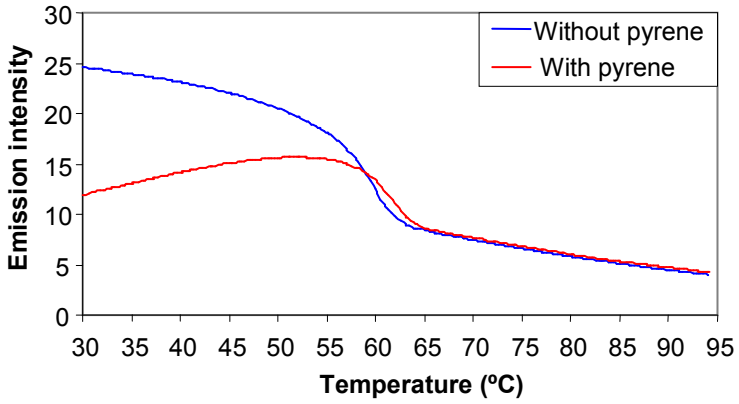

Figure 3.20. Melting curves of FRET HyBeacons using Cy5 acceptor labelled using 2'-aminoethoxy-T, both with and without a 3'-pyrene end-cap.

This clearly demonstrates that by placing the Cy5 label in the minor groove, the temperature dependant emission problem is eliminated. This meant that a suitable third probe system was now available, setting three probes in place for a multiplex system. Using the long target strand, all three probes could then be used simultaneously to probe the three mutations chosen from the CFTR gene (Figure 3.21) to simulate PCR products.

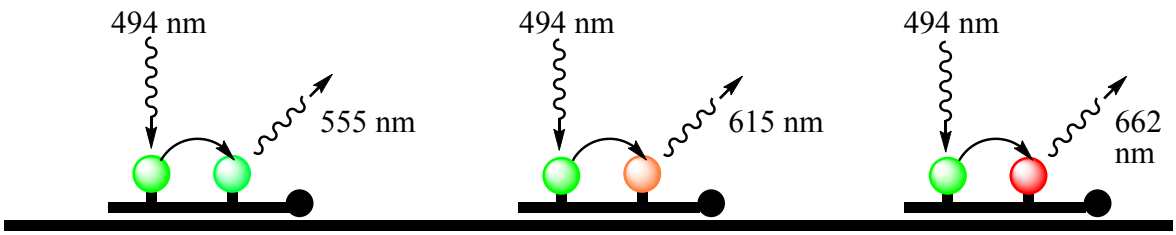

Figure 3.21. Schematic of three probe FRET system using JOE, Texas Red and Cy5 acceptor dyes

This system was tested using the LightCycler® 3 channel system, however, the different filters for the channels are not optimal for the three acceptor dyes and so the fluorimeter was used for a more reliable analysis. Using an excitation wavelength of 494 nm and performing an emission scan, at 1 ºC intervals, allowed a 3D plot to be obtained, displaying emission intensity as a function of wavelength and temperature. On this plot, the melting transitions can be seen, taking a cross section along the temperature axis at the corresponding acceptor dye emission wavelengths (Figure 3.22).

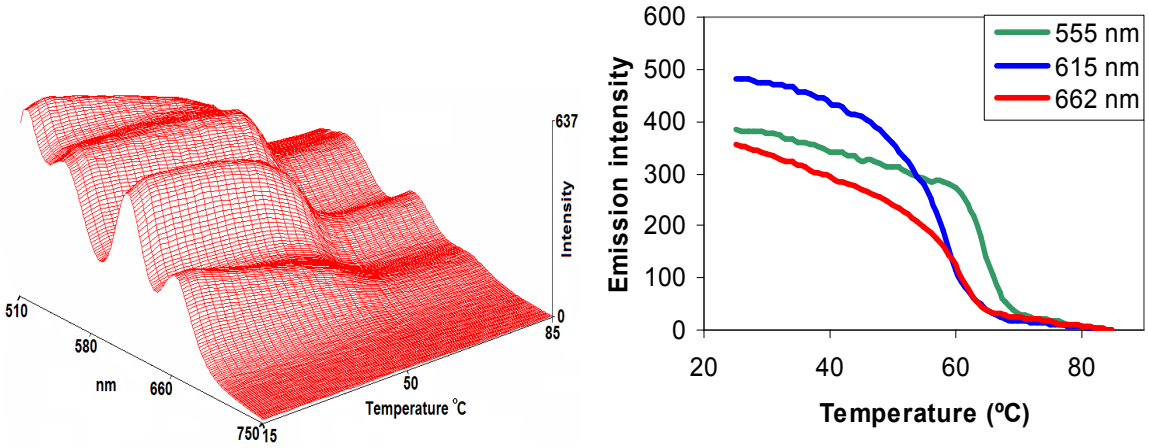

Figure 3.22. 3D melting plot of three probe system and corresponding melting curves of the three probes taken from cross sections at specific wavelengths.

This three probe system was then used to analyse the three mutation sequences, and provide melting temperature analysis to detect the presence of the wild type or mutant sequence for each of the target mutations (Table 3.3).

Target	res0571 Cy5	res0436 TxR	res0437 JOE
WT	62.3	60.1	66.1
ΔF508	54.8	59.8	66.4
R516G	63.0	56.1	66.2
C524X	62.9	60.6	63.6

Table 3.3. Melting temperatures of HyBeacon probes in three probe system for wild type and mutant sequences using res0571 (ΔF508 probe, Cy5 acceptor), res0436 (R516G probe, Texas Red acceptor) and res0437 (C524X probe, JOE acceptor).

This system appears to work well, where the maximum variation in wild type T_m for any of the probes is 0.8 ºC and the smallest ΔT_m for wild type *vs* mutant is 2.5 ºC, for example the ΔF508 probe as a wild type T_m of 62.3 ºC and in the presence of the R516G and C524X mutations (also wild type) 63.0 ºC and 62.9 ºC. However in the presence of the ΔF508 target (mutant type) the T_m drops to 54.8 ºC. All probes demonstrate good melting curves with no discernible interference from each other (Figure 3.23).

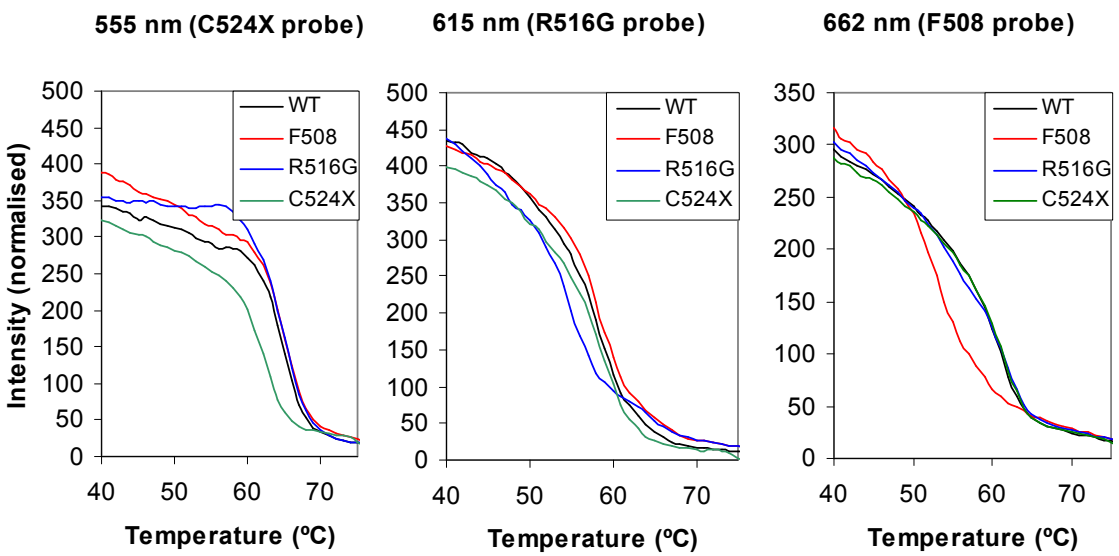

Figure 3.23. Melting curves of each probe in the presence of the four different target sequences (one wild type, one mutant type and two negative control mutant sequences).

These results provide proof of concept for the FRET HyBeacon system, demonstrating that multiplex detection using three probes with individual emission wavelengths and a single excitation wavelength is possible.

3.4 Cyanine dye analysis

Due to the abnormal melting curves and temperature dependant emission produced when labelling oligonucleotides with cyanine based dyes, a study was performed to investigate the effect more thoroughly. The FRET system used in the multiplex HyBeacons showed the Cy5 acceptor probe had a temperature dependant emission, with no melting curve when labelled using amino-C6-dT. However, if the residual fluorescein emission was monitored, with the same probe, there was a melting curve present. This means that the steady decrease in Cy5 emission is a function of the Cy5 radiative decay process and not a result of energy transfer problems. Using the same probe sequence (appendix Table 8.9), further oligonucleotides were synthesised and labelled with Cy3, Cy3.5 and Cy5.5, all of which

showed the same, expected steady decrease in emission as a function of temperature. There was a slight increase in emission upon melting with the Cy3 and Cy3.5 samples, providing enough of a change to observe a T_m. Although, much less change was observed than what can be achieved using other dyes, and the change could be due to residual emission from the fluorescein (Figure 3.24).

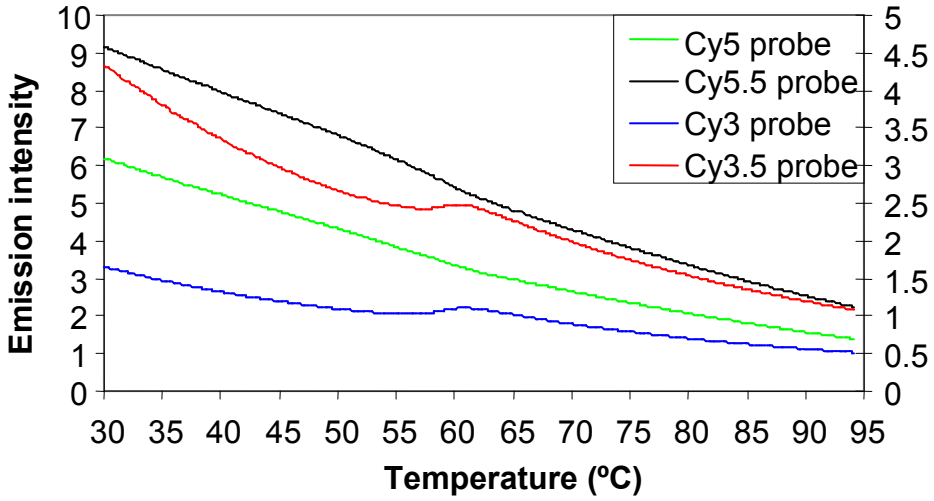

Figure 3.24. Melting curves of a ΔF508 FRET HyBeacon with FAM donor and different cyanine acceptors.

This suggests that this effect is caused by an inherent feature of the symmetric cyanine dyes, but is affected by the subsequent binding of the dye by placing it in the minor groove. The most likely cause of this temperature-dependant emission is the rotation around the polymethine bridge between the two indoles. To test this theory, a modified cyanine dye Cy3b was used to label a probe with the same sequence using amino-C6-dT, and was subsequently analysed in the same way. Cy3b has similar optical properties to Cy3 with an excitation maximum of 558 nm, an emission maximum of 572 nm and a high quantum yield (0.67)[116], but its polymethine bridge is part of a ring system and therefore cannot be rotated around (Figure 3.25).

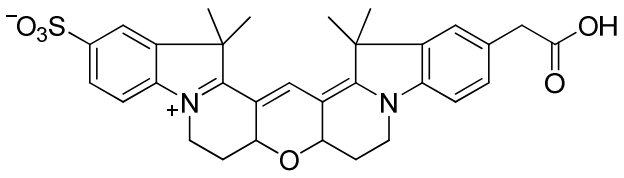

Figure 3.25. Structure of Cy3b.

This FRET probe gave a clean melting curve with a reasonable change in emission and did not display any significant temperature-dependant emission (Figure 3.26).

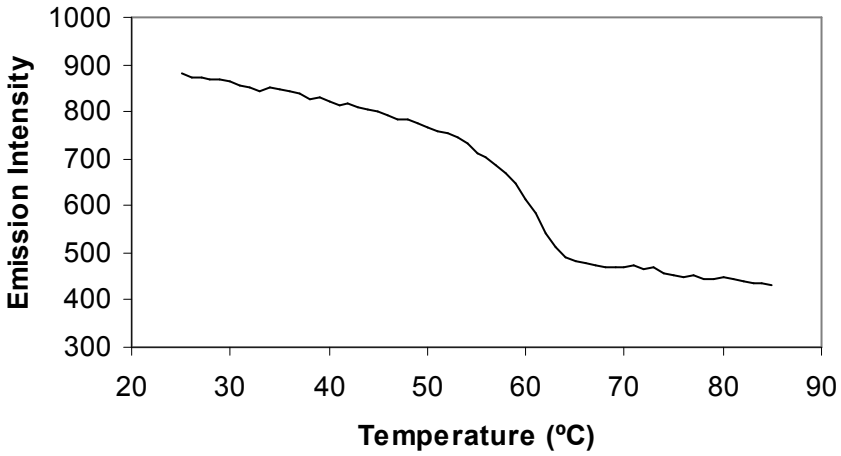

Figure 3.26. Melting curve of ΔF508 FRET HyBeacon using Cy3b acceptor dye**.**

This is strong evidence to suggest that the rotation around the polymethine bridge is the main cause of the temperature-dependant emission and to confirm that the effect is not limited to oligonucleotide-bound labels, NHS esters of Cy3 and Cy3b were analysed in the same way, with and without oligonucleotide present. This produced the expected observation, of strong temperature-dependence of emission for Cy3 but not for Cy3b. These results have outlined a major limitation in the use of cyanine dyes for biophysical analysis and have provided evidence of a cause, as well as how the use of specific modifications to the dye structure can alleviate the problem.

During analysis of the FRET probes, containing cyanine acceptors, with the fluorimeter, emission scans performed at specific temperature intervals provided a 3D plot of temperature/wavelength/intensity as previously used in Section 3.3 (Figure 3.22). When recording melting curves using these plots, cross-sections were taken at the corresponding dye-emission wavelengths. However, when this technique was applied to the probes using cyanine acceptor dyes, it became apparent that the emission wavelength experienced a slight red shift upon duplex melting. This effect was present for Cy3, Cy3.5, Cy5 and Cy5.5 acceptor ΔF508 probes and can clearly be seen in a contour plot of the fluorescence melting (Figure 3.27).

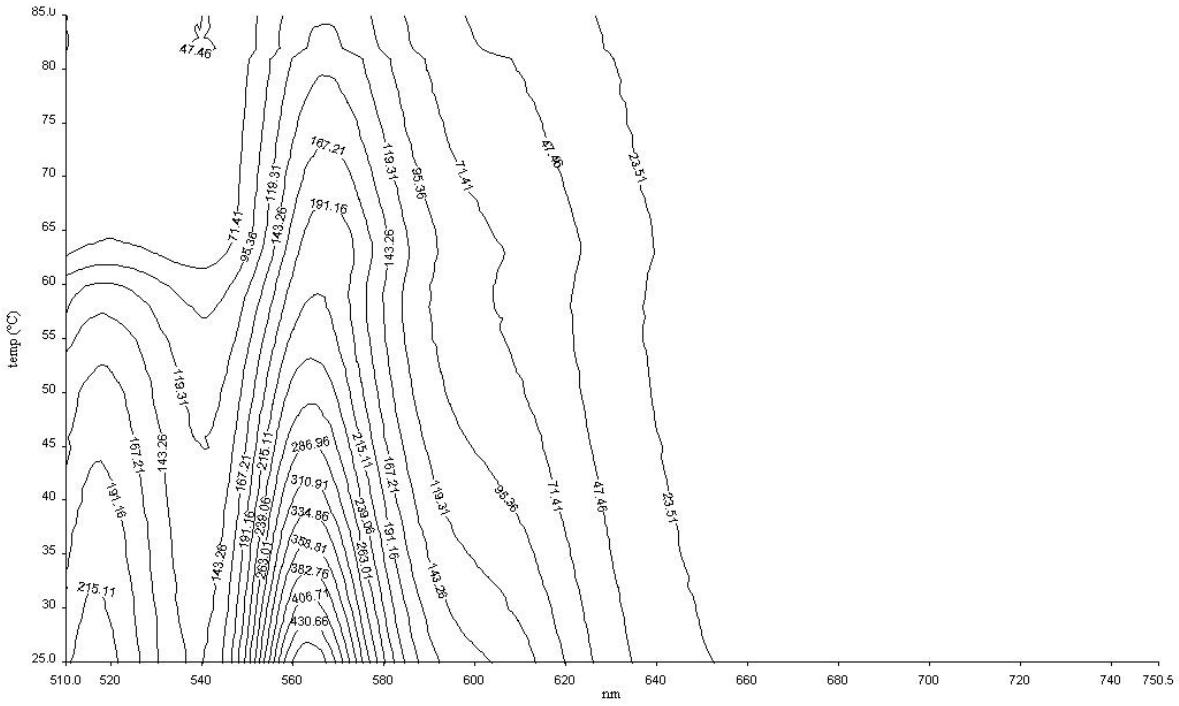

Figure 3.27. Contour plot of fluorescence melting using a FRET HyBeacon with a FAM donor and Cy3 acceptor.

To convert the change in emission into a more appropriate format, a melting curve was plotted using the wavelength of maximum emission intensity against temperature. This was compared alongside the melting curve derived from the fluorescein emission at 525 nm, showing that the change in emission wavelength occurs at the same temperature as the

traditional fluorescence melting for both a wild type target and ΔF508 mutant target (Figure 3.28).

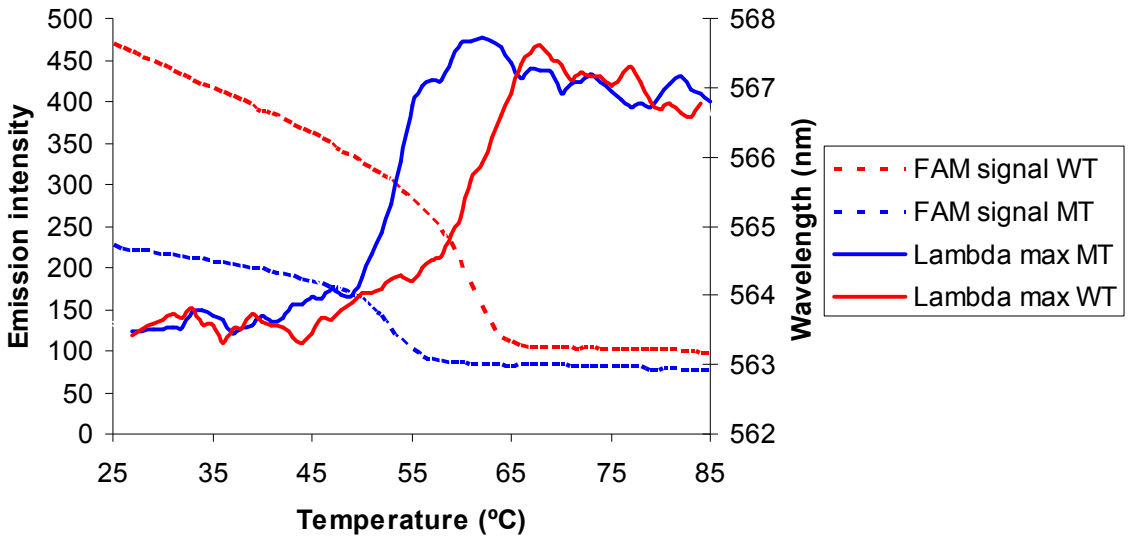

Figure 3.28. Melting curves from FRET probes using FAM donor and Cy3 acceptor, monitoring emission intensity (dashed) and λ max (solid) for both wild type (red) and ΔF508 mutant (blue) sequences.

The same procedure was applied to the probe using a Cy5 acceptor, which gave similar results displaying the same 4 nm red shift. This means that the size of red-shift is independent of spectral proximity to the fluorescein emission, and therefore is not a factor of residual fluorescein emission decrease.

Two more FRET probes were synthesised to probe the R616G and C524X mutations as previously employed in Section 3.3 using the same sequence (appendix Table 8.10). These were labelled with Cy3 and Cy5 respectively to provide a three-probe system with acceptor dyes Cy3.5, Cy3 and Cy5 to probe for ΔF508, R516G and C524X mutations. These probes were then analysed simultaneously using a multiplex system with the long template strand containing either none or one of the mutations. This demonstrated, as expected, that the

wavelength shift can be used to provide melting temperature analysis for mutation discrimination in a three probe multiplex system (Figure 3.29).

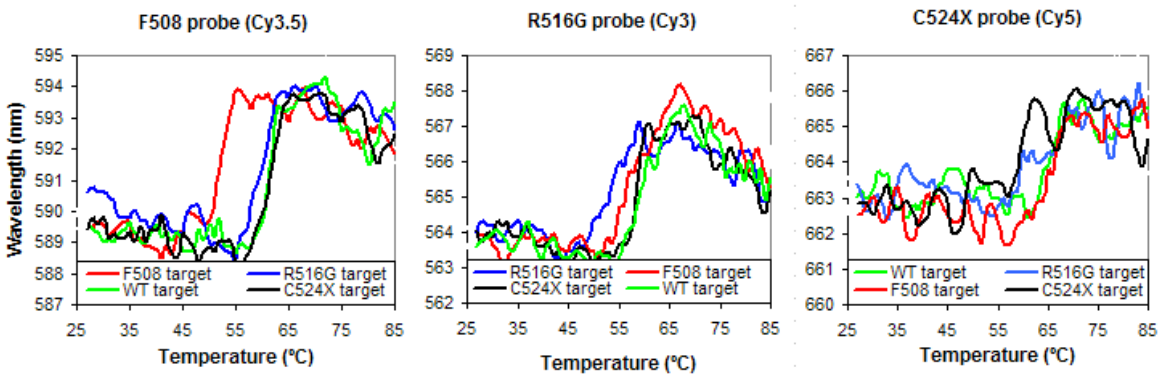

Figure 3.29. Melting curves of multiplex melting temperature analysis of a three probe system using λ-max detection.

The melting curves produced from this technique have a lower signal to noise ratio than those produced by emission intensity, and for the multiplex sample, the C524X probe did not show a clear distinction between wild types and mutant. However, these results do provide a proof-of-concept for an alternative method of measuring melting temperatures using a FRET multiplex system.

3.5 Conclusions and further work

The choice of fluorescent dye in HyBeacon synthesis can have a large effect on the performance of the HyBeacon, with some dyes such as cyanine dyes being unsuitable without careful design. The performance of these single-dye probes can be improved through the addition of stabilising and quenching end-capping monomers such as pyrene. However, the single-dye HyBeacons are limited in their multiplex capabilities.

Experiments using FRET based HyBeacons have demonstrated their ability to perform melting temperature analysis of three mutation sites within a target DNA sequence simultaneously. Using a single excitation wavelength, three separate detection emission wavelengths can be produced, allowing for use in equipment currently used for genetic analysis. Furthermore, the separation of the acceptor and donor and rigidity of the labels is important for efficient energy transfer. FRET HyBeacons using cyanine dyes have also shown differing degrees of success depending on the method of attachment to the probe, as well as changes in the emission wavelength. These phenomenon demonstrate the importance of dye selection and probe design when using FRET-based systems.

Chapter 4

4.0 SERS probes

4.0 SERS probes

This chapter describes the development of SERS as a method of DNA detection for high throughput genetic analysis. The following work was a collaboration with Dr Sumeet Mahajan and Professor Phil Bartlett.

4.1 Introduction

Recent developments in SERS substrates have led to the use of SERS in genetic analysis techniques with both metallic surfaces and nanoparticles[87-89,91,92]. These surface based detection and analysis techniques potentially provide rapid and accurate DNA diagnostics. We have developed such a technique using a spherical micro cavity gold surface with high sensitivity and reproducibility. A custom flow cell was designed (Figure 4.1) to allow the surface to be washed with buffers/samples in a closed environment with precise control of the temperature and potential applied to the surface. This flow cell could hold a substrate and provide a 150 μM film of the sample material.

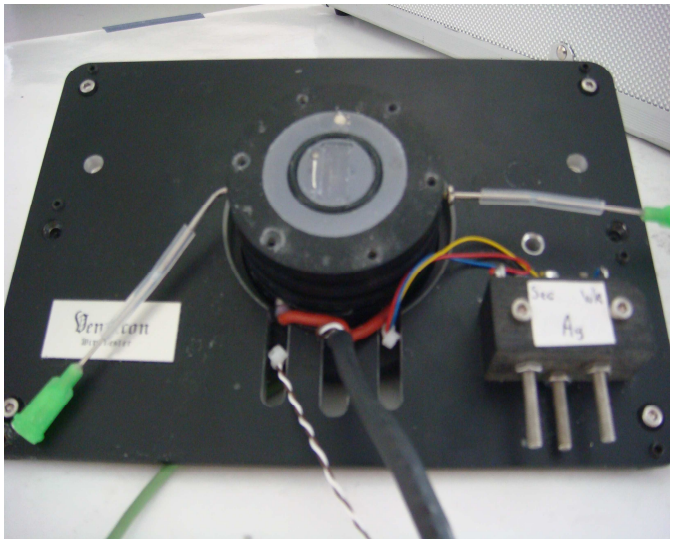

Figure 4.1. Custom made flow cell containing substrate holder, heating element and electrodes.

4.2 Spherical micro cavity gold surface

A novel SERS substrate was recently developed by Bartlett *et al.* which contains ordered spherical cavities in a gold substrate[117]. This surface is manufactured by the electrochemical deposition of gold around a template of closely packed polystyrene spheres. Once the deposition of gold is complete the spheres can be washed away using DMF or another suitable solvent. By controlling both the sphere diameter and the amount of electrochemical deposition the cavity diameter and depth can be controlled. These highly ordered surfaces have been shown to be excellent substrates for SERS[118,119] and due to their controllable nature, their optical properties can be tuned[120,121]. The highly ordered nature of these surfaces can be seen by SEM (Figure 4.2) and is highly reproducible, making the surface ideal for analytical techniques where reproducibility is essential.

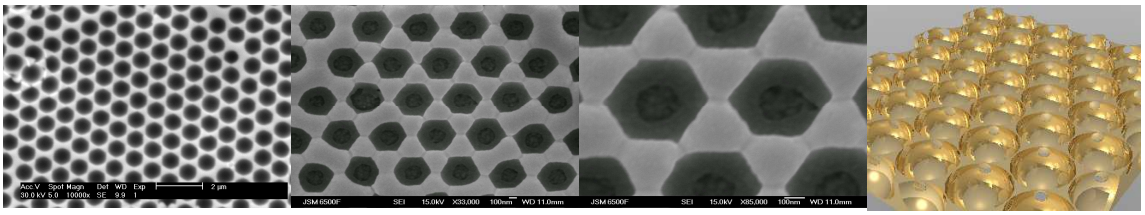

Figure 4.2. SEM images of spherical micro cavity gold surfaces and a graphical representation of the surface (right).

For the experiments discussed in this thesis a void diameter of 600 nm was used and gold was deposited to give a void depth of 480 nm.

4.3 Raman labelled oligonucleotide analysis

The majority of analytical techniques for genetic analysis use a fluorescent molecule as a reporter, many of these molecules are also Raman active and give unique molecule specific signals. We have used commercially available oligonucleotide monomers, traditionally employed in fluorescent strategies to provide oligonucleotide probes which can be immobilised onto a spherical micro cavity gold surface and display high intensity Raman signals. We have used this to provide melting temperature analysis of both synthetic templates and PCR products, detecting mutations present in the CFTR gene.

4.3.1 Short synthetic templates

Initial experiments used a short (22-mer, for sequences see Appendix Table 8.12) oligonucleotide probe containing three additions of a commercially available disulphide monomer, separated by HEG spacers (Figure 4.3).

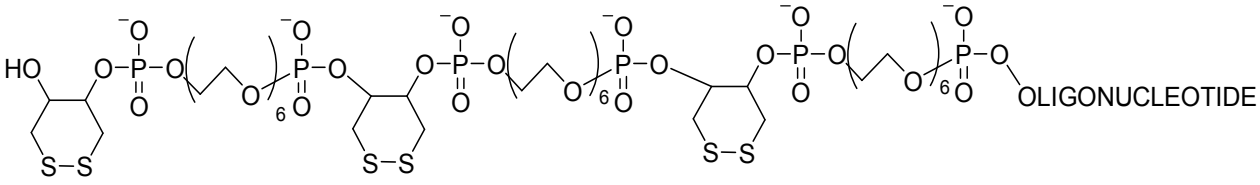

Figure 4.3. Oligonucleotide modification for attachment to structured gold substrate.

These were incorporated at the 5' terminus of the oligonucleotide to allow surface immobilisation. By immersing the gold substrate into a solution of the disulphide modified oligonucleotide, the disulphide could form two stable gold sulphur bonds. The substrate could then be washed to remove any unbound oligonucleotide, leaving a functionalised gold substrate. To monitor this immobilisation an oligonucleotide was synthesised containing the 5'-disulphide modifications, as well as a 3'-fluorescein, which once

immobilised could be detected using the SERS signal from the fluorescein. Once the probe strand was immobilised, to prevent non specific binding of oligonucleotides to the surface, a passivation step was performed. This process consisted of submerging the surface in a solution of mercaptohexanol to bind to any free space on the surface, preventing further non-specific binding of oligonucleotides. This was optimised by washing a non-complementary Cy3 labelled oligonucleotide over the surface, after various lengths of immersion in mercaptohexanol (Figure 4.4).

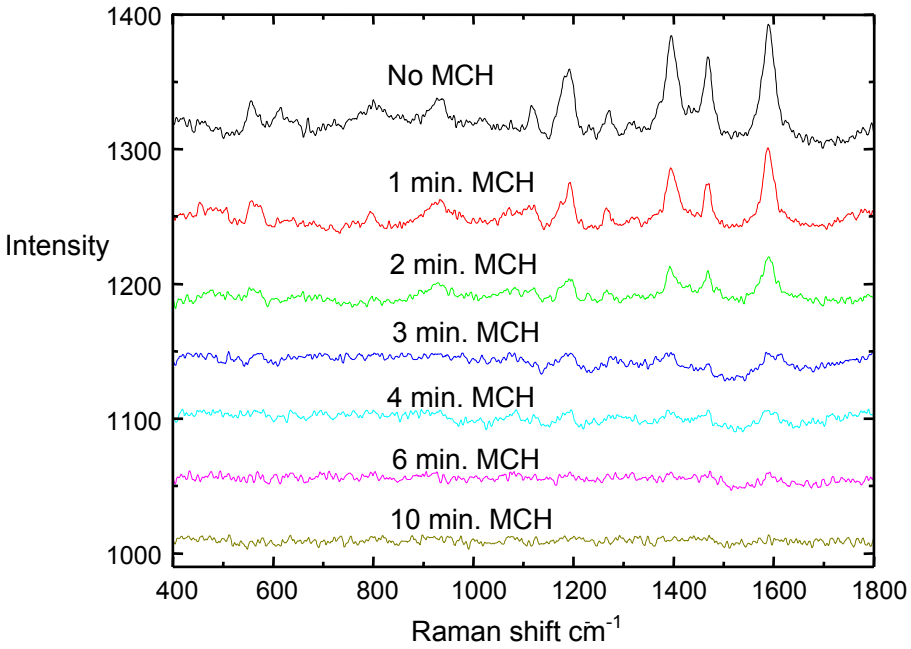

Figure 4.4. Raman spectra of a non-complementary Cy3 labelled oligonucleotide washed over a mercaptohexanol (MCH) passivated probe modified gold substrate.

Once a substrate was modified with an oligonucleotide probe and the surface had been passivated, a complementary target oligonucleotide with a 3' Texas red label was washed through in buffer. This then hybridised to the immobilised probe and due to the 3' label in close proximity to the surface (Figure 4.5) an intense SERS signal could be recorded.

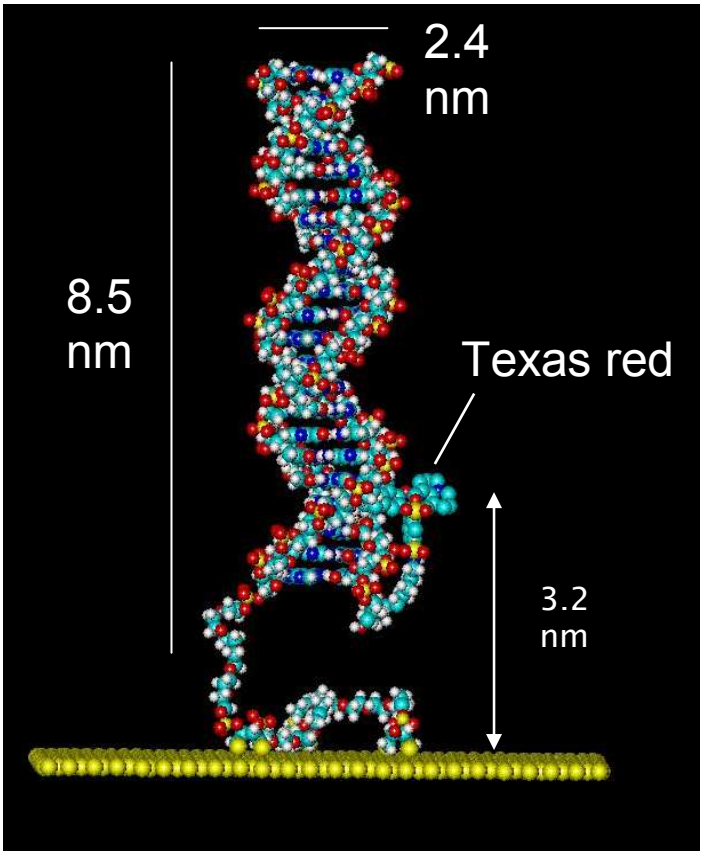

Figure 4.5. Hyperchem image of surface bound probe target duplex with Texas red label.

By using a heating element embedded into the flow cell, the temperature could then be increased at a controlled rate. By recording the Raman spectra as a function of temperature the denaturation of the surface bound duplex could be monitored. As the duplex melts the target oligonucleotide leaves the surface by diffusion/electrostatic repulsion and the label-surface distance increases, therefore signal intensity decreases (Figure 4.6).

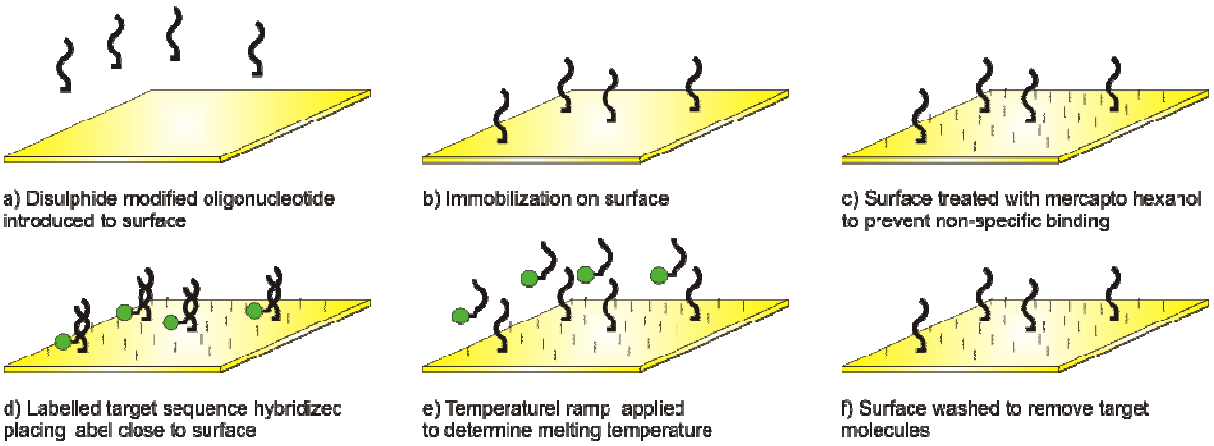

Figure 4.6. Procedure for capturing labelled target sequences and subsequence melting analysis.

By monitoring the intensity of a predetermined peak in the Raman spectra, melting curves akin to fluorescence melting can be produced by plotting Raman intensity as a function of temperature (Figure 4.7). By taking the derivative of the SERS melting profile the melting temperature of the duplex could be determined similar to traditional fluorescence/UV-vis melting.

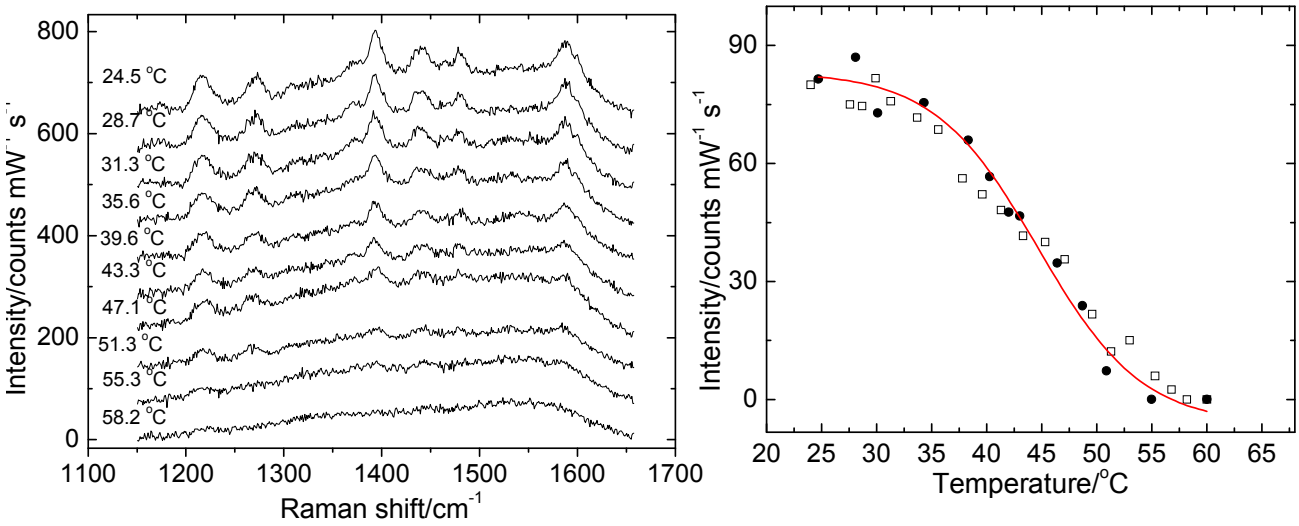

Figure 4.7. Raman spectra recorded at temperature intervals (left) and a plot of intensity *vs* temperature monitoring the 1400 cm^{-1} peak.

To test the reproducibility and reusability of the substrates, the process of hybridisation was repeated using complementary Cy3 labelled oligonucleotides. After denaturation the surface was washed, before another sample was passed through the cell, hybridising to the surface probe. This demonstrated the complete removal of the target strand from the surface after denaturation and the surface bound probe was reusable (Figure 4.8).

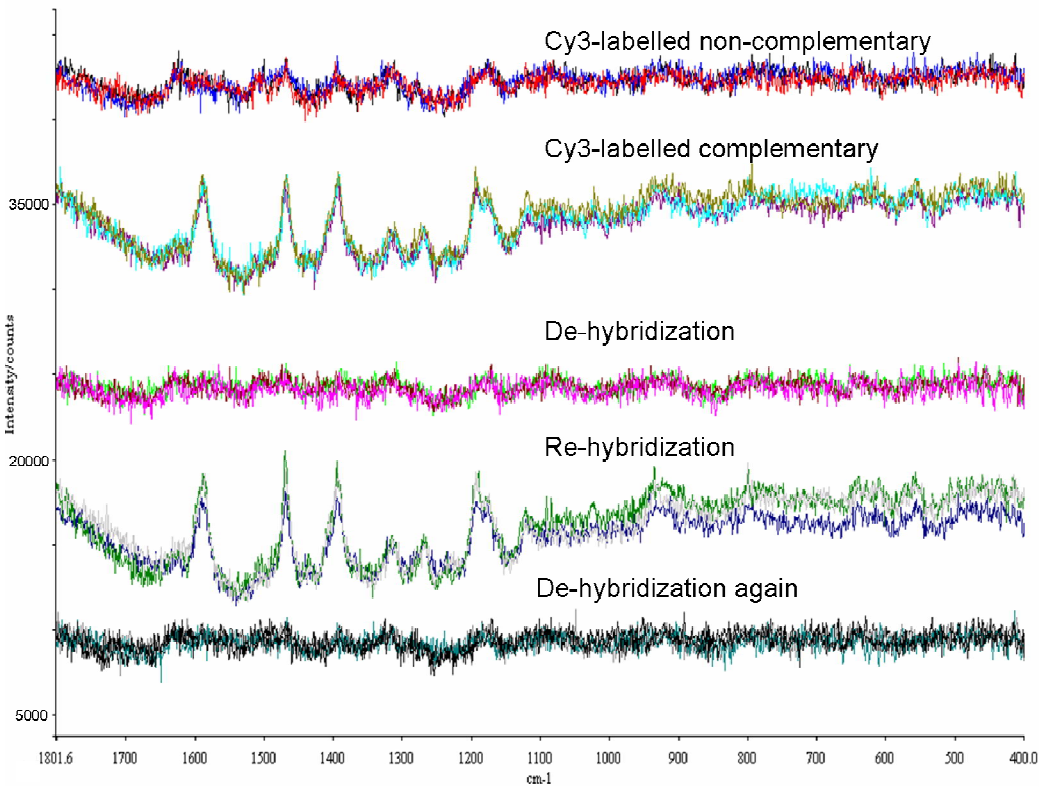

Figure 4.8. Raman spectra of substrate with complementary, non-complementary and no target strand, demonstrating the reusability of the substrate (Cy3 label).

Due to the reusable nature of probe and the reproducibility of the surface, this technique is highly suited to the analysis of genetic material, and melting temperature analysis is commonly used for mutation discrimination. To determine whether the SERS melting can discriminate between mutations, a series of synthetic targets were synthesised to mimic a region of the CFTR gene. Two different mutations were studied, the ΔF508 (triple T

deletion) and 1653C/T (single point mutation) to demonstrate the ability of mutation discrimination between different mutation types (for sequences see appendix Table 8.12). This gave three different targets for a single probe sequence, the wild type and two mutations. Each of these targets were labelled with Texas red or Cy5, due to the strong Raman signal when using the 633 nm laser. Each probe target duplex was then analysed separately by SERS melting using the same procedure as the previous experiments, except a different peak (1500 cm^{-1}) was used to produce the melting curves due to the different label. All three target sequences gave clear melting curves with different T_m's analogous to the T_m's you would expect from traditional melting analysis (Figure 4.9).

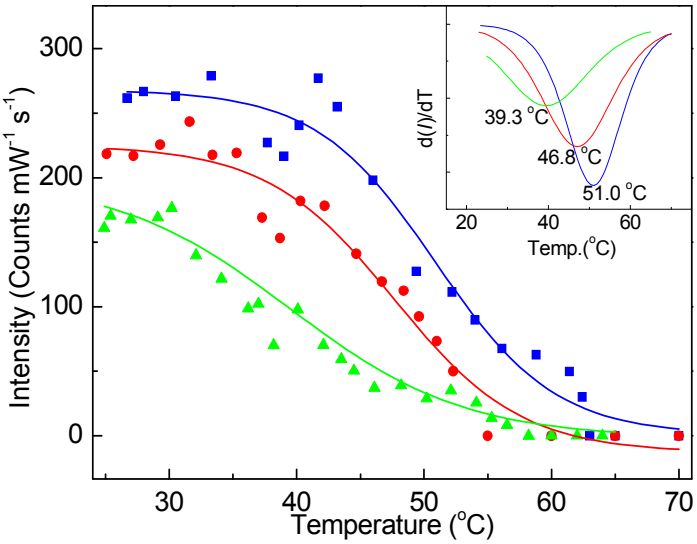

Figure 4.9. Melting curves and derivatives (inset) of wildtype (blue), ΔF508 (green) and 1653C/T (red) target sequences measured using the 1500 cm^{-1} band of a texas red label.

This ability to distinguish between mutant target oligonucleotides and the ability of SERS to multiplex, results in a potentially very useful technique, especially if resonant Raman spectroscopy can be used to increase sensitivity.

4.3.2 PCR product analysis

The success of the synthetic template analysis indicated that the SERS melting is a potential tool in genetic diagnostics, however, samples analysed in commercial/medical applications rarely use short sequences such as the synthetic targets used in section *4.3.1*. This led to the analysis of longer target oligonucleotides prepared by PCR. This is closer to a genetic analysis application, as PCR is routinely used in the production of target DNA for analysis.

We synthesised a long (138-mer) region of the CFTR gene containing the ΔF508 mutation site to act as a PCR template, simulating genomic DNA. We then synthesised two primers, one unlabelled and one containing a 5' Cy5 modification, using a commercially available Cy5 phosphoramidite (for sequences see appendix Table 8.13). Cy5 was chosen as the label due to its absorption maximum of 646 nm, resulting in a large spectral overlap with the 633 nm laser and therefore resonant Raman is possible, increasing signal strength to achieve sensitivity similar to that which can be achieved by fluorescence[54]. To capture the target DNA a new probe was synthesised using the same combination of disulphide and HEG monomers used in section *4.3.1*, except the modifications were at the 3'-end. This was to allow the probe to capture the target positioning the 5'-end of the target with close proximity to the surface. This allowed the Cy5 label from the primer to give a strong SERS signal. However, this meant that excess labelled primer could potentially give a false positive and so the probe sequence was complementary to part of the primer, but also the primer extension product. This meant that there were no false positives from primers, although it had the effect of the label being slightly further from the surface (Figure 4.10).

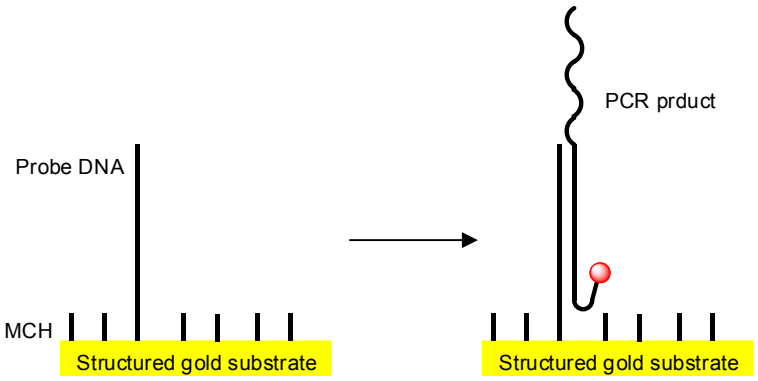

Figure 4.10. Schematic demonstrating PCR product capture and label/primer position.

Asymmetric PCR was then used to amplify the template DNA using a 4 times excess of the labelled primer. This gave a 20 µL sample containing the labelled target DNA, which could then be washed through the flow cell with no purification and captured by the immobilised probe. Once complete the sample could then be analysed by SERS melting using the same technique as with the synthetic templates and a melting temperature could be determined. This was applied to PCR templates of the wild type and also a ΔF508 template in order to use melting temperature analysis for mutation discrimination, yielding similar results to the synthetic targets.

4.4 Electrochemical melting

DNA duplexes are highly charged due to the poly anionic backbone and as such are susceptible to manipulation by both ionic strength and electric fields. A common example of DNA manipulation by electric fields is the use of gel electrophoresis, where a sample of DNA moves through a gel medium towards a cathode due a potential difference across the gel. This effect was applied to the probe-target duplexes bound to the structured gold surface, taking advantage of the properties of the gold surface allowing its uses as an electrode. A potential was applied across the sample, with the surface being used as an anode and a cathode in the buffer solution at the top of the flow cell. By applying the

potential in an incremental manner from 0 to -1.6 V and recording the Raman spectra at each step, any duplex melting could be observed in a similar fashion to the SERS thermal melting. This process was performed on both the synthetic targets as well as the PCR products used in sections *4.3.1* and *4.3.2* respectively.

Experiments using the synthetic templates demonstrated that the electrochemical melting (*E*melting) gave similar results to the thermal melting previously used, with the ΔF508 target displaying the least stability, followed by the 1653C/T, then the wild type sample. The *E*melting curves produced could then be differentiated to provide *E*melting potentials for each of the targets, akin to the T_m's achieved with the thermal melting (Figure 4.11).

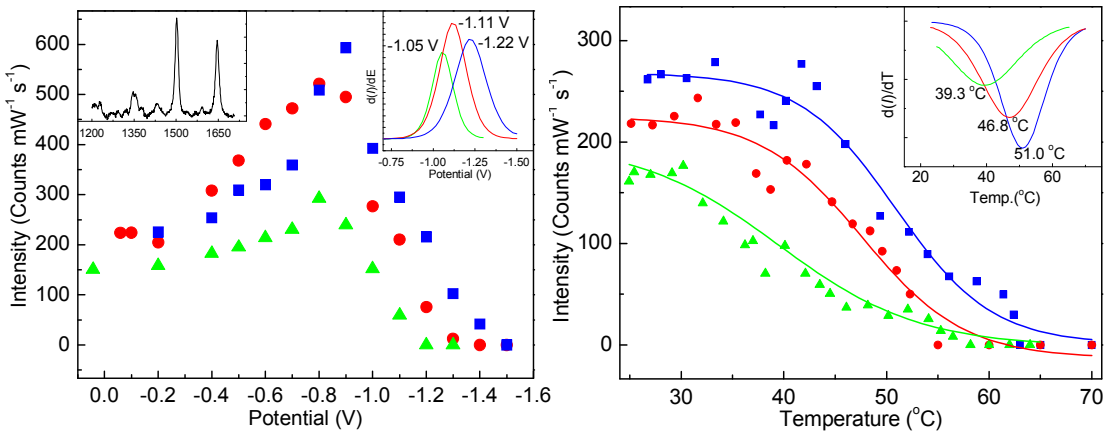

Figure 4.11. *E*melting (left) and thermal melting (right) profiles and derivatives (inset) of synthetic DNA targets from the CFTR gene, wild type (blue), 1653C/T (red) and ΔF508 (green).

The synthetic templates gave sharp melting curves and the difference in potential between the wild type and mutant variants was clearly significant enough to provide melting temperature analysis of the mutations.

The same approach was applied to target sequences labelled with an anthraquinone derivative (Figure 4.12) allowing a similar method for mutation discrimination[122]. However anthraquinones are electrochemically active and can allow further

characterisation of the probe target duplex through cyclic voltammetry and coulometric measurements. These extra analytical techniques allow the surface coverage of the target sequence to be measured.

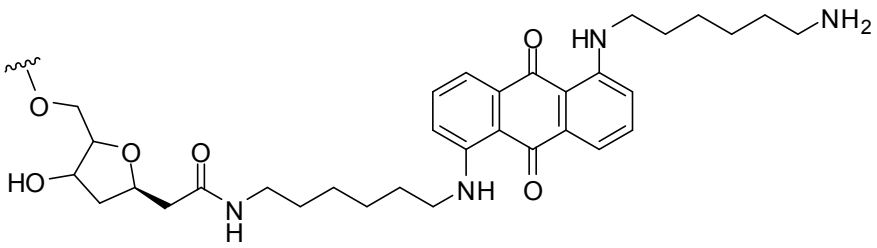

Figure 4.12. Structure of 3' anthraquinone label

Mutation discrimination was measured using the same procedure of *E*melting monitoring the 1559 cm^{-1} peak in the anthraquinone SERS spectra. The 1559 cm^{-1} peak is characteristic of ring stretching and is independent of the redox state of the anthraquinone and so is not affected by the applied potential during *E*melting. This results in the measured *E*melting transitions being accurate for mutation discrimination.

The exact same *E*melting procedure was then applied to the Cy5 labelled PCR amplicons used in previous experiments, yielding a similar result (Figure 4.13).

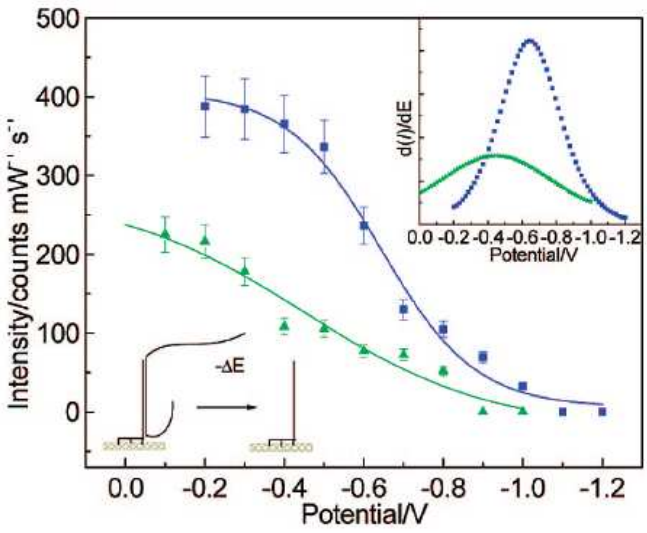

Figure 4.13. *E*melting profile and derivative (inset) of PCR amplicons of a wild type (blue) and ΔF508 (green) template.

Further experiments altering the ionic strength of the buffer solution were performed using the synthetic ΔF508 target (texas red label) to determine if *E*melting would show the same stability relationship as thermal melting. Using a pH 7, 10 mM Tris buffer the NaCl concentration was increased from 10 mM to ~6 M and the *E*melting profile recorded (Figure 4.14). This gave a clear relationship between the melting potential and the ionic strength, with higher ionic strengths giving a lower melting potential.

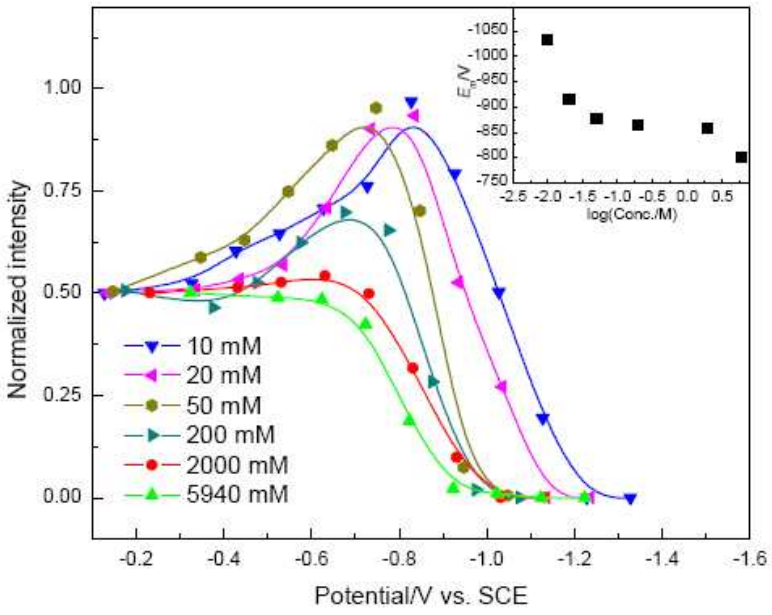

Figure 4.14. *E*melting profiles of a synthetic target with different ionic strengths and their melting potentials (inset).

The expected effect of altering the ionic strength is that an increase in ionic strength would reduce the inter-strand repulsion in the duplex, increasing the stability and also it would screen the potential from the bulk solution and duplex. However, the opposite effect was observed, which was an unusual discovery, as it rules out that the mechanism for the *E*melting could be simply due to electrostatic repulsion. If the mechanism of *E*melting was electrostatic repulsion, then at ionic strengths of >1 M the *E*melting would be inhibited due to screening of the potential. At concentrations above 1 M NaCl the effect of the electric field extends less than 0.1 nm from the surface and so the DNA duplex should not be influenced. When a similar comparison was made using the same probe-target duplex and thermal melting the expected relationship between duplex stability and ionic strength was observed (Figure 4.15). This confirms that the observed effect using *E*melting is a direct effect of the applied potential and not the surface affecting stability.

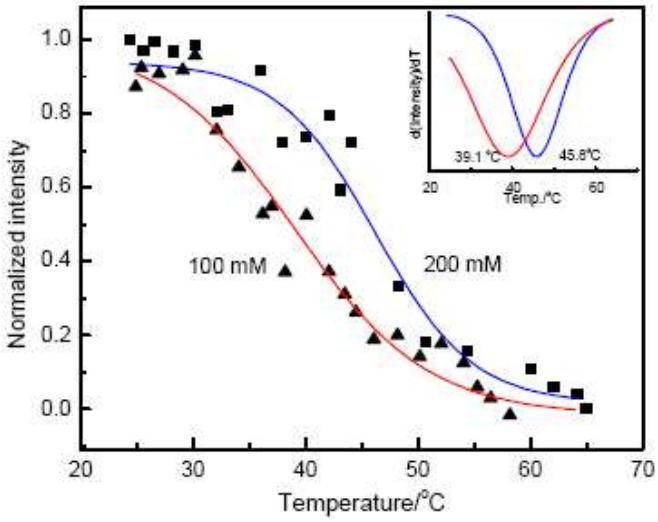

Figure 4.15. Effect of ionic strength on thermal SERS melting, showing melting profiles and derivatives (inset) at 100 mM and 100 mM NaCl.

As well as a shift in the melting potential the ionic strength appears to have an effect on the shape of the melting curve. At low potentials prior to melting there appears to be an increase in the label intensity, which is less predominant in high salt concentrations (Figure 4.13). This is most likely due to the flexible linker used to attach the Raman label, in this case Texas red. Dyes such as Texas red and cyanine dyes carry positive charges and so upon application of a negative potential to the surface it is not unreasonable to expect the dye to be attracted to the surface. With many commercially available dyes the linker used for conjugation to an oligonucleotide can be as many as 6 carbons long, this combined with the length of the amine modification in the oligonucleotide provides the label with an alkyl tether, which can be in the region of 12-13 carbons long (Figure 4.5). This can allow the label to move closer to the surface and therefore give an increase in the Raman signal. The increase in Raman signal clearly has a dependence on the ionic strength and appears to follow the 1 M screening effect. This means that the duplex is clearly no longer experiencing electrostatic repulsion from the surface at high ionic strengths, but the application of a potential can still cause melting.

The effect of pH on duplex stability is well documented using thermal melting in solution and so the pH was altered and the stability of a duplex was measured using *E*melting. The ΔF508 synthetic template labelled with texas red was analysed by *E*melting using Tris buffer at pH 7, 8 and 9 keeping the ionic strength constant at 10 mM (NaCl). This gave the expected decrease in melting potential as the pH increased (Figure 4.16) demonstrating a reduction in the duplex stability as the pH increases.

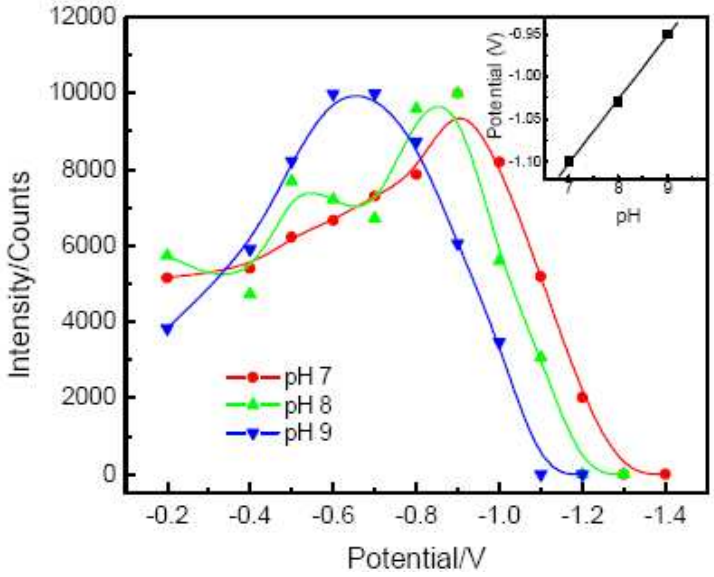

Figure 4.16. *E*melting profiles of a synthetic texas red labelled target using Tris buffer at pH 7, 8 and 9 with a constant ionic strength (10 mM NaCl).

To determine whether the pH is causing the melting in *E*melting experiments the synthetic target was analysed using a high concentration (500 mM) pH 7 Tris buffer. This high strength buffer would overcome any minor pH changes at the surface which could have caused the duplex melting. This gave a normal *E*melting profile with a small change in the melting potential (0.2 V) when compared to the pH 7 10 mM Tris sample with no significant abnormalities. This meant that small pH changes caused by the applied potential are not the main cause of the mechanism of *E*melting but could possibly be a contributing factor.

4.5 Unlabelled oligonucleotide SERS analysis

The detection and analysis of unlabelled DNA duplexes is routinely used in techniques such as PCR and gel electrophoresis through the use of DNA binding dyes such as those described in section *1.3.1.1*. A similar approach was applied to the SERS melting in order to detect unlabelled DNA duplexes in the same way. When using a fluorescent DNA binding dye typically there is an observed change in emission intensity between the free dye and the DNA-dye complex. It is unlikely that there would be any equally significant change in the Raman spectra between bound and unbound dye and so a different approach was used. This used the distance dependant nature of SERS, where a DNA binding dye could be washed through a sample containing a surface-bound DNA duplex. This dye would then be bound to the duplex, providing the DNA with an intense Raman signal with no background signal from the free dye in the bulk solution due the large distance from the surface. The DNA duplex was then analysed by *E*melting and upon melting of the duplex the now unbound dye diffused into the bulk solution, providing a decrease in the Raman signal. Initial experiments used a chloro-anthraquinone and 7-aminoactinamycin as the Raman reporters, however, these did not give interpretable results. We then selected DRAQ5 (Biostatus Ltd. Figure 4.17) as the DNA binding dye due to its maximum absorption at 646 nm, resulting in a resonant Raman response as well as its selective binding for double stranded DNA.

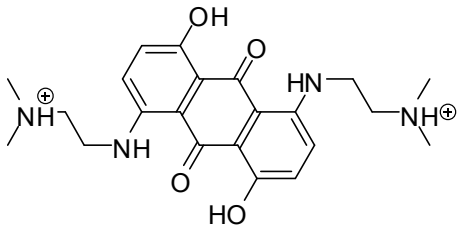

Figure 4.17. Structure of DNA binding dye DRAQ5.

Unlabelled PCR primers and the same template region of the CFTR gene as used in section *4.3.2* were used in asymmetric PCR in a similar manner to previous experiments. The unlabelled PCR products were captured by the surface probe and then the DNA binding dye was washed through the flow cell to facilitate binding to the surface-bound duplex. Then the *E*melting procedure as previously described was used to provide a melting profile (Figure 4.18).

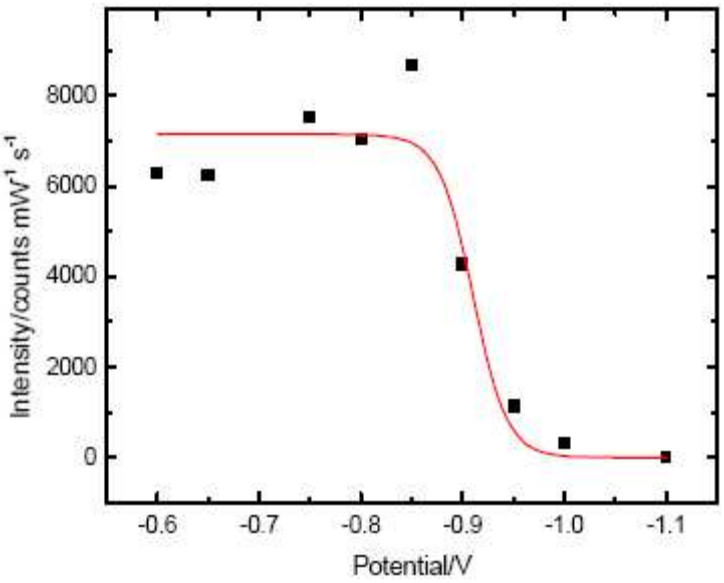

Figure 4.18. Melting profile of an unlabelled PCR amplicon using DRAQ5 as a Raman reporter.

The resulting melting profile was clear enough to provide information about the melting potential, however mutation discrimination was not possible as the difference between the wild type and mutant was too small. This could be due to observed non-specific binding of the DRAQ5 due to its high hydrophobicity and electropositive nature. This could potentially be overcome using optimisation of the passiviating surface layer.

4.6 Conclusions and further work

Initial experiments using a temperature controlled flow cell have provided a proof of concept for the application of SERS melting in genetic analysis. This has significant advantages over existing SERS technologies due to the high sensitivity and reproducibility. Furthermore we have demonstrated that electrochemical potentials can be used in a manner parallel to heating in order to provide information about the stability of DNA duplexes bound to an anodic surface. Both the thermal melting and *E*melting have shown that commercially available monomers with well proven chemistries can be used in SERS analysis of DNA alongside a structured gold surface. The sensitivity of the experiments and use of impure PCR reaction mixtures has demonstrated the ability of these techniques to compete with current existing fluorescence-based technologies[123]. Further work is required to investigate the ability of the systems to multiplex information to increase the potential in high thoughput analysis. Also the analysis of unlabelled DNA duplexes using DNA binding dyes should be optimised.

Chapter 5

5.0 Conclusions and further work

5.1 Conclusions

Quantum dots with minimal modification have shown to have a number of problematic properties; strongly temperature dependent emission, inconsistent aqueous solubility and potentially DNA binding properties. Each of these factors contribute to the difficulty in using quantum dots as a direct replacement of organic fluorophores without significant further modification to either the quantum dots or the procedure in which they are used.

The performance of HyBeacon probes has been improved through the use of end-capping moieties, resulting in increased melting peaks and improved melting temperatures. Furthermore the use of HyBeacon probes in multiplex systems has been improved through the use of FRET to allow multiplex detection with a single excitation wavelength. This has allowed multiplex detection of multiple genetic mutations simultaneously with no significant signal interference. This work has also demonstrated that the temperature dependant emission from cyanine dyes can be controlled through alternative linker methods allowing their use in current genetic analysis systems.

Experiments with SERS detection of PCR products have demonstrated that SERS can be used to successfully capture and detect PCR products and using either thermal or electrochemical melting allelic analysis can be performed. The high sensitivity and selectivity of the technique has been demonstrated and the potential for unlabelled detection explored. This technique provides a genetic analysis system with the potential for high sensitivity and the ability to multiplex up to 10 samples simultaneously and therefore improve high-throughput genetic analysis.

5.2 Further work

The multiplex potential of HyBeacons can be improved further through the use of multiple excitation wavelength machines such as the Rotorgene systems (Qiagen) and to exploit the multiple excitation wavelengths probes using a selection of dyes must be used. This would require a study into which dyes perform well as HyBeacons and which modifications are required to provide a good HyBeacon effect. This would provide a system in which multiple probes, each labelled with a different fluorophore can be excited in rapid succession in order to provide multiplex analysis.

The multiplex potential of SERS-melting can be explored through PCR amplification of multiple loci with multiple labelled primers each with a different label. This could then be used to monitor the SERS signal of the primers during capture and melting of the PCR products. Furthermore the use of DNA binding dyes to detect and interrogate unlabelled PCR products needs to be optimised in order to improve the sensitivity of detection.

Chapter 6

6.0 Experimental

6.0 Experimental

6.1 Preparation of compounds

6.1.1 General methods

All reagents and solvents were purchased from Aldrich, Avocado, Biostatus, Eppendorf, Evident technologies, Fluka, Glen research, Invitrogen, Link Technologies Ltd, Nanoco or Qiagen and used without prior purification except for the following solvents which were purified by distillation: i) THF over sodium wire and benzophenone), i) DCM (over calcium hydride), iii) pyridine/triethylamine (over calcium hydride).

All reactions which required anhydrous conditions were performed using dry glassware, under an atmosphere of argon.

6.1.2 Mass spectrometry

Small molecule low resolution mass spectra were performed using electrospray ionisation using a Waters ZMD quadrupole mass spectrometer and acetonitrile. Oligonucleotide mass spectra were performed by electrospray ionisation using a HP 1050 single quadrupole mass spectrometer. MALDI-TOF oligonucleotide analysis was performed using a ThermoBioAnalysis Dynamo linear mode with a matrix of 4:1 3-hydroxypicolinic acid (HPA):picolinic acid (PA).

6.1.3 NMR

NMR spectra were recorded using a Bruker AV 300 spectrometer, ^{1}H spectra at 300 MHz, ^{13}C NMR spectra were measured at 75 MHz and ^{31}P NMR spectra were measured at 121 MHz. All spectra were internally referenced using the appropriate residual undeuterated DMSO. The multiplicities of ^{13}C signals were determined using distortionless enhancement by phase transfer (DEPT) spectral editing.

6.1.4 List of compounds

[1] 5'-*O*-(4,4'-Dimethoxytrityl)-2'-deoxy-5-iodo-uridine

[2] Prop-2-ynyl 4-oxopentanoate

[3] 5'-*O*- (4,4'-Dimethoxytrityl)-2'-deoxy-5-(prop-1-ynyl-3-oxopentanoyl) uridine

[4] 5'-*O*- (4,4'-Dimethoxytrityl)-2'-deoxy-5-(prop-1-ynyl-3-oxopentanoyl) uridine phosphoramidite

[5] 5'-*O*- (4,4'-Dimethoxytrityl)-2'-deoxy-5-(pentyn-1-yl-5-Fmoc) uridine

[6] 5'-*O*- (4,4'-Dimethoxytrityl)-2'-deoxy-3'-cyanoethyl, N,N disopropyl phosphoramidite-5-(pentyn-1-yl-5-Fmoc) uridine

6.1.5 Experimental

5'-*O*-(4,4'-Dimethoxytrityl)-2'-deoxy-5-iodo-uridine [1]

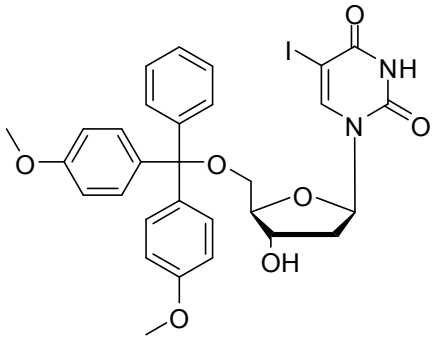

5-IDU (4.00 g/0.0113 mol) was dissolved in pyridine (30 mL), and dimethoxytritylchloride was added (4.595 g/0.01356 mol). The solution was stirred under an inert atmosphere for 2.5 hours. The reaction was monitored by TLC (eluent 5 % MeOH/DCM) and upon completion the solution was evaporated on a low-vac Buchi. Toluene (~5 mL) was added and the solution was dried on a high vacuum Buchi. The crude product was purified using column chromatography (eluent 2 % MeOH/DCM), giving 5.90 g (8.69 mmol) of pure product as a white foam (80 % yield).

^{1}H NMR **δ_H ppm** (300MHz, DMSO), 8.00 (1H, s, H6 uridine), 7.22-7.42 (10H, m, ArCH), 6.10 (1H, t, *J* 6.8, 1' CH), 5.40 (1H, bs, 3'OH), 4.24 (1H, s, 4'), 3.89 (1H, s, 3'), 3.75 (6H, s, 2 x OCH_3), 3.18 (2H, s, 2 x 5'CH), 2.09-2.32 (2H, m, 2')

^{13}C NMR **δ_c ppm**, (75MHz, DMSO), 160.6 (C4), 158.1 (C11), 150.1 (C2), 144.2 (C6), 135.4 (C13), 129.7 (C9), 127.9 (C15), 127.6 (C14), 126.7 (C16), 113.3 (C10), 85.8 (C4'), 84.9 (C11), 70.5 (C3'), 69.8 (C5), 63.7 (C5'), 55.0 (C12), 39.8 (C2')

LRMS **(ES^+)** 679.21 $[M+Na]^+$

R_f (5 % MeOH/DCM) 0.29 Visualised by UV light and anisaldehyde stain

Prop-2-ynyl 4-oxopentanoate [2]

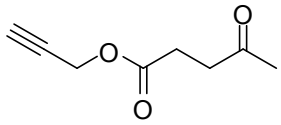

Levulinic acid (5.25 mL/50 mmol) was added to a solution of DCC (N,N'dicyclohexylcarbodiimide, 10.50 g/50 mmol) in DCM (50ml) and stirred at room temperature for ten minutes. Propargyl alcohol (1.5 mL/25 mmol) was then added to the reaction slurry dropwise, and then after fifteen minutes DMAP (0.3 g/2.4 mmol) and the reaction was monitored by TLC (eluent 10 % MeOH/DCM) for two hours. When the reaction had gone to completion (2 hours) the mixture was filtered, and the filtrate was washed with saturated sodium bicarbonate and saturated KCl. The organic layer was then dried over sodium sulphate and evaporated to dryness *in vacuo*, then purified using column chromatography (eluent 9.5:0.5 toluene:ethyl acetate), giving 3.813 g (24.6 mmol) of pure product as a colourless oil (98 % yield).

^{1}H NMR **δ_H ppm** (300MHz, DMSO), 4.67 (2H, d, *J* 2.5, H2), 3.53 (1H, t, *J* 2.4, H1), 2.73 (2H, t, *J* 6.5, H4), 2.50 (2H, m, H3), 2.11 (3H, s, H5)

^{13}C NMR **δ_c ppm**, (75MHz, DMSO) 206.6 (C8), 171.5 (C5), 78.4 (C2), 77.5 (C1), 51.6 (C3), 37.2 (C7), 29.5 (C9), 27.3 (C6)

LRMS **(ES^+)** 177.1 $[M+Na]^+$

R_f (10 % MeOH/DCM) 0.73 Visualised by UV light and $KMnO_4$ stain.

5'-*O*- (4,4'-Dimethoxytrityl)-2'-deoxy-5-(prop-1-ynyl-3-oxopentanoyl) uridine [3]

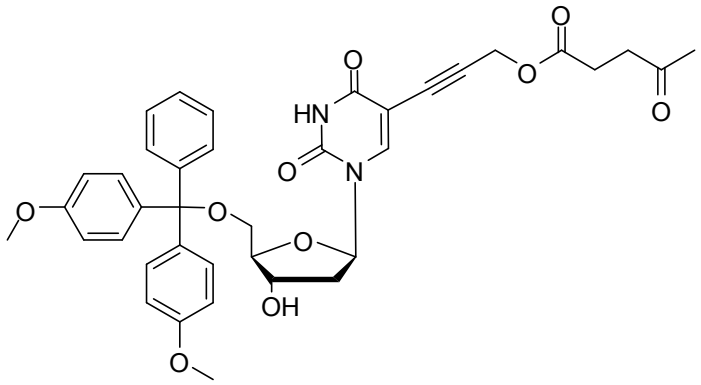

Compound **1** (1.50 g/2.2 mmol) was dissolved in anhydrous DMF (~5 mL) then copper iodide (83.6 mg/440 μmol) and triethylamine (1.53 mL/11 mmol) were added. Compound 2 (0.367 g/2.42 mmol) was then added and the solution was stirred in a dark inert atmosphere for 15 minutes. After this time tetrakistriphenylphosphinepalladium (0.307 g/220 μmol) was added and the reaction mixture was stirred in a dark inert atmosphere for 2 hours. At his point upon TLC visualization it became apparent that an impurity had begun to form, and so the reaction was partitioned between DCM and sat.KCl, and the organic layer was dried over $NaSO_4$ before being evaporated to dryness resulting in a yellow foam. This was then purified using column chromatography (eluent 4:1 EtOAc:hexane), giving 0.404 g of a white foam (27% yield).

^{1}H NMR **δ_H ppm** (300MHz, DMSO), 7.98 (1H, s, H6), 7.29 (9H, m, DMT Ar CH) 6.89 (4H, dd, *J* 1.2, 9.0, DMT Ar CH), 6.09 (1H, t, *J* 14, 1'CH), 5.31 (1H, d, *J* 4.6, 3'OH), 4.64 (2H, d, *J* 1.5, H9 CH_2), 4.29 (1H, m, 4'CH), 3.93 (1H, m, 3'CH), 3.74 (6H, s, DMT OMe), 3.25 (2H, m, 5'CH_2), 3.12 (2H, m, H13 CH_2), 2.70 (2H, t, *J* 6.5, H12 CH_2), 2.25 (2H, m, 2' CH_2), 2.09 (3H, s, H15 CH_3)

^{13}C NMR **δ_c ppm**, (75MHz, DMSO), 207.0 (C13), 172.3 (C10), 162.0 (C4), 159.0 (C10'), 149.8 (C2), 144.9 (C12'), 144.1 (C6), 136.0 (C7'), 130.4 (C8'), 128.5 (C14'), 128.3 (C13'), 127.5 (C15'), 113.6 (C9'), 99.6 (C5), 87.9 (C6'), 87.1 (C4'), 86.4 (C1'), 77.5 (C8), 77.1 (C7), 72.7 (C3'), 64.0 (C5'), 55.7 (C11'), 53.2 (C9), 42.0 (C12), 38.2 (C2'), 30.2 (C14), 28.1 (C11)

LRMS (**ES$^+$**) 705.2 $[M+Na]^+$

HRMS 705.2421 $[M+Na]^+$ Expected 705.2419 ($C_{38}H_{38}N_2NaO_{10}$)

R_f 0.64 (eluent 5:1:1, EtOAc:MeOH:NH_3) visualized using UV light and anisaldehyde stain.

5'-*O*- (4,4'-Dimethoxytrityl)-2'-deoxy-5-(prop-1-ynyl-3-oxopentanoyl) uridine phosphoramidite [4]

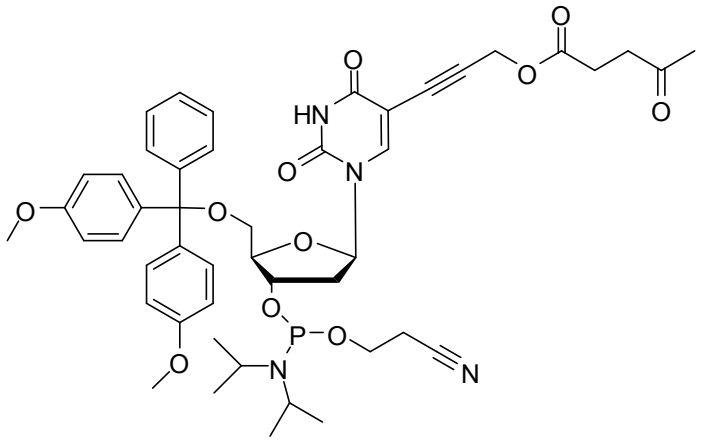

Compound **3** (400 mg/0.586 mmol) was dissolved in distilled DCM (5ml) in an inert atmosphere and distilled DIPEA (0.255 mL/1.465 mmol). The phosphitylating agent (0.160

mL/0.703 mmol) was then added and the reaction mixture was stirred under argon for 1.5 hours, monitored by TLC (eluent 4:1 EtOAc:Hexane). Once the reaction was complete the reaction mixture was washed using saturated KCl and dried over sodium sulphate (still in an inert atmosphere). The resulting solvent was evaporated off and the resulting solid was dried under high vacuum for 1 hour and the purified using column chromatography (eluent 70% EtOAc:Hexane) under argon and evaporated to dryness and dried under high vacuum. This gave 414 mg of a pure white foam (80% yield).

^{1}H NMR **δ_H ppm** (300MHz, DMSO) 11.63 (1H, bs, NH) 8.02 (1H, s, H6 CH), 7.29 (9H, m, DMT Ar CH), 6.88 (4H, dd, *J* 3.30, 8.97 DMT Ar CH) 6.30 (1H, q, *J* 7.0, 1'CH), 4.66 (2H, d, *J* 11.7, H9 CH_2), 4.51 (1H, m, 4'CH) 4.09 (1H, m, 3'CH), 3.74 (6H, s, DMT OMe), 3.64 (2H, m, CH_2 21), 3.53 (1H, m, CH 18), 3.22 (2H, m, 5'CH_2), 2.69 (2H, m, CH_2 22), 2.46 (2H, m, 2'CH_2), 2.09 (3H, s, CH_3 15)

^{31}P NMR **δ_H ppm** 148.7 (d)
(300MHz, DMSO)

LRMS **(ES^+)** 905.3 $[M+Na]^+$

R_f 0.42 (eluent 4:1, EtOAc:Hexane) visualized using UV light and anisaldehyde stain.

5'-*O*- (4,4'-Dimethoxytrityl)-2'-deoxy-5-(pentyn-1-yl-5-Fmoc) uridine [5]

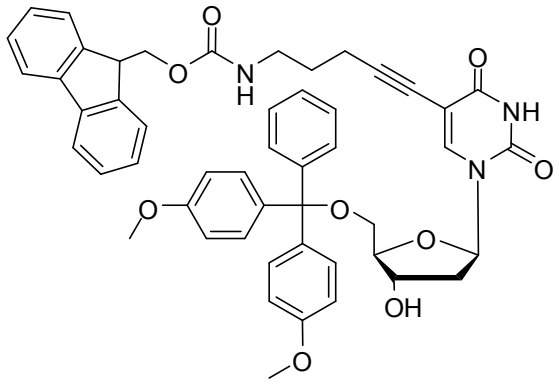

5'-*O*- (4,4'-Dimethoxytrityl)-2'-deoxy-5-(hex-5-ynylamine)uridine (2.000 g/3.0 mmol) was dissolved in DCM (20mL) and stirred, whilst diisopropylamine (0.46 mL/3.3 mmol) was added and then shortly after Fmoc-OSu (1.012 g/3.0 mmol) was added to the solution. After 2 hours the reaction was complete and the reaction mixture was washed with saturated sodium bicarbonate, and then the organic layer was dried over sodium sulphate and evaporated to dryness. This was then purified using column chromatography (eluent 4% MeOH/DCM 0.5% pyridine) and then dried under high vacuum to give a white foam (2.1514 g 86% yield).

^{1}H NMR **δ_H ppm** (300MHz, DMSO), 11.42 (1H, s, N3-H), 7.82 (m, Fmoc) 7.44 (m, DMT C-H g), 7.37 (m, DMT C-H h), 7.33 (d, *J* 8.24 DMT C-H c), 6.92 (d, *J* 8.0 DMT C-H d), 6.18 (1H, t, *J* 6.6 1'), 5.36 (1H, s, 3'OH), 4.24 (1H, m 3'), 3.97 (1H, m, 4'), 3.79 (6H, s, DMT OMe), 3.00 (2H, q, *J* 6.4, CH_2 11), 2.24 (2H, m, 2'), 2.21 (2H, t, *J* 7.3, CH_2 9), 1.50 (2H, t, *J* 7.0. CH_2 10)

^{13}C NMR **δ_c ppm**, (75MHz, DMSO), 161.7 (C2), 149.6 (C6), 143.9 (H13), 140.7 (**C**), 135.3 (**C**H), 129.6 (**C**H), 127.5 127.0 126.6 125.1 213.85 120.0 113.2 (**C**H), 99.3 (C9), 85.8 (4'C), 84.8 (1'C), 70.4 (3'C), 65.2 (5'C), 55.0 (OCH_3), 39.5 (C11), 28.4 (C10), 16.3 (C9)

LRMS **(ES^+)** 856.4 $[M+Na]^+$

HRMS 856.3208 $[M+Na]^+$ Expected 856.3205 ($C_{50}H_{47}N_3NaO_9$)

R_f 0.47 (eluent 10%MeOH/DCM) visualized using UV light and anisaldehyde stain.

5'-*O*- (4,4'-Dimethoxytrityl)-2'-deoxy-3'-cyanoethyl, N,N disopropyl phosphoramidite-5-(pentyn-1-yl-5-Fmoc) uridine [6]

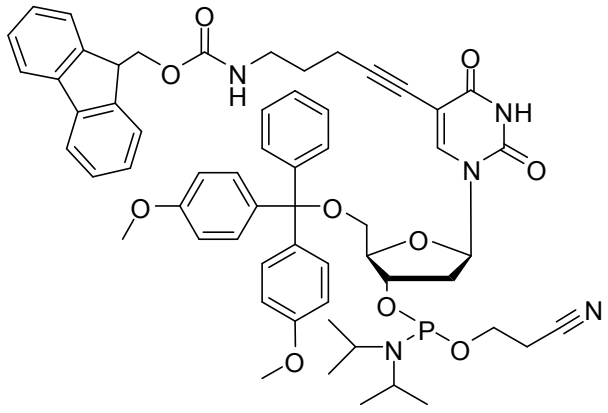

Compound 5 (1.889 g/2.27 mmol) was dissolved in distilled DCM (25ml) in an inert atmosphere and distilled DIPEA (0.82 mL/4.72 mmol). The phosphitylating agent (0.61 mL/2.72 mmol) was then added and the reaction mixture was stirred under argon for 1.5 hours, monitored by TLC (eluent 4:1 EtOAc:Hexane). Once the reaction was complete the

reaction mixture was washed using saturated KCl and dried over sodium sulphate (still in an inert atmosphere). The resulting solvent was evaporated off and the resulting solid was dried under high vacuum for 1 hour and the purified using column chromatography (eluent 70% EtOAc:Hexane) under argon and evaporated to dryness and dried under high vacuum. This gave 1.576 g of a pure white foam (67% yield).

^{1}H NMR **δ_H ppm** (300MHz, DMSO) 7.89 (4H, m, Fmoc) , 7.68 (2H, m, Fmoc), 7.2-7.4 (m, DMT Ar CH), 6.87 (4H, m, DMT Ar C-H), 6.13 (1H, q, *J* 6.2, 1'CH), 5.42 (1H, s, 3'OH), 4.20 (1H, m, 3'CH), 3.72 (6H, s, DMT OMe), 3.62 (m, CH_2, 29), 3.55 (m, CH, 26), 3.25 (2H, m, 5'CH_2), 2.96 (2H, m, CH_2, 11), 2.75 (2H, t, *J* 5.86, CH_2, 30), 2.67 (2H, t, *J* 6.0, CH_2, 30), 2.39 (2H, m, 2' CH_2), 2.18 (2H, q, *J* 7.5, CH_2, 9), 1.46 (2H, q, *J* 6.6, CH_2, 10), 1.13 (9H, m, CH_3, 27), 0.99 (2H, d, *J* 6.8, CH_3, 27)

^{13}C NMR **δ_c ppm**, 158.1 (C2), 149.3 (C6), 143.9 (C13), 140.7 135.2 128.9 127.5 127.0 125.1 (**C**H^{Ar}), 121.3 (C31), 120.0 113.1 (**C**H^{Ar}), 99.3 (C9), 85.9 (4'C), 84.8 (1'C), 72.4 (3'C), 65.2 (5'C), 58.5 (C29), 54.8 (OCH_3), 46.8 (C5), 39.5 (C11), 28.4 (C10), 24.2 (C27), 19.7 (C30), 16.3 (C9)

^{31}P NMR **δ_H ppm** 148.1 (d, *J* 17920.0)
(300MHz, DMSO)

R_f 0.49 (eluent 5%MeOH/DCM) visualized using UV light and anisaldehyde stain.

6.2 Analytical techniques

6.2.1 Chromatography

6.2.1.1 Column chromatography

Column chromatography was carried out under pressure using Fisher Scientific Davisil 60A (35-70 μ) silica. TLC was performed using Merck Kieselgel 60 F_{24} sheets (0.22 mm thickness, aluminium backed). Compounds were visualized using irradiation at 254/365 nm, as well as staining with either anisaldhyde or potassium permanganate. Anisaldehyde (*para*-anisaldehyde 13.80 ml, glacial acetic acid 5.70 ml, concentrated sulphuric acid 18.75 ml, ethanol 507 ml) was used to stain compounds containing sugars and potassium permanganate (potassium permanganate 2 g, potassium carbonate 13.33 g, sodium hydroxide 3.33 ml, water 200 ml) was used to stain all other compounds. Compounds which also contained a 4, 4'-dimethoxytrityl group could be visualized prior to staining via heating, resulting in a strong orange colour.

6.2.1.2 Reverse phase HPLC

For reverse phase HPLC the purification was carried out using a Gilson pump system coupled to an ABI Aquapore column (C8), 8 mm x 250 mm, pore size 300 Å. Gradient elutions were performed varying the gradient depending on individual sample under analysis, using a mixture of 0.1 M ammonium acetate, pH 7.0 and 0.1 M ammonium acetate with 50% acetonitrile pH 7.0. The run time was 30 minutes and the samples were eluted at a rate of 4 mL/ minute and monitored by ultraviolet absorbance at 260 nm with an Applied Biosystems 785A absorbance detector.

6.2.1.3 Gel Filtration

Gel filtration was performed using an XK 16/20 column packed with either superdex^{TM} 75 or superdex^{TM} 200 resin purchased from GE Healthcare and a Gilson 306 pump combined with an Applied Biosystems 785A absorbance detector. The column was equilibrated using 10 mM phosphate buffer containing 0.1 M sodium chloride and the samples were loaded in 300 μL volumes. The samples were eluted at a rate of 0.5 mL/minute using 10 mM phosphate buffer containing 0.1 M sodium chloride and were monitored using ultraviolet absorbance at 260 nm.

6.3 Oligonucleotide synthesis

Standard DNA phosphoramidites, solid supports and additional reagents were purchased from Link Technologies Ltd, Sigma and Applied Biosystems Ltd. For 3'-labelling, C7-aminoalkyl and C7-fluorescein (FAM) synthesis columns were obtained from Link Technologies Ltd and Cy3, Cy5 and dithiol phosphoramidites were purchased from Glen Research Inc. Fluorescein, JOE, texas red, Cy3, Cy3.5, Cy5, Cy5.5 and Cy3B NHS esters were purchased from Invitrogen Inc and C6-amino dT was purchased from Link Technologies Ltd. All oligonucleotides were synthesized on an Applied Biosystems 394 automated DNA/RNA synthesizer using a standard 0.2 or 1.0 μmole phosphoramidite cycles of acid-catalyzed detritylation, coupling, capping and iodine oxidation. Stepwise coupling efficiencies and overall yields were determined by the automated trityl cation conductivity monitoring facility and in all cases were >98.0%. All β-cyanoethyl phosphoramidite monomers were dissolved in anhydrous acetonitrile to a concentration of 0.1 M immediately prior to use. The coupling time for normal (A, G, C, T) monomers was 25 s and the coupling time for the modified monomers was extended to 360 s. Cleavage of oligonucleotides from the solid support and deprotection was achieved by exposure to concentrated aqueous ammonia for 60 min at room temperature followed by heating in a sealed tube for 5 h at 55 °C. Oligonucleotides labeled with 5'-Cy3 and 5'-Cy5 were

prepared by adding the appropriate Cy phosphoramidite monomer at the final addition in solid-phase synthesis. The Cy3 and Cy5 chromophores are unstable to prolonged exposure to ammonia so 5'-Cy oligonucleotides were synthesized using fast deprotecting dmf-G and Ac-dC phosphoramidite monomers, cleaved from the resin by treatment with concentrated aqueous ammonia for 60 min at room temperature then deprotected for 1 h at 55 °C. The 3'-FAM oligonucleotide was synthesised starting from a FAM C7 column and 3'- Cy5 and Texas Red-labelled oligonucleotides and internal Cy3, Cy3.5, Cy5, Cy5.5, Cy3B, JOE and Texas Red oligonucleotides were synthesised by post-synthetic labeling of C6-amino dT or 3'-aminoalkyl oligonucleotides which were assembled using C7-aminolink solid support. These oligonucleotides were then labeled with the appropriate dye NHS ester as described below.

To incorporate the Cy3, Cy3.5, Cy5, Cy5.5, Cy3B, JOE or Texas Red chromophores at the 3'-end of C7-aminoalkyl oligonucleotides or internal C6-amino dT oligonucleotides, 50-150 nmol of the oligonucleotide in 70 µL of 0.5 M Na_2CO_3/$NaHCO_3$ buffer (pH 8.75) was incubated for 4 h at room temperature with 1 mg of the succinimidyl ester of Cy3, Cy3.5, Cy5, Cy5.5, Cy3B, JOE or Texas Red (Invitrogen) in 40 µL of DMSO. The crude oligonucleotides were purified by reversed-phase HPLC and desalted by NAP-10 gel-filtration according to the manufacturer's instructions (GE Healthcare). Reversed-phase HPLC purification was carried out on a Gilson system using an ABI Aquapore column (C8), 8 mm x 250 mm, pore size 300 Å. The following protocols were used: run time 30 min, flow rate 4 mL per min, binary system, gradient: time in min (% buffer B);0 (0); 3 (0); 5 (10); 21 (40); 21(60)* 25 (100); 27 (0); 30 (0). Elution buffer A: 0.1 M ammonium acetate, pH 7.0, buffer B: 0.1 M ammonium acetate with 50% acetonitrile pH 7.0. **The % buffer B at 21 min was 40% for all oligonucleotides except those containing the hydrophobic Cy3, Cy3.5, Cy5, Cy5.5, Cy3B, JOE or Texas Red dyes which required 60% buffer B.* Elution of oligonucleotides was monitored by ultraviolet absorption at 295 nm. Texas Red oligonucleotides gave two product peaks corresponding to the 5- and 6-regioisomers of Texas Red. The first peak (5-isomer) was collected and used in the subsequent SERS and FRET efficiency experiments and the second peak was discarded. After HPLC purification oligonucleotides were desalted using NAP-10 Sephadex columns

(GE Healthcare), aliquoted into eppendorf tubes and stored at –20 ºC. All oligonucleotides were characterized by MALDI-TOF or electrospray mass spectrometry.

6.4 Quantum dot conjugation

6.4.1 Solution phase coupling

Peptide coated quantum dots (0.25 mg) were dissolved in 100 μL water and to this 100 μL of EDC in water (0.03 M) was added and the solution was mixed at room temperature for 20 minutes. To this solutions of either N-hydroxysuccinamide (0.25 mg) or pentafluorophenol (0.25 mg) were added dissolved in the minimum amount of water. This was left at toom temperature for a further 15 minutes. Reaction mixtures diluted to 1 mL with water and then purified using gel filtration (NAP 10 sephadex). The resulting solution was then freeze dried, and was dissolved in 100 μL of pH 8.68 buffer ($NaHCO_3$) and 100 μL of the amino modified oligonucleotide (200 μM) was added and the mixture was left at room temperature for 6 hours then analyzed by HPLC.

6.4.2 Solid phase Coupling

Peptide coated quantum dots (0.25 mg) were dissolved in 100 μL pH 7.2 buffer (NaH_2PO_4 0.1 M) and to this HBTU in DMF (0.76 mg/10 μL) was added. This was left at room temperature for 15 minutes. The reaction mixture was added to 3.3 mg of oligonucleotide modified CPG resin direct from oligonucleotide synthesis. This was then mixed and left at room temperature in dark conditions for three hours and then the resin was washed with water, methanol and ether, and then the resin was dried by mild heating to remove any remaining ether. This resin was then treated with a 1:1 mixture of concentrated ammonia and methylamine (40 % in water, 300 μL) at 55°C for 15 minutes. The resulting solution

was then decanted off of the resin and mildly heated to remove the methylamine and ammonia.

6.5 Biophysical analysis

6.5.1 Fluorescence melting

Fluorescence melting samples were prepared using a labelled oligonucleotide concentration of 0.15 μM and a target oligonucleotide concentration of 0.5 μM. Standard experiments used salt concentrations of either 100 mM NaCl or 2.5 mM $MgCl_2$ and an appropriate buffer to achieve desired pH (either phosphate or PCR).

For fixed wavelength samples experiments were performed using a Roche LightCycler 1.5 using glass capillaries with a 20 μL sample volume with an excitation wavelength of 470 nm and detection wavelengths of 530, 645 and 710 nm. Samples were heated to 95 ºC for 2 minutes then cooled to 30 ºC at a rate of 0.1 ºC/sec with a 1 ºC step size and 30 second incubation time. The sample was then incubated at 30 ºC for 5 minutes then heated to 95 ºC at a rate of 0.1 ºC/sec with a 1 ºC step size and 30 second incubation time before being cooled to room temperature. The fluorescence intensity was recorded during both the cooling/heating stages to provide annealing/melting information.

Single wavelength analysis was performed using a Perkin Elmer LS 50B luminescence spectrometer fitted with a Perkin Elmer PTP1 peltier temperature control device using sample volumes of 200 μL and a collection angle of 90º. Prior to fluorescence melting the samples were annealed by heating to 75 ºC in a water bath and cooling to room temperature slowly. The sample specific optimal excitation and emission wavelengths were used and the sample was heated from 25 ºC to 85 ºC at a rate of 1 ºC/minute with a 1 ºC step size and 30 second equilibration time, recording the emission intensity as each step.

Multiplex samples or samples which required a range of emission wavelengths were analysed using a Perkin Elmer LS 50B luminescence spectrometer fitted with a Perkin Elmer PTP1 peltier temperature control device using sample volumes of 200 µL and a collection angle of 90º. Prior to fluorescence melting the samples were annealed by heating to 75 ºC in a water bath and cooling to room temperature slowly. A single excitation wavelength could be set at the optimal wavelength and an emission scan range covering all desired wavelengths. The sample was heated from 25 ºC to 85 ºC at a rate of 1 ºC/minute with a 1 ºC step size and 30 second equilibration time and emission scans performed at each step at a rate of 300 nm/minute.

6.5.2 Gel electrophoresis

6.5.2.1 Agarose gel electrophoresis

Agarose gel electrophoresis was performed using LE agarose (Promega, UK) stained with ethidium bromide and using a horizontal tank with TBE buffer. 1.6 g of LE agarose was added to 80 mL of TBE buffer and heated to boiling using a microwave. Once heated 50 µL of ethidium bromide in water (1 mg/mL) was added and the solution mixed and allowed to cool to below 50 ºC. Once cool the solution was added to the horizontal gel tank, adding the appropriate comb and then allowed to cool to room temperature. The comb was then removed and the gel immersed in TBE buffer. 10 µL of each sample and the appropriate DNA stepladder were mixed with 2 µL of a 6x loading dye (Promega, UK) and loaded onto the gel. A voltage of 120 V was then applied to the gel until the marker dye had reached approximately 2/3 of the gel distance. The gel was then removed from the tank and imaged using a Syngene genius bio-imaging system using UV light.

6.5.2.2 Polyacrylamide gel electrophoresis

Polyacrylamide gel electrophoresis was performed using acrylamide (40% in water, Fisher) with TBE buffer containing urea and crosslinked using N, N, N', N'-tetramethylethylenediamine and ammonium perfulphate, and the concentration of acrylamide varied to alter separation (10-20%). This was performed using a vertical electrophoresis tank with an applied power of 20 W. Once complete the gel was imaged using a Syngene genius bio-imaging system using UV light.

6.5.3 Atomic Force microscopy

All AFM imaging was performed using a Multimode Nanoscope IIIa (Digital instruments, Santa Barbara) in tapping mode, using silicon nitride tips (Si3N4) for aqueous samples and FESP tips for samples in air. The scan size was 0.5-2 μm with scan rates of 1-2 Hz at a resolution of 256x256 and 512x512 pixels. Samples were prepared by making a 2-5 μM sample in water (sometimes containing 500mM NaCl). A 9 mm mica sample disc was prepared by removing the top layer using selotape, to give a freshly cleaved mica surface. This surface was then treated with 5 μL $MgCl_2$ (25 mM) and left for two minutes and then washed with a flow of water for ten seconds. The excess water was then removed using the corner of a piece of filter paper and the sample disc carefully dried using compressed air. The sample solution could then be deposited onto the sample disc and left to dry by evaporation and water added if the sample is to be scanned in water leaving the sample ready for imaging.

6.6 Molecular biology

6.6.1 PCR

Standard asymmetric PCR experiments were performed using a reaction volume of 20 μL containing a forward primer concentration of 0.2 μM and reverse primer concentration of 0.05 μM. 1 mM dNTPs (Promega, UK) and 1 unit hot start DNA polymerase (either Eppendorf HotMaster® or Qiagen Taq DNA polymerase) were used. Salt concentration was 2.5 mM $MgCl_2$ as standard (optimised for specific primer/template sequences) and buffers used were specific to the enzyme source (Promega/Qiagen) and diluted as per manufacturers instructions. The PCR reactions were performed using a thermocycler (Eppendorf Mastercycler Gradient) with a denaturation step of 95 °C for 2 minutes (15 minutes for Qiagen Taq DNA polymerase), followed by 15 cycles of 94 °C for 20 s, 54 °C for 45 s and 70 °C for 45 s. PCR products were analysed by 2% agarose gel electrophoresis stained with ethidium bromide.

6.7 SERS melting

SERS melting experiments were carried out using a custom designed micro-Raman cell (Ventacon Ltd, UK) and Raman spectra recorded using a ULWD 50x objective (NA: 0.5) on a Renishaw 2000 Raman microscope instrument equipped with a 632.8 nm He-Ne laser with a laser spot size of 1 μM.

Thermal melting ramped the temperature from 25 °C to 70 °C at a rate of 1 °C/minute and the Raman spectra recorded at 1 °C intervals using 10 mM phosphate buffer containing 100 mM. *E*melting experiments ramped the potential from 0.0 V to -1.6 V in 100 mV steps with an equilibration time of 5 minutes and the Raman spectra recorded at each step.

Chapter 7

7.0 References

7.0 References

(1) Blackburn, G. M. *Nucleic acids in chemistry and biology*; Oxford University Press, 1990.
(2) Watson J.D; Crick, F. C. *Nature* **1953**, *171*, 737.
(3) Chargaff, E.; Vischer, E.; Doniger, R.; Green, C.; Misani, F. *J. Biol. Chem.* **1949**, *177*, 405.
(4) Chargaff, E. *Fed Proc* **1951**, *10*, 654.
(5) Egholm, M.; Buchardt, O.; Christensen, L.; Behrens, C.; Freier, S. M.*et al. Nature* **1993**, *365*, 566.
(6) Watson, J. D. *Molecular Biology of the Gene (5th edition)*; Cold Spring Harbor Laboratory Press, 2005.
(7) Newton, G.; Welcome trust: 2005.
(8) Ju, J. Y.; Kim, D. H.; Bi, L. R.; Meng, Q. L.; Bai, X. P.*et al. Proc. Natl. Acad. Sci. U. S. A.* **2006**, *103*, 19635.
(9) Bentley, D. R.; Balasubramanian, S.; Swerdlow, H. P.; Smith, G. P.; Milton, J.*et al. Nature* **2008**, *456*, 53.
(10) Lakowicz, J. R. *Principles of fluorescence spectroscopy*; Springer, 1999.
(11) Cox, W. G.; Singer, V. L. *Biotechniques* **2004**, *36*, 114.
(12) Kurian, A.; George, N. A.; George, S. D.; Unnikrishnan, K. P.; Paul, B.*et al. J. Opt.* **2002**, *31*, 29.
(13) Crimaldi, J. P. *Exp. Fluids* **1997**, *23*, 325.
(14) Ernst, L. A.; Gupta, R. K.; Mujumdar, R. B.; Waggoner, A. S. *Cytometry* **1989**, *10*, 3.
(15) Kvach, M. V.; Ustinov, A. V.; Stepanova, I. A.; Malakhov, A. D.; Skorobogatyi, M. V.*et al. Eur. J. Org. Chem.* **2008**, 2107.
(16) Xu, C. L.; Losytskyy, M. Y.; Kovalska, V. B.; Kryvorotenko, D. V.; Yarmoluk, S. M.*et al. J. Fluoresc.* **2007**, *17*, 671.
(17) Mader, O.; Reiner, K.; Egelhaaf, H. J.; Fischer, R.; Brock, R. *Bioconjugate Chem.* **2004**, *15*, 70.
(18) Grabolle, M.; Spieles, M.; Lesnyak, V.; Gaponik, N.; Eychmu□ller, A.*et al. Anal. Chem.* **2009**, *81*, 6285.
(19) Klimov, V. I. *Los Alamos science* **2003**, *28*, 214.
(20) Kloepfer, J. A.; Bradforth, S. E.; Nadeau, J. L. *J. Phys. Chem. B* **2005**, *109*, 9996.
(21) Chan, W. C. W.; Nie, S. M. *Science* **1998**, *281*, 2016.
(22) Kim, J. H.; Morikis, D.; Ozkan, M. *Sens. Actuator B-Chem.* **2004**, *102*, 315.
(23) Zhou, D. J.; Piper, J. D.; Abell, C.; Klenerman, D.; Kang, D. J.*et al. Chem. Commun.* **2005**, 4807.
(24) Mitchell, G. P.; Mirkin, C. A.; Letsinger, R. L. *J. Am. Chem. Soc.* **1999**, *121*, 8122.
(25) Wan, Y.; Wang, L. P.; Lin, Z. B.; Chen, Q. D.; Zhang, H.*et al. Can. J. Anal. Sci. Spectrosc.* **2004**, *49*, 99.
(26) Aldana, J.; Wang, Y. A.; Peng, X. G. *J. Am. Chem. Soc.* **2001**, *123*, 8844.

(27) Pathak, S.; Choi, S. K.; Arnheim, N.; Thompson, M. E. *J. Am. Chem. Soc.* **2001**, *123*, 4103.
(28) Gao, X. H.; Cui, Y. Y.; Levenson, R. M.; Chung, L. W. K.; Nie, S. M. *Nat. Biotechnol.* **2004**, *22*, 969.
(29) Wang, Y. A.; Li, J. J.; Chen, H. Y.; Peng, X. G. *J. Am. Chem. Soc.* **2002**, *124*, 2293.
(30) Han, M. Y.; Gao, X. H.; Su, J. Z.; Nie, S. *Nat. Biotechnol.* **2001**, *19*, 631.
(31) Selvin, P. R.; Hearst, J. E. *Proc. Natl. Acad. Sci. U. S. A.* **1994**, *91*, 10024.
(32) Matsumoto, K. In *11th International Conference on Biological Inorganic Chemistry*; Elsevier Science Inc: Caims, Australia, 2003, p 29.
(33) Nojima, T.; Kondoh, Y.; Takenaka, S.; Ichihara, T.; Takagi, M.*et al. Nucleic Acids Res Suppl* **2001**, 105.
(34) Carey, P. R.; Bernstei.Hj; Schneide.H *Biochem. Biophys. Res. Commun.* **1972**, *47*, 588.
(35) Carey, P. R. *J. Raman Spectrosc.* **1998**, *29*, 861.
(36) Cao, Y. W. C.; Jin, R. C.; Mirkin, C. A. *Science* **2002**, *297*, 1536.
(37) Stokes, R. J.; Macaskill, A.; Lundahl, P. J.; Smith, W. E.; Faulds, K.*et al. Small* **2007**, *3*, 1593.
(38) Arnheim, N.; Levenson, C. H. *Chem. Eng. News* **1990**, *68*, 36.
(39) Lenstra, J. A. *Cell. Mol. Biol.* **1995**, *41*, 603.
(40) Southern, E. M. *J. Mol. Biol.* **1975**, *98*, 503.
(41) Hammond, N.; Koumi, P.; Langley, G. J.; Lowe, A.; Brown, T. *Org. Biomol. Chem.* **2007**, *5*, 1878.
(42) Lakowicz, J. R.
(43) *Reviews in Molecular Biotechnology* **2002**, *82*, 177.
(44) Ciruela, F. *Curr. Opin. Biotechnol.* **2008**, *19*, 338.
(45) LeTilly, V.; Royer, C. A. *Biochemistry* **1993**, *32*, 7753.
(46) Patel, S.; Datta, A. *J. Phys. Chem. B* **2007**, *111*, 10557.
(47) Krishnan, C. V. R. K. S. *Nature* **1928**, *121*, 501.
(48) Mandelstam, G. L. L. *Naturwissenschaften*
1928, *16*, 557.
(49) Fleischmann, M.; Hendra, P. J.; McQuillan, A. J. *Chemical Physics Letters* **1974**, *26*, 163.
(50) Nie, S.; Emory, S. R. *Science* **1997**, *275*, 1102.
(51) Moskovits, M. *J. Chem. Phys.* **1978**, *69*, 1459.
(52) Moskovits, M. *Surface enhanced Raman scattering: Physics and applications*; Springer, 2006.
(53) Grasselli, J. *Analytical Raman spectroscopy*; Wiley-Interscience 1991.
(54) Mahajan, S.; Baumberg, J. J.; Russell, A. E.; Bartlett, P. N. *Phys. Chem. Chem. Phys.* **2007**, *9*, 6016.
(55) Orlando, C.; Pinzani, P.; Pazzagli, M. *Clin. Chem. Lab. Med.* **1998**, *36*, 255.
(56) Joo, C.; Balci, H.; Ishitsuka, Y.; Buranachai, C.; Ha, T. *Annual Review of Biochemistry* **2008**, *77*, 51.
(57) Cheng, S.; Fockler, C.; Barnes, W. M.; Higuchi, R. *Proc. Natl. Acad. Sci. U. S. A.* **1994**, *91*, 5695.

(58) Whitcombe, D.; Theaker, J.; Guy, S. P.; Brown, T.; Little, S. *Nat Biotech* **1999**, *17*, 804.
(59) Livak, K. J.; Flood, S. J.; Marmaro, J.; Giusti, W.; Deetz, K. *Genome. Res.* **1995**, *4*, 357.
(60) French, D. J.; Howard, R. L.; Gale, N.; Brown, T.; McDowell, D. G.*et al. Forensic Sci. Int.-Genet.* **2008**, *2*, 333.
(61) Saiki, R.; Gelfand, D.; Stoffel, S.; Scharf, S.; Higuchi, R.*et al. Science* **1988**, *239*, 487.
(62) Mackay, I. M.; Arden, K. E.; Nitsche, A. *Nucl. Acids Res.* **2002**, *30*, 1292.
(63) Innis, M. A.; Myambo, K. B.; Gelfand, D. H.; Brow, M. A. *Proc. Natl. Acad. Sci. U. S. A.* **1988**, *85*, 9436.
(64) Eaker, S.; Johnson, M.; Jenkins, J.; Bauer, M.; Little, S. *Biosense. Bioelectron* **2005**, *21*, 933.
(65) Costa, C.; Costa, J.-M.; Martin, J.; Boissier, B.; Goossens, M.*et al. Clin Chem* **2008**, *54*, 1564.
(66) Newton, C. R.; Graham, A.; Heptinstall, L. E.; Powell, S. J.; Summers, C.*et al. Nucl. Acids Res.* **1989**, *17*, 2503.
(67) Pinkel, D.; Landegent, J.; Collins, C.; Fuscoe, J.; Segraves, R.*et al. Proc. Natl. Acad. Sci. U. S. A.* **1988**, *85*, 9138.
(68) Nath, J.; Johnson, K. L. *Biotech. Histochem.* **2000**, *75*, 54.
(69) Sieben, V. J.; Marun, C. S. D.; Pilarski, P. M.; Kaigala, G. V.; Pilarski, L. M.*et al. IET Nanobiotechnol.* **2007**, *1*, 27.
(70) Patrinos, G. P. *Molecular diagnostics*; Academic Press, 2005.
(71) French, D. J.; Archard, C. L.; Brown, T.; McDowell, D. G. *Mol. Cell. Probes* **2001**, *15*, 363.
(72) French, D. J.; McDowell, D. G.; Debenham, P.; Gale, N.; Brown, T. In *Methods in Molecular Biology*; Marx, A., Seitz, O., Eds.; Humana Press Inc: 2008, p 171.
(73) Dobson, N.; McDowell, D. G.; French, D. J.; Brown, L. J.; Mellor, J. M.*et al. Chem. Commun.* **2003**, 1234.
(74) Gale, N.; French, D. J.; Howard, R. L.; McDowell, D. G.; Debenham, P. G.*et al. Org. Biomol. Chem.* **2008**, *6*, 4553.
(75) Broude, N. E. *Trends. Biotechnol.* **2002**, *20*, 249.
(76) Tyagi, S.; Kramer, F. R. *Nat. Biotechnol.* **1996**, *14*, 303.
(77) Tyagi, S.; Bratu, D. P.; Kramer, F. R. *Nat Biotech* **1998**, *16*, 49.
(78) Kostrikis, L. G.; Tyagi, S.; Mhlanga, M. M.; Ho, D. D.; Kramer, R. F. *Science* **1998**, *279*, 1228.
(79) Piatek, A. S.; Tyagi, S.; Pol, A. C.; Telenti, A.; Miller, L. P.*et al. Nat Biotech* **1998**, *16*, 359.
(80) Vet, J. A. M.; Majithia, A. R.; Marras, S. A. E.; Tyagi, S.; Dube, S.*et al. Proc. Natl. Acad. Sci. U. S. A.* **1999**, *96*, 6394.
(81) Kim, J. H.; Morikis, D.; Ozkan, M. *Sensors and Actuators B: Chemical* **2004**, *102*, 315.
(82) Dubertret, B.; Calame, M.; Libchaber, A. J. *Nat Biotech* **2001**, *19*, 365.
(83) Ortiz, E.; Estrada, G.; Lizardi, P. M. *Mol. Cell. Probes* **1998**, *12*, 219.

(84) Solinas, A.; Brown, L. J.; McKeen, C.; Mellor, J. M.; Nicol, J.*et al. Nucl. Acids Res.* **2001**, *29*, e96.
(85) Thelwell, N.; Millington, S.; Solinas, A.; Booth, J.; Brown, T. *Nucl. Acids Res.* **2000**, *28*, 3752.
(86) Milanovich, F. *Science & Technology Review* **1998**, *June*, 4.
(87) Vo-Dinh, T.; Houck, K.; Stokes, D. L. *Anal. Chem.* **1994**, *66*, 3379.
(88) Culha, M.; Stokes, D.; Allain, L. R.; Vo-Dinh, T. *Anal. Chem.* **2003**, *75*, 6196.
(89) T. Vo-Dinh, D. L. S., G. D. Griffin, M. Volkan, U. J. Kim, M. I. Simon, *J. Raman Spectrosc.* **1999**, *30*, 785.
(90) Graham, D.; Mallinder, B. J.; Whitcombe, D.; Watson, N. D.; Smith, W. E. *Anal. Chem.* **2002**, *74*, 1069.
(91) Faulds, K.; Fruk, L.; Robson, D. C.; Thompson, D. G.; Enright, A.*et al. Faraday. Discuss.* **2006**, *132*, 261.
(92) Duncan Graham, B. J. M., W. Ewan Smith, *Angewandte Chemie International Edition* **2000**, *39*, 1061.
(93) Sosnowski, R. G.; Tu, E.; Butler, W. F.; Oâ€™Connell, J. P.; Heller, M. J. *Proc. Natl. Acad. Sci. U. S. A.* **1997**, *94*, 1119.
(94) Wei, F.; Chen, C.; Zhai, L.; Zhang, N.; Zhao, X. S. *J. Am. Chem. Soc.* **2005**, *127*, 5306.
(95) Murray, C. B.; Kagan, C. R.; Bawendi, M. G. *Annual Review of Materials Science* **2000**, *30*, 545.
(96) Alivisatos, A. P. *The Journal of Physical Chemistry* **1996**, *100*, 13226.
(97) Yu, M.; Fernando, G. W.; Li, R.; Papadimitrakopoulos, F.; Shi, N.*et al. Applied Physics Letters* **2006**, *88*, 231910.
(98) Wang, X.; Qu, L.; Zhang, J.; Peng, X.; Xiao, M. *Nano Letters* **2003**, *3*, 1103.
(99) Xia, Y.; Zhang, T.; Diao, X.; Zhu, C. *Chemistry Letters* **2007**, *36*, 242.
(100) Pinaud, F.; King, D.; Moore, H. P.; Weiss, S. *J. Am. Chem. Soc.* **2004**, *126*, 6115.
(101) Tsay, J. M.; Doose, S.; Pinaud, F.; Weiss, S. *J. Phys. Chem. B* **2005**, *109*, 1669.
(102) Tsay, J. M.; Doose, S.; Pinaud, F.; Weiss, S. *P. Soc. Photo-opt. Ins.* **2005**, *5705*, 139.
(103) French, D. J.; McDowell, D. G.; Debenham, P.; Gale, N.; Brown, T. *Method. Mol. Biol.* **2008**, 171.
(104) Robins, M. J.; Barr, P. J. *The Journal of Organic Chemistry* **1983**, *48*, 1854.
(105) Dogan, Z.; Paulini, R.; Rojas Stutz, J. A.; Narayanan, S.; Richert, C. *J. Am. Chem. Soc.* **2004**, *126*, 4762.
(106) Tuma, J.; Paulini, R.; Rojas Stutz, J. A.; Richert, C. *Biochemistry* **2004**, *43*, 15680.
(107) Cruickshank, K. A.; Daniel L, S. *Tetrahedron Letters* **1988**, *29*, 5221.
(108) Ranasinghe, R. T.; Rusling, D. A.; Powers, V. E. C.; Fox, K. R.; Brown, T. *Chem. Commun.* **2005**, 2555.
(109) McGuigan, C.; Barucki, H.; Blewett, S.; Carangio, A.; Erichsen, J. T.*et al. Journal of Medicinal Chemistry* **2000**, *43*, 4993.

(110) Karunakaran, V.; Perez Lustres, J. L.; Zhao, L.; Ernsting, N. P.; Seitz, O. *J. Am. Chem. Soc.* **2006**, *128*, 2954.
(111) Yarmoluk, S. M.; Lukashov, S. S.; Ogul'chansky, T. Y.; Losytskyy, M. Y.; Kornyushyna, O. S. *Biopolymers* **2001**, *62*, 219.
(112) Karunakaran, V.; Lustres, J. L. F.; Zhao, L. J.; Ernsting, N. P.; Seitz, O. *J. Am. Chem. Soc.* **2006**, *128*, 2954.
(113) Hannah, K. C.; Armitage, B. A. *Accounts Chem. Res.* **2004**, *37*, 845.
(114) Chowdhury, A.; Wachsmann-Hogiu, S.; Bangal, P. R.; Raheem, I.; Peteanu, L. A. *J. Phys. Chem. B* **2001**, *105*, 12196.
(115) Mikheikin, A. L.; Zhuze, A. L.; Zasedatelev, A. S. *J. Biomol. Struct. Dyn.* **2000**, *18*, 59.
(116) Cooper, M.; Ebner, A.; Briggs, M.; Burrows, M.; Gardner, N.*et al. J. Fluoresc.* **2004**, *14*, 145.
(117) Bartlett, P. N.; Baumberg, J. J.; Birkin, P. R.; Ghanem, M. A.; Netti, M. C. *Chemistry of Materials* **2002**, *14*, 2199.
(118) Kelf, T. A.; Sugawara, Y.; Baumberg, J. J.; Abdelsalam, M.; Bartlett, P. N. *Physical Review Letters* **2005**, *95*, 116802.
(119) Abdelsalam, M. E.; Bartlett, P. N.; Baumberg, J. J.; Cintra, S.; Kelf, T. A.*et al. Electrochemistry Communications* **2005**, *7*, 740.
(120) Baumberg, J. J.; Kelf, T. A.; Sugawara, Y.; Cintra, S.; Abdelsalam, M. E.*et al. Nano Letters* **2005**, *5*, 2262.
(121) Mahajan, S.; Abdelsalam, M.; Suguwara, Y.; Cintra, S.; Russell, A.*et al. Physical Chemistry Chemical Physics* **2007**, *9*, 104.
(122) Mahajan, S.; Richardson, J.; Ben Gaied, N.; Zhao, Z.; Brown, T.*et al. Electroanalysis*, *In press*.
(123) Mahajan, S.; Richardson, J.; Brown, T.; Bartlett, P. N. *J. Am. Chem. Soc.* **2008**, *130*, 15589.

Chapter 8

8.0 Publications

J|A|C|S
ARTICLES
Published on Web 10/29/2008

SERS-Melting: A New Method for Discriminating Mutations in DNA Sequences

Sumeet Mahajan, James Richardson, Tom Brown, and Philip N. Bartlett*

School of Chemistry, University of Southampton, Southampton SO17 1BJ, United Kingdom

Received July 16, 2008; E-mail: pnb@soton.ac.uk

Abstract: The reliable discrimination of mutations, single nucleotide polymorphisms (SNPs), and other differences in genomic sequence is an essential part of DNA diagnostics and forensics. It is commonly achieved using fluorescently labeled DNA probes and thermal gradients to distinguish between the matched and mismatched DNA. Here, we describe a novel method that uses surface enhanced (resonance) Raman spectroscopy (SER(R)S) to follow denaturation of dsDNA attached to a structured gold surface. This denaturation is driven either electrochemically or thermally on SERS active sphere segment void (SSV) gold substrates. Using this method, we can distinguish between wild type, a single point mutation (1653C/T), and a triple deletion (ΔF 508) in the CFTR gene at the 0.02 attomole level, and the method can be used to differentiate the unpurified PCR products of the wild type and ΔF 508 mutation. Our method has the potential to provide small, rapid, sensitive, reproducible platforms for detecting genetic variations and sequencing genes.

Introduction

The development of simple, reliable, high-throughput methods to detect genetic variations in DNA is crucial for the development of DNA-based diagnostics and forensics. A variety of methods for identifying mutations[1] have been described in the literature using either solution-based or surface methods. Solution-based methods include the identification of single-strand conformational polymorphism,[2,3] use of denaturing gradient gel electrophoresis,[2,4] or quantitative polymerase chain reaction-based approaches. The latter have the advantages that they do not require a chromatographic separation step and that they can be used to detect several sequences simultaneously. The most widely used methods are based on fluorescent detection schemes such as those used in Molecular Beacons,[5] Taqman,[6] Scorpions,[7] or Hybridization Probes.[8]

The use of surface-based approaches offers the attraction of an array approach to the detection of mutations, the opportunity to control the conditions locally at the surface, and the ability to produce simple, portable biosensor devices. A variety of sensing approaches have been investigated including the measurement of mass changes using a quartz crystal microbalance,[9,10] nanomechanical detection using microcantilevers,[11] local refractive index changes using surface plasmon resonance,[12,13] electrochemical changes[14−16] using either impedance measurements[17−20] or redox labels,[21−26] and fluorescence;[27−29] of these, only a few utilize differential denaturation (melting analysis) on solid substrates.[13]

In a typical solid-phase analytical system relying on differential denaturation analysis, a single-strand DNA (ssDNA)

(1) Nollau, P.; Wagener, C. *Clin. Chem.* **1997**, *43*, 1114.
(2) Bernat, M.; Titos, E.; Clària, J. *Genet. Mol. Res.* **2002**, *1*, 72.
(3) Orita, M.; Iwahana, H.; Kanazawa, H.; Hayashi, K.; Sekiya, T. *Proc. Natl. Acad. Sci. U.S.A.* **1989**, *86*, 2766.
(4) Myers, R.; Fischer, S.; Lerman, L.; Maniatis, T. *Nucleic Acids Res.* **1985**, *13*, 3131.
(5) Tyagi, S.; Kramer, F. R. *Nat. Biotechnol.* **1996**, *14*, 303.
(6) Holland, P. M.; Abramson, R. D.; Watson, R.; Gelfand, D. H. *Proc. Natl. Acad. Sci. U.S.A.* **1991**, *88*, 7276.
(7) Whitcombe, D.; Theaker, J.; Guy, S. P.; Brown, T.; Little, S. *Nat. Biotechnol.* **1999**, *17*, 804.
(8) Wittwer, C. T.; Herrmann, M. G.; Moss, A. A.; Rasmussen, R. P. *BioTechniques* **1997**, *22*, 130.
(9) Caruso, F.; Rodda, E.; Furlong, D. N.; Niikura, K.; Okahata, Y. *Anal. Chem.* **1997**, *69*, 2043.
(10) Okahata, Y.; Kawase, M.; Niikura, K.; Ohtake, F.; Furusawa, H.; Ebara, Y. *Anal. Chem.* **1998**, *70*, 1288.
(11) McKendry, R.; Zhang, J. Y.; Arntz, Y.; Strunz, T.; Hegner, M.; Lang, H. P.; Baller, M. K.; Certa, U.; Meyer, E.; Guntherodt, H. J.; Gerber, C. *Proc. Natl. Acad. Sci. U.S.A.* **2002**, *99*, 9783.
(12) Nakatani, K.; Sando, S.; Saito, I. *Nat. Biotechnol.* **2001**, *19*, 51.
(13) Thiel, A. J.; Frutos, A. G.; Jordan, C. E.; Corn, R. M.; Smith, L. M. *Anal. Chem.* **1997**, *69*, 4948.
(14) Gooding, J. J. *Electroanalysis* **2002**, *14*, 1149.
(15) Kerman, K.; Kobayashi, M.; Tamiya, E. *Meas. Sci. Technol.* **2004**, *15*, R1.
(16) Drummond, T. G.; Hill, M. G.; Barton, J. K. *Nat. Biotechnol.* **2003**, *21*, 1192.
(17) Li, X.; Lee, J. S.; Kraatz, H.-B. *Anal. Chem.* **2006**, *78*, 6096.
(18) Lee, T.; Shim, Y. *Anal. Chem.* **2001**, *73*, 5629.
(19) Li, C. Z.; Long, Y. T.; Lee, J. S.; Kraatz, H. B. *Chem. Commun.* **2004**, 574.
(20) Long, Y.-T.; Li, C.-Z.; Sutherland, T. C.; Kraatz, H.-B.; Lee, J. S. *Anal. Chem.* **2004**, *76*, 4059.
(21) Hashimoto, K.; Ito, K.; Ishlmori, Y. *Anal. Chem.* **1994**, *66*, 3830.
(22) Ihara, T.; Nakayama, M.; Murata, M.; Nakano, K.; Maeda, M. *Chem. Commun.* **1997**, 1609.
(23) Millan, K. M.; Mikkelsen, S. R. *Anal. Chem.* **1993**, *65*, 2317.
(24) Paleček, E.; Masaň´k, M.; Kizek, R.; Kuhlmeier, D.; Hassmann, J.; Schülein, J. *Anal. Chem.* **2004**, *76*, 5930.
(25) Wang, J.; Xu, D.; Kawde, A.; Polsky, R. *Anal. Chem.* **2001**, *73*, 5576.
(26) Yu, C. J.; Wan, Y.; Yowanto, H.; Li, J.; Tao, C.; James, M. D.; Tan, C. L.; Blackburn, G. F.; Meade, T. J. *J. Am. Chem. Soc.* **2001**, *123*, 11155.
(27) Ramachandran, A.; Flinchbauch, J.; Ayoubi, P.; Olah, G. A.; Malayer, J. R. *Biosens. Bioelectron.* **2003**, *19*, 727.
(28) Du, H.; Strohsahl, C. M.; Camera, J.; Miller, B. L.; Krauss, T. D. *J. Am. Chem. Soc.* **2005**, *127*, 7932.
(29) Wang, H.; Li, J.; Liu, H.; Liu, Q.; Mei, Q.; Wang, Y.; Zhu, J.; He, N.; Lu, Z. *Nucleic Acids Res.* **2002**, *30*, e61.

10.1021/ja805517q CCC: $40.75

probe is immobilized on the substrate and then hydridized to "target" sequences from solution. The resulting DNA duplexes are then denatured, typically either by ramping the temperature or by washing with solutions of decreasing ionic strength (stringency washing). Mutations are detected by monitoring the denaturation process; the mutations possess base pair mismatches, which destabilize the duplex relative to the perfectly complementary target, and therefore these duplexes denature more readily.

Although optical wave guides,[30] optical scan arrays,[31] and temperature gradient assay platforms[32] have been employed, fluorescence is currently the preferred technique for detecting mutations using this hybridization/denaturation strategy.[33] However, surface-enhanced Raman or resonant Raman scattering (SER(R)S) has been shown to possess significant advantages as compared to fluorescence;[34−36] these include the ability to multiplex because of the narrow line width (~10 nm) and molecular specificity of SER(R) spectra,[35,37] flexibility in the choice of labels,[38−40] insensitivity to quenching by oxygen or other species,[34] and excellent sensitivity.[38] In addition, SER(R)S has the benefit of using a single excitation wavelength without imposing any inflexibility on the choice of donor, which is the case in FRET (Forster or fluorescence resonance energy transfer). When compared to surface-plasmon resonance (SPR)[13] or electrochemical detection methods,[16] SER(R)S is molecule-specific and much more sensitive. Finally, SER(R)S is a highly surface-sensitive technique so that there is no significant interference from species that are not at or close to (typically <100 nm) the surface.

The application of SERS to analysis of DNA was pioneered by Vo-Dinh and colleagues[41] using rough silver surfaces formed by thermal evaporation of thin silver films onto 100 nm alumina particles dropped coated on glass. In these original experiments, DNA was hybridized on nitrocellulose membranes, and then the labeled double-stranded DNA was spotted onto the SERS substrate for analysis. In subsequent studies, they showed that SERS detection could be used on DNA arrays with multispectral imaging[42] and when the DNA probes were attached to the SERS active rough silver surface.[36,43,44] Flocculated silver colloids have also been used very successfully by Graham, Smith, and their colleagues for SER(R)S detection of DNA, including the use of different labels for multiplex geneotyping,[45] quantitative SERRS using two wavelengths and different dyes,[46,47] and the development of SERRS beacons.[48] In their recent work, they have shown that the same methods can be used on a commercially available structured gold surface.[49]

In our laboratory, we have been developing the fabrication of ordered sphere segment void (SSV) substrates by electrodeposition around templates made from close packed monolayers of uniform submicrometer diameter polystyrene spheres.[50] Removal of the polystyrene template by dissolution in a suitable solvent leaves a smooth sculpted metal surface with low surface roughness. We have studied the reflection spectra of these structures in detail[51−55] and shown that these metamaterials generate intense local electric fields under illumination and that, as a result, they are excellent substrates for SERS.[52,56] The optical properties of these substrates can be tuned[57,58] through the choice of sphere diameter and film thickness so that typical surface enhancements of the order of 10^6 have been demonstrated for structured gold substrates.[59] The sensitivity of detection can be further increased by selecting molecules that have an electronic transition in resonance with the laser excitation so that the surface enhancement is accompanied by a further resonant enhancement of $\sim 10^3$ to give surface-enhanced resonance Raman scattering (SERRS).[60] These SSV surfaces show excellent stability in solution and can be used as electrodes and still give stable repeatable SER(R)S.[61] The SSV surfaces differ in their structure from both the nanotriangle surfaces[62] and the metal film on nanosphere (MFON) surfaces[63] produced by Van Duyne and co-workers using similar colloidal particle templates. In the case of the SSV surfaces, both the sphere diameter and the film thickness can be varied independently to control the optical properties.

(30) Stimpson, D. I.; Hoijer, J. V.; Hsieh, W. T.; Jou, C.; Gordon, J.; Theriault, T.; Gamble, R.; Baldeschwieler, J. D. *Proc. Natl. Acad. Sci. U.S.A.* **1995**, *92*, 6379.
(31) Khomyakova, E. B.; Dreval, E. V.; Tran-Dang, M.; Potier, M. C.; Soussaline, F. P. *Cell. Mol. Biol.* **2004**, *50*, 217.
(32) Mao, H.; Holden, M. A.; You, M.; Cremer, P. S. *Anal. Chem.* **2002**, *74*, 5071.
(33) Ranasinghe, R. T.; Brown, T. *Chem. Commun.* **2005**, 5487.
(34) Braun, G.; Lee, S. J.; Dante, M.; Nguyen, T. Q.; Moskovits, M.; Reich, N. *J. Am. Chem. Soc.* **2007**, *129*, 6378.
(35) Cao, Y. C.; Jin, R.; Mirkin, C. A. *Science* **2002**, 1536.
(36) Culha, M.; Stokes, D.; Allain, L. R.; Vo-Dinh, T. *Anal. Chem.* **2003**, *75*, 6196.
(37) Stokes, R. J.; Macaskill, A.; Lundahl, P. J.; Smith, W. E.; Faulds, K.; Graham, D. *Small* **2007**, *3*, 1593.
(38) Faulds, K.; Barbagallo, R. P.; Keer, J. T.; Smith, W. E.; Graham, D. *Analyst* **2004**, *129*, 567.
(39) Faulds, K.; Smith, W. E.; Graham, D. *Anal. Chem.* **2004**, *76*, 412.
(40) Graham, D.; Smith, W. E.; Linacre, A. M. T.; Munro, C. H.; Watson, N. D.; White, P. C. *Anal. Chem.* **1997**, *69*, 4703.
(41) Vo-Dinh, T.; Houck, K.; Stokes, D. L. *Anal. Chem.* **1994**, *66*, 3379.
(42) Vo-Dinh, T.; Stokes, D. L.; Griffin, G. D.; Volkan, M.; Kim, U. J.; Simon, M. I. *J. Raman Spectrosc.* **1999**, *30*, 785.
(43) Isola, N. R.; Stokes, D. L.; Vo-Dinh, T. *Anal. Chem.* **1998**, *70*, 1352.
(44) Vo-Dinh, T.; Allain, L. R.; Stokes, D. L. *J. Raman Spectrosc.* **2002**, *33*, 511.
(45) Graham, D.; Mallinder, B. J.; Whitcombe, D.; Watson, N. D.; Smith, W. E. *Anal. Chem.* **2002**, *74*, 1069.
(46) Faulds, K.; Stewart, L.; Smith, W. E.; Graham, D. *Talanta* **2005**, *67*, 667.
(47) Faulds, K.; McKenzie, F.; Smith, W. E.; Graham, D. *Angew. Chem., Int. Ed.* **2007**, *46*, 1829.
(48) Faulds, K.; Fruk, L.; Robson, D. C.; Thompson, D. G.; Enright, A.; Smith, W. E.; Graham, D. *Faraday Discuss.* **2006**, *132*, 261.
(49) Stokes, R. J.; Macaskill, A.; Dougan, J. A.; Hargreaves, P. G.; Stanford, H. M.; Smith, W. E.; Faulds, K.; Graham, D. *Chem. Commun.* **2007**, 2811.
(50) Bartlett, P. N.; Baumberg, J. J.; Birkin, P. R.; Ghanem, M. A.; Netti, M. C. *Chem. Mater.* **2002**, *14*, 2199.
(51) Netti, M. C.; Coyle, S.; Baumberg, J. J.; Ghanem, M. A.; Birkin, P. R.; Bartlett, P. N.; Whitaker, D. M. *Adv. Mater.* **2001**, *13*, 1368.
(52) Kelf, T. A.; Sugawara, Y.; Baumberg, J. J.; Abdelsalam, M.; Bartlett, P. N. *Phys. Rev. Lett.* **2005**, *95*, 116802.
(53) Kelf, T. A.; Sugawara, Y.; Cole, R. M.; Baumberg, J. J.; Abdelsalam, M. E.; Cintra, S.; Mahajan, S.; Russell, A. E.; Bartlett, P. N. *Phys. Rev. B* **2006**, *74*, 245415.
(54) Bartlett, P. N.; Baumberg, J. J.; Coyle, S.; Abdelsalem, M. *Faraday Discuss.* **2004**, *125*, 117.
(55) Cole, R. M.; Baumberg, J. J.; Abajo, F. J. G. d.; Mahajan, S.; Abdelsalam, M.; Bartlett, P. N. *Nano Lett.* **2007**, *7*, 2094.
(56) Abdelsalam, M. E.; Bartlett, P. N.; Baumberg, J. J.; Cintra, S.; Kelf, T.; Russell, A. E. *Electrochem. Commun.* **2005**, *7*, 740.
(57) Baumberg, J. J.; Kelf, T.; Sugawara, Y.; Cintra, S.; Abdelsalam, M.; Bartlett, P. N.; Russell, A. E. *Nano Lett.* **2005**, 2262.
(58) Mahajan, S.; Abdelsalam, M.; Suguwara, Y.; Cintra, S.; Russell, A.; Baumberg, J.; Bartlett, P. *Phys. Chem. Chem. Phys.* **2007**, *9*, 104.
(59) Cintra, S.; Abdelsalem, M.; Bartlett, P. N.; Baumberg, J. J.; Kelf, T.; Sugawara, Y.; Russell, A. E. *Faraday Discuss.* **2005**, *132*, 191.
(60) Mahajan, S.; Baumberg, J.; Russell, A.; Bartlett, P. *Phys. Chem. Chem. Phys.* **2007**, *9*, 6016.
(61) Abdelsalam, M.; Bartlett, P. N.; Russell, A. E.; Baumberg, J. J.; Calvo, E. J.; Tognalli, N. G.; Fainstein, A. *Langmuir* **2008**, *24*, 7018.
(62) Haynes, C. L.; Van Duyne, R. P. *J. Phys. Chem. B* **2001**, *105*, 5599.
(63) Dick, L. A.; McFarland, A. D.; Haynes, C. L.; Van Duyne, R. P. *J. Phys. Chem. B* **2002**, *106*, 853.

Although advances have been made in the application of SERS for DNA diagnostics by hybridization to surface bound probes,[36,43−45] including techniques that avoid direct labeling of the target sequences by using molecular beacons[48] or silver nanoparticles,[34] none of these methods have been used in dsDNA melting studies to discriminate between mutations. In this Article, we describe the use of SERS combined with either thermal or electrochemical cycling to discriminate mutations. Although there are a few reports of mutation detection by monitoring temperature- or potential-induced denaturation using SPR,[64,65] to date fluorescence monitoring remains the dominant technique with several systems commercially available.[66,67] The use of an applied electric field to affect hybridization and to determine mutations by the application of a constant potential (−300 mV) followed by measuring the change in fluorescence with time has been described by Sosnowski et al.[68] In their work, the probes were immobilized in a 1 μm thick gel-permeation layer coating the electrode, and denaturation was brought about by a complex mechanism involving a mixture of effects rather than as the result of simple electrostatic repulsion at the metal surface.[69,70] The use of electrochemical scanning dehybridization using fluorescence monitoring for SNP recognition has been recently demonstrated on silicon substrates with surface-bound hairpin (molecular beacons) probes.[71,72] However, in these experiments, the authors were unable to generate sufficient difference to distinguish SNP targets from the perfect match when using linear DNA probes. There are also a few reports on monitoring electrochemical denaturation with other techniques such as SPR[64] and chemiluminescence[73] in which a constant potential was applied[68] and denaturation was monitored with time.

In this work, we show that the SSV substrates can be used to obtain stable reproducible SERS signals for labeled ssDNA during hybridization onto surface attached DNA probe sequences. We show that these target sequences can be melted from the surface and rehybridized and that the method is highly sensitive with detection at sub attomole levels. Further, sequences in the gene responsible for coding the Cystic Fibrosis Transmembrane Regulator (CFTR) protein were used as a model system to demonstrate the discrimination of different mutations. Mutations in this gene cause cystic fibrosis, which is one of the most common inherited genetic life-shortening diseases, reducing the life expectancy to 37.5 years, across different populations.[74] Two particular mutations, ΔF 508 the most common CFTR mutation (70% and 90% of cystic fibrosis cases in U.K. and U.S., respectively) and 1653C/T a relatively rare single point mutation occurring in the same gene fragment, were targeted. We show that we can distinguish between the wild type, the single nucleotide mutation, and the most common triplet deletion in the human CFTR gene by employing SER(R)S to follow melting of the dsDNA from the SSV surface as either the temperature or the applied potential is scanned. Finally, we demonstrate the applicability of this approach in real systems by discriminating between the unpurified amplicons of the wild type and triplet deletion in the human CFTR gene following asymmetric PCR of a DNA sample.

Experimental Section

Fabrication of Substrates. For a typical fabrication procedure, glass microscope slides were coated with a 10 nm chromium adhesion layer followed by 200 nm of gold using standard thermal evaporation. 2 cm × 1.5 cm pieces were cut from the gold-coated slide, cleaned by sonicating in isopropanol for 90 min, washed, and dipped in 10 mM cysteamine in ethanol for at least 48 h. Subsequently, these treated surfaces are washed with water and assembly of polystyrene spheres (obtained as 1% solutions from Duke Scientific) was carried out. This served as the template for the formation of sphere segment voids. Electrodeposition was carried out using a commercial gold electroplating bath (ECF 60, Technic Inc.) to which an additive (Brightener E3, Technic Inc.) was added for a bright and smooth finish. A fixed area was masked, and the charge required for a particular height was calculated. Electrodeposition was carried under potentiostatic control at −0.73 V versus a homemade saturated calomel electrode (SCE) with a platinum counter electrode. The deposition was terminated when the requisite amount of charge had been passed. The polystyrene spheres were then removed by dissolution in DMF to obtain ordered sphere segment void substrates. In the present work, 600 nm diameter spheres were employed, and the gold film was electrodeposited to 480 nm.

Oligonucleotide Synthesis. Standard DNA phosphoramidites, solid supports, and additional reagents were purchased from Link Technologies Ltd., Sigma, and Applied Biosystems Ltd. For 3′-labeling, C7-aminoalkyl and C7-fluorescein (FAM) synthesis columns were obtained from Link Technologies Ltd., and Cy3, Cy5, and dithiol phosphoramidites were purchased from Glen Research Inc. All oligonucleotides were synthesized on an Applied Biosystems 394 automated DNA/RNA synthesizer using standard 0.2 or 1.0 μmol phosphoramidite cycles of acid-catalyzed detritylation, coupling, capping, and iodine oxidation. Stepwise coupling efficiencies and overall yields were determined by the automated trityl cation conductivity monitoring facility and in all cases were >98.0%. All β-cyanoethyl phosphoramidite monomers were dissolved in anhydrous acetonitrile to a concentration of 0.1 M immediately prior to use. The coupling time for normal (A, G, C, T) monomers was 25 s, and the coupling time for the Cy3, Cy5, and dithiol monomers was extended to 360 s. Cleavage of oligonucleotides from the solid support and deprotection was achieved by exposure to concentrated aqueous ammonia for 60 min at room temperature followed by heating in a sealed tube for 5 h at 55 °C. Oligonucleotides labeled with 5′-Cy3 and 5′-Cy5 were prepared by adding the appropriate Cy phosphoramidite monomer at the final addition in solid-phase synthesis. The Cy3 and Cy5 chromophores are unstable to prolonged exposure to ammonia, so 5′-Cy oligonucleotides were synthesized using fast deprotecting dmf-G and Ac-dC phosphoramidite monomers, cleaved from the resin by treatment with concentrated aqueous ammonia for 60 min

(64) Heaton, R. J.; Peterson, A. W.; Georgiadis, R. M. *Proc. Natl. Acad. Sci. U.S.A.* **2001**, *98*, 3701.
(65) Peterlinz, K. A.; Georgiadis, R. M.; Herne, T. M.; Tarlov, M. J. *J. Am. Chem. Soc.* **1997**, *119*, 3401.
(66) Herrmann, M. G.; Durtschi, J. D.; Wittwer, C. T.; Voelkerding, K. V. *Clin. Chem.* **2007**, *53*, 1544.
(67) Meuzelaar, L. S.; Hopkins, K.; Liebana, E.; Brookes, A. J. *J. Mol. Diagn.* **2007**, *9*, 30.
(68) Sosnowski, R. G.; Tu, E.; Butler, W. F.; O'Connell, J. P.; Heller, M. J. *Proc. Natl. Acad. Sci. U.S.A.* **1997**, *94*, 1119.
(69) Kassegne, S. K.; Reese, H.; Hodko, D.; Yang, J. M.; Sarkar, K.; Smolko, D.; Swanson, P.; Raymond, D. E.; Heller, M. J.; Madou, M. J. *Sens. Actuators, B* **2003**, *94*, 81.
(70) Edman, C. F.; Raymond, D. E.; Wu, D. J.; Tu, E.; Sosnowski, R. G.; Butler, W. F.; Nerenberg, M.; Heller, M. J. *Nucleic Acids Res.* **1997**, *25*, 4907.
(71) Wei, F.; Chen, C. L.; Zhai, L.; Zhang, N.; Zhao, X. S. *J. Am. Chem. Soc.* **2005**, *127*, 5306.
(72) Wei, F.; Qu, P.; Zhai, L.; Chen, C. L.; Wang, H. F.; Zhao, X. S. *Langmuir* **2006**, *22*, 6280.
(73) Spehar-Deleze, A. M.; Schmidt, L.; Neier, R.; Kulmala, S.; de Rooij, N.; Koudelka-Hep, M. *Biosens. Bioelectron.* **2006**, *22*, 722.
(74) Kerem, B.-S.; Rommens, J. M.; Buchanan, J. A.; Markiewicz, D.; Cox, T. K.; Chakravarti, A.; Buchwald, M.; Tsui, L.-C. *Science* **1989**, *245*, 1073.

Scheme 1. Structures of (a) Cy3, (b) Cy5, and (c) Texas Red Labels Coupled to the 3′ End of the Oligonucleotide

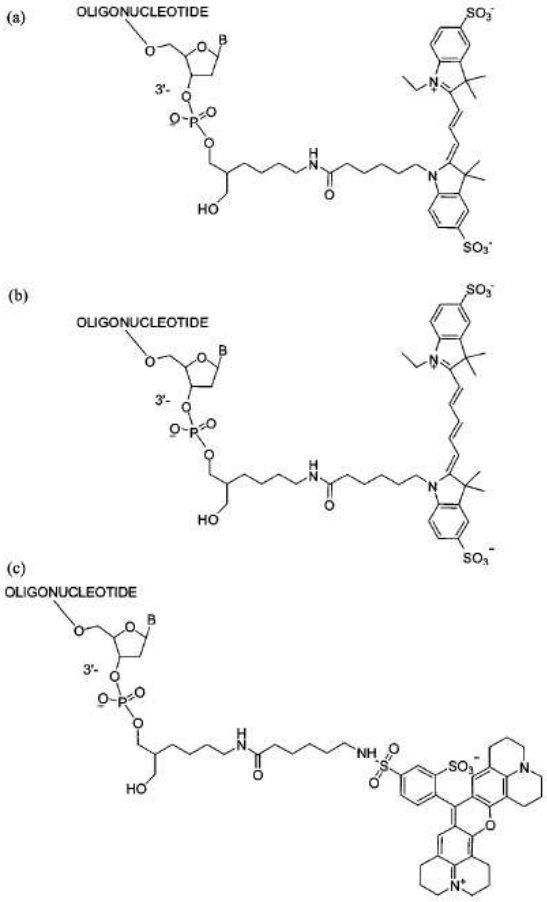

Table 1. Oligonucleotide Sequences Used in Preliminary SERS Experiments

probe	XHXHXHGCAGCAAATTGCACTGGAGTGCGAG-3′-(**FAM**), where X is a disulfide monomer and H is a hexaethyleneglycol (Heg) spacer
target	3′-GTGACCTCACGCTC-5′-**Cy3**

at room temperature, and then deprotected for 1 h at 55 °C. The 3′-FAM oligonucleotide was synthesized starting from a FAM C7 column, and 3′-Cy5 and Texas Red-labeled oligonucleotides were synthesized by postsynthetic labeling of 3′-aminoalkyl oligonucleotides, which were assembled using C7-aminolink solid support. These oligonucleotides were then labeled with the appropriate dye NHS ester (Scheme 1) as described below. The labeled probe and target sequences used in the preliminary SERS experiments are given in Table 1.

To incorporate the Cy3, Cy5, or Texas Red chromophores at the 3′-end of C7-aminoalkyl oligonucleotide, 50−150 nmol of the oligonucleotide in 70 μL of 0.5 M Na_2CO_3/$NaHCO_3$ buffer (pH 8.75) was incubated for 4 h at room temperature with 1 mg of the succinimidyl ester of Cy3, Cy5, or Texas Red (Invitrogen) in 40 μL of DMSO. The crude oligonucleotides were purified by reversed-phase HPLC and desalted by NAP-10 gel-filtration according to the manufacturer's instructions (GE Healthcare). Reversed-phase HPLC purification was carried out on a Gilson system using an ABI Aquapore column (C8), 8 mm × 250 mm, pore size 300 Å. The following protocols were used: run time 30 min, flow rate 4 mL per min, binary system, gradient, time in min (% buffer B), 0 (0); 3 (0); 5 (10); 21 (40); 21 (60); 25 (100); 27 (0); 30 (0). Elution buffer A: 0.1 M ammonium acetate, pH 7.0. Buffer B: 0.1 M ammonium acetate with 50% acetonitrile pH 7.0. (The % buffer B at 21 min was 40% for all oligonucleotides except those containing the hydrophobic Cy3, Cy5, and Texas Red dyes, which required 60% buffer B.) Elution of oligonucleotides was monitored by ultraviolet absorption at 295 nm. Texas Red oligonucleotides gave two product peaks corresponding to the 5- and 6-regioisomers of Texas Red. The first peak (5-isomer) was collected and used in the subsequent SERS experiments, and the second peak was discarded. After HPLC purification, oligonucleotides were desalted using NAP-10 Sephadex columns (GE Healthcare), aliquoted into eppendorf tubes, and stored at −20 °C. All oligonucleotides were characterized by MALDI-TOF mass spectrometry.

PCR Amplification. For the SERS-melting experiments with PCR amplicons, a synthetic DNA template (50 ng) containing the wild-type sequence or the ΔF 508 mutation was amplified in a sample volume of 20 μL, containing 0.2 μM 5′ Cy5-labeled forward primer, 0.05 μM reverse primer, 1 mM dNTPs (Promega, UK), 2.5 mM $MgCl_2$, and 1 unit hot start DNA polymerase (Eppendorf HotMaster) in 1 × PCR buffer. The PCR reactions were performed using a thermocycler (Eppendorf Mastercycler Gradient) with a denaturation step of 95 °C for 2 min, followed by 15 cycles of 94 °C for 20 s, 54 °C for 45 s, and 70 °C for 45 s. The sequences used and amplified along with that of the probe immobilized on the surface for detecting the amplicons are shown in Table 2.

Immobilization of Probe Oligonucleotides on the Substrate. The dithiol-modified oligonucleotides were diluted to 1 μM concentration with pH 8.1 phosphate buffer containing 0.1 M NaCl. It was extremely important that the substrates were clean. This was ensured by thoroughly cleaning them by sonicating in DMF for at least 3 h. Thereafter, they were immediately transferred to deionized water and sonicated for another 15 min. The substrates were preserved in water until used. For immobilizing the probe oligonucleotides, the substrates were dipped in the 1 μM solutions and kept in a refrigerator maintained at 6 °C for 48 h. After this, the substrates were taken out and washed with pH 8.1 phosphate (0.1 M NaCl) buffer several times and dipped in 10 μM mercaptohexanol solution prepared in pH 8.1 phosphate (1 M NaCl) buffer for 20 min. This ensured that any nonspecific binding of the target oligonucleotides with the substrate was prevented. The substrates were taken out and rinsed with pH 8.1 phosphate (0.1 M NaCl) buffer several times and employed for detection or mutation analysis.

Surface Coverage Determination of Probe on Gold Surface. The coulometric procedure of Steel et al.[75] using $[Ru(NH_3)_6]^{3+}$ was used to determine the coverage of immobilized probes on the gold surfaces. In this method, the $[Ru(NH_3)_6]^{3+}$ cation binds electrostatically to the phosphate groups on the DNA. Under saturating conditions, assuming that the charge on the phosphate groups is entirely compensated by $[Ru(NH_3)_6]^{3+}$, the amount of DNA bound at the surface can be deduced. This is done by measuring the charge required to reduce the DNA bound $[Ru(NH_3)_6]^{3+}$ using a short reductive potential pulse. Thus, a 500 ms pulse from an initial potential of 0.1 to −0.4 V vs SCE was employed to completely reduce the $[Ru(NH_3)_6]^{3+}$, and the charge transient was recorded. Prior to the application of the potential pulse, the solutions were deoxygenated by purging with argon for 20 min and thereafter blanketed with argon during the experiment. The electrode was allowed to equilibrate for 2 min with the solution at each concentration of $[Ru(NH_3)_6]^{3+}$ before recording the transient.

SERS-*T*melting Procedure. The thermally induced melting experiments were carried out in custom designed micro-Raman cell (Ventacon Ltd., www.ventacon.com). It utilizes a horizontal

(75) Steel, A. B.; Herne, T. M.; Tarlov, M. J. *Anal. Chem.* **1998**, *70*, 4670.

Table 2. Oligonucleotide Sequences for PCR, the Products, and the Probe Used in the Detection of Amplicons

oligonucleotide	sequence
forward primer	**Cy5**-GTATCTATATTCATCATAGGAAACACC
reverse primer	CATTGGAAGAATTTCATTCTGTTCTCAG
wild-type template	GCACATTGGAAGAATTTCATTCTGTTCTCAGTTTTCCTGGATTATGCCTGGCACCATTAAA**GAAAATATCATC-TTTGGTGTTTCCT**ATGATGAATATAGATACAGA
mutant template(ΔF 508)	GCACATTGGAAGAATTTCATTCTGTTCTCAGTTTTCCTGGATTATGCCTGGCACCATTAAA**GAAAATAT-CATC---GGTGTTTCCT**ATGATGAATATAGATACAGA
wild-type amplicon	**Cy5**-5′-GTATCTATATTCATCAT**AGGAAACACCAAAGATGATATTTTC**TTTAATGGTGCCAGGCATAATCCAG-GAAAACTGAGAACAGAATGAAATTCTTCCAATG-3′
mutant amplicon	**Cy5**-5′-GTATCTATATTCATCAT**AGGAAACACC---GATGATATTTTC**TTTAATGGTGCCAGGCATAATCCAGG-AAAACTGAGAACAGAATGAAATTCTTCCAATG-3′
probe for amplicons	$(dithiol)_3$-3′-TCCTTTGTGGTTTCTACTATAAAAG-5′

geometry for viewing under the Raman microscope, maintaining a thin 150 μm liquid film on the substrate. It is possible to flow solutions over the substrate during an experiment without disturbing the position of the substrate. A heating element is provided in the body of the cell and can be controlled with a microcontroller circuit. Two thermocouple probes are incorporated, with digital display, for controlling and monitoring the heating temperature and the temperature of the substrate, respectively. In the thermal melting, the temperature was ramped up from room temperature at 1 °C per minute to 60 °C or as appropriate in pH 8.1, 0.01 M phosphate buffer containing 0.1 M NaCl. The temperature of the substrate was recorded at the time the acquisition of each Raman spectrum was started.

SERS-*E*melting Procedure. The procedure for electrochemical melting was essentially similar to that used in *T*melting except that the temperature was held constant. The electrochemically induced melting experiments were carried out in the same custom designed micro-Raman cell. For the *E*melting experiments, the reference (Ag/AgCl) and counter (platinum wire) electrodes are placed on the side.

For a typical *E*melting experiment, the substrates were dipped in pH 7, 10 mM TRIS buffer, and the buffer was flushed over the substrates several times in the cell at open circuit potential. The experiments were carried out at room temperature. All electrochemical studies were carried out employing an EcoChemie μAutolabIII potentiostat/galvanostat. A potential sequence was applied, typically starting at -0.2 V and then -0.4 V, followed by 100 mV decrements until -1.3 V or less. The potential was held at each step for 300 s. Raman spectra were also recorded every 300 s with the first spectrum recorded 250 s after the beginning of the potential pulse.

The choice of buffers is of no particular significance except that in low ionic strength buffers we expected the electrostatic effects to be more pronounced. Hence, in this work, we show the *E*melting results in 10 mM TRIS buffer. However, it is possible to obtain *E*melting profiles in a phosphate buffer containing 100 mM NaCl and also carry out *T*melting in Tris buffer.

Raman Instrumentation. Raman spectra were acquired using a ULWD 50× objective (NA: 0.5) on a Renishaw 2000 Raman microscope instrument equipped with a 632.8 nm He−Ne laser. The diameter of the laser spot in the work presented here was 1 μm. The Raman microscope system has a motorized stage with a precision XYZ stage controller. Typically, Raman spectra were acquired from a 4 μm × 4 μm or larger area on the substrate with the laser being moved 1−2 μm each time using the stage controller. This was done to avoid any bleaching effects of the dye and was aided by the fact that signals on our substrates are reproducible.

Typically, for the targets with Cy3 label, the spectra were acquired for 20−30 s; with Texas Red, the spectra were acquired for 10 s, and for Cy5-labeled oligonucleotides it was 2−10 s, under either static mode centered at 1400 or 1450 cm^{-1} or extended mode between 3200 and 400 cm^{-1} with the laser power measured at the sample being 3 mW. When presenting the results, the spectra have been normalized by the laser power and the collection times.

Data Analysis. Unless otherwise stated, the SERS spectra presented in this Article have been background corrected using a polynomial multipoint fitting function (WiRe software, Renishaw). The Raman intensities of the peaks mentioned in this work are their heights over and above the baseline. A Boltzmann function has been used to fit sigmoidal curves to the melting profiles using Origin 7.0 software, and the first derivative of the fits was used to determine the melting points (midpoint of melting curves).

SEM Images. A Philips XL30 environmental scanning electron microscope (ESEM) and a Jeol JSM 6500F thermal field emission scanning electron microscope (FESEM) were used for taking the images of the structured substrates.

Results

Preparation of DNA SSV Surfaces. The gold sphere segment void (SSV) surfaces were made by electrodeposition of 480 nm of gold through a close-packed template of 600 nm diameter polystyrene spheres assembled on an evaporated gold surface. Efficient surface enhancement on the SSV surface requires coupling of both the incoming laser excitation and the outgoing, Stokes shifted, light to surface plasmons on the structured metal surface.[58,76] It is therefore important to choose an appropriate film thickness and sphere diameter. In this case, the values were selected to be resonant with 633 nm excitation (see Supporting Information) on the basis of earlier studies in aqueous solution.[56] Removal of the template spheres leaves the surface structured as shown in Figure 1a. SEM and voltammetric studies show that the surface of the templated structure is smooth with a surface roughness that is lower than that of the original evaporated gold film.

Single-strand DNA probe sequences, Figure 1b, were attached to the surface through three dithiol linkages and hexaethyleneglycol (HEG) spacers (Scheme 2) attached at the 5′ end of the oligonucleotide sequence by soaking the clean SSV surfaces in a 1 μM solution of the probe in pH 8.1 phosphate buffer containing 0.1 M NaCl at 6 °C for 48 h. The 6 thiol groups on the linker ensure strong binding of the DNA to the surface. For efficient hybridization with target strands from the solution, it is important to ensure that the probe sequences are not too closely packed on the surface,[77,78] and the immobilization conditions used here were chosen for that reason. The large footprint of the disulfide monomers and HEG spacers between them ensures that the surface bound probes are well spaced on the surface with enough room between them to prevent any cross-hybridization and to ensure efficient hybridization with

(76) Baumberg, J. J.; Kelf, T. A.; Sugawara, Y.; Cintra, S.; Abdelsalam, M. E.; Bartlett, P. N.; Russell, A. E. *Nano Lett.* **2005**, *5*, 2262.
(77) Herne, T. M.; Tarlov, M. J. *J. Am. Chem. Soc.* **1997**, *119*, 8916.
(78) Peterson, A. W.; Heaton, R. J.; Georgiadis, R. M. *Nucleic Acids Res.* **2001**, *21*, 5163.

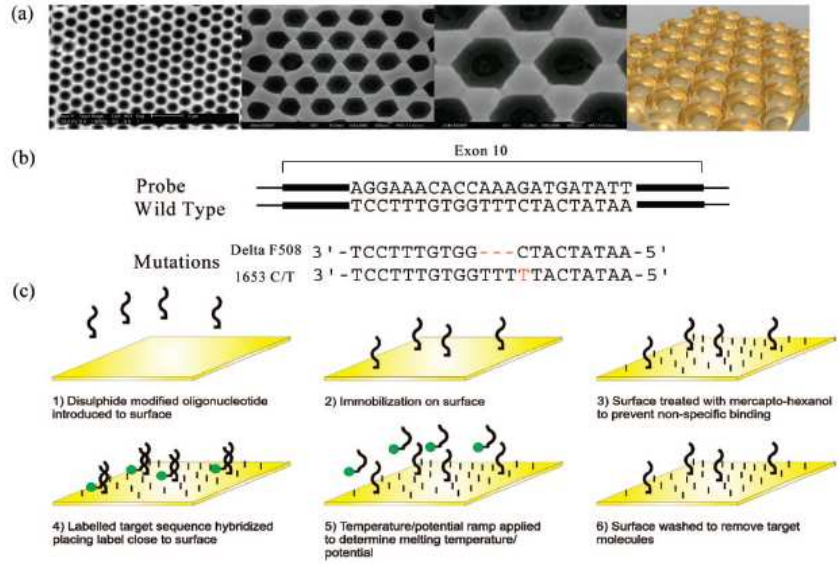

Figure 1. Substrate, scheme for detection, and sequences used. (a) Three SEM images at different magnifications of the SSV gold substrates (templated with 600 nm spheres and electroplated to 480 nm) and (right) a 3-D model of the structure. The scale bar is 2 μm for the first SEM image and 100 nm for the other two. (b) The probe and the target CFTR sequences for the synthetic oligonucleotides. The labels were attached to the 3′ end (proximal to the surface) of the target in all cases, unless mentioned otherwise. (c) The process of detection and characterization of DNA sequences beginning with (1) and (2) preparation of the sensing surface followed by (3) passivation with mercapto-hexanol to prevent nonspecific binding, (4) detection using SER(R)S-labeled targets, (5) dehybridization with either temperature or potential, and ending with (6) regeneration of the surface for reuse starting again at step 4. The dehybridization process is the key step and yields the information that characterizes mutations.

Scheme 2. Structure of the Disulfide Linkages Attached to the 5′ End of the Probe Oligonucleotides[a]

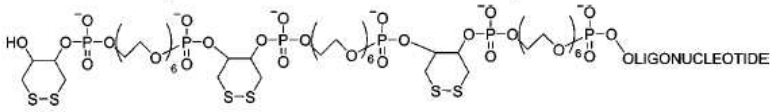

[a] The dithiol linkages ensure strong bonding with gold on immobilization.

target species from solution. Following attachment of the probe sequences, the substrates were washed and soaked in a 10 μM solution of mercapto-hexanol in pH 8.1 phosphate buffer, 1 M NaCl for 20 min, Figure 1c. The mercapto-hexanol adsorbs to the gold surface around the attached DNA and reduces nonspecific binding of target DNA from the solution at the gold surface.[77] The mercaptohexanol also has the effect of reorienting the ssDNA attached to the surface into a more upright conformation.[79,80]

Measurement of Surface Coverage. The coulometric method of Steel et al.[75] was used to determine the coverage of the immobilized DNA on the gold surfaces. Figure 2shows a typical charge transient recorded in the experiment (Figure 2a) together with the adsorption isotherm (Figure 2b). The adsorption isotherm was constructed by fitting coulometric curves of the type shown in Figure 2a recorded for different concentrations of $[Ru(NH_3)_6]^{3+}$ to the following expression for the total charge, Q,

$$Q = \frac{2nFAD_O^{1/2}c_O t^{1/2}}{\pi^{1/2}} + Q_{dl} + nFA\Gamma_O \qquad (1)$$

where t is the time, n is the number of electrons transferred, F is the Faraday constant, A is the area of the electrode, D_O is diffusion coefficient and c_O the bulk concentration of $[Ru(NH_3)_6]^{3+}$, Q_{dl} is the double layer charge, and Γ_O is the surface coverage of bound $[Ru(NH_3)_6]^{3+}$. The first term in eq 1 describes the mass transport limited reaction of $[Ru(NH_3)_6]^{3+}$ from the solution, the second term the double layer charging contribution, and the final term the contribution from the electrostatically bound $[Ru(NH_3)_6]^{3+}$. The coverage was found to be 1.6×10^{12} molecules per cm^2 so that on an average the 25 base long ssDNA molecules are 8.5 nm apart, leaving sufficient room to hybridize while preventing any cross-hybridization with target DNA from solution.

Preliminary SERS Experiments. Initial experiments were carried out using a 3′ fluorescein (FAM)-labeled 25 base long probe to test the stability and reusability of the DNA-coated SSV substrates. Figure 3 shows a set of SERS spectra recorded from the same substrate at different stages in the experiment. Spectrum a was recorded for the ssDNA immobilized on the SSV substrate at open circuit in buffer solution. The bands at 1179, 1322, and 1637 cm^{-1} correspond to the 3′ fluorescein (FAM) label[47,48] attached to the probe and are assigned to the C−OH bending, C−O phenoxide stretching, and the ring stretching vibrations, respectively.[81] There was no observable change in the spectrum when a noncomplementary 25-mer DNA labeled at the 5′ end with Cy3 was introduced into the solution,

(79) Lee, C.-Y.; Gong, P.; Harbers, G. M.; Grainger, D. W.; Castner, D. G.; Gamble, L. J. *Anal. Chem.* **2006**, *78*, 3316.
(80) Erts, D.; Polyakov, B.; Olin, H.; Tuite, E. *J. Phys. Chem. B* **2003**, *107*, 3591.

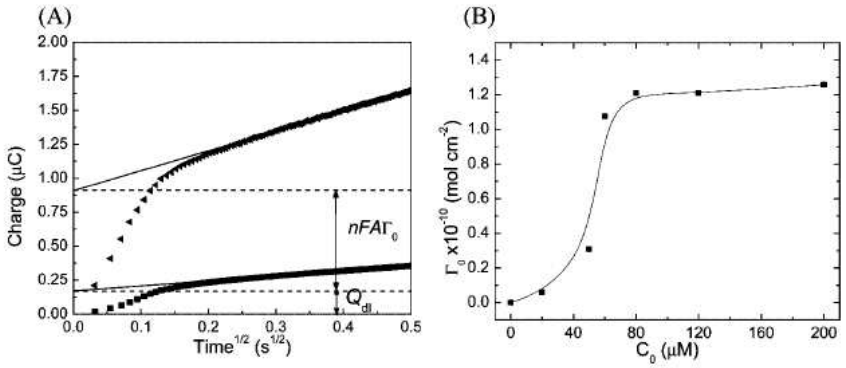

Figure 2. Coulometric determination of surface coverage of immobilized DNA. (A) Coulometric curves recorded by stepping the potential from 0.1 to −0.4 V vs SCE at a ssDNA-coated electrode (6.18 mm^2) in blank electrolyte solution (pH 7, 10 mM Tris buffer) (■) and in the same electrolyte solution containing 80 μM $[Ru(NH_3)_6]^{3+}$ (▲). (B) The adsorption isotherm for $[Ru(NH_3)_6]^{3+}$ calculated from the coulometric measurements.

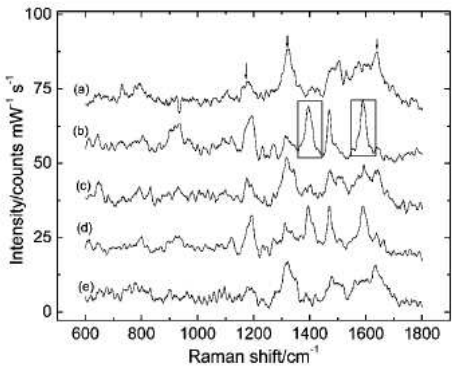

Figure 3. DNA assay and reusability. Demonstrated employing a fluorescein (FAM) 3′-labeled 25 base long probe and 14 bases long Cy3 5′-labeled target. In this study, both of the labels are at the distal end from the surface. (a) Even after incubation with a noncomplementary Cy3-labeled strand, only peaks due to FAM-labeled probe (marked with arrows) are observed in the spectrum, which is identical to that of the probe DNA alone. (b) Hybridization with a complementary Cy3-labeled target (peaks enclosed in boxes), and (d) rehybridization occurs with almost no loss in signal from Cy3-labeled target. (c and e) Dehybridization is achieved by flowing hot water (~55 °C) for 5 min over the substrate, resulting in regeneration of the sensor substrate as inferred by the reappearance of the FAM peaks and loss of Cy3 peaks. Spectra are baseline corrected and smoothed. The spectra were recorded with an extended scan set to 30 s collection time (1 and 3 accumulations for Cy3 and FAM, respectively), 3 mW laser power in pH 8.1 phosphate buffer containing 100 mM NaCl.

confirming that the mercapto-hexanol suppresses nonspecific binding. In contrast, when the 14-mer cDNA strand labeled with Cy3 at the 5′ end is introduced into the solution the spectrum changes, Figure 3b, and new bands corresponding to the Cy3 label[35,48] appear at 1272 and 1393 cm^{-1} assigned to C−N stretch and CH deformation modes, and at 1590 cm^{-1} assigned to C═N stretching vibration (based on work on indocarbocyanine dyes by Sato et al.[82]). At the same time, the fluorescein bands become less prominent. We attribute the changes to the hybridization of the Cy3-labeled target to the DNA probe attached to the surface and the subsequent change in conformation of the DNA, which probably moves the 3′ fluorescein label further from the surface, thus reducing its SERS intensity.[83] In this case, the fluorescein label on the probe and the Cy3 label on the target are on the same end distal to the surface; yet the intensities of the fluorescein peaks are much weaker as compared to Cy3. This difference could be due to the lower Raman cross section of fluorescein as compared to Cy3 with the 633 nm laser used in this experiment. This suggests that in principle any molecule with a high Raman cross section could be employed as a label in these experiments. On the basis of the measured coverage of DNA on the surface and given the area illuminated by the 1 μm diameter laser spot in the spectrometer, we calculate that the spectra are recorded from approximately 12 500 molecules, giving a sensitivity of detection by SER(R)S of better than 0.02 amol. Note this is not the same as the limit of detection of the method for DNA in solution because this will also depend on the hybridization step. To test the stability of the system, the dsDNA was dehydridized by washing the surface with water at ~55 °C for 5 min, Figure 3c, then rehybridized to the complementary target, spectrum d, and finally dehybridized with hot water again, spectrum e. Comparing the spectra in Figure 3, we can see that on dehybridization the original spectrum for the fluorescein (FAM)-labeled probe is recovered, compare spectra (a), (c), and (e), with very similar intensities. Comparing spectra (b) and (d) in Figure 3, we also find excellent reproducibility in the hybridization of the target with very similar spectral intensities of the Cy3 peaks in the two cases.

These preliminary experiments show that SERS detection on the SSV substrates gives excellent sensitivity, that we can clearly distinguish the signals of the two different dye labels, fluorescein (FAM) and Cy3, that attachment of the probe to the gold surface through the 6 thiols (3 disulfides) is robust, that the mercapto-hexanol prevents nonspecific binding of labeled DNA to the surface, and that the surfaces are reuseable.

Discrimination of Mutations by Thermal Melting. The allele-specific 22-mer probes for detecting the wild type and mutated sequences in the CFTR gene were synthesized with three dithiol linkages (Scheme 2) at the 5′-end for attachment to the gold surface. Similarly, the oligonucleotide targets were synthesized by standard solid-phase techniques and labeled at the 3′-end

(81) Wang, L.; Roitberg, A.; Meuse, C.; Gaigalas, A. K. *Spectrochim. Acta, Part A* **2001**, *57*, 1781.
(82) Sato, H.; Kawasaki, M.; Kasatani, K.; Katsumata, M.-A. *J. Raman Spectrosc.* **1988**, *19*, 129.
(83) Ye, Q.; Fang, J.; Sun, L. *J. Phys. Chem. B* **1997**, *101*, 8221.

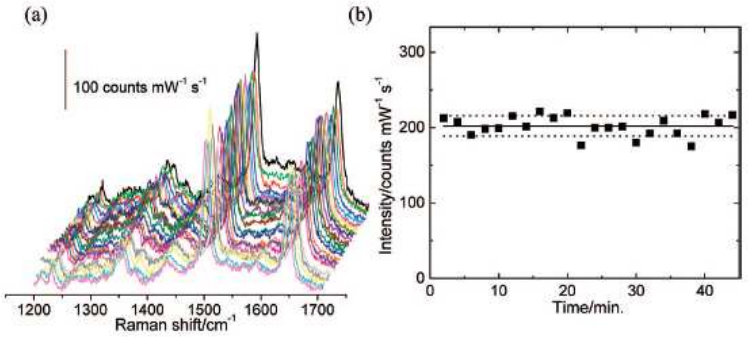

Figure 4. Reproducibility on the substrate with time. (a) Spectra of a Texas Red-labeled target with a single mismatch (1653 C/T point mutation) after hybridization recorded on a SSV substrate recorded in blank pH 8.1, 0.01 M phosphate buffer containing 100 mM NaCl. The laser spot was moved 2 μm every ~2 min while recording the spectra in static mode with a single 10 s exposure at 3 mW laser power. All spectra have been baseline corrected. (b) The peak intensity for the 1500 cm^{-1} band attributed to ring stretching mode of Texas Red plotted as a function of time for the different spectra in (a); the solid and the dotted lines show the average and std dev (7%) range, respectively. The spectra were acquired at room temperature and open circuit potential.

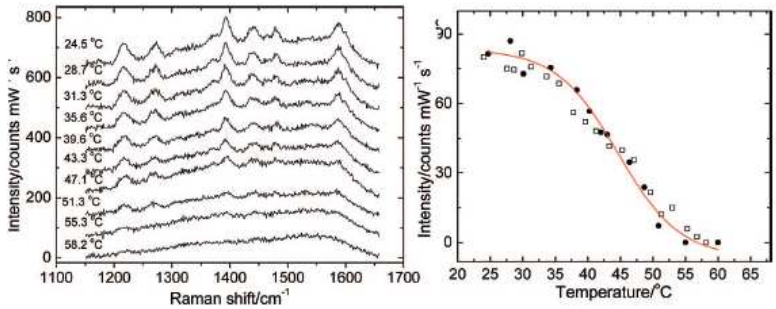

Figure 5. SERS-*T*melting experiment. (a) A sequential set of spectra recorded at different temperatures in a thermally induced dehybridization experiment using the Cy3-labeled wild-type CFTR target sequence. The temperature of the sample was ramped at 1 °C min^{-1} in blank pH 8.1, 0.01 M phosphate buffer containing 100 mM NaCl. All spectra are baseline corrected by a straight line offset between the extremities. (b) Plot of the intensity of the 1437 cm^{-1} SERS band, corresponding to the −CH asymmetric deformation mode of the Cy3 label, as a function of temperature. Data for two consecutive replicate measurements on the same substrate are shown. Spectra were acquired under a single static scan for 20 s at 3 mW laser power.

with common fluorophores, which served as SERS labels. In this case, 3′ labeling brings the label closer to surface, which is expected to increase the SER(R)S signals. The synthetic probe and target sequences are shown in Figure 1b.

The targets were detected in a hybridization assay; the entire scheme for detection and mutation discrimination is shown in Figure 1c. SER(R)S detection was carried out in a custom-made cell with electrochemical and temperature control. Hybridization was carried out in 10 μM solutions of the labeled targets in pH 8.1 phosphate buffer containing 0.1 M NaCl for 30 min. Thereafter, the substrates were rinsed by flushing the cell with the buffer at least 3 to 4 times. In experiments to discriminate mutations, the same substrate was used each time with the different targets, and spectra were collected from the same area on the substrate, although for each spectrum the laser spot was moved by 1−2 μm. This not only reduced any bleaching and photodegradation effects but also serves to demonstrate that the SERS sensitivity, surface modification, and melting effects are reproducible across the SSV surface. In fact, the substrates are reusable, and no change in melting characteristics was observed on repeated measurements. Figure 4a shows a set of 22 spectra recorded for the Texas Red-labeled 1653 C/T point mutation target hybridized to the probe on the SSV surface in the blank buffer solution at room temperature (~23 °C). The bands at 1500 and 1643 cm^{-1} correspond to the Texas Red dye[35] and are assigned to the ring stretching and −NH deformation modes in the molecule. The spectra were recorded by moving the laser spot sequentially across the surface, and again each spectrum is recorded from around 12 500 molecules in a single 10 s exposure without any spectral averaging. Texas Red has an absorption maximum at 596 nm; therefore, it is in preresonance (see Supporting Information) with the 633 nm laser used here. Figure 4b shows a plot of the intensity of the 1500 cm^{-1} band as a function of time for the set of spectra recorded at different places on the surface. The results show excellent reproducibility and stability, <7% variation.

When the temperature is increased the dsDNA begins to melt, or dehybridize, and the temperature at which this occurs will be lower if there are mismatches between the target and the probe. In the next set of experiments, the temperature was ramped at 1 °C min^{-1}, and a series of spectra were recorded at different temperatures; Figure 5a shows a representative set of data recorded for the Cy3-labeled wild-type CFTR sequence recorded in pH 8.1, 0.01 M phosphate buffer containing 100 mM NaCl. As before, the bands at 1216, 1393, 1437, 1479, and 1589 cm^{-1} are characteristic for the Cy3 label, although the intensity pattern of the peaks in this case with the label on the 3′ end is different as compared to that observed in the case of 5′-labeled target in Figure 3. Also, the signal-to-noise for the 3′-Cy3 peaks in this case is higher than that in the earlier

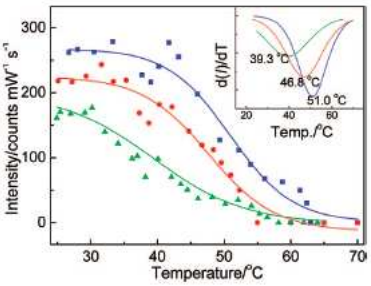

Figure 6. Thermally induced dehybridization monitored with SERS (SERS-*T*melting). The SERS intensity of the 1500 cm^{-1} band of the Texas Red label for the three targets, (■) wild type (no mutation), (●) 1653C/T mutation (single point mutation), and (▲) Δ*F* 508 mutation (triple deletion), is plotted against the temperature. The first derivatives of the sigmoidal fits of the intensity curves are shown in the inset. The temperature of the sample was ramped at 1 °C min^{-1} in blank pH 8.1, 0.01 M phosphate buffer containing 100 mM NaCl. Spectra were acquired in static mode with a single 10 s exposure at 3 mW laser power on the same substrate beginning with the triple deletion, followed by the single point mutation and then the perfect match.

experiments. As the temperature increases, we can see that the intensity of the Cy3 bands decreases sequentially, eventually disappearing at high temperature when all of the dsDNA has melted and the labeled target molecules diffuse away from the surface. Note that the SERS signal decreases because the enhancement is strongly surface specific; labeled DNA molecules that are not close to the surface (less than about 100 nm) do not contribute to the signal. We can analyze the thermal melting of the dsDNA on the surface by plotting the intensity of the SERS signal as a function of temperature. Figure 5b shows results for two consecutive measurements made on the same surface, showing excellent agreement in both overall signal intensity and in the temperature variation. In both cases, there is a sigmoidal drop in signal with a mid point temperature of about 45 °C. This type of SERS-*T*melting measurement is reproducible and can be used to discriminate mutations with high sensitivity.

Figure 6 shows SERS-*T*melting for the three different targets, wild type and two mutations each labeled with Texas Red. As expected, the wild type, which is a perfect match for the probe, melts at the highest temperature, while the Δ*F* 508 triple deletion, which is the worst match, melts at the lowest temperature. Analysis of the melting curves gives melting temperatures (T_m), which show a difference of 4.2 °C for the single point mutation and 11.7 °C for the triple deletion as compared to the wild type. It is also noticeable that the triple deletion shows the lowest SERS intensity at all temperatures, possibly indicating lower surface coverage as a result of weaker binding to the probe. Again, these spectra were acquired from around 12 500 molecules on the surface, demonstrating that SERS-*T*melting on the SSV substrate is a very sensitive method to discriminate single nucleotide mutations.

Discrimination of Mutations by Electrochemical Melting. The results presented above show that SERS at the SSV substrates is a very sensitive method to discriminate mutations by recording spectra as the temperature is increased. However, close control over the temperature and reproducible heating of the system requires special equipment and cannot be applied selectively to one region of a surface and not to a nearby region. We therefore also investigated the effects of using the SSV substrate as an electrode and slow ramping of its potential.

In a typical SERS-electrochemical-melting (SERS-*E*melting) experiment, after hybridization with the target the cell was flushed several times with 10 mM TRIS buffer, pH 7, and the surface was equilibrated at open circuit potential for several minutes. Thereafter, the SSV electrode was potentiostatted and the potential decreased in steps from −0.2 to −1.5 V vs Ag/AgCl. SER spectra were recorded at each potential step after a fixed time interval of 250 s. A typical SERS-*E*melting analysis in the present, unoptimized form therefore took less than an hour. Figure 7 shows results for a SERS-*E*melting experiment using the same probes and the same three Texas Red-labeled targets as in the SERS-*T*melting experiment shown in Figure 6. As the potential is taken cathodic, Figure 7a, we see that the bands at 1500 and 1643 cm^{-1} characteristic of the Texas Red label first increase and then decrease in intensity, eventually disappearing at the most cathodic potential. It is notable that the spectra are again much clearer than in the spectra presented in Figure 3. This is because Texas Red is in preresonance with the 633 nm laser, resulting in an additional resonance enhancement over and above the surface enhancement. Plotting the extracted SERS intensities of the Texas Red aromatic ring stretching band at 1500 cm^{-1} against potential yields the SERS-*E*melting profiles, which are shown in Figure 7b. The first derivatives of the sigmoidal curve fits to the melting curves (inset) were used to define the melting potentials (E_m). As evident in Figure 7b, the profiles for the perfect match and the two mutations are clearly distinguishable with shifts in the melting potentials (ΔE_m) of 110 and 60 mV, respectively. Again, as expected, the mutation with the triple deletion is the least stable and shows the most positive melting potential. In all cases, the intensity of the peak for the SERS marker increases as the potential becomes more negative from −0.2 to −0.8 V before then decreasing and ultimately falling to zero at potentials more negative than −0.8 V. The initial increase is reversible, and we speculate that this is due to a potential-dependent change in the orientation of the dsDNA and the 3′ Texas Red label. This requires further study, but it is worth noting that we do not see the same effect when we use Cy5 as a label or in the case of thermal melting with either of the dyes; see Figure 9 and discussion below.

Reproducibility of SERS-*E*melting. Figure 8 shows results for consecutive SERS-*E*melting experiments using the same SSV substrate and the Texas Red-labeled Δ*F* 508 target. After the first SERS-*E*melting measurement, the substrate was stored in buffer solution for 3 days and then rehybridized with the same target. There is good reproducibility in both the intensity profiles of the SERS signal and the *E*melting characteristic with excellent agreement in the melting potential, E_m, for the two measurements. These results show that the loss of SERS signal at high cathodic potentials arises from melting of the dsDNA and loss of labeled target from the surface and not through reductive desorption of the DNA probe (reductive desorption can occur in our experiments, but it does not become significant until the potential is taken more negative than −1.3 V vs Ag/AgCl). These results demonstrate the excellent reusability of these surfaces for DNA detection and mutation discrimination and also show the stability and reproducibility of the SSV gold SERS substrates used in this work.

Potential Dependence of the SERS Spectra. SER(R)S spectra are quite rich in information about changes in orientation and can in principle be used to study the melting process in detail.

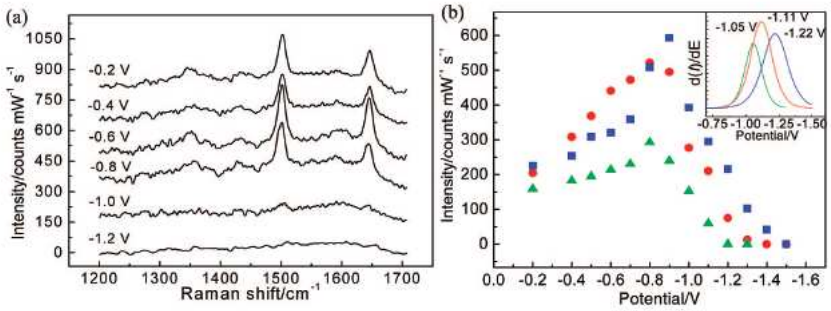

Figure 7. Electrochemical dehybridization monitored with SERS (SERS-*E*melting) for mutation discrimination. (a) Representative spectra of Texas Red-labeled Δ*F* 508 synthetic target at various potentials in an actual SERS-*E*melting experiment with the intensity of peaks changing with applied potential. (b) The SERS intensities of the 1500 cm^{-1} band of the dye label (Texas Red) for the three targets, (■) wild type (no mutation), the (●) 1653C/T mutation (single point mutation), and the (▲) Δ*F* 508 mutation (triple deletion), are plotted against the applied potential. The first derivatives of the sigmoidal fits of the intensity curves are shown in the inset with the melting potentials shown above each curve. Spectra were acquired in static mode with a single 10 s exposure at 3 mW laser power on the same substrate beginning with the triple deletion, followed by the single point mutation and then the perfect match, in pH 7, 10 mM Tris buffer.

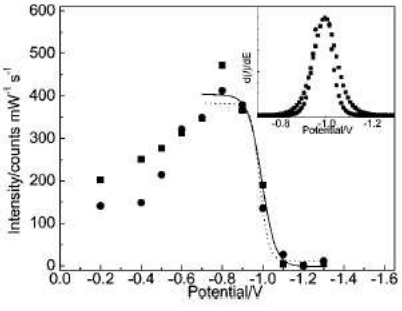

Figure 8. Reproducibility of SERS-*E*melting. The peak intensities for the 1500 cm^{-1} band for Texas Red-labeled Δ*F* 508 target oligonucleotides are plotted as the function of potential for two successive measurements carried out 3 days apart on the same DNA probe-modified SSV substrate (■ first run, ● second run). The dehybridization profiles are reproducible on the substrates with almost no variation in the melting potential values, 0.99 and 0.98 V, respectively (the first derivatives of the fitted profiles are shown in the inset). Spectra were acquired in static mode with a single 10 s exposure at 3 mW laser power in pH 7, 10 mM Tris buffer.

Figure 9a shows a set of SERRS (also called resonant SERS) spectra recorded at different potentials for the 3′ Cy5-labeled complementary target hybridized to the immobilized probe on the SSV surface. Cy5 is a cyanine dye with an absorption maximum of 647 nm (see Supporting Information). It is therefore resonant with the 633 nm laser used in these experiments, and so, as expected, the signals in the SERR spectra of this label are significantly more intense (in this case by a factor of 4−5) than those for the partially resonant Texas Red label shown in Figure 7. The bands at 583 and 935 cm^{-1} are assigned to alkene chain and aromatic CH deformation modes, and those at 1367 and 1597 cm^{-1} to methine chain deformation and *C*═N stretching modes, respectively, and are characteristic of Cy5.[35] Figure 9b shows normalized melting profiles calculated from four different bands in the Cy5 spectrum. In each case, the intensity of the band decreases as the potential moves cathodic, but it is noticeable that there are no significant shifts in band position. The melting profiles derived from each band may give some information about the conformational changes that accompany partial melting of the dsDNA. This is an area that deserves further study.

With Cy5 as the label, the electrochemical melting profile is shifted 400−450 mV less negative, depending on which band we take, as compared to the value for the corresponding Texas Red-labeled target (Figure 7). Thus, the particular choice of the label has a significant effect on the stability of the surface bound dsDNA. At neutral pH, Cy5 is a dianion whereas Texas Red is a zwitterion; we speculate that the difference in the SERS-*E*melting profiles is caused by the additional negative charge on the Cy5 label at the 3′ end of the target leading to dehybridization at lower potentials and temperatures (data not shown). The melting temperature of the perfect match with 3′ Cy5 label was found to be 45 °C, which is 6 °C lower than that measured for the corresponding 3′ Texas Red-labeled target. We also note that for the Cy5-labeled system the initial increase in SER(R)S intensity observed with Texas Red (Figure 7b) is not found but that the melting profiles for Texas Red-labeled oligonucleotides are sharper as compared to Cy5-labeled sequences. These effects highlight the possibility of optimizing the choice of SER(R)S label in future work.

Application of SERS-*E*melting to Analysis of PCR Products. The examples described above clearly demonstrate that there are readily measurable differences in the SERS-melting responses and that discrimination of mutations is possible for a model system. To demonstrate the potential practical utility of the method, we carried out mutation discrimination experiments with PCR products of the wild type and Δ*F* 508 mutated sequences from the CFTR gene. The primers in this case were labeled with Cy5, and the surface bound probe sequence was redesigned (see Table 2). For the PCR product, the target strand is much longer; we use a 103-mer as compared to the synthetic 22-mer oligonucleotides used above. When hybridized to the probe sequence on the surface, the PCR product has overhanging sequences at both ends with a 15 base long nonoverlapping part of the primer on the 3′-end.

Figure 10 shows results for the SERS-*E*melting experiment with the PCR product. The target solution was as obtained after PCR without any purification; hence, it contained residual dNTPs, primer, $MgCl_2$, and DNA polymerase besides the amplicon. In comparison with the results in Figure 9, the positions of several of the Cy5 bands are shifted (see Supporting Information); this is because a 5′-Cy5 phosphoramidite label was used in this case rather than the 3′-Cy5 added as an NHS

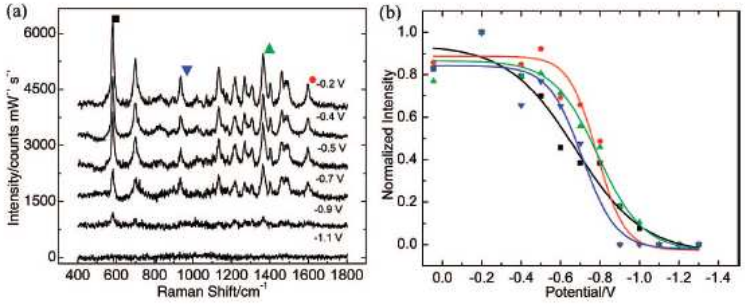

Figure 9. (a) SERRS (or resonant SERS) spectra of Cy5-labeled complementary strand recorded at the different potentials indicated beside each spectrum. The spectra are offset for clarity. (b) Normalized resonant SERS-*E*melting profiles extracted from the SERRS bands at (■) 583 cm^{-1}, (▼) 935 cm^{-1}, (▲) 1367 cm^{-1}, and (●) 1597 cm^{-1} for the Cy5-labeled synthetic target strand. Spectra were acquired in the extended mode with a single scan set to 3 s collection time at 3 mW laser power in pH 7, 10 mM Tris buffer.

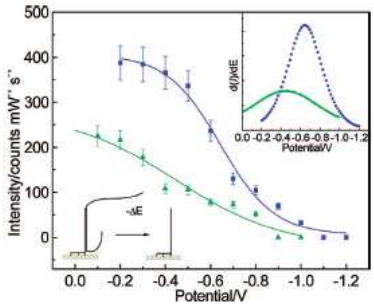

Figure 10. The resonant SERS-melting profiles of the PCR products for wild type (■) and Δ*F* 508 mutation (▲) using the 1347 cm^{-1} SERRS (resonant SERS) band for Cy5. A schematic of the dehybridization process of the PCR products is shown. The first derivatives of the melting profiles are shown in the inset. The mutation has a melting potential of −0.44 V, while that of the wild type is −0.64 V vs SCE. Spectra were acquired with a single static scan of 2 s exposure at 1.5 mW laser power in pH 7, 10 mM Tris buffer.

ester. Once again, there is still a significant difference of 200 mV between the melting potential (ΔE_m) of the mutation and the wild type. As compared to the results for the model system, Figure 9, the melting profile is shifted to less negative potentials by about 200 mV. It is possible that this is due to the increased destabilization of the duplex at the surface due to the longer overhanging strands of the PCR product. The negative control for the PCR products was also tested with the same procedure, and no signal from the Cy5 label could be observed, confirming that there is no nonspecific binding and no contamination of the sample during PCR, which was also separately confirmed by gel electrophoresis.

Discussion

Thermal melting of dsDNA to discriminate mutations is usually applied in solution with fluorescence monitoring rather than to surface bound DNA, although such approaches have been used in microarrays. Our thermal melting study demonstrates the first use of in situ SER(R)S dehybridization of dsDNA, which we show can be employed for distinguishing mutations. Peterlinz et al.[65] have described the application of thermal melting to dsDNA attached to a gold surface followed by SPR where they showed a clear difference in the melting temperature depending on the electrolyte concentration but did not discriminate between different DNA target strands. In our case, as described above, the approach shows excellent selectivity for single point mutations and excellent sensitivity. This is in large part due to the high sensitivity of the SER(R)S technique coupled to the excellent stability of our SSV substrates, which provide a stable SERS enhancement, even when the temperature is cycled and the substrates are reused, and the robust attachment of the probe DNA through the six thiol (three disulfide) linkages.

Although the SERS-*T*melting method works well, the SERS-*E*melting approach has significant advantages because potential control can be localized more easily and is therefore more suitable for miniaturization, addressability, integration with integrated circuit (IC) technology, and lower implementation costs than is precise temperature control. The use of applied potential to direct or in some way control the immobilization, hydridization, or denaturation of DNA has a long history. As early as 1957, Hill[84] pointed out, based on a statistical thermodynamic treatment, that the stability of double-stranded DNA should be affected by an electric field and predicted that fields of the order of 10^4 V cm^{-1} could bring about melting of dsDNA. Early work on the electrochemistry of calf thymus DNA at mercury electrodes[85,86] provided evidence, based on the accessibility or otherwise of cytosine and adenine nucleotides for reduction at mercury, for partial melting of dsDNA at around −1.2 V vs SCE. In this case, the dsDNA was assumed to be adsorbed parallel to the electrode surface so that it experienced the full effect of the potential drop across the double layer at the electrode surface.

There have been a limited number of studies of field effects on the immobilization,[78,87] hybridization,[64,88] or denaturation[64,71−73,89] of DNA directly attached to electrode surfaces. A significant increase in the rate of hybridization was found by Heaton et al.[64] in a study of the reaction of target DNA sequences with probe sequences attached to a gold surface through a thiol link. In the same paper, they also show that denaturation of dsDNA at the surface can be driven by the potential. In these experiments, they found that a fixed potential of −0.3 V led to the denaturation of a two base mismatched target strand from the

(84) Hill, T. L. *J. Am. Chem. Soc.* **1958**, *80*, 2142.
(85) Brabec, V.; Paleček, E. *Biophys. Chem.* **1976**, *4*, 79.
(86) Valenta, P.; Nürnberg, H. W. *Biophys. Struct. Mech.* **1974**, *1*, 17.
(87) Ge, C.; Liao, J.; Yu, W.; Gu, N. *Biosens. Bioelectron.* **2003**, *18*, 53.
(88) Su, H.-J.; Surrey, S.; McKenzie, S. E.; Fortina, P.; Graves, D. J. *Electrophoresis* **2002**, *23*, 1551.
(89) Wei, F.; Sun, B.; Liao, W.; Ouyang, J.; Zhao, X. S. *Biosens. Bioelectron.* **2003**, *18*, 1149.

probe in the hybridization buffer in a few minutes, whereas there was little loss of the fully complementary strand over several hours. A similar effect of moderate negative potentials on the rate of denaturation was observed by Spehar-Deleze et al.[73] using electrochemiluminescent detection at gold electrodes. In a recent series of papers, Wei et al.[71,72,89] demonstrated that scanning electrode potential could be used to discriminate single nucleotide polymorphisms using hairpin probes. In these experiments, the DNA hairpin probes were immobilized on doped p-Si (111) substrates, and experiments were carried out in 10 mM TRIS buffer containing 1 mM EDTA. Duplex dissociation was monitored either by impedance measurements[89] or by fluorescence.[71,72] Significantly, the authors found that in their experiments it was essential to use a hairpin probe and there was no discrimination when the experiment was repeated with a linear probe.[71]

It is of interest to consider the mechanism of discrimination in our experiments. The persistence length for double-stranded DNA is 80 nm,[90] significantly longer than the 25 base and 22 base long duplexes used in our experiments, which were only around 9.5 and 8.5 nm long, respectively. Thus, the dsDNA approximates to a rigid cylinder with an effective diameter, including the 0.5 nm thick countercation sheath due to Manning condensation,[91] of 3 nm attached to the gold surface through the six gold thiol bonds by a flexible hexaethyleneglycol (HEG) linkage 1.2 nm long. The measurements of surface coverage give an average surface area of 0.016 nm^2 for the 25 base long DNA probe so that, on average, the strands are 8.5 nm apart. The gold between the DNA probes is covered by a layer of mercapto-hexanol around 0.8 nm thick. Several studies using a range of techniques have established that for dsDNA immobilized on gold surfaces coimmobilized with mercapto-hexanol the DNA stands up and extends out into the solution[92,93] and that as the applied potential changes the orientation of the attached dsDNA can be switched from near the surface at potentials close to the potential of zero charge (pzc) to perpendicular to the surface at potentials negative of the pzc.[94,95] Thus, we can picture the dsDNA at the electrode surface at the negative potentials where the electrochemically driven denaturation occurs as shown in Figure 11. The reversible change in orientation of the dsDNA with applied potential reported in the literature[92,94,95] is consistent with the reversible changes in SERS intensity seen in Figures 7b and 8 for the Texas Red-labeled molecules. The results of our experiments are in general agreement with the thermodynamic calculations of Vainrub and Pettitt[96,97] on the electrostatic effects on DNA hybridization at electrode surfaces, which predict that potentials negative of the potential of zero charge should decrease the stability of the dsDNA at the electrode surface and enhance melting. This simple model partially explains our *E*melting data. In the simple Gouy−Chapman model, the bulk of the potential in the double layer at the electrode surface is dropped over the Debye length,[95−97] which for our buffer solution is ~3 nm, with the field decaying to zero over three multiples of the Debye length. Thus, in the current work most of the dsDNA might be expected to be within the double layer. However, it is possible that the *E*melting effect is not only due to the effect of the potential but also to local changes in pH caused by electrode reactions, but this seems unlikely given the large range of *E*melting potential we observe (from −0.44 V for the Cy5-labeled Δ*F* 508 PCR product to −1.22 V for Texas Red-labeled wild type). Comparing the *E*melting and *T*melting experiments, there is a reasonable correlation between the two, Figure 12, suggesting that the *E*melting effect is directly probing the thermodynamic stability of the duplex. Clearly, further work is required to understand the full details of the *E*melting process. Nevertheless, it is clear from the results presented here that it is a simple reproducible, sensitive, and accurate method to discriminate single nucleotide polymorphisms.

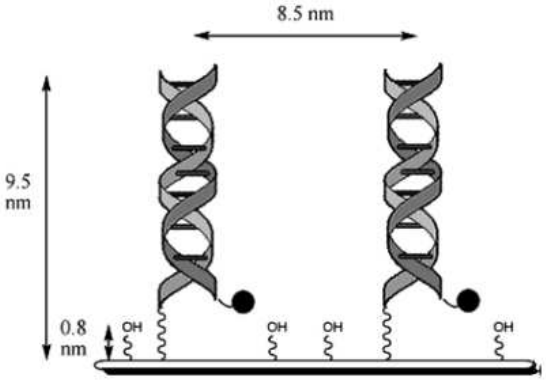

Figure 11. Schematic showing the configuration at negative electrochemical potentials on a gold surface with estimated dimensions (approximately to scale) of the distribution of the DNA sequences in the mercaptohexanol layer for a 25 base long duplex.

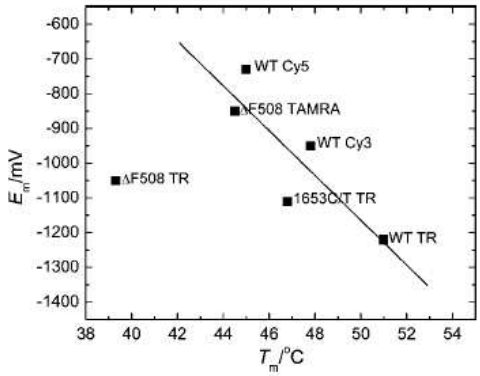

Figure 12. The melting potentials (E_m) plotted versus melting temperatures (T_m) for different targets bearing various labels determined from the SERS-melting experiments with the 22-mer oligonucleotide targets.

Conclusions

In this work, we have provided "proof of concept" of a new method for distinguishing mutations employing SERS detection

(90) Bednar, J.; Furrer, P.; Katritch, V.; Stasiak, A. Z.; Dubochet, J.; Stasiak, A. *J. Mol. Biol.* **1995**, *254*, 579.
(91) Manning, G. *Acc. Chem. Res.* **1979**, *12*, 443.
(92) Kelley, S. O.; Barton, J. K.; Jackson, N. M.; McPherson, L. D.; Potter, A. B.; Spain, E. M.; Allen, M. J.; Hill, M. G. *Langmuir* **1998**, *14*, 6781.
(93) Levicky, R.; Herne, T. M.; Tarlov, M. J.; Satija, S. K. *J. Am. Chem. Soc.* **1998**, *120*, 9787.
(94) Rant, U.; Arinaga, K.; Fujita, S.; Yokoyama, N.; Abstreiter, G.; Tornow, M. *Nano Lett.* **2004**, *4*, 2441.
(95) Rant, U.; Arinaga, K.; Fujita, S.; Yokoyama, N.; Abstreitera, G.; Tornowa, M. *Org. Biomol. Chem.* **2006**, *4*, 3448.
(96) Vainrub, A.; Pettitt, B. M. *Chem. Phys. Lett.* **2000**, 323.
(97) Vainrub, A.; Pettitt, B. M. *Biopolymers* **2003**, *68*, 265.

(termed SERS-melting) on ordered gold sphere segment void substrates, and we have demonstrated its potential utility in a PCR-based application. Many practical applications are envisaged leveraging the advantages of SER(R)S over fluorescence and other detection methods especially in being able to combine immense molecule-specific information with high sensitivity. The other advantage of our SERS substrate approach is its fundamental suitability for high throughput analysis, miniaturization, and the possibility of multidimensional control of the denaturation process by electrochemical potential, temperature, and/or solution composition. Thus, SERS-melting could prove to be an important enabling technology in the fields of diagnostics, genomics, and forensic science.

Acknowledgment. S.M. thanks ORSAS for a scholarship.

Supporting Information Available: Reflectance spectrum of the SSV structure used in this work, absorption spectra of the dye labels, and SERRS spectra of 3′- and 5′-Cy5-labeled targets corresponding to Figures 9 and 10, respectively. This material is available free of charge via the Internet at http://pubs.acs.org.

JA805517Q

The use of an electroactive marker as a SERS label in an *E*-melting mutation discrimination assay

*Sumeet Mahajan, James Richardson, Nouha Ben Gaied, Zhengyun Zhao, Tom Brown, Philip N. Bartlett**

School of Chemistry, University of Southampton, Highfield, Southampton, SO17 1BJ, UK

*e-mail:pnb@soton.ac.uk

Abstract

In this paper we describe the first example of the use of an electroactive label as a SERS marker for detecting and quantifying target oligonucleotides and distinguishing mutations using a combination of voltammetry and electrochemically induced melting (*E*-melting). The experiments were carried out on sphere segment void substrates selected to show strong surface enhancement for SERS at 633 nm. DNA analysis was carried out for CFTR sequences using synthetic 22-mer oligonucleotides labelled with a modified anthraquinone at the 3'-end. Discrimination between the wide type, 1653C/T (point mutation) and ΔF508 (triple deletion) is demonstrated.

Keywords

DNA hydridization, SERS, Electrochemical melting curve, Anthraquinone label, Base pair mismatches.

1. Introduction

The advancement of surface enhanced Raman spectroscopy (SERS) based solid phase analytical techniques for DNA diagnostics has been hampered over the last decade due to the lack of suitable substrates and the irreproducibility of signals on those in use. Nevertheless, researchers have continued to demonstrate the advantages of SERS over other techniques, such as ability to multiplex [1], high sensitivity, and flexibility in the choice of labels [2-4] in nanoparticle and colloidal silver systems. Utilization of SERS for gene diagnostics by hybridization of labelled probes on rough silver surfaces was first demonstrated by Vo-Dinh and co-workers [5-7]. Very recently DNA detection with surface enhanced resonance Raman spectroscopy (SERRS) on a commercially available reproducible substrate using labelled oligonucleotides in a hybridization assay [8] has also been shown. Most of the labels that have been used for DNA detection are common fluorophores which also serve as SER(R)S

(SERS or SERRS) markers. However, none of the SER(R)S based DNA detection systems have been shown to distinguish between mutations and/or simultaneously quantify the hybrid on the surface.

Over the past few years we have developed sphere segment void (SSV) substrates [9] with tuneable SER(R)S properties [10-13]. We have also recently developed a new technique of distinguishing mutations employing SER(R)S monitoring of thermally or electrochemically induced melting on gold SSV substrates [14]. These gold SSV substrates are easily fabricated by templated electrodeposition around colloidal templates, have low surface roughness, and can be used as electrodes. Here we describe for the first time the use of an electroactive label, a modified anthraquinone [15, 16] as a SERS marker for detecting and quantifying target oligonucleotides and distinguishing mutations using a combination of voltammetry and electrochemically induced melting (*E*-melting). This was demonstrated using synthetic 22-mer oligonucleotides labelled with a modified anthraquinone at the 3'-end. Mutation discrimination was achieved using the differences in the melting behaviour, monitored by SERS, of the duplex on the surface as the potential was scanned cathodic. We assume that increasing cathodic potential under our experimental conditions increases the electrostatic repulsion between the surface and duplex causing it to denature, though the exact mechanism is under investigation. The method relies on the surface specificity of SERS and therefore on denaturation; as the labelled target DNA strands leave the surface and diffuse into the bulk the SERS signal reduces ultimately to zero allowing a melting profile based on SERS peak intensities to be generated. The *E*-melting approach is fast, simple and does not rely on the position of the label for differentiation of mutations [17]. By using anthraquinone labels on target oligonucleotides we combine for the first time the advantages of both SERS and amperometric electrochemical detection on SSV substrates.

2. Experimental

2.1 Fabrication of sphere segment void (SSV) substrates

Glass microscope slides were coated with a 10 nm chromium adhesion layer followed by 200 nm of gold using standard thermal evaporation. The gold coated slide was cut into pieces, typically 2 cm x 1.5 cm, and these were cleaned by sonicating in isopropanol (HPLC grade, Rathburn) for 90 min, then washed and dipped in 10 mM cysteamine (Sigma-Aldrich) in ethanol (HPLC grade, Rathburn) for at least 48 h. Subsequently, these treated surfaces were washed with water and assembly of a monolayer of 600 nm polystyrene spheres (obtained as

1 % solutions from Duke Scientific) was carried out by slow evaporation in a thin layer cell [18, 19]. This monolayer of spheres served as the template for the formation of ordered spherical cavities. Electrodeposition was carried out using a commercial cyanide free gold electroplating bath (ECF 60, Metalor) to which an additive (Brightener E3, Metalor) was added for a bright and smooth finish. A fixed area was masked using an insulating varnish and the charge required to deposit a film 480 nm thick was calculated. Electrodeposition was carried out under potentiostatic control (Autolab PGSTAT30) at -0.73 V *vs.* a homemade saturated calomel electrode (SCE) in a three electrode cell with a large area platinum counter electrode. The deposition was terminated when the requisite amount of charge had been passed. Thereafter, the polystyrene spheres were removed by dissolution in DMF (HPLC grade, Fisher) to obtain ordered spherical segment void (SSV) gold substrates.

2.2 Chemical synthesis

Reagents for chemical synthesis were purchased from Sigma-Aldrich or Fluka and used without further purification. DNA phosphoramidite monomers, solid supports (including phosphate-on synthesis columns for 3'-phosphate addition) and additional reagents were purchased from Link Technologies Ltd or Applied Biosystems Ltd. Flash chromatography was performed on silica (40-63 μm) purchased from VWR and thin layer chromatography was performed on Merck Kieselgel $60F_{254}$ coated plates (0.22 mm thickness, aluminium backed). Compounds were visualized by staining with vanillin (2 g of vanillin in 100 mL of EtOH/ H_2SO_4 98:2) or by ultraviolet absorbance at 254 nm.

^{1}H and ^{13}C NMR spectra were recorded on a Bruker DPX 400 spectrometer. All spectra were internally referenced to the appropriate residual undeuterated solvent signal. Chemical shifts are given in ppm relative to tetramethylsilane, and *J* values are given in Hz and are corrected to within 0.5 Hz. Multiplicities of ^{13}C signals were determined using the DEPT spectral editing technique. Low-resolution mass spectra were recorded using the electrospray technique on a Waters ZMD single quadrupole instrument in MeOH (HPLC grade). High-resolution mass spectra were recorded in acetonitrile, methanol or water (HPLC grade) using the electrospray technique on a Bruker APEX III FT-ICR mass spectrometer.

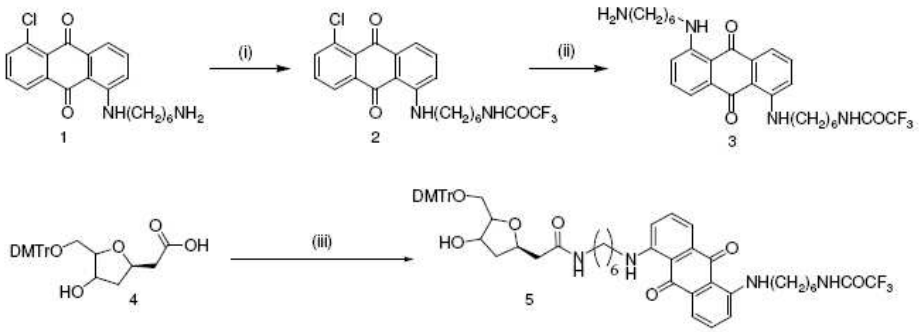

Scheme 1. Synthesis of anthraquinone labelled deoxyribose monomer (**5**). i) Ethyl trifluoroacetate, NEt_3, DCM, RT, 90 min, 63%; ii) hexamethylenediamine (5 eq), xylene, reflux, overnight (82%); iii) compound (**3**), HBTU (2 eq), DMAP (1 eq), DMF, RT, 2h, 26%.

2.2.1 1-(6-Trifluoroacetamidohexylamino)-5-chloroanthraquinone (2)

Ethyl trifluoroacetate (1.2 ml, 10 mmol) was added to a solution of 1-(6-aminohexylamino)-5-chloroanthraquinone [20] **1** (0.72 g, 2 mmol) and dried triethylamine (2.8 ml, 20 mmol) in CH_2Cl_2 (20 ml). The reaction was stirred at room temperature (RT) for 90 min before removing the solvent under vacuum. The crude material was purified on silica gel packed with CH_2Cl_2. A gradient of MeOH (from 0 to 4%) in CH_2Cl_2 gave compound **2** (0.57 g, 63%) as a red solid foam.

R_f CH_2Cl_2 (100%) 0.66. δ_H (400 MHz, DMSO-d_6) 9.43-9.40 (1H, t, J= 5.2 Hz, NH), 9.38 (1H, s, $NHCOCF_3$), 8.12-8.09 (1H, dd, J_1= 1.6 Hz, J_2= 7.4 Hz, ArH), 7.79-7.77 (1H, dd, J_1= 1.6 Hz, J_2= 7.9 Hz, ArH), 7.76-7.70 (1H, q, J= 7.6 Hz, ArH), 7.55-7.51 (1H, t, J= 8 Hz, ArH), 7.26-7.25 (1H, d, J= 6.7 Hz, ArH), 7.09-7.07 (1H, d, J= 8.5 Hz, ArH), 3.28-3.23 (2H, q, J= 6.4 Hz, CH_2), 3.21-3.16 (2H, q, J= 6.2 Hz, CH_2), 1.62-1.33 (8H, m, CH_2). δ_C (100 MHz, DMSO-d_6) 182.24 (CO), 181.40 (CO), 150.86 (C-Ar), 136.28, 135.71, 134.91 (CH-Ar), 134.16, 132.89 (C-Ar), 126.04, 117.67, 114.97 (CH-Ar), 114.54, 111.17 (C-Ar), 42.54, 32.07, 28.85, 28.60, 26.56, 26.34 (CH_2). m/z LRMS (ES^+, MeOH) 457.3 ($M+Na^+$, 100%), 927.6 ($2M+Na^+$, 50). m/z HRMS ($M+H^+$) $C_{22}H_{21}ClF_3N_2O_3$ calc. 453.1195 found 453.1188.

2.2.2 1-(6-Trifluoroacetamidohexylamino)-5-(6-aminohexylamino)-anthraquinone (3)

A mixture of 1-(6-trifluoroacetamidohexylamino)-5-chloroanthraquinone (**2**) (0.11 g, 0.25 mmol) and hexamethylenediamine (0.14 g, 1.25 mmol) in xylene (1 ml) was heated under reflux overnight. The solvent was removed under reduced pressure before purifying the crude

mixture on flash column chromatography. A gradient of methanol (1-10%) in CH_2Cl_2 containing 0.5% NEt_3 gave compound **3** (0.11 g, 82%) as a red foam.

R_f Hexane/EtOAc (50:50) 0.61. δ_H (400 MHz, DMSO-d_6) 9.66-9.64 (2H, t, *J*= 4 Hz, NH-$COCF_3$), 7.62-7.58 (2H, t, *J*= 7.93 Hz, Ar), 7.42-7.40 (2H, d, *J*=7.3 Hz, Ar), 7.14-7.12 (2H, d, *J*=8.6 Hz, Ar), 3.35-3.29 (8H, m, CH_2), 3.20-3.17 (4H, t, *J*= 7 Hz, CH_2), 2.70-2.66 (2H, t, *J*= 7.15 Hz, CH_2), 1.67-1.33 (10H, m, CH_2). δ_C (100 MHz, DMSO-d6) 184.76 (CO), 180.65 ($COCF_3$), 151.54 (C-NH), 136.04 (C-Ar), 135.94 (CH-Ar), 117.51, 114.73 (CH-Ar), 112.29 (CF_3), 42.50, 32.08, 28.90, 28.59, 26.66, 26.33 (CH_2). m/z LRMS (ES^+, MeOH) 533.5 ($M+Na^+$, 100%). m/z HRMS ($M+H^+$) $C_{28}H_{36}F_3N_4O_3$ calc. 533.2746 found 533.2734.

2.2.3 N-(6-(9,10-Dihydro-9,10-dioxoanthracen-1-ylamino)-5-yl-(6-aminohexyl)hexyl)-5'-*O*-(4,4'-dimethoxytrityl)-2'-deoxy-D-ribofuranose-1'-β-acetamide (5)

The entire scheme of synthesis of the anthraquinone tagged deoxyribose monomer is summarized in Scheme 1. Deoxyribose ethanoic acid derivative **4** [21] (0.17 g, 0.35 mmol), DMAP (86 mg, 0.70 mmol) and HBTU (0.27 g, 0.70 mmol) were combined and dissolved in dry pyridine (5 ml). The mixture was co-evaporated three times and dried under high vacuum overnight. In a separate flask *bis*-aminohexylanthraquinone **3** (0.12 g, 0.23 mmol) was also co-evaporated three times with dry pyridine, dried *in vacuo* overnight then dissolved in dry pyridine (5 ml). The mixture of **4**, HBTU and DMAP was dissolved in pyridine (1.2 ml) and added drop-wise to the solution of **3** in pyridine under argon at room temperature. After 2 h the reaction mixture was diluted with CH_2Cl_2 (25 ml). The organic phase was washed with $NaHCO_3$ (10 ml), H_2O (10 ml) and brine (10 ml), dried over Na_2SO_4, filtered and evaporated to dryness. The crude mixture was adsorbed on silica and purified by column chromatography using a gradient of acetone in cyclohexane (0 to 60 %) to give compound **5** (0.61 g, 26 %) as a purple foam.

R_f Cyclohexane:Acetone (40:60): 0.66. δ_H (400 MHz, $CDCl_3$) 9.74-9.70 (2H, m, NH), 7.57-7.23 (15H, m, DMTr, H-Ar), 7.0-6.96 (2H, t, *J*=7.5 Hz, H-Ar), 6.87-6.85 (4H, m, DMTr), 6.50-6.47 (2H, t, *J*= 5.52 Hz, H-Ar), 4.52-4.47 (1H, m, H1'), 4.36-4.35 (1H, m, H4'), 4.05-4.01 (1H, m, H3'), 3.83 (6H, s, OCH_3), 3.46-3.17 (10H, m, CH_2), 2.57-2.43 (2H, ddd, J_1=3.25 Hz, J_2= 8.75 Hz, J_3= 15.25 Hz, H5'), 2.08-2.01 (2H, m, H2'), 1.90-1.35 (14H, m, CH_2). δ_C (100 MHz, $CDCl_3$) 185.99 (CO), 185.80 (CO), 171.11 (CONH), 158.98 ($COCF_3$), 151.94 (C-NH), 151.90 (C-Ar), 145.16 (C-Ar), 136.77, 136.7 (C-DMTr), 136.33 (CH-Ar), 135.69 (C-DMTr), 135.63 (C-DMTr), 130.46, 128.75, 128.56, 128.26, 127.29 (CH-DMTr), 116.87, 115.2 (CH-Ar), 113.5 (CH-DMTr), 113.37 (CF_3), 86.73 (C1'), 75.53 (C4'), 74.42

(C3'), 64.8 (CH_2-CONH), 55.6 (OCH_3), 43.22 (C5'), 43.09, 43.03, 41.31, 40.27, 39.70, 29.90, 29.42, 29.26, 29.24, 27.22, 27.08, 27.04, 26.77 (CH_2, C2'). m/z LRMS (ES^+, MeOH) 1015.7 ($M+Na^+$, 100%).

2.2 Resin functionalization

Compound **5** was immobilized on an aminolink resin (LCAA-CPG-NH_2, 92 μmol/g amine loading, Link Technologies Ltd). The resin was firstly activated by conversion to the succinic acid derivative under microwave conditions [22]. The microwave activation was carried out as follows: LCAA-CPG-NH_2 (0.5 g, 46 μmol) was reacted with succinic anhydride (0.4 g, 4 mmol) dissolved in DMF (1 ml) in the presence of DMAP (0.05 g, 0.4 mmol). Three cycles of 30 s microwave excitation were performed on a CEM Explorer® 24 positions microwave at 150 °C and 300 watt. The resin was then washed with CH_3CN (3 x 5 ml, 2 min per wash), MeOH (3 x 5 ml, 15 min per wash) and CH_2Cl_2 (3 x 5 ml, 2 min per wash) and dried overnight under high vacuum. The activation efficiency was confirmed by the Kaiser test [23]. The resin functionalisation was performed on 200 mg (18.4 mmol). Compound **5** (67.8 mg, 73.6 mmol) was then dissolved in DMF (2.5 ml) in presence of HBTU (116.64 mg, 294.4 mmol) and DMAP (36 mg, 294.4 mmol), and the mixture was added to the succinylated resin. After 4 h of constant agitation, the resin was washed with CH_3CN (3 x 5 ml) and CH_2Cl_2 (3 x 5 ml). Free amino sites on the resin were then converted to unreactive acetamide derivatives by reaction with capping reagents from the ABI DNA synthesizer for 3 h (capping reagent A: 0.1 M acetic anhydride, pyridine/THF; capping reagent B: 0.1 M *N*-methylimidazole in THF). The resin was then washed with pyridine (3 x 5 ml), CH_3CN (3 x 5 ml) and CH_2Cl_2 (3 x 5 ml) before drying overnight under high vacuum. A detritylation step using a solution of 3% trichloroacetic acid in CH_2Cl_2 (DNA synthesis grade) was performed to measure the resin loading [24].

2.4 Oligonucleotide synthesis

Oligonucleotide synthesis was carried out on an Applied Biosystems 394 automated DNA/RNA synthesizer using a standard 0.2 μmol phosphoramidite cycle of acid-catalyzed detritylation, coupling, capping and iodine oxidation. All β-cyanoethyl phosphoramidite monomers were dissolved in anhydrous acetonitrile to a concentration of 0.1 M immediately prior to use. Stepwise coupling efficiencies and overall yields were determined by automated trityl cation conductivity monitoring and in all cases were >98.0 %. Cleavage of oligonucleotides from the solid support and deprotection were achieved by exposure to

concentrated aqueous ammonia for 60 min at room temperature followed by heating in a sealed tube for 5 h at 55 °C. Purification of oligonucleotides was carried out by reversed-phase HPLC on a Gilson system using a Brownlee Aquapore column (C8, 8 mm x 250 mm, 300 Å pore) with a gradient of CH_3CN in NH_4OAc increasing from 0 % to 50 % buffer B over 30 min with a flow rate of 4 ml/min (buffer A: 0.1 M NH_4OAc, pH 7.0, buffer B: 0.1 M NH_4OAc with 50 % CH_3CN pH 7.0). Elution of oligonucleotides was monitored by ultraviolet absorption at 295 nm. After HPLC purification, oligonucleotides were desalted using NAP-10 Sephadex columns (GE Healthcare) according to the manufacturer's instructions.

2.5 Oligonucleotide analysis

2.5.1 Capillary electrophoresis (CE) analysis

The purity of the oligonucleotides was confirmed by injection (0.4 OD/100 µl) of each sample individually on ssDNA 100-R Gel. Tris-Borate 7 M Urea were used (kit N° 477480) on a Beckman coulter P/ACE™ MDQ Capillary Electropheresis system using 32 Karat software. UV-254, inject voltage 10.0 kV and separate voltage 9.0 kV (45.0 min duration).

2.5.2 Mass Spectra

Mass spectrometry on oligonucleotides was performed using the electrospray technique on an HP 1050 single quadrupole mass spectrometer in water with 2 % triisopropylamine. The results are shown in Table 1.

Table 1. Results of mass spectrometry for the oligonucleotides employed

Oligonucleotide	Calculated mass	Observed mass
Dithiol surface probe	7850.52	7849.0
Wild Type	7336.29	7340.0
ΔF508 mutant	6424.29	6426.9
1653C/T mutant	7351.29	7352.0

2.6 Surface modification with probe DNA

For this study the dithiol modified oligonucleotides were diluted to 1 µM concentration with 10 mM pH 7 Tris buffer containing 1 M NaCl. It was extremely important that the substrates were clean. This was ensured by sonicating them in DMF for at least 3 h. Thereafter, they

were immediately transferred to de-ionized water and sonicated for another 15 min. The substrates were preserved in water until used. For immobilizing the probe oligonucleotides, the substrates were dipped in the 1 μM solutions and kept in a refrigerator maintained at 6 ºC for at least 24 h. After this the substrates were dipped in 20 μM mercapto-hexanol solution prepared in 10 mM pH 7 Tris buffer (0.1 M NaCl) for 20 min. Thereafter they were rinsed with 10 mM pH 7 Tris buffer (0.1 M NaCl) buffer several times. This ensured that any non-specific binding of the target oligonucleotides with the substrate was prevented.

2.7 Electrochemical measurements

The cyclic voltammetric and coulometric measurements were carried out with an Autolab PGSTAT30 potentiostat/galvanostat. Cyclic Voltammetry was conducted in 0.1 M pH 7 phosphate buffer while the coulometric transients were recorded in 10 mM pH 7 Tris buffer solutions. A homemade saturated calomel reference and a large area platinum mesh counter electrode were used in these measurements.

E-melting experiments were carried out in 10 mM pH 7 Tris buffer solutions and SERS spectra were simultaneously acquired in a custom designed micro-Raman spectroelectrochemical cell (Ventacon Ltd., www.ventacon.com). The cell has a horizontal geometry allowing it to be mounted under a microscope and at the same time allowing solution to be flowed over the surface of the substrate. The cell utilized a Ag/AgCl reference and a platinum ring as the counter electrode. A Renishaw 2000 Raman microscope was employed for recording SERS while a μAutolab III was used for controlling the potential during the *E*-melting experiment.

3. Results and Discussion

3.1 Preparation of the SSV surfaces

The gold SSV surfaces were prepared by electrodeposition through monolayer templates of polystyrene spheres assembled on evaporated gold surfaces. Strong SERS enhancement (of the order 10^7) on SSV surfaces requires strong coupling of both the incoming laser light, in this case at 633 nm, and the out going Raman scatter light, in this case between 675 and 725 nm, with plasmons on the SSV surface [10, 19]. In the present experiments this was achieved using a 600 nm diameter template and growing the films 480 nm thick. Figure 1 shows typical scanning electron micrographs of the surfaces used.

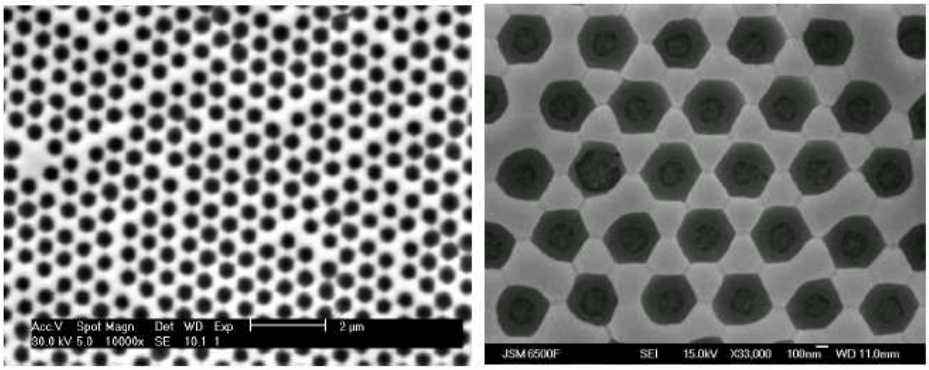

Fig. 1. Representative SEM images of the gold SSV surfaces used in these experiments. The films were grown 480 nm thick through a 600 nm template.

These SSV surfaces were used both for SERS and as electrodes in our studies. 3'-Anthraquinone labelled oligonucleotides were synthesized using standard solid phase techniques (see Experimental section). CFTR gene sequences corresponding to the wild type (perfect match), ΔF508 (triple deletion), which is the most common CFTR mutation, and 1653C/T (point mutation) were targeted. The probe and target sequences are shown in Table 2. The anthraquinone label has an absorption maximum (ε = 13580 M^{-1} cm^{-1}) at 550 nm with a slight tail at the Raman laser wavelength used here of 633 nm so that only partial resonance enhancement is expected, Figure 2.

Table 2. Probe and the target CFTR sequences for the synthetic oligonucleotides. The labels were attached to the 3' end (proximal to the surface) of the target in all cases.

Probe	XXXH–5′–AGGAAACACCAAAGATGATATT–3′
WT	AQ–3′–TCCTTTGTGG**TTT**CTACTATAA–5′
ΔF508	AQ–3'–TCCTTTGTGG---CTACTATAA–5'
1653C/T	AQ–3'–TCCTTTGTGGTTT**T**TACTATAA–5'

X is a disulfide monomer and H is a hexaethyleneglycol (HEG) spacer. AQ is anthraquinone.

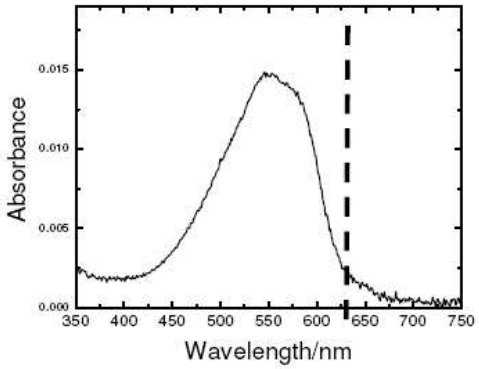

Fig. 2. Absorbance spectrum of a 1 μM solution of the anthraquinone labelled target. The dashed line marks the position of the 633 nm laser employed in the SERS measurements.

The probe sequence was attached to the SSV surface through six thiol linkages and a hexaethyleneglycol spacer to ensure good flexibility. The conditions for attachment of the probe were chosen to ensure that the probe molecules were well spaced on the surface (see below for details of coverage) so that hybridisation to the target would not be sterically or electrostatically inhibited [25, 26] and the remaining surface was passivated with mercaptohexanol to suppress non-specific binding to the gold [25]. The mercaptohexanol also serves to reorient the ssDNA on the surface to a more upright conformation [27, 28]. Scheme 2 shows the general arrangement for the dsDNA melting experiments. The anthraquinone label is attached to the 3' end of the target and is therefore held close to the electrode surface in the duplex, its structure and attachment to the target DNA is shown in the inset.

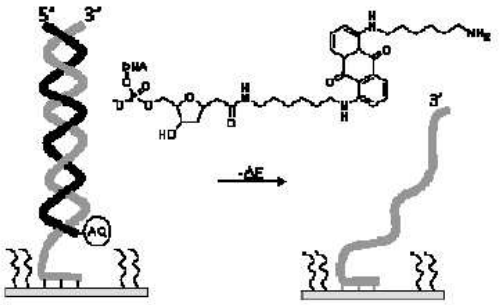

Scheme 2. DNA detection and mutation discrimination with anthraquinone (AQ) labelled target. The probe is immobilized on the surface along with mercapto-hexanol to prevents non-specific binding. Application of a cathodic potential causes the dsDNA to melt. The structure of the AQ label is shown in the inset.

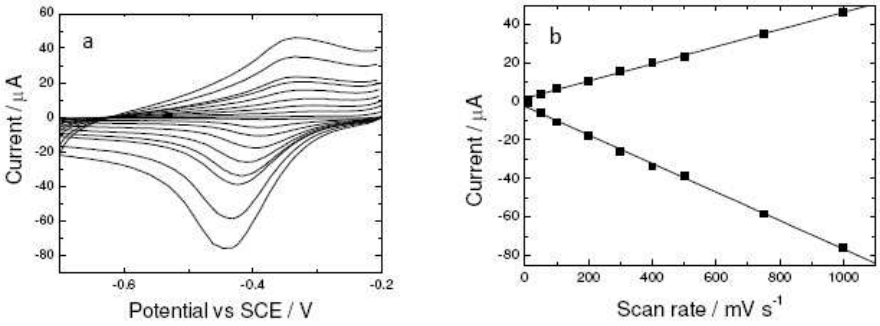

Fig. 3. (a) Cyclic voltammograms at different scan rates (10, 50, 100, 200, 300, 400, 500, 750 and 1000 mV s^{-1}) for anthraquinone labelled WT target hybridized to surface bound probe in pH 7, 100 mM phosphate buffer on gold surface (area : 0.5 cm^2). (b) Plot of peak current versus scan rate.

3.2 Electrochemical measurements

Cyclic voltammograms recorded at different scan rates in pH 7 buffer are shown in Figure 3(a) for the anthraquinone labeled wild type target hybridized to the probe on a SSV gold electrode. They show peaks for the oxidation and reduction of the anthraquinone label with a mid-peak potential of -0.35 V (at a scan rate of 100 mV/s) vs. SCE. The mid-peak potential is found to vary with scan rate from -0.34 V vs. SCE at 10 mV/s to -0.39 V vs. SCE at 1 V/s. The peak separation increases at higher scan rates indicating a kinetic limitation for the reaction, however both the anodic and cathodic peak currents increase linearly with scan rate as expected for a surface bound species, Figure 3(b). From the cyclic voltammetry we can infer that the anthraquinone label will be fully reduced at potentials more negative to -0.6 V.

The electroactive anthraquinone label was used to determine the surface coverage of the target after hybridization by coulometry. The electrochemical approach of using redox probes for detection and quantification of DNA hybridization is well known [29-31]. The method used here is similar to that used by Steel *et al.* [29] except that in this case the SERS label itself is electroactive and therefore it is not necessary to add ruthenium hexamine to the solution as a redox probe. The buffer solution was sparged with argon for 20 min and then blanketed with argon during the experiment. The electrode with dsDNA was held at -0.1 V for 60 s and then a 500 ms pulse from the initial potential of -0.1 V to -0.6 V *vs.* SCE was applied to reduce the anthraquinone label and the current was recorded. Figure 4 shows typical results for the charge transients recorded for the three different hybridised targets.

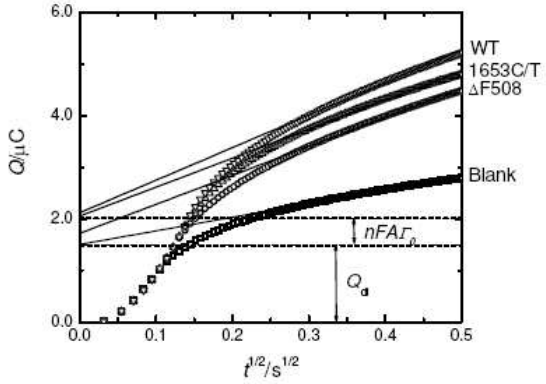

Fig. 4. Coulometric transients recorded by stepping the potential from -0.1 V to -0.6 V vs. SCE with just the (□) blank probe immobilized and MCH treated gold electrode (88 mm^2) in electrolyte solution (pH 7, 10 mM Tris buffer) and in the same electrolyte solution after hybridization with anthraquinone labelled ΔF508 (○), 1653C/T (Δ) and WT (∇) targets. The transients were acquired with the same electrode beginning with the blank, triple mismatch, single mismatch and finally perfect match. The hybridization was carried out separately in another reaction vessel and washed before recording the charge transient. After each coulometric curve was recorded with the respective target, the surface was regenerated by leaving the electrode in 10 mM NaOH for 15 min and subsequently washing with deionized water. The regeneration was checked as the charge transient with the probe only (blank) was recovered.

The coulometric curves shown in Figure 4 were fitted to the following expression for the total charge, Q,

$$Q = Bt^{1/2} + Q_{dl} + nFA\Gamma_O \qquad (1)$$

where t is the time, B is constant, Q_{dl} is the double layer charge, n is the number of electrons transferred, F is the Faraday constant, A is the area of the electrode, and Γ_O is the surface coverage of bound anthraquinone labelled target. The first term in Equation 1 describes the contribution from electroactive species in the solution. The second term is the double layer charging contribution and the final term is the contribution from the bound redox label by virtue of the hybridized target. The double layer charging contribution was found by performing the experiment on the same electrode prior to hybridization to the target, Figure 4.

The only underlying assumption in this analysis is that the double layer capacitance does not significantly change after hybridization, which is reasonable [29] particularly as the bulk of the surface is passivated by mercaptohexanol to prevent non-specific binding. The intercepts for the different charge transients were graphically determined for each target and the double layer charge was subtracted from the value obtained. From this value (equal to $nFA\,\Gamma_O$ and shown for the 1653C/T target in Figure 4) the surface coverage was determined using the number of electrons transferred (n = 2) and the area of the electrode. The area of the SSV electrode was calculated taking into account the geometry of the void surface. The exposed (5 mm x 5 mm in this case) of the SSV surface was multiplied by the geometrical roughness factor, G_R (=3.52) calculated based on the film thickness, h ($1<G_R<4.63$ for $0<h<2R$; where R is the radius of the sphere used for templating the SSV structure). The results are summarised in Table 3 together with the calculated numbers of molecules in the 1 micron laser spot used in the SERS measurements. The surface coverage decreases as the number of mismatches increase. Moreover, the difference between the fully complementary and the single point mutation is significantly less than that between it and the triple mismatch. Based on the coverages in Table 3 the DNA molecules on the surface are around 7 nm apart leaving sufficient space for hybridization to the target DNA.

Table 3. Calculated surface coverages for anthraquinone labelled targets

Target	$nFA\Gamma_0$ / C	Γ_0 / mol cm^{-2}	Γ_0 / molecules cm^{-2}	Molecules in 1 μm diameter laser spot
WT	6.20×10^{-7}	3.65×10^{-12}	2.19×10^{12}	17300
1653C/T	5.60×10^{-7}	3.29×10^{-12}	1.98×10^{12}	15600
ΔF508	2.30×10^{-7}	1.35×10^{-12}	8.15×10^{11}	6400

calculated using n =2 and A = 0.88 cm^2

3.3 SERS-*E*-melting

Representative SERS spectra are presented at different potentials (all potentials are quoted vs. Ag/AgCl reference) for the single point mutation target (1653C/T) on a gold SSV substrate in Figure 5. Anthraquinone labelled targets were found to have an absorbance spectrum with λ_{max} of 547 nm which slightly overlaps with the laser line at 633 nm used in the SERS experiments presented in this work. Hence, the high intensity of SERS peaks could be

attributed to this partial resonance. The SERS peaks in the spectra are similar to those observed for dimethylaminoanthraquinone on silver [32]. In particular, the peaks at 1559 cm^{-1} assigned to ring stretching and at 1375 cm^{-1} assigned to C-N stretching are among the strongest at all potentials. The peak attributed to ring stretching, observed at 1559 cm^{-1}, has been found to be independent of the redox state of the molecule [33]. Hence, for mutation discrimination using anthraquinone labelled probes the SERS-*E*-melting profiles are plotted for the 1559 cm^{-1} peak by extracting the peak intensity after background subtraction.

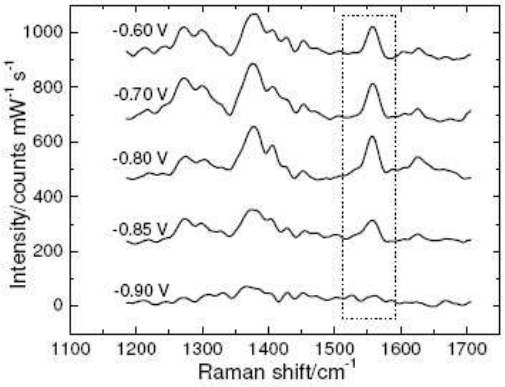

Fig. 5. SERS spectra for anthraquinone labelled 1653C/T (single point mutation) target hybridized to the probe on a gold SSV substrate at different potentials in an *E*-melting experiment. Spectra were acquired with a 633 nm laser with a single accumulation of 5 s at 1 mW laser power. The spectral intensity has been normalized by the laser power and collection time. The 1559 cm^{-1} peak (enclosed in dashed box) was used for SERS-*E*-melting analysis. The spectra are offset for clarity.

SERS-*E*-melting profiles for the three targets corresponding to the perfect match, single mismatch and triplet deletion are shown in Figure 6. The SERS peak intensity for the 1559 cm^{-1} band shows clearly distinct profiles for the three targets during electrochemical denaturation. The profiles are fitted to a Boltzmann function yielding the sigmoidal curve fits and the first derivatives are used to locate the mid-point potential for the melting curve (melting potential or E_m, shown in the inset). It is expected that the greater the number of mismatches the lower will be the thermodynamic stability of the duplex. Hence, as the potential is taken cathodic a duplex with mismatches will be easier to melt than the perfect match. This behaviour is evident in Figure 6 with the triple deletion melting at less negative potentials than the point mutation and the perfect match, which melt at more negative potentials, respectively. From the cyclic voltammetry of the anthraquinone labelled

oligonucleotide hybridized to the surface it was deduced that the label should be fully reduced beyond -0.6 V and hence, changes in the SERS peak intensity at more negative potentials can be wholly attributed to de-hybridization of the target and its diffusion away from the surface. The melting potentials (Figure 6 inset) show clear and unambiguous distinction between the three strands with E_m values determined at -0.98 V, -0.87 V and -0.76 V for Wild type, 1653C/T and ΔF508 sequences, respectively. The 110 mV difference between the melting potentials of each of the targets respectively is large enough to enable measurement by simple instrumentation. Thus, this experiment demonstrates the suitability of the modified anthraquinone label to detect and differentiate mutations in DNA sequences with SERS.

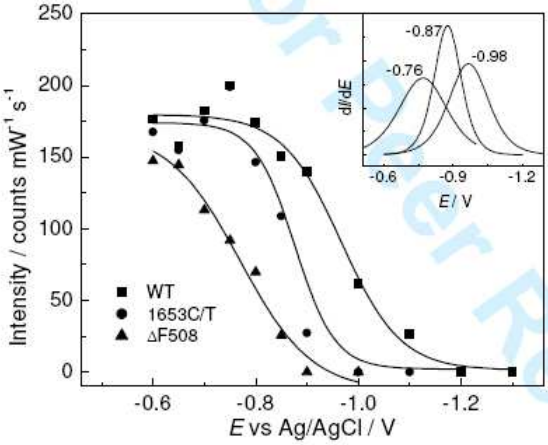

Fig. 6. SERS-*E*-melting profiles for (■) wild type, (●) 1653C/T single mismatch, and (▲) ΔF508 triple deletion, anthraquinone labelled targets on a gold SSV substrate. The first derivatives of the sigmoidal fits are shown in the inset along with the corresponding E_m values.

The initial SERS intensities of the three respective targets in Figure 6 also decrease as the number of mismatches increases though not as markedly as the electrochemical coverage. From the surface coverages, the number of molecules in the 1 micron diameter laser spot used in the SERS measurements (Table 3) was calculated to be only ~6400 molecules for the ΔF508 (triplet deletion), which reaffirms the extreme sensitivity of detection of SERS on SSV substrates.

4. Conclusions

In this work we have demonstrated the first use of an electroactive markers as a SERS label for highly sensitive detection and mutation discrimination in DNA sequences on gold SSV substrates. The electrochemical activity of the label, besides showing modulated SERS with potential, can be used to determine the coverage of the hybrid on the surface. The combination of electrochemistry and SERS is envisaged to be highly advantageous for determining copy number and relative distribution of mutations in a multiplexed high throughput SERS-*E*-melting assay.

5. Acknowledgements

S.M. thanks ORSAS for a scholarship.

6. References

[1]Y. C. Cao, R. Jin, C. A. Mirkin, *Science* **2002,** *297*, 1536.
[2]D. Graham, W. E. Smith, A. M. T. Linacre, C. H. Munro, N. D. Watson, P. C. White, *Anal. Chem.* **1997,** *69*, 4703.
[3]K. Faulds, R. P. Barbagallo, J. T. Keer, W. E. Smith, D. Graham, *Analyst* **2004,** *129*, 567.
[4]K. Faulds, W. E. Smith, D. Graham, *Anal. Chem.* **2004,** *76*, 412.
[5]L. R. Allain, T. Vo-Dinh, *Anal. Chim. Acta* **2002,** *469*, 149.
[6]M. Culha, D. Stokes, L. R. Allain, T. Vo-Dinh, *Anal. Chem.* **2003,** *75*, 6196.
[7]N. R. Isola, D. L. Stokes, T. Vo-Dinh, *Anal. Chem.* **1998,** *70*, 1352.
[8]R. J. Stokes, A. Macaskill, J. A. Dougan, P. G. Hargreaves, H. M. Stanford, W. E. Smith, K. Faulds, D. Graham, *Chem. Commun.* **2007**, 2811.
[9]P. N. Bartlett, J. J. Baumberg, P. R. Birkin, M. A. Ghanem, M. C. Netti, *Chem. Mater.* **2002,** *14*, 2199.
[10] J. J. Baumberg, T. Kelf, Y. Sugawara, S. Cintra, M. Abdelsalam, P. N. Bartlett, A. E. Russell, *Nano Lett.* **2005,** *5*, 2262.
[11] S. Cintra, M. Abdelsalem, P. N. Bartlett, J. J. Baumberg, T. Kelf, Y. Sugawara, A. E. Russell, *Faraday Discuss.* **2005,** *132*, 191.
[12] S. Mahajan, J. Baumberg, A. Russell, P. Bartlett, *Phys. Chem. Chem. Phys.* **2007,** *9*, 6016.
[13] S. Mahajan, M. Abdelsalam, Y. Suguwara, S. Cintra, A. Russell, J. Baumberg, P. Bartlett, *Phys. Chem. Chem. Phys.* **2007,** *9*, 104.
[14] S. Mahajan, J. Richardson, T. Brown, P. N. Bartlett, *J. Am. Chem. Soc.* **2008**.

[15] N. Ben-Gaied, Z. Zhao, S. R. Gerrard, K. R. Fox, T. Brown, *ChemBioChem* **2009,** *in press.*

[16] Z. Zhao, G. Peng, J. Michels, K. R. Fox, T. Brown, *Nucleos. Nucleot. Nucl.* **2007,** *26*, 921.

[17] S. Kumamoto, M. Watanabe, N. Kawakami, M. Nakamura, K. Yamana, *Bioconjugate Chem.* **2008,** *19*, 65.

[18] P. N. Bartlett, J. J. Baumberg, S. Coyle, M. Abdelsalem, *Faraday Discuss.* **2004,** *125*, 117.

[19] S. Mahajan, R. Cole, B. Soares, S. Pelfrey, A. Russell, J. Baumberg, P. Bartlett, *J. Phys. Chem. C* **in press,** *jp-2009-00661u.R1*.

[20] T. Moriguchi, H. Sekiguchi, M. Tachibana, K. Shinozuka, *Nucleos. Nucleot. Nucl.* **2006,** *25*, 601.

[21] J. Hovinen, H. Salo, *J. Chem. Soc., Perkin Trans. 1* **1997**, 3017.

[22] S. Padmanabhan, J. E. Coughlin, R. P. Iyer, *Tetrahedron Lett.* **2005,** *46*, 343.

[23] E. Kaiser, R. L. Colescott, C. D. Bossinger, P. I. Cook, *Anal. Biochem.* **1970,** *34*, 595.

[24] M. J. Gait, *Oligonucleotide synthesis a practical approach.* IRL Press: Oxford, 1984.

[25] T. M. Herne, M. J. Tarlov, *J. Am. Chem. Soc.* **1997,** *119*, 8916.

[26] A. W. Peterson, R. J. Heaton, R. M. Georgiadis, *Nucleic Acids Res.* **2001,** *21*, 5163.

[27] D. Erts, B. Polyakov, H. Olin, E. Tuite, *J. Phys. Chem. B* **2003,** *107*, 3591.

[28] C-Y. Lee, P. Gong, G. M. Harbers, D. W. Grainger, D. g. Castner, L. J. Gamble, *Anal. Chem.* **2006,** *78*, 3316.

[29] A. B. Steel, T. M. Herne, M. J. Tarlov, *Anal. Chem.* **1998,** *70*, 4670.

[30] K. Kerman, D. Ozkan, P. Kara, B. Meric, J. J. Gooding, M. Ozsoz, *Anal. Chim. Acta* **2002,** *462*, 39.

[31] Y. Wang, X. Zhu, Z. Hu, J. Wang, F. Zhouc, *Electroanalysis* **2005,** *17*, 2163.

[32] M. Umadevi, V. Ramakrishnan, *Spectrochim. Acta* **2002,** *58*, 2941.

[33] K. Nishiyama, S.-I. Tahara, Y. Uchida, S. Tanoue, I. Taniguchi, *J. Electroanal. Chem.* **1999,** *478*, 83.

Chapter 8

7.0 Appendix

9.0 Appendix

Peptide 1

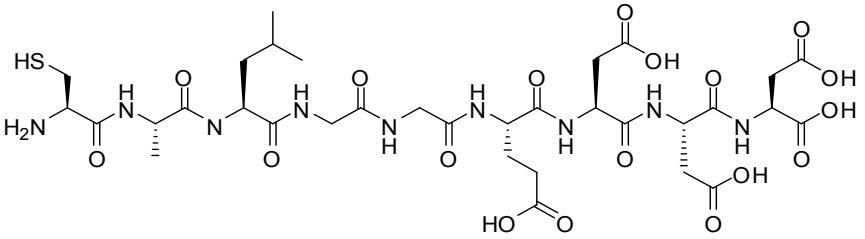

Peptide 2

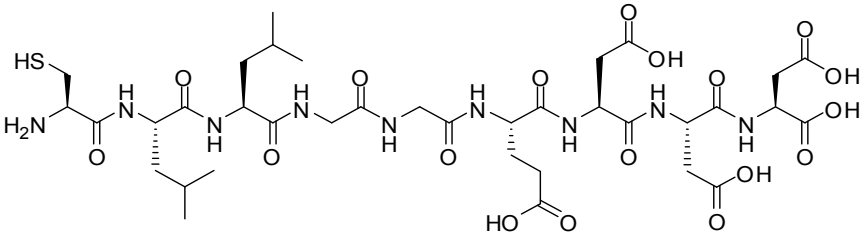

Peptide 3

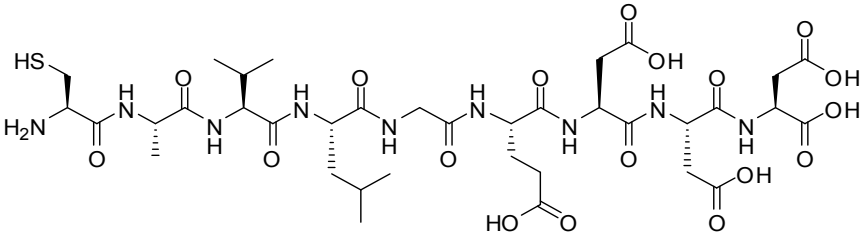

Peptide 4

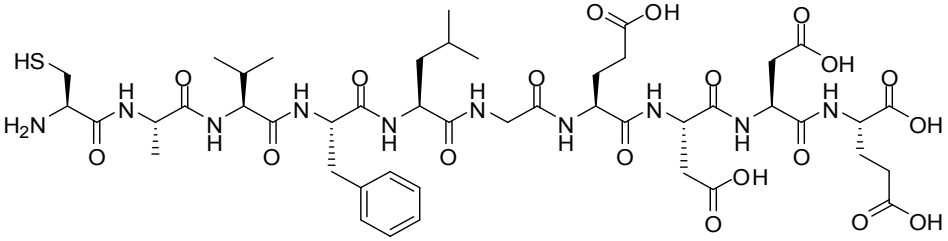

Peptide 5

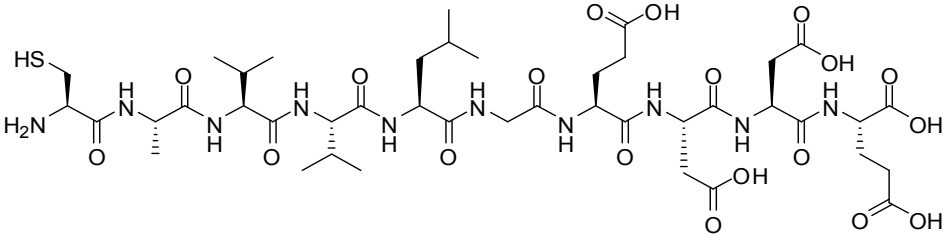

Peptide 6

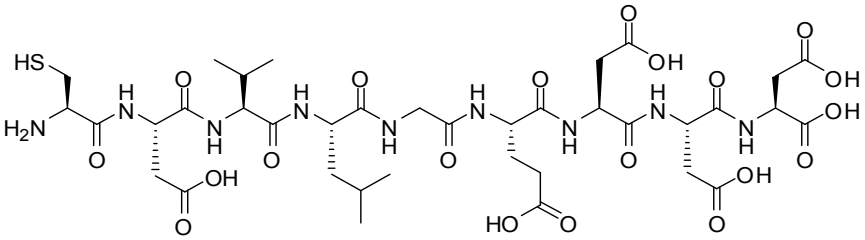

Figure 9.1. Structures of peptides used for quantum dot stabilisation.

Modification	Oligonucleotide sequence
Amino C6 dT (**X**)	**X**CTCGCACTCCAGTGCAATTTGCTGC
Amino C6 dT (**X**)	**X**GCAGCAAATTGCACTGGAGTGCGAG

Table 9.1. Sequences used for quantum dot oligonucleotides conjugates.

Modification	Oligonucleotide sequence
Dabcyl (**X**)	CTCGCACTCCAGTGCAATTTGCTGC**X**
Dabcyl (**X**)	GCAGCAAATTGCACTGGAGTGCGAG**X**

Table 9.2. DABCYL modified oligonucleotides.

Modification	Oligonucleotide sequence
TMSt (**2**) Propargyl dU (**X**) Phosphate (**3**)	**2**CTTTCC**X**CCAC**X**GTTGC**3**
TMSt (**2**) FAM dT (**F**) Phosphate (**3**)	**2**CTTTCC**F**CCAC**F**GTTGC**3**
TMSt (**2**) Aminopentynyl dU (**X**) Phosphate (**3**)	**2**CTTTCC**X**CCAC**X**GTTGC**3**
Aminopentynyl dU (**X**) FAM dT (**F**) Phosphate (**3**)	CTTTCC**F**CCAC**X**GTTGC**3**
Target (WT)	TCGATGGTGTGTCTTGGGATTCAATAACTTTGCAACAG**T**G GAGGAAAGCCTTTGGAGTGATACCACAGGTGAGCAAAAGG ACTTAGCCAGAT
Target (MT)	TCGATGGTGTGTCTTGGGATTCAATAACTTTGCAACAG**A**G GAGGAAAGCCTTTGGAGTGATACCACAGGTGAGCAAAAGG ACTTAGCCAGAT

Table 9.3. W1282X probe sequences, containing a 3' propanol (**3**) or phosphate (**P**), FAM dT (**F**) and aminopentynyl dU (**X**), labelled with JOE (R0547) and Texas red (R0548) NHS esters.

Code	Oligonucleotide sequence
Res0072	GCAT**F**GAGGACCG**F**GTTCAAG**1**
Res0073	GCAT**F**GAGGACCG**F**GTTCAAG**2**
Res0074	GCAT**F**GAGGACCG**F**GTTCAAG**3**
Res0075	GCAT**F**GAGGACCG**F**GTTCAAG**4**
Res0109	**5**GCAT**F**GAGGACCG**F**GTTCAAG**1**
Res0110	**5**GCAT**F**GAGGACCG**F**GTTCAAG**2**
Res0111	**5**GCAT**F**GAGGACCG**F**GTTCAAG**3**
Res0112	**5**GCAT**F**GAGGACCG**F**GTTCAAG**4**
WT	CTTGAACAC**G**GTCCTCAATGC
MT	CTTGAACAC**A**GTCCTCAATGC

Table 9.4. probe sequences, containing mixtures of 5' TMS (**5**), FAM dT (**F**), 3' anthraquinone NB4930-54 (**1**), NB4930-75 (**2**) and pyrene NB5037-18 (**3**), NB5037-19 (**4**).

Modification	Oligonucleotide sequence
Aminopentynyl dU (**X**) FAM dT (**F**) Propanol (**3**)	C**X**TTCC**F**CCAC**X**GTTGCT**P**
Target (WT)	TCGATGGTGTGTCTTGGGATTCAATAACTTTGCAACAG**T**G GAGGAAAGCCTTTGGAGTGATACCACAGGTGAGCAAAAGG ACTTAGCCAGAT
Target (MT)	TCGATGGTGTGTCTTGGGATTCAATAACTTTGCAACAG**A**G GAGGAAAGCCTTTGGAGTGATACCACAGGTGAGCAAAAGG ACTTAGCCAGAT

Table 9.5. W1282X probe sequence for FRET HyBeacons, containing a 3' propanol, FAM dT and aminopentynyl dU.

Code	Oligonucleotide sequence	Mutation target
Aminopentynyl dU (**X**) FAM dT (**F**) Propanol (**3**)	ACCAAAGA**X**GATA**F**TTTC**X**T**P**	ΔF508
Aminopentynyl dU (**X**) FAM dT (**F**) Propanol (**3**)	CTTC**X**GTA**F**CTATA**X**TCAT**P**	R516G
Aminopentynyl dU (**X**) FAM dT (**F**) Propanol (**3**)	CTAGT**X**GGCA**F**GCTT**X**GAT**P**	C524X
R0691 Target (WT)	CACCATTAAAGAAAATATCATC**TTT**GGTGTTTCCTATGATGAATAT**A**GATACAGAAGCGTCATCAAAGCATG**C**CAACTAGAAGAG	
R0692 Target (ΔF508)	CACCATTAAAGAAAATATCATCGGTGTTTCCTATGATGAATATAGATACAGAAGCGTCATCAAAGCATGCCAACTAGAAGAG	
R0693 Target (R516G)	CACCATTAAAGAAAATATCATCTTTGGTGTTTCCTATGATGAATAT**G**GATACAGAAGCGTCATCAAAGCATGCCAACTAGAAGAG	
R0694 Target (C524X)	CACCATTAAAGAAAATATCATCTTTGGTGTTTCCTATGATGAATATAGATACAGAAGCGTCATCAAAGCATG**A**CAACTAGAAGAG	

Table 9.6. CFTR FRET probe sequences for the ΔF508, R516G and C524X mutations.

Modification	Oligonucleotide sequence	Mutation target
Amino C6 dT (**X**) FAM dT (**F**) Propanol (**3**) TMSt (**5**)	**5**TTCTG**F**ATC**X**ATATTCATCAT**P**	R516G
Amino C6 dT (**X**) FAM dT (**F**) Pyrene (**3**)	CACCAAGATGA**X**ATTT**F**CTTTAATGG**3**	ΔF508
Amino C6 dT (**X**) FAM dT (**F**) Pyrene (**3**)	CGCTTC**X**GTA**F**CTATATTCATC**3**	R516G
Amino C6 dT (**X**) FAM dT (**F**) Pyrene (**3**)	CTTCTAGTTGGCA**X**GCTT**F**GATG**3**	C524X

Table 9.7. CFTR probe sequences using endcapping monomers.

Modification	Oligonucleotide sequence	Mutation target
Aminoethoxy T (**X**) FAM dT (**F**) Propanol (**3**)	CACCAAAGATGA**X**ATTT**F**CTTTAATGG**P**	ΔF508
Aminoethoxy T (**X**) FAM dT (**F**) Pyrene (**3**)	CACCAAAGATGA**X**ATTT**F**CTTTAATGG**3**	ΔF508

Table 9.8. HyBeacons using aminoethoxy T (**X**) for labelling with Cy5, containing FAM dT (**F**) and either a propanol (**P**) or pyrene (**3**) 3' modification.

Modification	Oligonucleotide sequence
Amino C6 dT (**X**) FAM dT (**F**) Propanol (**3**)	CACCAAAGATGA**X**ATTT**F**CTTTAATGG**P**

Table 9.9. FRET HyBeacon sequence for labelling with Cy3, Cy3.5, Cy5, Cy5.5 and Cy3b.

Code	Oligonucleotide sequence	Mutation target
Amino C6 dT (**X**) FAM dT (**F**) Propanol (**3**)	CACCAAAGATGA**X**ATTT**F**CTTTAATGG**P**	ΔF508
Amino C6 dT (**X**) FAM dT (**F**) Propanol (**3**)	CGCTTC**X**GTA**F**CTATATTCATC**P**	R516G
Amino C6 dT (**X**) FAM dT (**F**) Propanol (**3**)	CTTCTAGTTGGCA**X**GCTT**F**GATG**P**	C524X

Table 9.10. Cyanine labelled FRET HyBeacons for emission wavelength mutation discrimination.

Modification	Dye separation	Oligonucleotide sequence
Amino C6 dT (**X**) FAM dT (**F**)	5 bp	TT**X**AGCA**F**TAGATACCTTTGCATACCTTAT
Amino C6 dT (**X**) FAM dT (**F**)	5 bp	TTTAGCA**F**TAGA**X**ACCTTTGCATACCTTAT
Amino C6 dT (**X**) FAM dT (**F**)	7 bp	TTTAGCATTAGATACCTTTGCA**X**ACCTTA**F**T
Amino C6 dT (**X**) FAM dT (**F**)	10 bp	TTTAGCA**F**TAGATACCT**X**TGCATACCTTAT
Amino C6 dT (**X**) FAM dT (**F**)	12 bp	TTTAGCATTAGATACCT**X**TGCATACCTTA**F**T
Amino C6 dT (**X**) FAM dT (**F**)	13 bp	TTTAGCATTAGATACC**X**TTGCATACCTTA**F**T
Amino C6 dT (**X**) FAM dT (**F**)	15 bp	TTTAGCA**F**TAGATACCTTTGCA**X**ACCTTAT
Amino C6 dT (**X**) FAM dT (**F**)	17 bp	TTTAGCATTAGA**X**ACCTTTGCATACCTTA**F**T
Amino C6 dT (**X**) FAM dT (**F**)	20 bp	TTTAGCA**F**TAGATACCTTTGCATACCT**X**AT
Amino C6 dT (**X**) FAM dT (**F**)	22 bp	TTTAGCA**X**TAGATACCTTTGCATACCTTA**F**T
Target		ATAAGGTATGCAAAGGTATCTAATGCTAAA

Table 9.11. Oligonucleotides containing FAM-Texas red FRET pair with different donor-acceptor spacing used in FRET efficiency experiments.

Modification	Oligonucleotide sequence	Mutation target
Disulphide (**D**) HEG (**H**)	**DHDHDH**AGGAAACACCAAAGATGATATT	
Amino C7	AATATCATCTTTGGTGTTTCCT**X**	WT
Amino C7	AATATCATCGGTGTTTCCT**X**	ΔF508
Amino C7	AATATCATTTTTGGTGTTTCCT**X**	1653C/T

Table 9.12. Short synthetic oligonucleotides for SERS mutation discrimination experiments.

Oligonucleotide	Sequence
Forward primer	Cy5–GTATCTATATTCATCATAGGAAACACC
Reverse primer	CATTGGAAGAATTTCATTCTGTTCTCAG
Wild type template	GCACATTGGAAGAATTTCATTCTGTTCTCAGTTTTCCTGGATT ATGCCTGGCACCATTAAAGAAAATATCATCTTTGGTGTTTCCT ATGATGAATATAGATACAGA
Mutant template (ΔF508)	GCACATTGGAAGAATTTCATTCTGTTCTCAGTTTTCCTGGATT ATGCCTGGCACCATTAAAGAAAATATCATCGGTGTTTCCTATG ATGAATATAGATACAGA

Table 9.13. PCR primer and template sequences used in SERS PCR analysis.

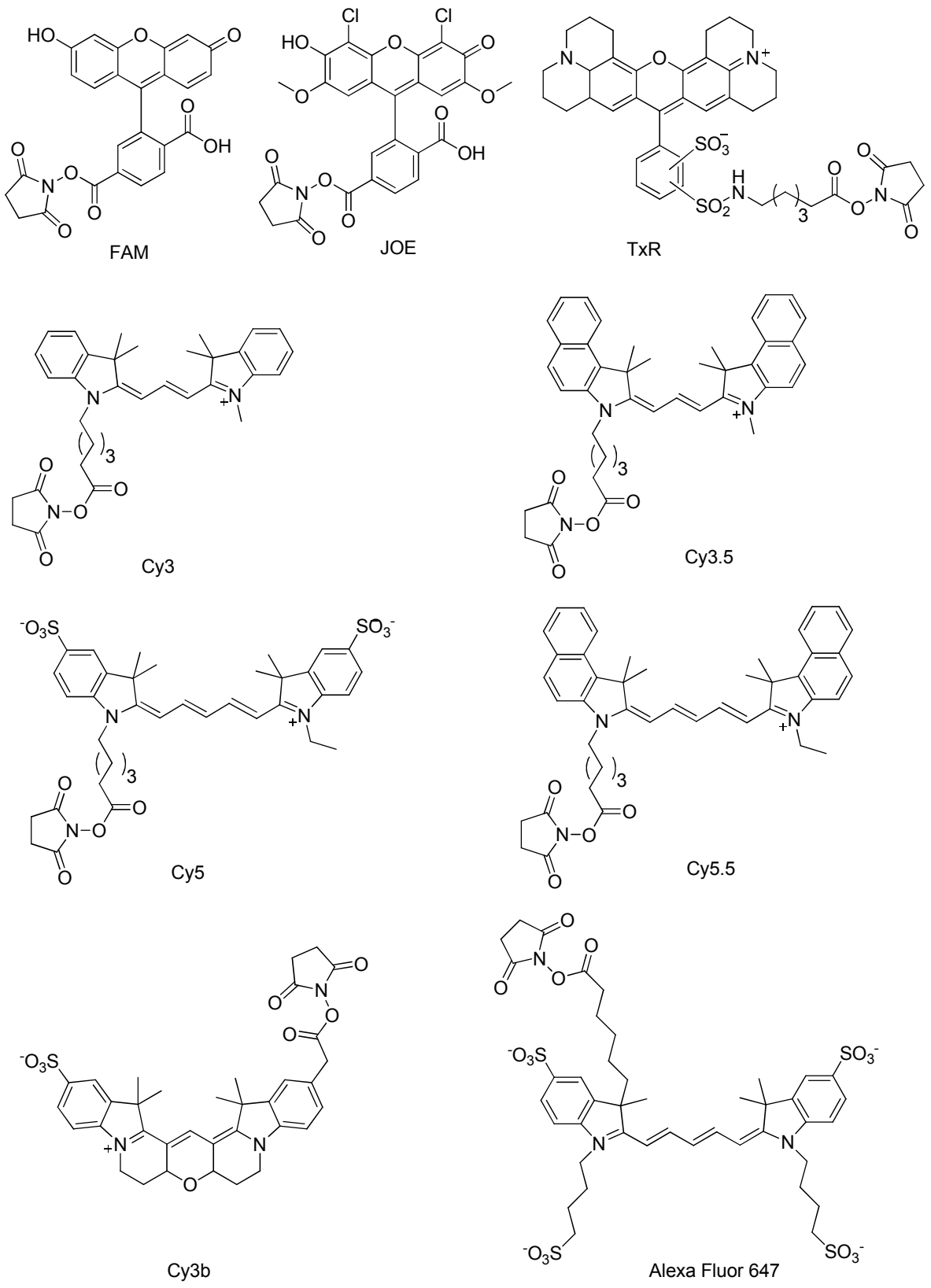

Figure 9.2. Structures of frequently used dyes.